USE OF SATELLITE OBSERVED SEASONAL SNOW COVER
IN HYDROLOGICAL MODELING AND SNOWMELT RUNOFF PREDICTION
IN UPPER EUPHRATES BASIN, TURKEY


A THESIS SUBMITTED TO
THE GRADUATE SCHOOL OF NATURAL AND APPLIED SCIENCES
OF
MIDDLE EAST TECHNICAL UNIVERSITY


BY


ALİ ARDA ŞORMAN


IN PARTIAL FULFILLMENT OF THE REQUIREMENTS
FOR
THE DEGREE OF DOCTOR OF PHILOSOPHY
IN
CIVIL ENGINEERING


JUNE 2005

Approval of the Graduate School of Natural and Applied Sciences

_____

Prof. Dr. Canan Özgen
Director

I certify that this thesis satisfies all the requirements as a thesis for the degree of Doctor of Philosophy.

_____

Prof. Dr. Erdal Çokca
Head of Department

This is to certify that we have read this thesis and that in our opinion it is fully adequate, in scope and quality, as a thesis for the degree of Doctor of Philosophy.

_____

Asst. Prof. Dr. Zuhal Akyürek
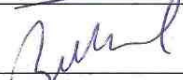Supervisor

Examining Committee Members

| | | |
|---|---|---|
| Prof. Dr. Ayşen Ergin | (METU, CE) | |
| Asst. Prof. Dr. Zuhal Akyürek | (METU, GGIT) | |
| Prof. Dr. Alparslan Arıkan | (HU, HYD) | |
| Prof. Dr. A. Ünal Şorman | (METU, CE) | |
| Asst. Prof. Dr. A. Burcu Altan Sakarya | (METU, CE) | |

I hereby declare that all information in this document has been obtained and presented in accordance with academic rules and ethical conduct. I also declare that, as required by these rules and conduct, I have fully cited and referenced all material and results that are not original to this work.

Name, Last name : Ali Arda ŞORMAN

Signature           :

# ABSTRACT

USE OF SATELLITE OBSERVED SEASONAL SNOW COVER
IN HYDROLOGICAL MODELING AND SNOWMELT RUNOFF PREDICTION
IN UPPER EUPHRATES BASIN, TURKEY

ŞORMAN, Ali Arda

Ph.D., Department of Civil Engineering

Supervisor: Asst. Prof. Dr. Zuhal AKYÜREK

June 2005, 213 pages

Snowmelt runoff in the mountainous eastern part of Turkey is of great importance as it constitutes 60-70% in volume of the total yearly runoff during spring and early summer months. Therefore, forecasting the amount and timing of snowmelt runoff especially in the Euphrates Basin, where large dams are located, is an important task in order to use the water resources of the country in an optimum manner.

The HBV model, being one of the well-known conceptual hydrological models used more than 45 countries over the world, is applied for the first time in Turkey to a small basin of 242 km$^2$ on the headwaters of Euphrates River for 2002-2004 water years. The input data are provided from the automatic snow-meteorological stations installed at various locations and altitudes in Upper Euphrates Basin operating in real-time. Since ground based observations can only represent a small part of the region of interest, spatially and temporally distributed snow cover data are acquired through the use of MODIS optical satellite. Automatic model parameter estimation methods, GML and SCE_UA, are utilized to calibrate the HBV model parameters with a multi-objective criteria using runoff as well as snow covered area to ensure the internal validity of the model and to generate a Pareto

front. Model simulations show that the choice of study years and timing of satellite images affect the results and further suggest that more study catchments and years should be included to achieve more comprehensible conclusions. In the second part of the study, the calibrated HBV model is applied to forecast runoff with a 1-day lead time using gridded input data from numerical weather prediction models of ECMWF and MM5 for the 2004 snowmelt period. Promising results indicate the possible operational use of runoff forecasting using numerical weather prediction models in order to prevent or at least take precautions before flooding ahead of time.

Keywords:     snowmelt runoff, HBV model, parameter estimation, snow cover, numerical weather prediction model, Turkey

# ÖZ

TÜRKİYE'NİN YUKARI FIRAT HAVZASINDA UYDU GÖZLEMLERİYLE BULUNAN
KARLA KAPLI ALANLARIN HİDROLOJİK MODELLEMEDE KULLANIMI VE
KAR ERİMESİNDEN OLUŞAN AKIMLARIN TAHMİNİ

ŞORMAN, Ali Arda

Doktora, İnşaat Mühendisliği Bölümü

Tez Yöneticisi: Yard. Doç. Dr. Zuhal AKYÜREK

Haziran 2005, 213 Sayfa

Türkiye'nin dağlık doğu bölümlerindeki kar erimesinin meydana getirdiği akımlar, bahar ve ilk yaz ayları süresince yıllık akımın % 60-70'ini oluşturduğu için büyük bir öneme sahiptir. Bu nedenle, büyük barajların yer aldığı Fırat Havzasında, kar erimesinden oluşan akımların miktarının ve zamanlamasının tahmin edilmesi, ülkenin su kaynaklarının verimli bir biçimde kullanılmasını sağlamak için önemli bir görevdir.

Dünyada 45'den fazla ülkede kullanılmış, iyi bilinen kavramsal hidrolojik modellerden biri olan HBV modeli, Türkiye'de ilk defa Fırat Nehri'nin kaynağında yer alan 242 km$^2$'lik bir havzada 2002-2004 su yılları için uygulanmıştır. Model girdi verileri, Yukarı Karasu Havzasında, gerçek zamanlı gözlem yapılması ve veri toplanması amacıyla farklı yer ve yüksekliklere kurulmuş otomatik kar ve meteoroloji istasyonlarından sağlanmıştır. Yer gözlem istasyonları, ilgili alanın ancak küçük bir kısmını temsil edebileceği için, alansal ve zamansal dağılımlı karla kaplı alanların saptanmasında MODIS optik uydu görüntülerinden faydalanılmıştır. Otomatik model parametre tahmin yöntemleri olan GML ve SCE_UA, akımın yanı sıra karla kaplı alan verisinin kullanıldığı; modelin içsel doğruluğunu saptayan ve Pareto düzlemi oluşturmaya olanak tanıyan çoklu objektif kriterleriyle HBV model

parametrerininin kalibre edilmesinde kullanılmıştır. Model simülasyonları, uygulanan süre ve seçilen uydu görüntülerinin sonuçları etkilediğini, bu nedenle kesin kararlara ulaşabilmek için modelin farklı havzalarda ve uzun yıllar boyunca uygulanması gerektiğini göstermektedir. Çalışmanın ikinci kısmında, ECMWF ve MM5 sayısal hava tahmin modellerinden sağlanan grid bazlı veriler, kalibre edilmiş HBV modeline girdi olarak kullanılarak 2004 su yılının kar erime periyodunda bir gün öncesinden akım tahmini gerçekleştirilmiştir. Sonuçlar, su taşkınlarının önlenebilmesi veya en azından tedbir alınabilmesi için, sayısal hava tahmin model verilerinin işlevsel akım tahmininde faydalı olduğunu göstermektedir.

Anahtar Kelimeler:    Kar erime akımı, HBV modeli, parametre tahmini, karla kaplı alan, sayısal hava tahmin modeli, Türkiye

*Dedicated to ŞORMAN and ŞENSOY families*

# ACKNOWLEDGEMENTS

# TABLE OF CONTENTS

# LIST OF FIGURES

FIGURES

# LIST OF TABLES

# CHAPTER 1

# INTRODUCTION

## 1.1 Importance of the Problem

In most parts of the world seasonal short term variations in streamflow reflect variations in rainfall only. However, at higher latitudes and altitudes where more precipitation falls as snow, runoff depends on heat supply for snowmelt rather than the timing of precipitation. The hydrological importance of snow is not restricted to areas where it lies for months: many dryland rivers in areas with little or no snow are fed largely by meltwater from high mountains many kilometers away. Snowmelt water is therefore an immensely important water resource in many parts of the world for public supply, hydropower, irrigated agriculture and other uses. Much of the value of meltwater as a resource lies in its reliable occurrence at a particular time of the year and enhanced, if total runoff and timing can be predicted. Accurate forecasting can also minimize risk and loss from floods caused by rapid snowmelt. Hydrologists have therefore devoted much effort to developing models to simulate and forecast snowmelt runoff.

A plethora of hydrologic models have been proposed during the last few decades for a variety of different applications ranging from purely statistical methods which neglect the physics of snowmelt process to the complicated energy budget equations. But most hydrological models fall in the category of conceptual models which try to represent a compromise between scientifically realistic complexity and practically realistic simplicity mainly because of the difficulties in obtaining input data varying in time and space.

1

Traditionally, input to hydrological models is obtained from point measurements of precipitation and temperature at the meteorological stations whereby supported by direct observations of the snow pack when possible. In the past, hydrologists relied mostly on conventional data network systems based on manual ground measurements. As the technological progress brought new impulses, automatic meteorological stations furnished real-time data from remote mountain areas which was particularly important for snow hydrology.

However, ground based observations can by necessity only represent a small part of the region of interest creating problems in basins with pronounced topography because of the high spatial variability of hydro-meteorological parameters. Since a long time, hydrologists have thus looked to remote sensing as an additional source of information. In this sense, remote sensing offers the advantage of spatially distributed observations which, in principle, are more directly linked to runoff than point data because measured runoff represents an integration across a drainage basin.

Snow cover mapping in mountainous areas is demanding due to the interfering topography and the heterogeneous ground properties. With the growing number of satellite platforms and improvements in processing and transmission of digital data obtained from them, it has become possible to obtain frequent snow cover information in near real-time through a variety of different sources. Other hydrologic information such as topographic, vegetation and soil characteristics can also be made available from digital databases through the use of Geographic Information Systems. The incorporation of these data sets into hydrologic modeling is considered highly desirable by hydrologists. The development of efficient and effective methods to determine the amount and timing of snowmelt runoff is still an active area of research.

## 1.2 Purpose of the Study

Water perhaps is the most valuable natural asset in the Middle East as it was a historical key for settlement and survival. The Euphrates and Tigris Rivers with their tributaries served as the cradle for many civilizations that evolved in Mesopotamia, "the land between two rivers". The headwaters of these two trans-boundary rivers originate within the boundaries of Turkey and are later shared by the riparian countries Syria, Iran, Iraq and Saudi Arabia along its way until linked by their natural course to drain into the Persian Gulf.

The Euphrates-Tigris basin is largely fed by snow precipitation over the uplands of northern and eastern Turkey. A sustained period of high flows during the spring months resulting from melting of the snowpack causes not only extensive flooding, inundating large areas, but also the loss of much needed water required for irrigation and power generation purposes during the summer season.

Many of the large dams in Turkey are located in the Euphrates-Tigris basin. The aridity of the region and the water requirements of the downstream nations necessitate accurate and optimum operation of these dams.

Accordingly, the importance of monitoring the seasonal snow cover and forecasting the river runoff in the mountainous regions of Eastern Turkey, as being one of the major headwaters of Euphrates-Tigris basin, is crucial from water resources management point of view.

As a result, a pilot basin, located on the Upper Euphrates River, is selected whereby five automatic meteorological and snow stations and three stream gauging stations are installed providing real-time data for hydrological modeling.

For this study, one of the well known hydrological models, HBV model, is used for the first time in Turkey. Being a conceptual model in trying to represent the physical processes with simplified yet logical algorithms, HBV model is

automatically calibrated both in a traditional manner with the collected hydro-meteorological data from the ground stations and with the additional snow cover area derived from optical satellite and later verified in the first part of the study.

In the second part, spatially and temporally distributed meteorological variables obtained from numerical weather prediction models are used as input to the calibrated HBV model to perform pre-operational runoff forecasts for part of the 2004 water year when snowmelt dominates runoff.

The study is targeted at individuals and organizations interested in operational snowmelt runoff modeling. It does not present a theoretical look at state-of-the-art snowmelt modeling, but an account for implementation of, and improvements to, established hydrological models assisted by Earth Observation data for real time snowmelt runoff forecasting at the very headwaters of Euphrates River.

So the objectives of the study can be listed as:
* real time snow, meteorological and hydrological data collection at the headwaters of Euphrates Basin,
* multi-objective hydrological model calibration using measured runoff and snow covered area derived from Earth Observation data by means of a population-based algorithm,
* integration of numerical weather prediction model outputs with a hydrological model in forecasting 1-day ahead runoff values,
* co-operation between university (METU) and government organizations (DSI and DMI) in order to use the water resources of the country in an optimum manner.

## 1.3 Organization of the Dissertation

The structure of this dissertation follows a clear and logical order for the reader to understand the work undertaken during the study. It consists of seven further chapters.

Chapter 2 discusses the fundamentals of snow hydrology starting from the physics of snow formation until snowmelt runoff. Physical properties of the snowpack and several different snow data collection methods are described. During this process, the most important factors affecting snow cover distribution in a catchment of various spatial scales are discussed. Different modeling approaches in snowmelt hydrology along with their data requirements are mentioned.

Chapter 3 introduces the hydrological model used in this thesis, the HBV model, which is one of the well known hydrologic models in the world. Each of its routines and corresponding model parameters is described in detail along with the input data requirements and output produced. The traditional model performance criterion is explained. Afterwards, a general view of model calibration concept both with manual and automatic methods are compared. The formulation of automatic calibration framework is illustrated. The concept of multi-objective calibration is presented with the aim to seek the Pareto (non-dominant) solutions of the problem. In the end, the future of hydrological model calibration is discussed.

Chapter 4 describes the selected field site and the locations of the automatic snow, meteorological and hydrological instrumentation installed in the region. The instrumentation collect high quality real time data and when needed can transmit this data online for use in near real time modeling in the basin. These equipments were essential to characterize the climate conditions over the rough mountainous topography of Eastern Anatolia and are the pioneer applications in Turkey. These comprehensive data sets form the basis of hydrological modeling work undertaken in subsequent chapters.

Chapter 5 summarizes the remote sensing techniques applied in snow hydrology. Although microwave portion of the electromagnetic spectrum provide more details about the snow properties along with the independency of measurements from weather conditions and illumination, because of the easy interpretation of snow and fine spatial resolution, the use of visible and near infrared region is still highly preferred. A recently launched optical satellite, Moderate Resolution Imaging Spectrometer (MODIS) is briefly described in addition to different MODIS snow products formed and MODIS snow detection algorithm is mentioned.

Chapter 6 constitutes the first part of the model application. Since HBV model is a semi-distributed conceptual hydrologic model, its several parameters need calibration. Calibration of the selected free parameters in the model is undertaken firstly in a traditional manner using only runoff and then runoff along with snow covered area derived from Earth Observation data to assess if internal simulations of the model could be improved without deteriorating the runoff results. The HBV model is later validated for periods not used in the calibration stage. Lastly the Pareto front is derived in order to determine the non-dominant parameter sets giving equally good results.

Chapter 7 forms the second part of the model application. The numerical weather prediction models used in the study and the procedures followed in coupling the gridded atmospheric model outputs into the calibrated HBV model are explained. 1-day ahead runoff forecasts are computed for the 2004 water year when snowmelt was dominant and the results are compared with the observed runoff values in the pilot basin.

Finally, Chapter 8 summarizes the main results of the previous two chapters, discusses the implications of the work within the context of existing snow hydrology literature and makes recommendations for further research.

# CHAPTER 2

# FUNDAMENTALS OF SNOW HYDROLOGY

## 2.1 Introduction

The occurrence of precipitation in the solid form (snow) as opposed to the liquid form (rain) typically causes a change in drainage basin response to the input of water, because snow is stored in a basin for an extended period of time before it enters into the runoff process.

In many regions of the world, snowfall and the resulting seasonal snowcover represent an important source of water. Although, volumetrically they form only a small fraction of the Earth's fresh water, their hydrological importance is immense. When the snowpacks melt, the snowmelt recharges the groundwater and replenishes surface water storage. Excessive snowmelt runoff can cause flooding, while inadequate snowmelt is often the prelude to later drought.

Snow accumulation and snow melt plays a major role in the hydrological cycle in temperate to cold regions and even in mountainous basins of tropical regions. Snow accumulation and melt also affect the runoff regime strongly, usually leading to a pronounced seasonal variation.

## 2.2 Snow - Formation, Distribution and Measurement

### 2.2.1 Physics of Formation

The atmospheric requirements for snowfall formation are the presence of water vapor and ice nuclei and an ambient temperature below 0°C. Ice nuclei are particles that cause ice crystals to form through either direct freezing of cloud droplets or freezing of water deposited on the particle surface as a vapor. At any time, there are billions of aerosol particles in the atmosphere, but a very small fraction of these particles are active as ice nuclei. Once ice crystals form, they may splinter and create large numbers of nuclei to aid the precipitation process.

Continued growth of an ice crystal leads to the formation of a snow crystal. This is a large particle, having a very complex shape and of such size that it is visible to the naked eye. A snowflake is an aggregation of snow crystals which may grow in size during its fall to the earth owing to the adhesion of colliding snow crystals. Snow scientists classify atmospheric snow crystals by their shapes and growth processes (Magono and Lee, 1966 as cited in Gray and Prowse, 1992), but a different system is used to classify seasonal snow on the ground (Colbeck et al., 1990 as cited in Gray and Prowse, 1992).

Whether a snowflake formed in the atmosphere arrives at the earth's surface as snow or rain depends primarily on the extent and temperature of layers of air through which it falls. Figure 2.1 illustrates the temperature dependent probability distribution of snow, sleet and rain occurrences in the interval from -2°C to +4°C from results observed at Donner Summit, USA (USACE, 1956) and Øvre Jervan, Norway (Killingtveit, 1976).
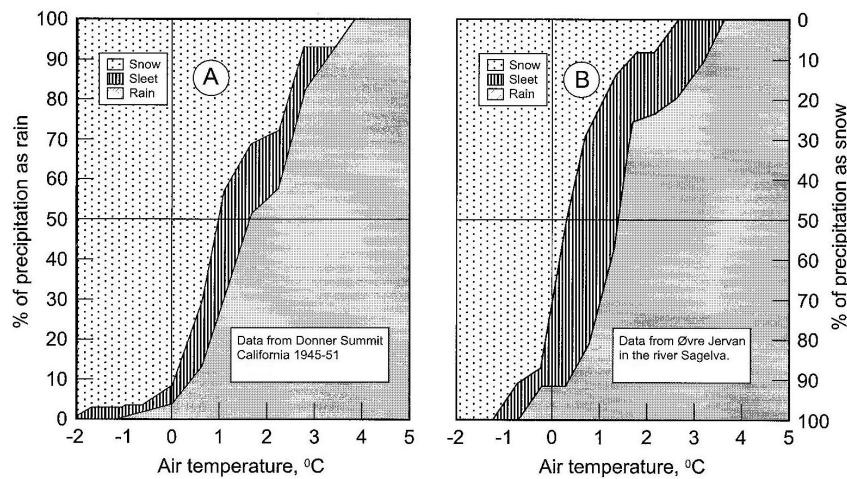
A: Data from USACE, 1956    B: Data from Killingtveit, 1976

Figure 2.1 Distribution of precipitation type as a function of air temperature

## 2.2.2 Physical Properties of the Snowpack

A number of physical parameters used to characterize the snowpack are:
* ❅ Water Equivalent (mm)
* ❅ Depth (cm)
* ❅ Density (g/cm$^3$ or kg/m$^3$)
* ❅ Liquid Water Content (% of weight or volume)
* ❅ Albedo
* ❅ Areal Extent

The water equivalent of snow is the vertical depth of water which would be obtained by melting the snowpack. It is usually obtained as the product of average snow depth and density. An average density of a freshly fallen snow can be assumed as 100 kg/m$^3$, which gives 1 unit of water for each 10 units of snow depth. But the density of a new snowfall varies widely depending on the amount of air contained within the lattice of the snow crystals. Densities in the range of 50 to 120 kg/m$^3$ are common. Lower values are generally found in snowfalls formed under dry, cold conditions and higher values are found in wet snows at warm temperatures.

9

Following deposition, the density of a new snow increases rapidly owing to metamorphism – changes in the size, shape and bonding of snow crystals due to temperature and water vapor gradients, settlement and wind packing with the rate of change being controlled primarily by meteorological conditions.

The average density of a snowpack also varies seasonally. During snowmelt, the densities commonly range between 350 and 500 kg/m$^3$ owing to the storage and loss of meltwater. Lower densities occur in the morning and increase during the day as the snowpack becomes primed by infiltrating water.

Liquid water content is the amount of liquid water (not frozen) retained in the snowpack. During the onset of snowmelt, the meltwater produced will first be retained in the snowpack as liquid water and no runoff is produced. Only when the retaining capacity is exceeded, usually 5-10% liquid water content per unit volume, additional snowmelt will be released from the snowpack and produce runoff. An example from measurements in Norway is shown in Figure 2.2 (Killingtveit and Saelthun, 1995).
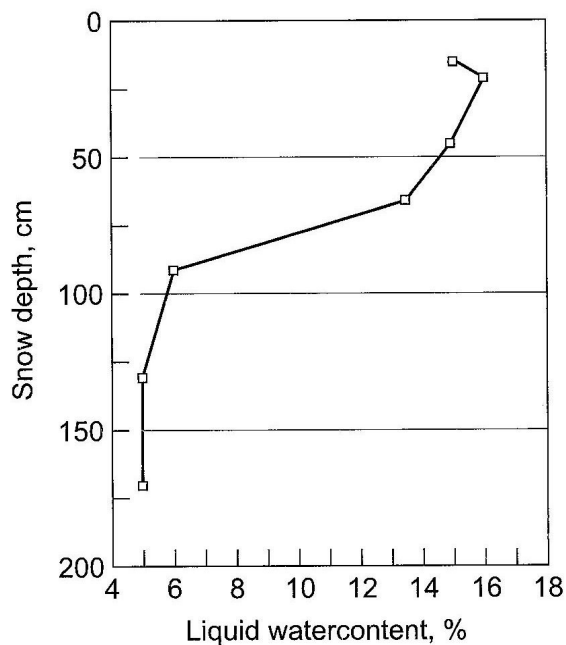


Figure 2.2 Liquid water content in a vertical snow profile for Nea basin, Norway (Killingtveit and Saelthun, 1995).

Snow albedo is the ratio of reflected radiation to the incoming radiation. It is usually averaged over the visible short-wave radiation spectrum (0.4 − 0.7 μm) and gives a good indication of the ability of the snow to absorb radiation energy. Generally the albedo of fresh, newly fallen snow is high, up to 95%, but decreases over time as metamorphosis of the snowpack changes the crystal structure to increasingly coarser grains. Old snow is often contaminated with dust and air pollution and albedo may be as low as 25%. Snow albedo varies widely with snow conditions and also with the wavelength of incoming radiation. This fact is used in remote sensing of snow, where measured albedo for different wavelengths can be used to distinguish between snow and bare ground or to identify wet and contaminated snow. Figure 2.3 shows albedo for snow of different age and for contaminated glacier ice (Winther, 1993).
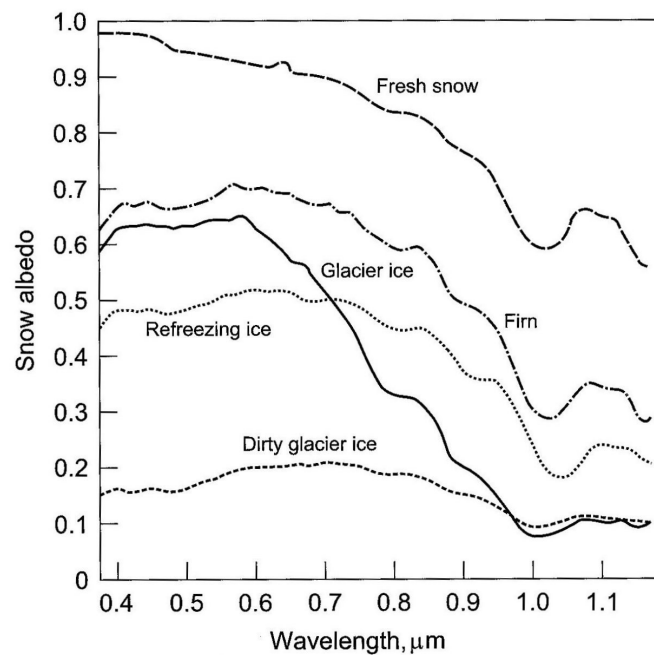


Figure 2.3 Spectral variability of snow albedo for different types of snow (Winther, 1993).

The location and extent of snowcover is usually estimated using remotely sensed data that can discriminate between snow and no snow. Snowcover extent is often expressed as a percentage or fraction of the total drainage area of interest that is covered by accumulated snow.

## 2.2.3 Collection of Snow Data

Knowledge of the amount of snow accumulation at a point (snowfall) on the ground and its spatial distribution (snowcover) throughout the area of interest is essential for snow modeling. Table 2.1 summarizes the techniques that are available to measure snowfall at a point and the areal extent of the snowcover (USACE, 1998).

There is uncertainty in all precipitation data (Isrealson, 1967; Larson, 1971; Sevruk, 1986 cited in Marks et al., 1992) but because rainfall is of higher and constant density than snow, rainfall data are not as difficult to analyze (Harris and Carder, 1974 cited in Marks et al., 1992). Peck (1972 in Marks et al., 1992) summarizes the problem of monitoring snowfall, stating that most measurements of snowfall rates and volumes are the least accurate of the meteorological measurements used in hydrological modeling. Even if the uncertainty in point snow data collection can not be removed completely, it may be reduced by careful gage placement and calibration (Larson and Peck, 1974). But precipitation evaluation at mountainous areas indicate that problems of wind during deposition are increased in rugged, high altitude regions where gage placement can significantly alter gage catch (Pagliuca, 1934; Garstka, 1944; Chadwick, 1972; Hamon, 1972 cited in Marks et al., 1992). In a comparison of gauge efficiency to snow deposition on snow boards show a systematic underestimate by collection gauges in windy alpine environments (Marks et al., 1988). Also numerous investigations have revealed that an unshielded gauge may only receive 50% of the true precipitation when the wind speed exceeds 4-5 m/s as shown in Figure 2.4 (Killingtveit and Saelthun, 1995). Hence in remote alpine environments, snow collection gages can not be relied upon for snowfall data. Instead, detailed ground measurements of snow should be made both on an event basis and at regular intervals (Marks et al., 1992). If the site is inaccessible on regular basis, being located at the higher parts of the basin, then snow pillows and depth sensors may be used. Although they may also represent only point data, if the location is carefully chosen, the continuous measurements can add valuable information.

Table 2.1 Snowfall and snowcover measurement techniques (USACE, 1998).

| Measurement Class | Method Name | Parameter Measured |
|---|---|---|
| Simple linear measurement | Graduated snow ruler | Depth |
| | Snow board | Depth |
| | | |
| Gravimetric | Precipitation gauges | |
| | a. Non-recording bucket | Water equivalent |
| | b. Recording | Water equivalent |
| | weighing/ tipping bucket | Snowfall rate |
| | c. Electronic balance | Water equivalent |
| | | Snowfall rate |
| | Snow samplers (snow tubes) | Depth |
| | | Water equivalent |
| | Snow pillows and snow triangles | Water equivalent |
| Calorimetric | Freezing, alcohol solution or dilution calorimetric methods | Liquid water content (weight basis) |
| Electromagnetic | | |
| A. In situ sensors | a. Gamma radiometers | Water equivalent |
| | b. Acoustic sensors | Depth |
| | c. Optical snow gauge | Snowfall rate |
| | (transmissiometer) | Snowfall mass conc. |
| B. Remote Sensors | Natural terrestrial | Water equivalent |
| (satellite or airborne) | gamma radiation | Snowcover |
| | Visible photography | Snowcover |
| | Microwave | Water equivalent |
| | | Snowcover |
| | Radar | Depth |
| | | Snowcover |
| | Multispectral Images | Snowcover |
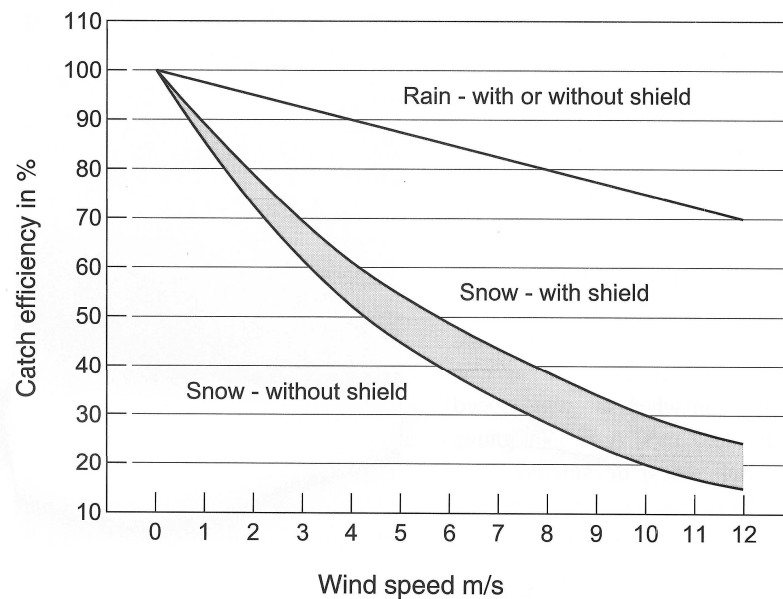
Figure 2.4 Gauge catch deficiency for rain and snow as a function of wind speed (Killingtveit and Saelthun, 1995).

Apart from the point snowfall data, the changing areal extent of the seasonal snow cover may be detected by remote sensors (satellite or airborne). Sometimes these sensors may even be used to determine snow water equivalent (e.g. microwave and gamma radiation), but firstly, they have to be calibrated with reliable ground truth point data to be used for operational purposes.

## 2.2.4 Snow Cover Distribution

The areal variability of snow cover can be studied at three spatial scales:
* Microscale (<100m)
* Mesoscale or Local (100 m to a few km)
* Macroscale or Regional (> a few km)

The most important factors affecting snow distribution in a catchment are:

❅ Climate

❅ Topography

❅ Vegetation

Climate

The important climatic parameters, in addition to the precipitation itself, are air temperature and wind. Air temperature affects the form of precipitation, melting/freezing and internal metamorphosis of the snowpack. Air temperature at snowfall determines the crystal structure and the degree of packing of the new snow. Snow falling at low temperatures consists of light crystals, easily moved by wind, while snow falling at around 0°C will usually be wet and dense and not so easily affected by wind. Since air temperature normally decreases with elevation, while precipitation normally increases, the effect is a net increase in snow with elevation. This effect can be very pronounced, with large snowpacks in high-lying areas and little or no snow in the lower-lying regions.

Wind has a strong influence on the redistribution of snow and consequently effect on the spatial variability in snow water equivalent. In addition, wind has great influence on the energy exchange between atmosphere and the snow surface and thus for evaporation, melting and refreezing of the snowpack. Wind hardens and compacts snow because of the drag forces exerted on the surface by the moving air and by impacting particles. Transported snow crystals undergo changes to their shape and size and form drifts and banks of higher density than the parent material. Generally, through erosion, transportation and redeposition, snow is redistributed significantly, especially in non-forested areas where the wind is strongest and snow drift is not hindered by trees. The net effect is that hills and ridges are blown free of snow and an accumulation of snow in the low-lying, gullies and within forests. This leads to an uneven or skew snow distribution in the catchment. Figure 2.5 depicts a snow distribution for a catchment in Norway compiled from 250 sampling points (Killingtveit and Sand, 1991).
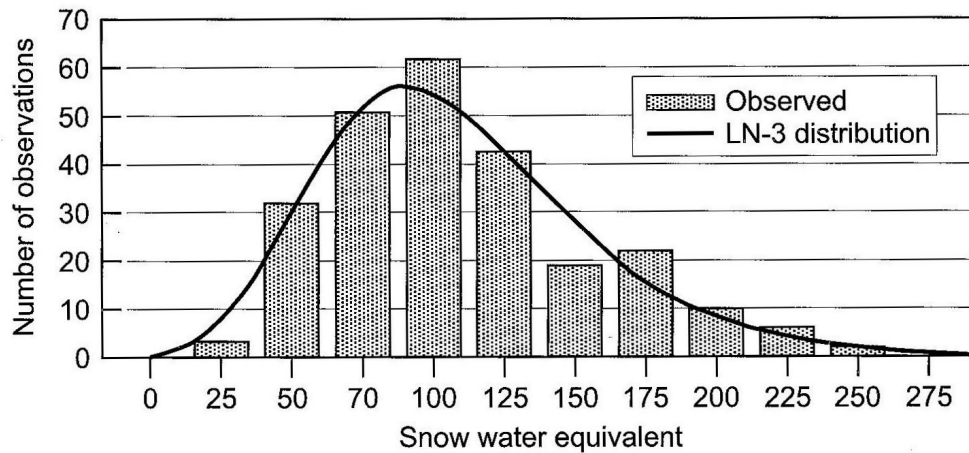
Figure 2.5 Snow distribution from Orkla river in Norway, based on 250 sampling points in the 800m zone (Killingtveit and Sand, 1991).

Topography

Depth of seasonal snow cover usually increases with elevation because of the larger number of snowfall events and lower amounts of evaporation and melt. Thus, at a particular location in a mountainous region, a strong linear association is often found between seasonal snow cover and elevation within a selected elevation band. However, even along specific transects the rate of increase in water equivalent with elevation may vary widely from year to year. Elevation alone is not a causative factor in snow cover distribution and a host of other variables such as slope and aspect must be considered to interpret distribution patterns accurately. Snow depth decreases with distance along a slope oriented in the direction of prevailing winds and major accumulations occur on lee slopes (sheltered from wind) and in abrupt depressions. A primary influence of aspect on snow distribution patterns is its effect on the surface energy exchange process and snowmelt.

Vegetation

Vegetation affects snow cover distribution through its influences on surface roughness and wind speed, therefore on snow erosion, transport and deposition; the surface energy exchange; and snowfall interception. It is commonly observed

that the snow distribution in a forested area is less uneven than in an open area. The proportion of snowfall accumulated in a forest depends on canopy density, the proportion of the ground surface protected (shaded) by vegetation and tree species. Interception by coniferous forests is much greater than by deciduous forests because deciduous trees lose their leaves during winter. This also affects the energy balance at the ground surface and the amount of snowfall lost to evaporation and sublimation.

## 2.3 Snowmelt

In many parts of the world, melt of the seasonal snow cover is the single most important event of the water year. Water produced by melting snow supplies reservoirs, lakes, rivers and infiltrating meltwater recharges soil moisture and groundwater.

When snow melts, the ice that composes the snow is converted into water. Since the conversion from ice to water requires the input of energy (or heat), the process of snowmelt is inextricably linked to the flow and storage of energy into and through the snowpack.

Whenever sufficient energy is available, some snow (ice) will melt and form liquid water (i.e. snowmelt). Since the physical structure of the snowpack is a porous matrix, this snowmelt will be held as liquid water (provided it does not refreeze) in the interstices between the snow grains and will increase snow density and snow water content. The snowpack is commonly called "ripe" when it is isothermal at 0°C and saturated. Whenever the capacity of the snowpack interstices to hold the liquid water is exceeded, some of the snowmelt will begin to move down-gradient called direct surface runoff to become a portion of the snowmelt runoff. Additionally, some of the snowmelt may infiltrate into the ground. The amounts that infiltrate depend on inherent soil characteristics, soil moisture content, as well as whether or not the ground surface is frozen. The infiltrated snowmelt later

reemerges as interflow into stream channels, or it percolates into deeper groundwater storage. Hence the snowmelt process can conceptually be divided into several different but interrelated processes:

❇ Heat balance of the snowpack

❇ Snowmelt at the atmosphere-snow and ground-snow interface

❇ Internal movement and retention of liquid water within the snowpack

❇ Release of water from bottom of snowpack with infiltration or surface runoff

There are many models for forecasting snowmelt runoff. These use either an energy balance or some empirically defined snowmelt index to compute melt. For extreme conditions and for short term forecasts, physically based systems are recommended. Most index models are designed for simulation periods of a month or longer and give good results under average conditions.

## 2.3.1 Energy and Mass Balance

The energy balance approach for calculating snowmelt applies the law of conservation of energy to a control volume. The control volume has its lower boundary as the snow-ground interface and its upper boundary as the snow-air interface. Use of a volume allows the energy fluxes into the snow to be expressed as internal energy changes.

The balance requires that the sum of the energy fluxes by radiation, convection, condensation and conduction plus the change in internal energy in the volume be zero. For a cube of snow of unit volume, assuming the energy transfers in the horizontal direction are negligible, the energy equation in the vertical direction gives the amount of net energy available for melt. The energy fluxes on a snowpack are quantified with the equation given below and depicted in Figure 2.6 (Killingtveit and Saelthun, 1995).

$$Q_m = Q_{sn} + Q_{ln} + Q_h + Q_e + Q_g + Q_p \pm \frac{dU}{dt}$$

Equation 2.1

$Q_m$ :  net energy available for melt

$Q_{sn}$ :  net short wave radiation flux absorbed by the snow

$Q_{ln}$ :  net long wave radiation flux at the snow-air interface

$Q_h$ :  sensible heat flux between air and snow by convection

$Q_e$ :  latent heat flux between snow and air by evaporation, sublimation, condensation

$Q_g$ :  heat flux between ground and snow by conduction

$Q_p$ :  heat from rain

$dU/dt$: rate of change of internal energy per unit area of snowpack
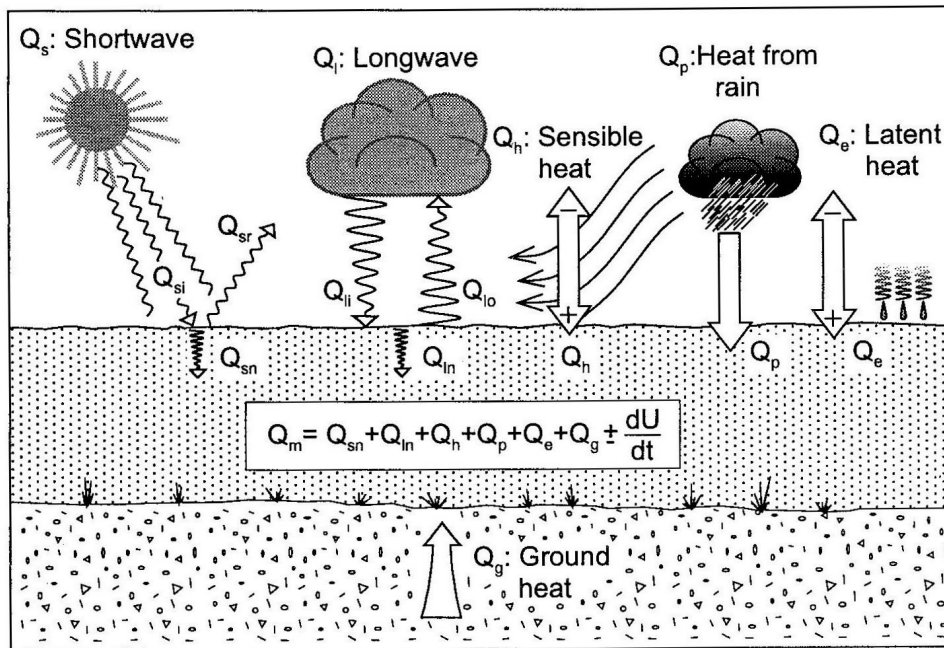


Figure 2.6 Energy fluxes in the vertical direction on a snowpack (Killingtveit and Saelthun, 1995).

The rate of change of internal energy in the snowpack is composed of the energy to melt the ice portion of the snowpack, freeze the liquid water in the snow and

19

change the temperature of the snow. Thus during periods of warming, the net flux of heat (dU/dt) is into the snow, while during periods of cooling, the net flux (dU/dt) is out of the snowpack. Therefore, the amount of energy available to cause snowmelt varies and can be dynamic, depending on the magnitudes of the various energy inputs to the snowpack. Male and Gray (1981) suggest that snowmelt is not homogeneous throughout the snowpack depth and point out that most of the melting occurs at the upper (snow-air) and lower (snow-ground) interfaces of the snow.

The summation of all sources of energy (heat) represents the total amount of energy available for melting the snowpack which may be expressed at a point by the general formula given in Equation 2.2.

$$M = \frac{Q_m}{h_f \, \rho_w \, B}$$
<div align="right">Equation 2.2</div>

M     : snow melt (mm/day)

$Q_m$     : net energy flux computed from Equ. 2.1 (kJ/m$^2$*day)

$h_f$     : latent heat of fusion of ice (kJ/kg)

$\rho_w$     : density of water (kg/m$^3$)

B     : thermal quality of snow or fraction of ice in a unit mass of wet snow (B≤1)

A melting snowpack consists of a mixture of snow (ice) and a small quantity of free (liquid) water trapped in the interstices between the snow grains. The relative proportion of a snowpack that consists of ice determines the thermal quality (B) of the snowpack. A snowpack that contains no free water has a thermal quality of 1.0. However, after melt has begun, there is some free water held within the snow matrix, yielding a thermal quality of less than 1.0. The heat energy required to release 1 g of water is somewhat less than the latent heat of fusion of water (that is the energy required to change state from ice to water; 334.9 kJ/kg or 80 cal/g for pure ice). For a melting snowpack, after free drainage by gravity for several hours, the thermal quality normally averages between 0.95 and 0.97, corresponding to 3 to 5 percent liquid water in the snow.

For normal melt conditions one can assume:

$h_f$     : 334.9 kJ/kg

$\rho_w$     : 1000 kg/m$^3$

B     : 0.97

Giving Equation 2.3 for snow melt in units of mm/day.

$$M = \frac{Q_m}{325}$$            Equation 2.3

The significant problem with implementing an energy balance approach to predicting snowmelt is the variability of the energy terms, particularly over time (at diurnal as well as synoptic and seasonal time scales), but also over space. Modern automatic weather stations allow the energy balance to be quantified at a point. It is rare for such instrumentation to be available at even a single point in a basin, and even then a problem remains in extrapolating the measurements to other parts of the basin. However, an alternative to measuring the energy balance is to approximate the main terms from more readily available data. There are many variants on this parametric energy balance approach. Net short wave radiation can be estimated from incident radiation (which in turn depends on latitude, altitude, and time of year, and can be corrected for relief shading effects), cloud cover, and snow albedo. The diurnal temperature range is sometimes used as a crude index. Sensible heat transfer varies as the product of air temperature and wind speed, and precipitation heat supply as the product of temperature and rainfall rate. All such approaches require extrapolation of, not just air temperature, but also wind speed and other variables from the base station to distant and higher parts of the basin.

Estimates of snowmelt amounts are derived through the use of energy balance equations as well as by some empirical defined snowmelt index.

## 2.3.2 Temperature Index Methods

Although energy balance models provide a physical basis for estimating snowmelt, the data required to solve the energy equation are very extensive. Therefore, operational systems for snowmelt prediction substitute a temperature index approach. Since air temperature was already a predominant variable used in the energy budget equations, it is logically connected with many of the energy exchanges involved in snowmelt. Also it is the meteorological variable that can most safely be extrapolated across a basin and since it is commonly available to hydrologists in historical and real-time databases, the studies concluded that air temperature is a useful index to snowmelt, particularly in forest covered basins. It is less reliable as an index in open, exposed areas because net short wave radiation, sensible and latent heat fluxes (none of which are related directly to air temperature) may exhibit wide variations in their relative importance to snowmelt. The temperature index approach is least applicable during extremes, e.g., when net radiation and latent heat are large and air temperature is low. It is also unsuitable for monitoring diurnal variations in melt because air temperatures usually lag and attenuate short term variations in net radiation. However, the low data and computational requirements make temperature indexes particularly attractive for operational modeling. Indeed, the method is at the heart of models such as SRM and HBV. The method is robust and can be applied to a variety of spatial scales and environmental conditions (WMO, 1986).

The simplest and most common expression relating snowmelt to air temperature is

$$M = a\left(T - T_c\right) \qquad \text{if } T \geq Tc \qquad \text{Equation 2.4}$$

$$M = 0 \qquad \text{if } T < T_c$$

M : snow melt (mm/day)
a : degree-day factor (mm/day/$^o$C)
T : mean air temperature ($^o$C)
$T_c$ : critical air temperature at which snow melts ($^o$C)

Since air temperature is only one of the several meteorological parameters influencing snowmelt, neither the degree-day factor nor the critical temperature can be truly constant. Solar radiation, cloudiness, wind speed, snow albedo, relative humidity and the effect of forest cover are some of the other parameters that can be used in order to account for the terms in the energy balance (Kuusisto, 1980).

The literature abounds with different values for the degree-day factor and the critical temperature. Although quite often a fixed critical temperature of $0^{o}C$ can be set without great loss in model performance, the degree-day factor is known to vary within a wide range of 2 - 15 mm/$^{o}$C/day. Normally, the value varies between 3 - 6 mm/$^{o}$C/day (Killingtveit and Saelthun, 1995).

The degree-day model has been extended in a number of ways, in numerous studies (Kustas and Rango, 1994; Cazorzi and Fontana, 1996; Hock, 1999; Ohmura, 2001; Pellicciotti et al., 2002; Şensoy, 2005). Typically, other climate parameters are included in order to account for other terms in the energy balance in addition to air temperature. Additional parameters commonly used are wind speed, relative humidity, short wave radiation and snow albedo. One of the most common extensions of the degree-day model is the addition of snow albedo with short wave radiation because radiation is a dominant flux in the energy balance snowmelt studies. Hence with the addition of new variables, Equation 2.4 can be renamed as modified (enhanced) degree-day and rewritten as below:

$$M = a\left(T - T_{c}\right) + b\left(1 - \alpha\right)S \qquad \text{Equation 2.5}$$

M : snowmelt (mm/day)

a : degree-day factor (mm/day/$^{o}$C)

T : mean air temperature ($^{o}$C)

$T_{c}$ : critical air temperature at which snow melts ($^{o}$C)

b : radiation index (mm/day/W/m$^{2}$)

$\alpha$ : snow albedo (units)

S : incoming shortwave radiation (W/m$^{2}$)

With the modified degree-day approach especially on a diurnal cycle, Pellicciotti et al. (2002) show that 80-90% of the energy balance terms can be explained. Hence it can be stated that with the addition of very limited data apart from the most common temperature and precipitation measurements, a very significant amount energy needed to melt the snow can be modeled. The only handicap for this modified method is the inability to incorporate it into operational modeling since radiation and albedo values are not very frequently found as forecast values.

## 2.4 Snowpack Meltwater Production and Movement

The metamorphosis from a loose, dry and subfreezing snowpack of low density to a coarse, granular and moist snowpack of high density is sometimes spoken of as "ripening" of the snowpack. A ripe snowpack is said to be "primed" to produce runoff when it becomes isothermal at 0°C and its liquid-water-holding capacity has been reached. At this point, the only storage effect of the snowpack is that of "transitory" storage, resulting in a temporary delay of liquid water transit through the pack.

As each new layer of snow is deposited, its upper surface is weathered by radiation, rain, and wind. The undersurface of the new layer may also be affected by ground heat. As a result, the snowpack is stratified, showing distinct layers and ice planes or lenses that separate individual snowstorm deposits. The interior of the pack is subjected to the action of percolating water and diffusing water vapor.

Analysis of meltwater movement through snow is more complicated than infiltration in a more static medium such as soil. The snowpack medium changes continuously as snow grains change in shape and size. In addition, as the snow melts and refreezes, impermeable ice layers form. Snowmelt moves through the snowpack vertically and horizontally. However, after the liquid-water conditioning of the snowpack has taken place, the movement of water through the pack is mostly straight downward to the snow-ground interface. Ice layers within the

snowpack, however, tend to deflect the path intermittently, thereby resulting in an irregularly stepped pattern.

Colbeck (1978 in Marks et al., 1992) and Yosida (1973 in Marks et al., 1992) have shown that as meltwater drains through the snowpack two zones are formed. An upper layer of wet snow that is isothermal at $0^{\circ}$C and a lower layer with a temperature below $0^{\circ}$C. The rate at which a wetting front moves downward is controlled by refreezing of water onto grains to release sufficient heat of fusion to raise the temperature of the snow to $0^{\circ}$C and to increase the water content. A wetting front does not advance as a uniform wave. Vertical flow fingers develop around inhomogeneities along the horizontal boundaries of the snowpack (Marsh and Woo 1984) which concentrate water that moves at a higher velocity than meltwater in the adjacent surrounding snow. These fingers cause instability in the flow regime and may extend through numerous stratigraphic layers.

## 2.5 Meltwater Infiltration

In snow hydrology, there will be essentially no direct runoff until the soil storage is filled to its field capacity, which is the amount of water that can be held against gravity. After this capacity, excess water may pass through the soil under gravitational force and appear later as subsurface or baseflow component of the streamflow. The time delay of transitory storage in the soil is integrated in the total basin storage effect.

Direct measurements of soil moisture in basins are generally lacking. Accordingly, basin soil moisture conditions are generally estimated from indirect relationships involving earlier precipitation, duration of rainless days, groundwater levels, stream discharges, time of year and other factors associated with soil moisture variation.

For areas of deep snow accumulation, the soil moisture deficit is satisfied early in the snowmelt period and in many areas it may often be satisfied in the fall from

rainfall or snowmelt. In the latter case, the soil beneath the snowpack remains at or above the field capacity throughout the winter and any loss by evapotranspiration will usually be supplied by winter snowmelt or rainfall. For years in which the soil moisture capacity is not filled by fall or winter rainfall or snowmelt, it is necessary to estimate the condition of the soil from preceding hydro-meteorological events.

Gray and Prowse (1992) state that the infiltrability of frozen ground is one of the most important factors affecting the apportioning of snow water between direct runoff and soil water in most northern regions. The ground is generally unfrozen beneath deep mountain snowpacks because of the flow of heat from the ground, together with the insulating effect of the snowpack. Frozen ground will occur during winter or early spring, in areas where snowpacks are shallow and where prolonged periods of subfreezing air temperatures prevail. Snowmelt infiltration into a frozen soil is influenced by the thermal and hydrophysical properties of the soil, the soil temperature and moisture regime and the quantity and rate of release of water from the snowpack. If the depth of frost is small, the energy exchanged between the soil and the meltwater may thaw the entire frozen profile, returning the infiltration characteristics of the soil to those of the unfrozen state. Studies by Komarov and Makarova (1973 in Gray and Prowse, 1992) suggest that a soil frozen to a depth less than 150 mm behaves the same as an unfrozen soil, but once a soil is frozen to 600 mm depth, freezing to greater depth has no further effect on infiltration. The principle effects of frozen ground on the outflow hydrograph of the watershed are faster response with higher peak flow and greater volume in the total hydrograph.

## 2.6 Runoff from Snowmelt

Many of the snow processes described in the preceding systems have been incorporated into operational systems for forecasting catchment runoff. The manner in which the various models available for snowmelt simulate the processes

varies widely in complexity, from single variable indices of melt to complete energy balances. Each model is most reliable in the area were it was developed and may require extensive calibration when applied elsewhere. In 1986, the results of a comprehensive study undertaken by the World Meteorological Organization compared the performance of eleven models using data sets from six different regions (WMO, 1986). This numerical assessment provides useful information on effects of basin size, relative elevation range, percentage forest cover and other factors on model performance.

# CHAPTER 3


# HYDROLOGICAL MODELING AND CALIBRATION


## 3.1 Introduction

Conceptual hydrologic models that account for the continuous dynamics of hydrologic processes were introduced in the early 1960's. The Stanford Watershed Model (Crawford and Linsley, 1962 cited in Duan et al., 2003) was the first integrated attempt to take advantage of the advent of digital computers to describe quantitatively the hydrologic processes that take place in a watershed within the limitations of current understanding and the limitations of the computer.

The limitations of our hydrologic understanding and the limitations of the computer both have evolved since 1960's. Computing power has increased immensely, but it still may pose practical limits for hydrologic modeling and parameter estimation today. Yet, hydrologic understanding remains limited and imperfect in several ways. A great challenge in hydrology is to make predictions and test hypotheses at space and time scales of practical interest. In the end, it is not possible to resolve every detail of every aspect of the hydrology of the real world. So, effective hydrologic modeling is both the art and the science of applying limited and imperfect understanding.

These issues were well understood by Crawford and Linsley (1966 cited in Duan et al., 2003) who wrote:

"A hydrologic model is nothing more than a collection of quantitative hydrologic concepts that are given mathematical representations. If each of these concepts is a well established physical law that has an exact mathematical representation, and

if every physical component of the watershed is present in the model, the entire model structure would be unique and all physical processes in the watershed could be accurately simulated. Prohibitive amounts of input data would be required, far beyond practical limitations even for small watershed plots."

Since most of the action in hydrology occurs underground where it cannot be directly observed, this assessment remains valid today.

A plethora of hydrologic models have been proposed during the last few decades and many are being used for a variety of different applications. These models have been valuable tools for water management problems (e.g. flood forecasting, water balance studies, computation of design floods) whilst the increasing awareness of environmental problems has also given additional impetus to hydrological modeling (Seibert, 2003). Twenty-six of the world's most popular computer models of watershed hydrology were documented by Singh (1995). More recently Singh and Frevert (2002a, 2002b) put together a 2-volume book that gives a comprehensive account of 38 mathematical models of large and small watershed hydrology not included in Singh's (1995) book. Some notable models that have been widely used throughout the world include: the Tank model (Sugawa, 1995) that was a contemporary of SWM; the Sacramento model in the National Weather Service River Forecast System (Burnash, 1995); the Precipitation Runoff Modeling System (PRMS) developed by the United States Geological Survey (Leavesley and Stannard, 1995); the SHE model developed in Europe (Bathurst et al., 1995) and the HBV model developed in Sweden (Bergström, 1995).

The first comprehensive attempt to intercompare different hydrologic models was the World Meteorological Organization (WMO) hydrologic model intercomparison study (WMO, 1975). Subsequently, WMO led intercomparison studies of snowmelt models (WMO, 1986) and real-time applications of hydrologic models (WMO, 1992). Recently there has been a number of intercomparison studies of models used to represent the land surface in atmospheric models (Henderson-Sellers et al., 1993).

Every conceptual model has parameters that are the coefficients and exponents in the model equations. These parameters must be estimated for a given catchment and for each computational segment of the model. They must be estimated either by some relationship with physical characteristics or by tuning the parameters so that model response approximates observed response, a process known as calibration.

In this section of the thesis, one of the well known hydrologic models, HBV model, is introduced and a general calibration process framework is discussed.

## 3.2 HBV Model

The HBV model is a conceptual precipitation-runoff model which is used to simulate the runoff process in a catchment based on data for precipitation, air temperature and potential evapotranspiration. The model computes snow accumulation, snow melt, actual evapotranspiration, storage in soil moisture and groundwater and runoff from the catchment.

The HBV model was developed during the early 1970s by Dr. Sten Bergström and colleagues at the Hydrologiska Byrans Vattenbalansavdelning, HBV, (Hydrological Bureau Waterbalance section), a former section at the Swedish Meteorological and Hydrological Institute (SMHI). Today the HBV model concept is widespread. In different model versions HBV has been applied in some 45 countries with different climate conditions ranging in size from small research basins to the continental scale. The model is a standard method for hydrological forecasting in many countries, it is used for design studies as well as being a hydrological research tool. Lately, it has been used in water quality modeling, transport of nutrients and in studies of impacts due to global warming.

The main principles behind the HBV model are:

❋ The model must be based on a sound scientific foundation

❋ It must be possible to meet its data demands in most areas

❋ Its complexity must be justified by its performance

❋ It must be properly validated

❋ The user must be able to understand the model


## 3.2.1 Model Structure

The HBV model can be best classified as a semi-distributed conceptual model based on a representation of a few main components in the land phase of the hydrological cycle. It uses subbasins as primary hydrological units and within these, an area-elevation distribution and crude classification of land use is employed. The subbasin option is used in geographically or climatologically heterogeneous basins or in presence of large lakes. Runoff from a catchment is computed from climatic data like precipitation, air temperature and potential evapotranspiration. To accomplish this, the model computes water balance for the main storage types in the catchment and show how these storages change dynamically in response to the varying meteorological inputs. The normal time step is usually daily, though shorter time steps are available as an option. The HBV model consists of three main storage components shown in Figure 3.1.

❋ Snow Routine
❋ Soil Moisture Routine
❋ Runoff Response and Routing Routine

The model consists of a number of parameters grouped into two main categories named as confined and free parameters. Confined parameters are values that are provided to the model once and never changed (e.g. catchment area, area-elevation curve and lake percentage). Free parameters must be determined by a process of calibration of the model. Free parameters are normally determined

31

before the model is taken in operational use and later kept constant. The model, however, be recalibrated as more and better input data are collected form the catchment. The most important free parameters in the HBV model are listed in Table 3.1, together with their normal range and commonly used default values.
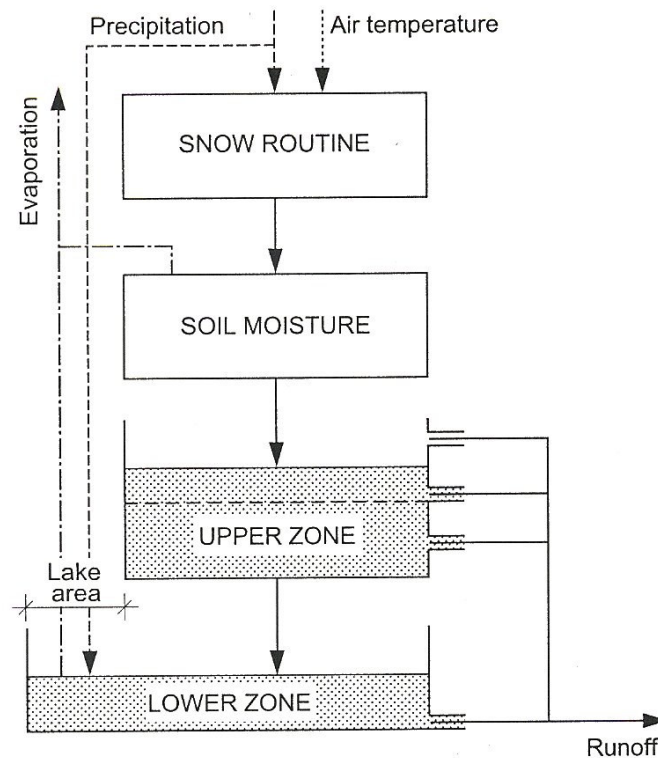


Figure 3.1 Main structure of the HBV-model (Killingtveit and Saelthun, 1995)

## 3.2.1.1 Catchment Description

The most important characteristics of the catchment are described by the following parameters in the HBV-model:

❋ The catchment area ($km^2$)

❋ Area of natural lakes ($km^2$)

❋ Area of regulated lakes ($km^2$)

❋ Area-elevation curve (hypsographic curve)

The catchment may be divided in as many as ten elevation levels. The area and average elevation of each level is used to construct the area-elevation curve.

Table 3.1 Free parameters in the HBV model

| Name | Meaning | Default value | Value range Min | Max | Units |
|------|---------|---------------|-----------------|-----|-------|
| Tx | Threshold temperature for rain/snow | 1.0 | -1.0 | 2.0 | °C |
| Ts | Threshold temperature for snowmelt | 0.0 | -1.0 | 2.0 | °C |
| Cx | Degree-day factor | 4.0 | 3.0 | 6.0 | mm/°C/day |
| LV | Liquid water content | 0.08 | 0.0 | 0.1 | --- |
| CFR | Refreezing efficiency in snow | 0.05 | 0.0 | 0.1 | --- |
| PKOR | Precipitation correction rainfall | 1.05 | 1.05 | 1.2 | --- |
| SKOR | Precipitation correction snowfall | 1.2 | 1.15 | 1.5 | --- |
| TTGD | Temperature lapse rate for clear days | - 0.6 | -1.0 | - 0.6 | °C/100 m |
| TVGD | Temperature lapse rate during precipitation | - 0.4 | - 0.6 | - 0.4 | °C/100 m |
| PGRD | Precipitation lapse rate | 0.05 | 0.0 | 0.1 | --- |
| FC | Field capacity in soil moisture zone | 150 | 75 | 300 | mm |
| LP | Threshold value for PET in soil moisture | 1.0 | 0.7 | 1.0 | frac. of FC |
| $\beta$ | Parameter in soil moisture routine | 2.0 | 1.0 | 4.0 | --- |
| KUZ2 | Fast recession constant in Upper zone | 0.3 | 0.1 | 0.5 | 1/day |
| UZ | Threshold level for quick runoff in Upper zone | 20 | 10 | 40 | mm |
| KUZ1 | Slow recession constant in Upper zone | 0.1 | 0.05 | 0.15 | 1/day |
| PERC | Percolation from Upper to Lower zone | 0.6 | 0.5 | 1.0 | mm/day |
| KLZ | Recession constant in Lower zone | 0.001 | 0.0005 | 0.002 | 1/day |

## 3.2.1.2 Snow Routine

The snow routine of the model, Figure 3.2, controls snow accumulation and snow melt and works separately for each elevation and vegetation zone. The precipitation is assumed to accumulate as snow when the air temperature drops below a threshold value ($T_x$). To account for undercatch of snow precipitation and winter evaporation, snow accumulation is adjusted by the snow correction factor. A temperature and precipitation lapse rate is provided according to elevation. Melt starts with temperatures above a threshold ($T_s$) according to a simple degree-day factor ($C_x$) which is assumed to remain constant throughout the melt season. The liquid water holding capacity of snow has to be exceeded before any runoff is generated (CPRO) and a refreezing coefficient is fixed in the model when snowmelt is interrupted (CFR).



P : Precipitation
$T_a$ : Air temperature, daily mean

Snow-melt SM = $C_x*(T_a-T_s)$
INSOIL > 0 when SW exceeds ST

$T_x$ : Threshold temp. rain/snow
$T_s$ : Threshold temp. snowmelt
$C_x$ : Degree-day factor
ST : Threshold = SN*CPRO
CPRO : Max. free water in snow

$T_a < T_x$
Snow

$T_a > T_x$
Rain

SN : Dry snow
$T_a > T_s$ : Snow melt $C_x \cdot (T_a-T_s)$
$T_a < T_s$ : Snow refreezing
$C_x \cdot$ CFR $(T_a -T_s)$

SW : Free water in snow   ST

INSOIL
To soil moisture zone
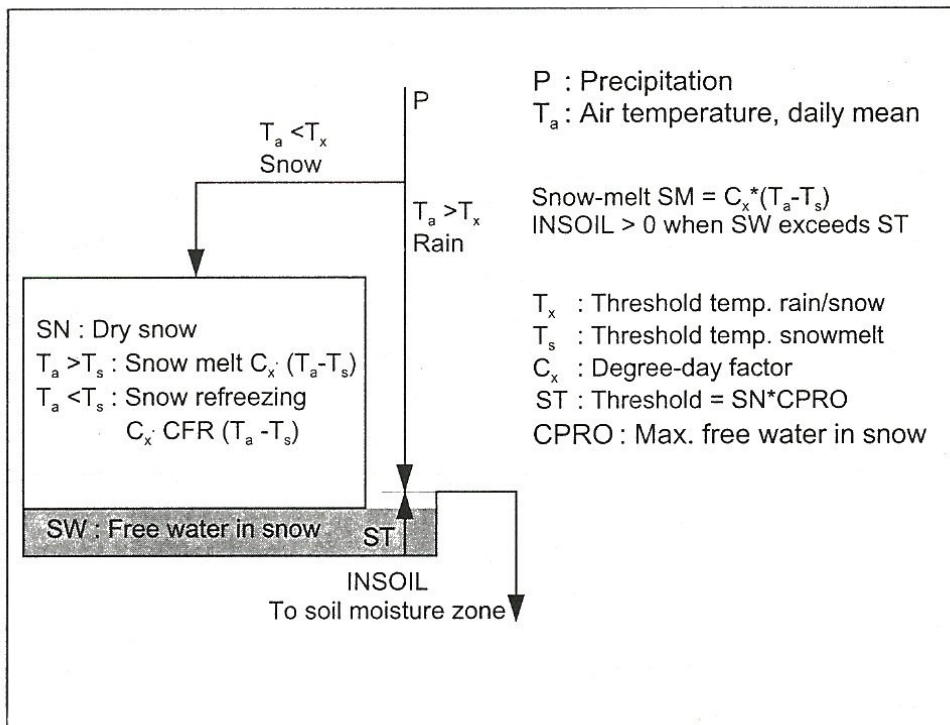
Figure 3.2 The snow routine in the HBV-model (Killingtveit and Saelthun, 1995)

By dividing the catchment into elevation zones the model is able to simulate the elevation dependent variability in snow storage, usually with higher precipitation and more snow at high elevations in the catchment than in the lower areas. This results in an elevation-dependent distributed snow storage in the catchment.

In addition to this elevation-dependent variation, there is another type of variation in snow storage that sometimes needs to be modeled. Within each elevation zone the snow cover will normally be unevenly distributed, mainly due to the effect of wind drift. In most implementations of the HBV model in Norway what is called a distributed snow-routine is used to simulate the effect of this uneven or skew distribution of snow within each elevation level. This computation is performed by distributing the snow storage within each elevation level using snow distribution curves.

The main results of the computations in the snow routine are the following three variables which are computed for each elevation zone and time step:
❋ Snow storage in mm of water equivalent
❋ Free (liquid) water contents in snow in mm
❋ Snow melt in mm/time step

## 3.2.1.3 Soil Moisture Routine

The soil moisture accounting of the HBV model is based on a modification of the bucket theory in that it assumes a statistical distribution of storage capacities in a basin.

The soil moisture routine receives rainfall or snowmelt as input from the snow routine and computes the storage of water in soil moisture, actual evapotranspiration and what may be called the net runoff generating precipitation as output to the runoff response routine.

The soil moisture routine is based on two simple equations with three empirical parameters, β, FC and LP as shown in Figure 3.3. The parameter β controls the contribution to the runoff response routine (dUZ) and the increase in soil moisture storage (dSM) for a precipitation or snow melt input of 1 mm into the soil moisture storage. The equation is non-linear if β is not equal to 1. Usually β has a value in the range 2-3, making the equation strongly non-linear.
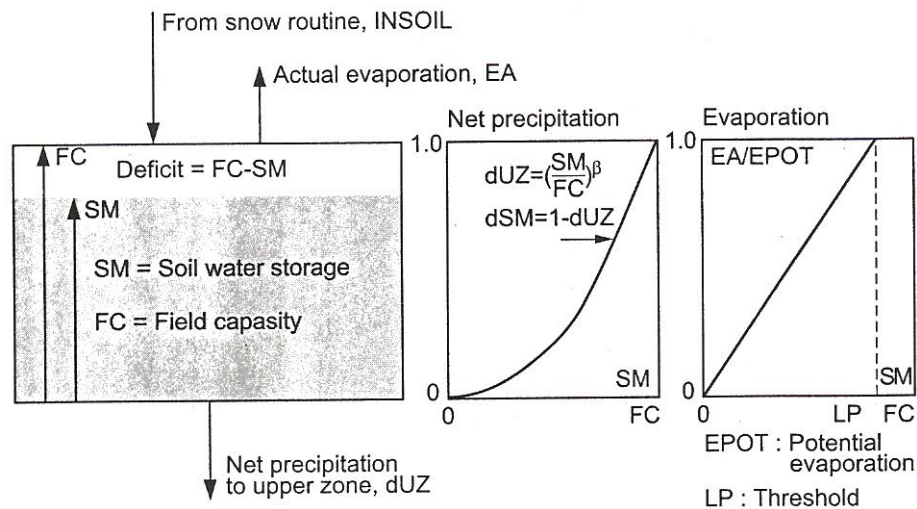


Figure 3.3 The soil moisture routine in the HBV-Model, (Killingtveit and Saelthun, 1995)

This structure results in a small percentage contribution to runoff (small net precipitation) when the soil moisture is low and a high contribution when the soil moisture is high. The Field Capacity (FC) is the maximum soil moisture storage in the model. If the soil moisture storage is filled up to FC, no more precipitation or snow melt can be stored as soil moisture and all input to soil moisture storage will be transformed directly to runoff. This may lead to high runoff even from moderate rain.

The soil moisture storage is depleted by evapotranspiration. The computation of actual evapotranspiration (EA) is a function of potential evapotranspiration (EP) and relative soil moisture storage (SM/FC). If the soil moisture exceeds a threshold

36

value (LP), the actual evapotranspiration equals the potential value. If soil moisture is below LP, the actual evapotranspiration decreases linearly with the decrease in storage as shown in Figure 3.3. Evapotranspiration in the model is only computed from the snow-free part of a catchment.

Both β, LP and FC are free parameters and must be determined by model calibration. They can not be determined directly from maps or field surveys. In some versions of the model an additional parameter controls the infiltration of water into the soil moisture routine. If the intensity of rainfall or snowmelt exceeds infiltration capacity the excess water is transferred directly to the runoff response function.

## 3.2.1.4 Runoff Response and Routing Routine

The runoff response routine transforms the net precipitation (excess water) produced in the soil moisture routine into runoff. The runoff response function in the HBV model consists of two linear tanks or reservoirs arranged as shown in Figure 3.4. This routine also includes the effect of direct precipitation on and evaporation from rivers and lakes in the catchment.

The two linear reservoirs called upper zone and lower zone delay the runoff in time and by choosing suitable values for the parameters the model can obtain both a quick response for high flows and slow response for low flows, as normally seen in observed hydrographs. The total combined flow from upper and lower zones can finally be filtered through a separate routine for river routing using a modified Muskingum method or simply for smoothing the flow with a triangular weighing function. The total effect of the runoff response function is very similar to the use of a unit hydrograph, transforming a sequence of net precipitation values into a runoff hydrograph.

The figure shows a schematic diagram with labels:

- Precipitation on lakes P
- From soilmoisture zone dUZ
- Lake evaporation EA=EPOT
- UPPER ZONE
- UZ, KUZ2 → Q12
- UZ2, KUZ1 → Q11
- UZ1
- KUZ → Q10
- Lake area
- PERC
- River/lake routing
- LOWER ZONE
- LZ, KLZ
- Q2, Runoff, Q
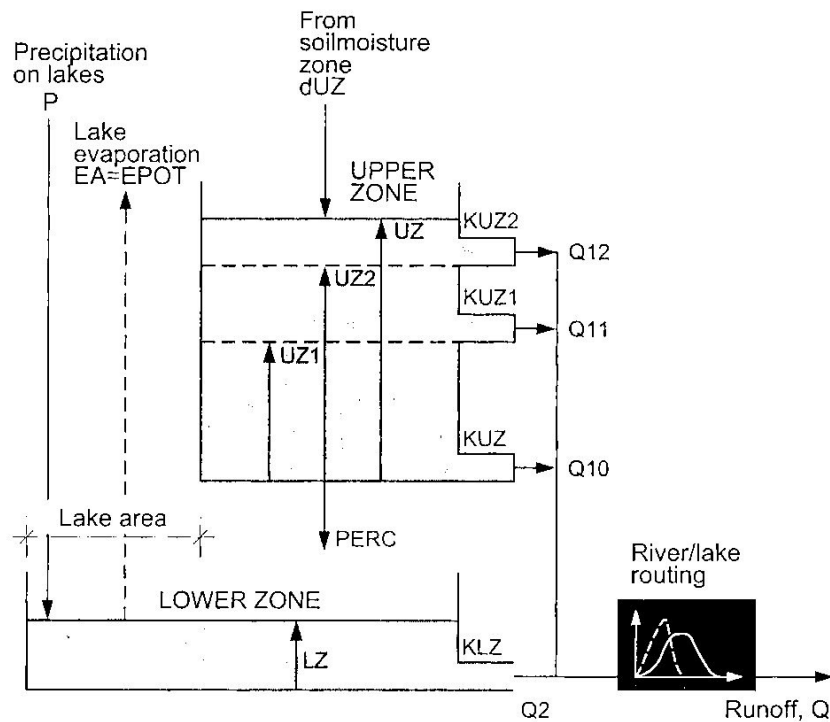
PARAMETERS IN THE RESPONSE FUNCTION :

KLZ   : Time constant, lower zone, 1/t
KUZ   : Time constant, upper zone, 1/t
KUZ1  : Time constant, upper zone, 1/t
KUZ2  : Time constant, upper zone, 1/t
UZ1   : Threshold for quick flow, mm
UZ2   : Threshold for very quick flow, mm
PERC  : Percolation to lower zone, mm/day

RUNOFF COMPONENTS :

$Q = Q10 + Q11 + Q12 + Q2$
$Q10 = MIN (UZ, UZ1)*KUZ$
$Q11 = MAX (0, ((MIN (UZ, UZ2) - UZ1)*KUZ1))$
$Q12 = MAX (0, (UZ - UZ2))*KUZ2$
$Q2 = KLZ*LZ$

Figure 3.4 The runoff response routine in the HBV-Model, (Killingtveit and Saelthun, 1995)

The upper zone conceptually represents the quick runoff components, both from overland flow and from groundwater drained through more superficial channels, interflow. When the input of net precipitation from soil moisture zone exceeds a percolation capacity (PERC), the storage in upper zone will start to fill and simultaneously be drained through the lower outlet. The speed of drainage is determined by the recession coefficient for the lower outlet (KUZ). If the storage exceeds a threshold (UZ1), an even quicker drainage will start through the upper outlet, the drainage speed controlled by the upper recession coefficient (KUZ1). In

some implementation of the model even an additional threshold and recession coefficient is used for still higher storage and quicker runoff components as shown in Figure 3.4. The combined effect of the upper zone is a variable response which can be adjusted to fit the observed quick runoff response in a catchment.

The lower zone conceptually represents the groundwater and lake storage that contributes to base flow in the catchment. The drainage speed is controlled by only one recession parameter (KLZ). The lower zone gets water input by percolation from upper zone and by direct precipitation on lakes and rivers. The lower zone is depleted through base flow runoff and also through evaporation from lakes and rivers. This evaporation always equals the potential as long as there is water in the lower zone storage.

## 3.2.1.5 HBV Model Calibration

Model calibration in this context means to determine the set of free parameters in the model that gives the best possible correspondance between observed and simulated runoff for a cathment. A general method for model calibration process is outlined in Figure 3.5.

The calibration of the HBV model is basically a trial and error procedure, where free parameters are chosen, model simulations are performed and the computed and observed runoff compared. The most difficult part of the procedure is the evaluation of the difference between observed and simulated runoff and to decide which parameter(s) should be changed and how much. To decide if another set of parameters really give better fit for the model, a method or criterion to determine the *goodness of fit* is needed. To test the goodness of fit in the HBV model, subjective and objective methods are utilized.
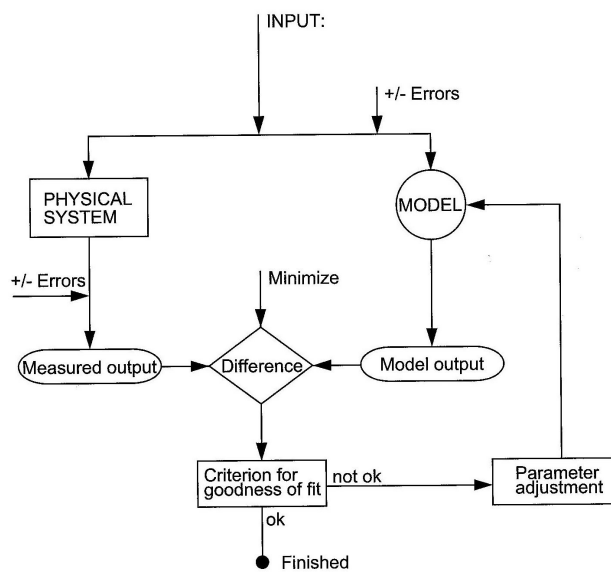
Figure 3.5 Model calibration process (Killingtveit and Saelthun, 1995)

The subjective method is usually based on study of plots of input data and observed and computed hydrographs as shown in Figure 3.6. A graph of the accumulated difference between the simulated and the recorded runoff reveals any volume bias in the water balance. Also scatter plots, flow duration curves and cumulative deviation curves may be used. A trained hydrologist can usually see how several parameters should be corrected from the study of observed and simulated runoff from one simulation. The subjective method is most efficient in the initial phase of model calibration, where several parameters need to be changed simultaneously. The use of objective methods is more appropriate during the "fine tuning" of the model where parameters are close to their optimal value. It is then difficult to see from the plots if the model has been improved by a slight change in parameter values.

To judge the model performance when using an objective method, a statistical criterion, normally the $R^2$-value according to Nash and Sutcliffe (1970) is employed as given in Equation 3.1.
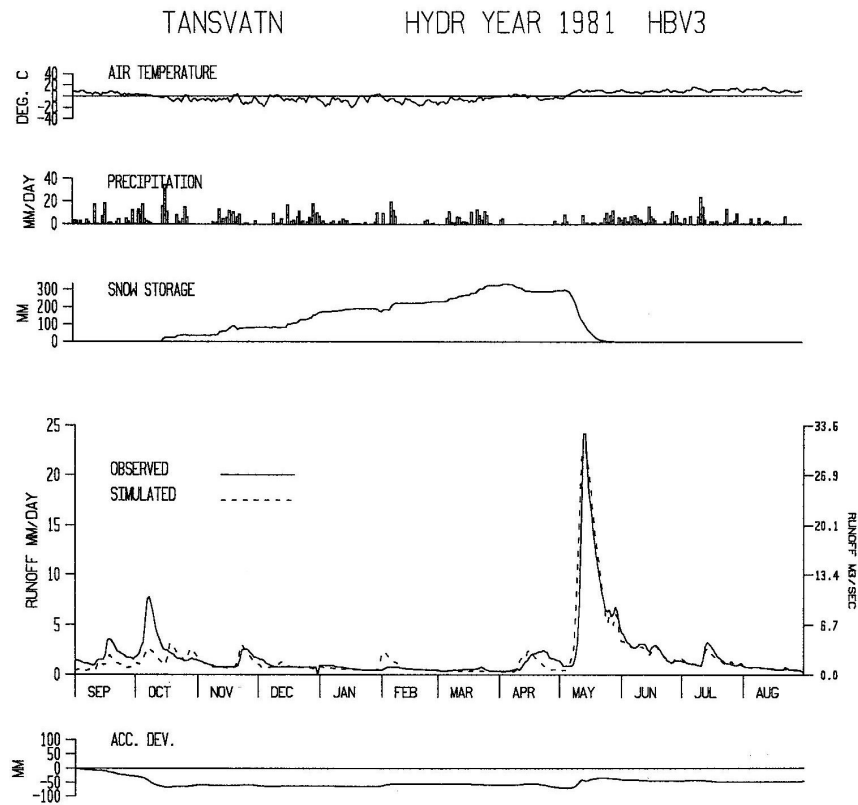
Figure 3.6 An example of a simulation output based on the HBV-model (Killingtveit and Saelthun, 1995)

$$R^2 = 1 - \frac{\sum (Q_{obs} - Q_{sim})^2}{\sum (Q_{obs} - \overline{Q_{obs}})^2}$$

Equation 3.1

where  $Q_{obs}$ = observed runoff

     $\overline{Q_{obs}}$ = mean of observed runoff

     $Q_{sim}$ = simulated runoff

$R^2$, often termed as the model efficiency criterion, varies from $-\infty$ to $+1.0$, the higher the value the better the model fit. $R^2$ has a value of 1.0, if the simulation and observation values agree completely and 0 if the model does not perform any better than the mean value of the recorded runoff. Negative values can be result of poor model performance or poor data. Normal values during HBV model calibrations are within the range 0.6-0.9.

Once the error functions are selected, the best (optimal) set of parameters may be found by systematically varying models parameters and computing the error functions for each parameter set. It is possible to search for and locate the optimal parameter set by different strategies, based on manual or automatic searching methods.

When the model has been optimally fitted to the observed data either by manual or automatic calibration, the goodness of fit should be tested (validated) on an independent set of data. This is often referred to as a split sample test.

## 3.3 Hydrologic Model Calibration

The increasing use of hydrologic models as tools for the study of hydroclimatology has prompted hydrologists and climatologists to examine complex problems and utilize new data sources. Hydrologic models, however, are only as reliable as their structure and the accuracy of their inputs and parameter estimates. While they are often mathematical in their structure, for reasons of parsimony and mathematical tractability, they must remain simple while being able to accurately simulate and predict complex hydrological phenomena. It is often assumed that the model structure is correct (even though this assumption can be questionable) and to devote much attention to model inputs and parameter estimates (Yapo, 1996).

Various techniques exist by which parameter estimates can be deduced: (a) field measurements, (b) prior information and (c) calibration. For as much as it is desirable to infer model parameters using (a) and (b) as witnessed by the gaining importance of the former, virtually all models require that some parameters be calibrated.

Hydrological model calibration is the process by which some or all parameters of a model are systematically adjusted in order to provide model outputs that closely resemble the observed data. The goal of calibration is to reduce the uncertainty

associated with the model parameters. (Maximum uncertainty is when parameters are assigned their initial range, whereas minimum uncertainty is when a single parameter set of values is found). Depending on the techniques used to infer parameter estimates, calibration can be separated into manual and automatic calibration.

## 3.3.1 Manual Calibration

Manual calibration is a procedure in which various subjective adjustments to model parameters, usually one at a time, are made on the basis of specific characteristics of the modeled output. Evaluation of model parameters by manual calibration can yield a good set of estimates. The method is, however, a tedious and time consuming task, depending on the number of free parameters and the degree of parameter interaction. In addition, subjective adjustments of parameters make the success of manual calibration user-dependent. In fact the user must possess a significant level of experience with the model to achieve good parameters. Besides the subjectivity of the method, it is possible that, on separate occasions, a single user can obtain different sets of acceptable parameters because of changing experience with the model or because of the order in which some parameters are estimated. Although these parameters may be different, they still provide similar output results. Due to the subjectivity involved, it is difficult to explicitly assess the confidence of the model simulations.

Perhaps the best argument for the use of manual calibration is that the user gains experience with the model and valuable insights into parameter interaction and sensitivity. Manual calibration is often used for initialization of model parameters including initial ranges and starting values.

### 3.3.2 Automatic Calibration

Automatic calibration consists of techniques in which the computer adjusts parameters in a rule-based fashion using a single objective function. The implementation of an automatic model calibration procedure requires the selection of (a) a calibration data set, (b) a goodness-of-fit measure (objective function), (c) an automatic parameter search procedure (optimization algorithm), (d) a region of the parameter to be searched (feasible parameter space), (e) a validation procedure (tests to determine the degree of uncertainty remaining in the model).

The main advantages of automatic calibration are its speed and ease of use. With the availability of fast and powerful computers automatic calibration has gained in importance as witnessed by the multitude of computer optimization algorithms. Automatic calibration can be viewed as an objective tool which even a novice can use because the user is not required to intervene during the search for the best parameter set.

The main disadvantages of automatic calibration are its dependence on a single objective function to direct the search for the best parameter and failure to obtain a unique global optimum. Another disadvantage is that, without the proper selection of an objective function, automatic calibration can degenerate to pure curve fitting. Thus, there appears to be a need for methods to infuse hydrological reasoning into the automatic calibration process.

In recent years, application of automatic calibration routines in hydrological modeling has advanced considerably. The routines, however, has evolved in various directions in different application areas. For parameter estimation in groundwater modeling, gradient-based local search techniques have mainly been applied (e.g. McLaughlin and Townley, 1996). In lumped, conceptual hydrological models, population-evolution-based global optimization methods, such as the shuffled complex evolution algorithm (Duan et al., 1992), have shown to be more efficient. Application of automatic calibration in complex, integrated and distributed

44

hydrological catchment models is an ongoing research area with limited experience.

### 3.3.3 Formulation of Calibration Framework

The process of model calibration is illustrated in Figure 3.7 (Madsen and Jacobsen, 2001). In automatic calibration, parameters are adjusted automatically according to a specific search scheme for optimization of certain calibration criteria (objective functions) that measure the goodness-of-fit of the simulation model. The process is repeated until a specified stopping criterion is satisfied, e.g. maximum number of model evaluations, convergence of the objective function or convergence of the parameter set.
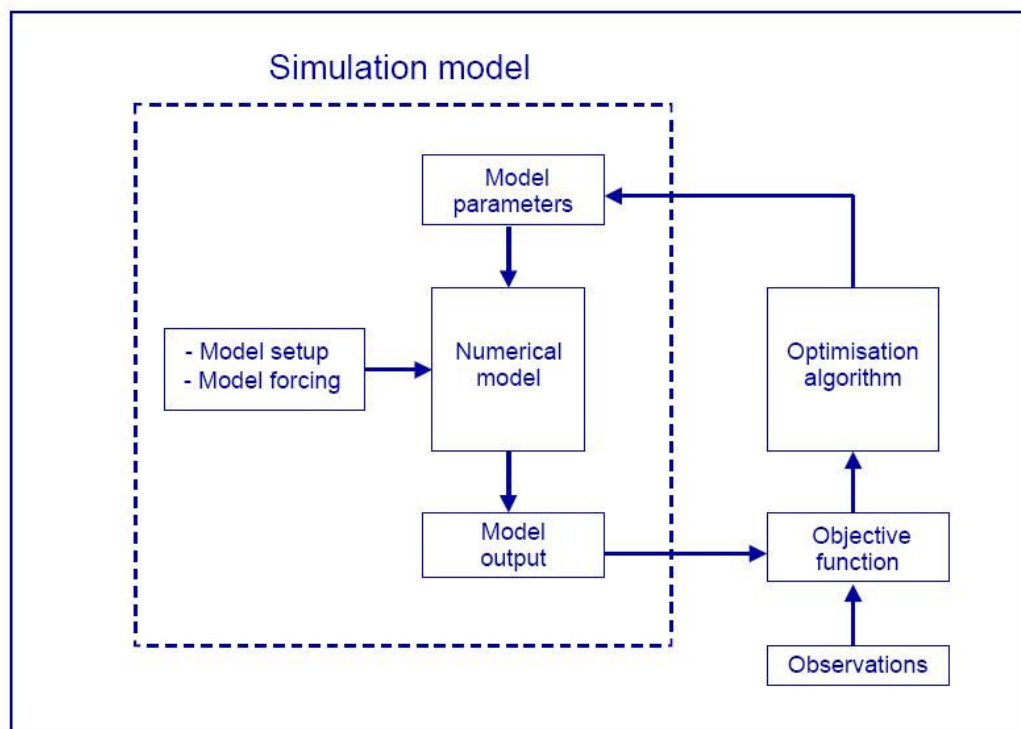


Figure 3.7 Outline of automatic calibration scheme, interfacing an optimization algorithm with the simulation model (Madsen and Jacobsen, 2001)

Formulation of a proper framework for automatic calibration involves the following key elements:

❊ Model parameterization and choice of calibration parameters
❊ Specification of calibration criteria
❊ Choice of optimization algorithm

## 3.3.3.1 Model Parameterization and Choice of Calibration Parameters

A semi-distributed hydrological modeling system potentially involves a large number of model parameters to be specified by the user during the model setup. Comprehensive field data, however, are seldomly available to fully support specification of all model parameters. In addition, some model parameters are of a more conceptual nature and cannot be directly assessed from field data.

In the model parameterization, the available field data should be used to define the spatial patterns of the parameter values to describe the most significant variations. This is often done by defining a conceptual model with appropriate parameter classes of geological units, soil types, vegetation types etc. For each class, some parameters are then assessed directly from field data while other parameters may be subject to calibration. The challenge is to formulate a relatively simple model parameterization in order to provide a well-posed calibration problem but at the same time keep it sufficiently complex in order to capture the spatial variability of key model parameters. The importance of a rigorous model parameterization for calibration of distributed hydrological models was emphasized by Refsgaard (1997). This aspect becomes even more important when automatic procedures are applied for parameter estimation.

Sensitivity analysis can be conducted to investigate which parameters can be considered to be well determined (sensitive) and which are poorly determined

(insensitive) with respect to the available observations. In Hill (1998), dimensionless, scaled sensitivities are used which measure the change in simulated values with respect to each of the parameters. Spear and Hornberger (1980) introduced a generalized sensitivity analysis procedure based on Monte Carlo sampling where a number of randomly generated parameter sets is evaluated and compared. Sensitivity analysis can be used in the initial model parameterization process to decide which parameters are insensitive and can be set to fixed values. The results of such an analysis, however, should be carefully interpreted. The dimensionless, scaled sensitivities in Hill (1998) depends on the parameter values, and hence sensitivity statistics evaluated at some initial parameter values may be very different from the statistics obtained using other parameter sets. In addition, sensitivity statistics do not properly account for parameter correlations, implying that parameters that seem to be insensitive may have important correlations with other parameters that are essential for the model behavior (Madsen, 2000b)

It should be noted that model parameterization and model calibration is an iterative process. If the calibration results in poorly defined parameter values, one should reconsider the model parameterization and define a simpler conceptual model that includes fewer calibration parameters. On the other hand, if the model is not able to sufficiently describe the spatial variability reflected in the observations, one should consider distributing key model parameters or including other process descriptions in the calibration.

### 3.3.3.2 Specification of Calibration Criteria

The automatic calibration scheme involves optimization of numerical measures (objective functions) that compare observations of the state of the system with corresponding simulated values. For hydrological model calibration river runoff or water level data are the most available measurements. In other cases, groundwater level data, water content in the unsaturated zone, snow covered area and snow water equivalent (snowpack) can also be used. In this respect, it is

important to note that for a proper evaluation of the validity of a catchment model, distributed data rather than just catchment-integrated values such as river runoff are necessary for calibration. In addition, parameters are usually better determined (more sensitive) when new types of field data are used for calibration rather than adding more data of the same variable.

If $F(\theta)$ is denoted as an objective function that measures the goodness-of-fit of the simulated model with respect to the parameter set $\theta$, the optimal parameter set $\theta_{opt}$ is found by solving the optimization problem

$$\theta_{opt} = \text{Min} \left\{ F(\theta) \right\}, \theta \in \Theta \qquad \text{Equation 3.2}$$

In this case the optimization problem is constrained in the sense that $\theta$ is restricted to the feasible parameter space $\Theta$. The parameter space is usually defined as a hypercube by specifying lower and upper limits on each parameter. These limits are chosen according to physical and mathematical constraints, information about physical characteristics of the system, and from modeling experiences. The feasible parameter space can also be defined as a hyperellipsoid by using prior knowledge about the correlation between the different parameters (Kuczera, 1997).

Automatic calibration can also be defined as an unconstrained optimization problem. In this case, prior information about the parameters can be used by adding a penalty term in the objective function that measures the departure of the parameters from their prior estimates (e.g. Hill, 1998).

The most commonly used objective function adopted in automatic optimization is the sum of squared errors between the observed and simulated model response. Calibration based on a single performance measure, however, is often inadequate to properly measure the simulation of all the important characteristics of the system that are reflected in the observations. Recently, automatic procedures have

been developed that allow a simultaneous optimization of a number of different calibration objectives (Gupta et al., 1998; Madsen, 2000a).

In a multi-objective context, model calibration can, in general, be performed on the basis of:

* Multi-variable measurements, i.e. groundwater level, river runoff and other types of measurements.
* Multi-site measurements, i.e. several groundwater level and runoff measurement sites distributed within the catchment.
* Multi-response modes, i.e. objective functions that measure various responses of the hydrological processes such as the general water balance, peak flows, and low flows.

When using multiple objectives, the calibration problem can be stated as follows:

$$\text{Min} \left\{ F_1 (\theta) , F_2 (\theta) , ...., F_m (\theta) \right\} , \ \theta \in \Theta \qquad \text{Equation 3.3}$$

where $F_i(\theta)$, i = 1, 2,.., m are the different objective functions. The solution of Equation 3.3 will not, in general, be a single unique set of parameters but will consist of the so called Pareto set of solutions (non-dominated solutions), according to various trade-offs between the different objectives. The definition of the Pareto front is illustrated in Figure 3.8 in the simple case of two objectives $F_1$ and $F_2$. Points on the Pareto front have the characteristics that no other points have both a smaller value of $F_1$ and a smaller value of $F_2$ (illustrated for point B in Figure 3.8 where no points exist in the hatched rectangle). When moving along the Pareto front from A to C results in successively smaller values of $F_2$ at the expense of larger values of $F_1$.
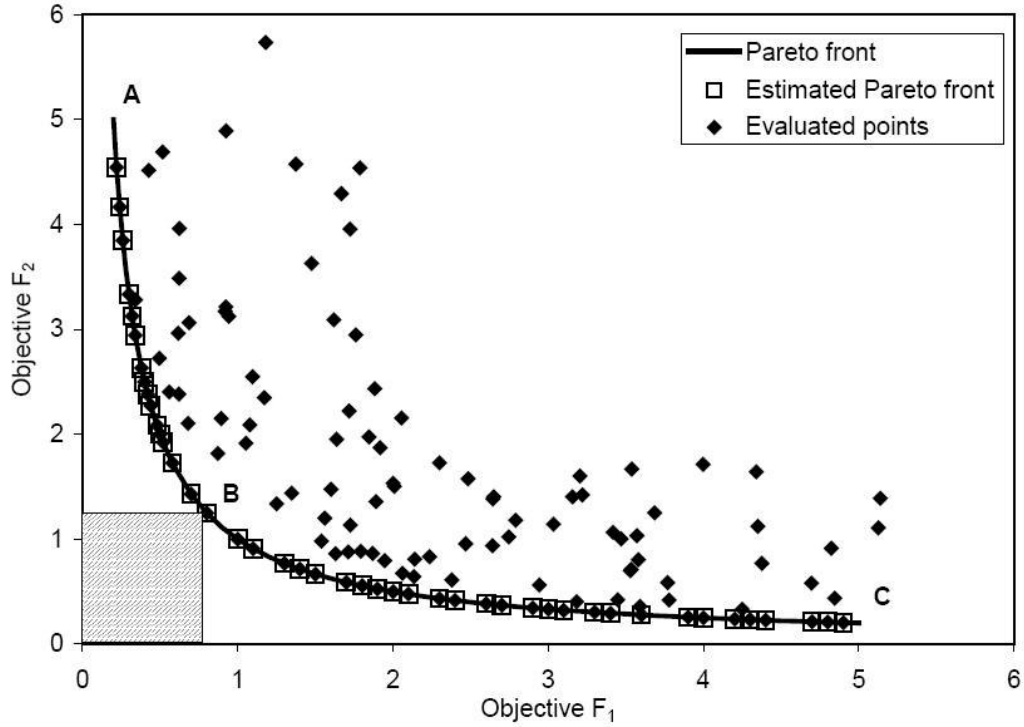
Figure 3.8 Definition of Pareto front for optimization of two objectives

When solving the multi-objective calibration problem, the problem is usually transformed into a single-objective optimization problem by defining a scalar that aggregates the various objective functions. One such aggregate measure is the weighted average

$$F_{agg}(\theta) = \sum_{i=1}^{m} w_i F_i(\theta) \quad , \quad \sum_{i=1}^{m} w_i = 1 \qquad \text{Equation 3.4}$$

where $w_i$ are weights assigned to the different objectives. For investigating the entire Pareto front, the aggregated measure can be adopted by performing several optimization runs using different values of $w_i$.

In practical applications, the entire Pareto set may be computationally too expensive to calculate, and one is only interested in part of the Pareto optimal solutions. In this case, the user can specify the weights to reflect the relative

priorities given to certain objectives, depending on the specific model application being considered. Furthermore, the weights should also reflect the measurement errors, i.e. smaller weights are given to measurements with larger errors. The selection of weights, however, is not straightforward, since the priority also depends on the value of $F_i$ itself. For instance, if all $w_i$ are equal, implicitly larger weights are given to objectives with larger F-values. A proper scaling of the objective functions in the aggregated measure can be defined as

$$F_{agg}(\theta) = \sum_{i=1}^{m} w_i \, g_i \left(F_i(\theta)\right) \quad , \quad \sum_{i=1}^{m} w_i = 1 \qquad \text{Equation 3.5}$$

where $g_i$ are functions that transform the different objectives to a common scale. When using a population-based optimization algorithm, an initial population within the feasible region is evaluated. From this initial population, the transformation functions can be evaluated. Madsen (2000a) used an Euclidian distance function in which all the objective functions are transformed to having about the same distance to the origin near the optimum. Van Griensven and Bauwens (2001) adopted a probability distribution function for $F_i$ for transformation of the objective functions into a probability scale.

### 3.3.3.3 Choice of Optimization Algorithm

Optimization algorithms can, in general, be categorized as "local" and "global" search methods (Sorooshian and Gupta, 1995). Depending on the hill climbing strategy employed, local search algorithms may be further divided into "direct" and "gradient-based" methods. Direct search methods use only information on the objective function value, whereas gradient-based methods also use information about the gradient of the objective function. Local search methods are efficient for locating the optimum of a uni-modal function since in this case the hill climbing search will eventually reach the global optimum, irrespective of the starting point. One of the more popular direct search methods is the simplex method (Nelder and

Mead, 1965). Gradient-based methods include the steepest descent method and various approximations of the Newton method (e.g. the Gauss–Marquardt algorithm).

Numerical simulation models may have numerous local optima on the objective function surface, and in such cases local search methods are less effective because the estimated optimum will depend on the starting point of the search. For such multi-modal objective functions global search methods are more effective ("global" in the sense that these algorithms are especially designed for locating the global optimum and not being trapped in local optima). Popular global search methods are the so-called population-evolution-based search strategies such as the shuffled complex evolution (SCE) algorithm (Duan et al., 1992) and genetic algorithms (GA) (Wang, 1991).

For calibration of lumped, conceptual hydrological catchment models a large number of studies have been conducted that compare different automatic algorithms (e.g. Duan et al., 1992; Gan and Biftu, 1996; Cooper et al., 1997; Kuzcera, 1997; Franchini et al., 1998; Thyer et al., 1999). The main conclusion from these studies is that the global population-evolution-based algorithms are more effective than multi-start local search procedures, which in turn perform better than pure local search methods.

### 3.3.4 Multi-Objective Calibration Problem

Previous research has focused extensively on the proper selection of an objective function for calibration of hydrological models. The development of an objective function is typically based on assumptions regarding the distributions of measurement errors present in the data. In general, these functions can be summarized by a weighted least square (WLS) of the following mathematical form (Troutman, 1985):

$$WLS = \frac{1}{n} \sum_{t=1}^{n} w_t \left| q_t^{obs} - q_t^{sim}(\theta) \right|^{\xi} \qquad \text{Equation 3.6}$$

where $q_t^{obs}$ and $q_t^{sim}(\theta)$ are the observed and model response at time t, respectively and n is the number of observations. The model response is dependent on parameters $\theta$ and exogenous inputs for hydrologic models include rainfall or temperature measurements. The WLS function scales and weights the difference between observed and modeled response, the prediction error $e_t = q_t^{obs} - q_t^{sim}(\theta)$ by constant factors $\xi$ and $w_t$, respectively. Depending of the values for $\xi$ and $w_t$ and assumption regarding the distribution of the prediction error, Equation 3.6 corresponds to the Maximum Likelihood Estimator (MLE). For example, when all the constants are set to unity ($\xi = 1$ and $w_t = 1$), Equation 3.6 reduces to Mean Absolute Error (MAE) and corresponds to the MLE for independent and identically uniform distributed errors. For $\xi = 2$ and $w_t=1$, WLS becomes the well-known Simple Least Square (SLS), where errors are assumed to be normally distributed with zero mean and constant variance, i.e. $e_t \sim N(0, \sigma^2)$. For cases where the weights are different than unity, their correct form can be deduced via maximum likelihood theory. The Autocorrelated Maximum Likelihood Estimator (AMLE) and Heteroscedastic Maximum Likelihood Estimator (HMLE) developed by Sorooshian and Dracup (1980) are examples where $\xi = 2$ and correspond to gaussian errors. AMLE assumes correlated errors ($e_t = a * e_{t-1} + e_t$), while HMLE assumes that the errors have unequal variances.

Choosing the proper objective for calibration can be difficult. The selection of an objective function requires prior knowledge or some assumption of the type of distribution present in the measurement errors associated with the data. For that reason, it is highly recommended that, for any calibration, results should be validated by residual analysis in order to verify the assumptions made with the use of a specific objective function. For example, the performances of two objective functions were carefully examined by Yapo et al. (1996). The objectives were: (a) Daily Root Mean Square (DRMS = $\sqrt{SLS/n}$) objective function and (b) HMLE

objective function. Using DRMS as objective resulted in better matching of high flow events and HMLE provided better results on low flow events. Therefore it was concluded that neither DRMS nor HMLE was superior but, depending on the intended purpose of the model either objective function could be used for calibration.

Model calibration requires the usage of an objective function where the goal is to determine a parameter set which minimizes the errors between observed and model outputs. Two fundamentally different ways exist to improve the closeness of model outputs to the observed data. (1) Each error can be minimized independently but simultaneously, (2) the errors can be aggregated under different functional relationship (e.g. weighted sum or weighted product) to account for specific characteristics present in the errors. In general, the second option is adopted because of its feasibility and mathematical attractiveness.

The calibration of hydrologic model is inherently a multi-objective problem because several objective functions can be used in matching different portions of the hydrographs or matching multiple outputs. The goal of multi-objective programming (MOP) is to seek non-dominant, efficient or Pareto solutions. Pareto solutions represent tradeoffs among different objective functions; as one moves from one non-dominant solution to another, one objective function improves whereas the other objective function(s) must decrease in value.

## 3.3.5 Reflections on the Future of Model Calibration

A problem in hydrological modeling is the great number of parameters and the risk for compensating errors. The fact that many, quite different, parameter sets can produce almost equally good agreement with observations is referred to as "model equifinality" (Beven 1993, 2001). Two 'ways forward' on the equifinality issue include: (1) making more detailed use out of the comparison between simulated

and observed runoff series or (2) incorporating additional data into the model calibration procedure (Seibert, 2003).

The need to utilize additional endogenous data such as, snow covered area, snow reservoir, evapotranspiration, soil moisture, groundwater levels, water quality or even qualitative information, for model calibration and testing has been emphasized by others in the recent years as one remedy to the problem (Kuczera, 1983; Hooper et al., 1988; de Grosbois et al., 1988; Ambroise et al., 1995; Rafsgaard, 1997; Kuczera and Mroczkowski, 1998; Seibert, 2000; Bergström, 2002; Seibert, 2003; Alfnes et al., 2005). Testing models against variables other than simply catchment outlet runoff is important for two main reasons:

1. in many hydrological questions and for other sciences as well such as ecology, it may be of much more interest to know what happens within a catchment than at the outlet alone,
2. to have confidence in model predictions, which are sometimes extrapolations beyond the testable conditions, it must be ensured that the model not only works but also does for the right reason.

In this sense multi-criteria application would be the most straightforward method to calibrate the model and in doing so, a small compromise in terms of runoff simulation may lead to better simulations on the other output variables. This can lead not only to improved parameter estimates but to better understanding of limitations of our models because different sets of parameter values may be needed to match different sets of observed data. Although some special measurements may only be available for brief periods during special research projects, others may become available routinely, especially from satellite remote sensing.

Generally, a large number of model parameters need to be specified in conceptual runoff models. Reducing the number of parameters is an unattractive option because it might transform the gray-box representation of the precipitation-runoff

process into a pure black-box description. Another more attractive way to reduce parameter uncertainty is the use of additional data. However, the worth of additional data varies depending on the kind of data, but also on the structure of the applied model.

To conclude, the use of multi-criteria calibration may not be the only solution to the problem of non-uniqueness of model parameters. The comparison of model results to more information than only runoff does, however, lead to increased confidence in the physical relevance of the model and provides new insight for further realistic conceptual model development.

# CHAPTER 4

# FIELD SITE AND INSTRUMENTATION

## 4.1 Introduction

Water perhaps is the most valuable natural asset in the Middle East as it was a historical key for settlement and survival. The Euphrates and Tigris rivers with their tributaries served as the cradle for many civilizations that evolved in Mesopotamia, "the land between two rivers". The Euphrates and Tigris rivers are the two largest trans-boundary rivers in Western Asia that are linked by their natural course where after named as Shatt-al-Arab, forming a river almost a kilometer wide and drain into the Persian Gulf. The riparian countries sharing the Euphrates-Tigris basin are Turkey, Syria, Iran, Iraq and Saudi Arabia as shown in Figure 4.1. The surface area that each country contributes is given in Table 4.1 (UNEP, 2001) and the estimates of mean annual natural runoff of the Euphrates and Tigris rivers are presented in Table 4.2 (Altınbilek, 2004).

Turkey is contributing a surface area of around 21.1% for the Euphrates basin and 14.3% for the Tigris basin even though an overwhelming 98% of Euphrates runoff is produced in the highlands of Turkey as compared to an estimated 53% of the discharge of the Tigris. On the overall, Turkey contributes 71.4% of the Euphrates and Tigris basin's combined natural flow.
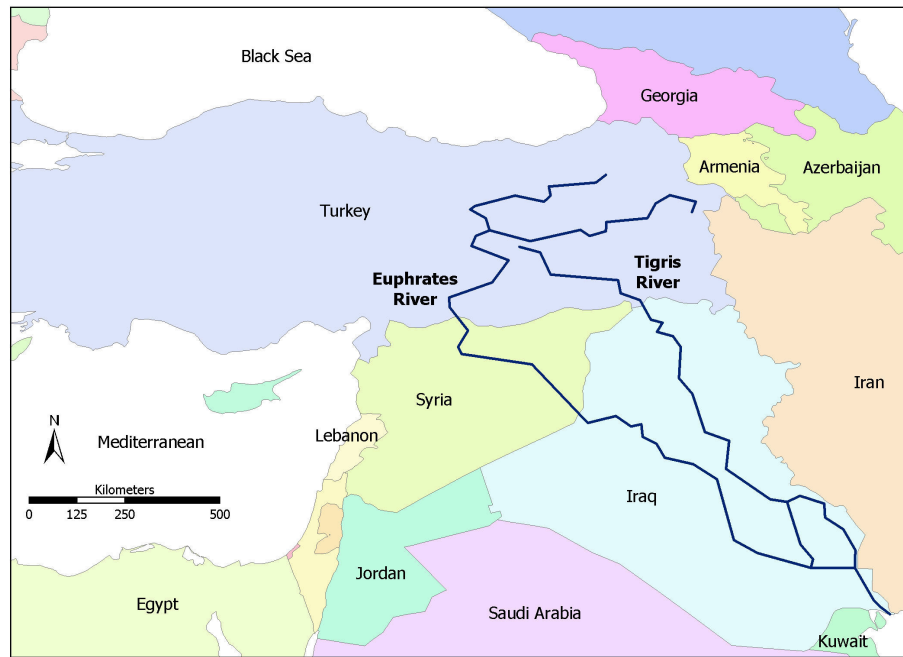
Figure 4.1 Euphrates and Tigris rivers

Table 4.1 Area of the Euphrates-Tigris drainage basin in riparian countries (UNEP, 2001)

| Country | Euphrates Basin | | Tigris Basin | |
|---|---|---|---|---|
| | km$^2$ | % | km$^2$ | % |
| Turkey | 121 787 | 21.1 | 53 052 | 14.3 |
| Syria | 95 405 | 16.5 | 948 | 0.2 |
| Iran | --- | --- | 175 386 | 47.2 |
| Iraq | 282 532 | 49.0 | 142 175 | 38.3 |
| Saudi Arabia | 77 090 | 13.4 | --- | --- |
| Total | 576 814 | 100.0 | 371 561 | 100.0 |

Table 4.2 Contribution of the riparian states to the Euphrates-Tigris basin (km$^3$/yr) (excluding river Karun) (Altınbilek, 2004)

| Country | Euphrates Basin | | Tigris Basin | |
|---|---|---|---|---|
| | km$^2$ | % | km$^2$ | % |
| Turkey | 121 787 | 21.1 | 53 052 | 14.3 |
| Syria | 95 405 | 16.5 | 948 | 0.2 |
| Iran | --- | --- | 175 386 | 47.2 |
| Iraq | 282 532 | 49.0 | 142 175 | 38.3 |
| Saudi Arabia | 77 090 | 13.4 | --- | --- |
| Total | 576 814 | 100.0 | 371 561 | 100.0 |

The characteristic feature that distinguishes the hydrologic regime of the Euphrates-Tigris river system is the irregularity of flow both between and within years, with large floods originating from the snowmelt in spring. About two-thirds of the precipitation occur in winter and may remain in the form of snow for half of the year. With the beginning of snowmelt in spring, the concentration of discharge over the months of March through June causes not only extensive flooding, inundating large areas, but also the loss of much needed water required for irrigation and power generation purposes during the summer season.

Accordingly, the importance of monitoring and modeling the areal snow cover cycle in the mountainous regions of Eastern Turkey, as being one of the major headwaters of Euphrates-Tigris basin, is crucial from water resources management point of view.

## 4.2 Area of Study

Within the borders of Turkey, the Euphrates river is formed by the union of two major tributaries at the mountainous Eastern Anatolia: the Karasu river which rises in the northeast highlands (elevation 2744 m) of the city of Erzurum and the Murat river which originates from the mountains (elevation 3135 m) surrounding the city of Ağrı. Keban dam is at the junction of these two tributaries and it the first major dam on the Euphrates River followed by Karakaya, Atatürk, Birecik and Karkamış dams respectively until the Syrian border.

Karasu basin, a subbasin of the Euphrates River, is selected as the representative pilot basin to monitor and model the snow cover cycle in Eastern Anatolia as shown in Figure 4.2. The main reasons for the selection of Karasu basin are its easier accessibility, better security and the high level of assistance received from the regional offices of the governmental organizations. Karasu basin outlet is controlled by the stream gauging station EIE 2119 under the supervision of General Directorate of Electrical Power Resources Survey and Development

Administration (EIE) in Turkey. The total catchment area is about 10,216 km$^2$ and the elevation ranges between 1125 m and 3487 m a.s.l. When the long-term runoff hydrographs at the EIE 2119 stream gauging station is analyzed, it can be seen that around 69% of total annual volume contribute to the flow during the snowmelt period of mid March through mid July (Kaya, 1999; Tekeli, 2005). This high percentage of snowmelt runoff indicates the necessity of accurate snowmelt runoff prediction in rate, volume and timing.
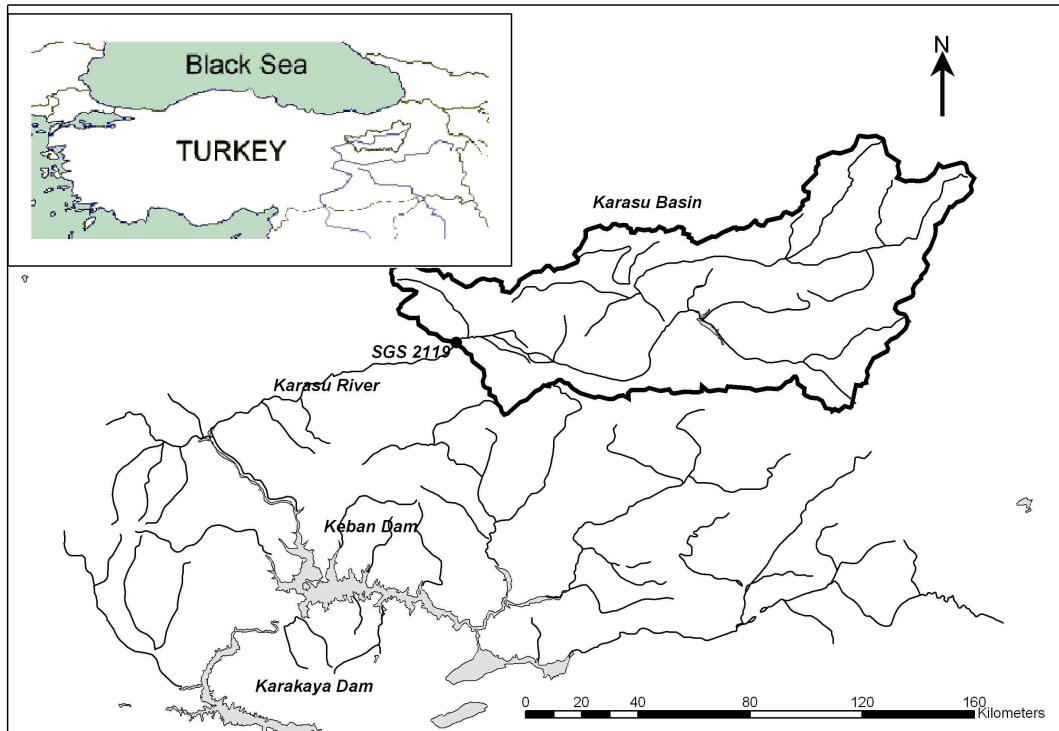


Figure 4.2 Location of Karasu basin in Turkey

Karasu basin is further divided into two smaller basins in order to simulate the snowmelt-runoff at different scales. The first of these is the basin with the outlet EIE 2154 again under the supervision of General Directorate of Electrical Power Resources Survey and Development Administration (EIE) (where more details can be found in Şensoy, 2005) with an area of 2818 km$^2$ and the other is the basin with the outlet DSI 21-01 under the supervision of General Directorate of State Hydraulic Works having an area of 242 km$^2$. The main focus in this thesis will be on the latter basin which will be named as the Kırkgöze basin from now on and will be discussed in detail in Chapter 6.

The seasonal snow cover in the region begins to accumulate in late November or early December. During winter nearly all precipitation falls as snow and partial areal precipitation events are common in the catchment. During spring and early summer, mixed rain/snow events occur. The climatic characteristics give rise to a typical hydrological regime: low flows generally prevail over the winter, while most incident precipitation accumulates as snow. This is followed by a sustained period of high flows during the spring resulting from melting of the winter snowpack. Flow generally declines after snow disappears from the catchment in early summer. Snow covered area of Turkey within the global framework of Northern Hemisphere can be seen in Figure 4.3.
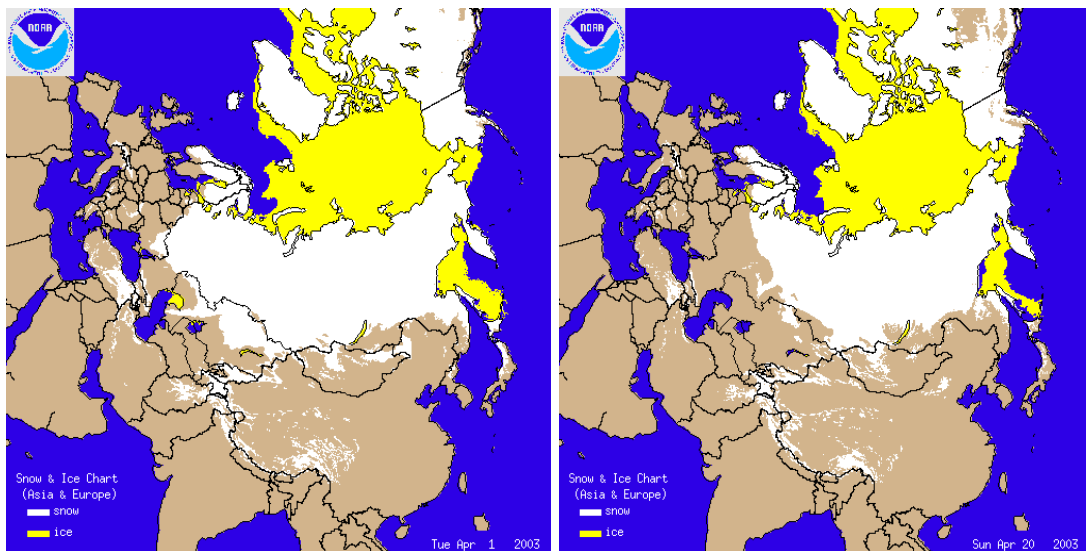


Figure 4.3 Daily snow cover conditions in Europe and Asia on 1 and 20 April 2003 from NOAA web site (URL-1)

## 4.3 Stations and Instrumentation

The science and practice of hydrology includes managing, assessing and forecasting the quantity and quality of water. Both historical and real-time hydrological data are collected, stored and analyzed. The resulting information is provided to the decision makers to manage the water resources and to mitigate floods, droughts, pollution incidents and similar water-related hazards. For this reason, an important prerequisite is the availability of accurate, reliable and timely data (WMO, 1999b). In developed countries, virtually all data collection is made by agencies with official program responsibilities and is available in computer databases. In addition to storing data, the databases allow for data retrieval, report generation, statistical analysis, model calibration and input data preparation for hydrologists and model users. In Turkey, several governmental organizations collect hydro-meteorological data, but the flow of information is slow and unorganized besides the scarce number of stations especially at higher elevations. Also, Turkey does not have a specific archiving organization and data source in terms of snow studies. Therefore, one of the main aspects of the present research is the formation of a continuous snow database in the eastern part of Turkey. In the end, the ultimate goals of graphical and tabular outputs, statistical analysis, remote sensing and geographic information systems integration capability and report availability should be satisfied with the cooperation of governmental organizations.

Investigations of the snow cover energy balance and snowmelt in remote alpine watersheds require detailed monitoring of the surface climate. Snow metamorphism, melting and runoff are controlled by the magnitude of energy available to drive these processes and these energy fluxes are determined by the combination of local meteorological inputs of precipitation and energy. Table 4.3 summarizes the possible data types that are needed in snow hydrological analysis along with comments on the purpose and application of the data (USACE, 1998).

Table 4.3 Data requirements for snow analysis (USACE, 1998)

| Data type | Physical element or purpose | Application |
|---|---|---|
| **Snow water Equivalent (SWE)** | Estimate of precipitation<br>Index to basin water supply<br>Snowpack during ablation | Analysis, model calibration<br>Water supply forecasting<br>Modeling snowmelt |
| **Snow depth** | Estimate of SWE, precipitation<br>Estimate of weight | SWE, precipitation applications<br>Snow load on structures |
| **Snow density** | Estimate of SWE, precipitation<br>Condition of snow | SWE, precipitation application<br>Avalanche conditions, snow loads |
| **Areal snowcover** | Extent of basin snowcover<br>Snowline elevation | Model calibration<br>Parameter in forecast models |
| **Precipitation** | Estimate of SWE<br>Basin moisture input | Hydrograph analysis, model calibration<br>Water supply forecasting |
| **Air temperature** | Rain/snow interface<br>Index to all energy exchanges<br>Factor in energy budget estimates | Modeling snow accumulation<br>Modeling snowmelt (temp. index / energy budget) |
| **Snow albedo** | Solar energy absorption | Modeling (energy budget) |
| **Solar radiation** | Solar energy flux | Modeling (energy budget) |
| **Longwave radiation** | Longwave energy flux | Modeling (energy budget) |
| **Wind velocity** | Estimate of convection / condensation energy flux | Modeling (energy budget) |
| **Humidity** | Estimate of condensation energy flux | Modeling (energy budget) |
| **Streamflow** | Continuous discharge<br>Runoff volumes | Hydrograph analysis, model calibration<br>Water supply analysis, forecasting |

It is hard, dangerous and expensive to collect hydro meteorological data at higher altitudes especially in extreme climatic conditions. However, it is essential to characterize the climate conditions over the rough topography of the remote mountainous catchments in Eastern Turkey where most of the water to the large dams is generated from snowmelt during spring and early summer months.

Detailed climatic observations in montane climates are limited and most of those that do exist come from locations at lower elevations (Smith and Berg, 1982 cited from Marks et al., 1992) and from nonalpine locations (Anderson, 1976 cited from Marks et al., 1992). This is the case in Karasu Basin as well. Meteorological stations at higher elevations, especially above 1850 m, are sparse and usually not continuous. On the other hand, snow course measurements by the governmental organizations are generally conducted once or twice a month during a snow season. In such situations, it becomes nearly impossible to monitor, model and forecast the amount and timing of important snow accumulation or melt events.

The increasing need for automatic data acquisition systems has led to considerable efforts in research and development to find optimal system designs and to improve accuracy and reliability. This work has led to development of sensors, electronics, software and complete systems which have been tested for extended periods both in experimental and operational networks.

With this idea, more sophisticated snow studies in the region started with the NATO-Sfs project in 1996. Under the guidance of Middle East Technical University and in cooperation with the governmental organizations of General Directorate of Electrical Power Resources Survey and Development Administration (EIE) and General Directorate of State Hydraulic Works (DSI) with their regional offices giving considerable effort, this project made it possible for the installation of four automated snow and meteorological (snow-met) stations at higher elevations of the study area in 1999. The stations were named as Çat (2340 m), Sakaltutan (2150 m), Ovacık (2130 m) and Hacımahmut (1965 m). The locations of the stations were selected according to their accessibility, safety and to represent the

characteristics of the basin with different subbasins, elevations, slopes and aspects. At the time, the instrumentation of the stations was not of great complexity. The sensors consisted of the main meteorological data such as temperature, humidity, wind speed and direction along with the collection of snow data using steel snow pillows (2 m by 2 m) to measure the snow water equivalent and an ultrasonic depth sensor to measure the depth of snow on the pillow. The measured data were recorded in a datalogger as minimum, maximum and daily averages.

With the data collected from this project, a number of master thesis using different hydrological models (SRM, SLURP, HEC-1) on different basin scales have been completed by Kaya (1999), Uzunoğlu (1999), Şensoy (2000) and Tekeli (2000).

With the existing infrastructure and experience gained on snow hydrology from the previous studies, it was decided that more fieldwork and additional data was necessary for further model development and testing. Hence, two projects funded by State Planning Organization (DPT), BAP-2001K120990 and BAP-2003K120920-01, made the continuation of the snow studies possible in the years 2001 and 2003. During this time, firstly, a new and well-equipped snow-meteorological station was set up in the basin in 2001, Güzelyayla (2065 m), and progressively, the previously installed stations were upgraded by increasing the number and accuracy of the instrumentation each year. With these upgrades, snow-met stations started to collect even higher quality data at a better time resolution than before. On top of these, key stream gauging stations were also renewed to collect automated discharge data during this period. But most important of all, as five snow-met stations and three stream gauging stations became automated collecting valuable data, this data could also be made available in real time format through satellite, GSM (Global System for Mobile Communication) or telephone communications whichever suited the station location. Therefore with this system, real time monitoring and near real time hydrological forecasting became possible. Figure 4.4 depicts the locations of the automated snow-met as well as the stream gauging stations in and around Karasu Basin on a digital elevation map and

Table 4.4 gives general information on the current situation of the established stations.
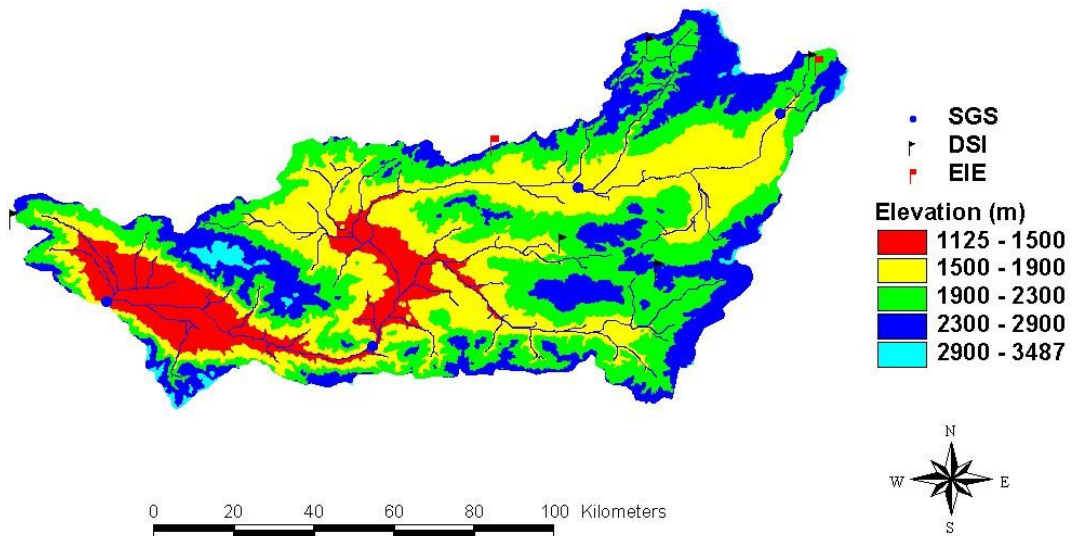


Figure 4.4 Locations of the automated snow-met and stream gauging stations in and around Karasu Basin

Even the most common meteorological parameters are difficult to measure continuously at a remote site because both the instrumentation and recording equipment exhibit varying degrees of instability depending on environmental conditions (Marks et al., 1992). On the rough topography and extreme climatic conditions of Eastern Anatolia, at times it may take days or weeks to attend instrumentation in case of a breakdown or malfunction in the sensors. This has happened a few times in the past years which resulted in loss of valuable data. But on the whole, the equipment worked quite well over the past years with minimum maintenance. Careful attention has been paid to both the precision and accuracy of the instrumentation, but the absolute uncertainty can not be known outside the laboratory.

Table 4.4 General information on the established automatic snow and meteorological (snow-met) stations and stream gauging stations (sgs) in and around Karasu Basin.

| Station | Elevation (m) | Type | Coordinates (Geographic) | Date of Construction |
|---|---|---|---|---|
| Çat | 2340 | Snow-met | 39° 44' 37" N 41° 00' 34" E | Feb-1999 |
| Sakaltutan | 2150 | Snow-met | 39° 52' 24" N 39° 07' 54" E | Feb-1999 |
| Ovacık | 2130 | Snow-met | 40° 14' 48" N 41° 00' 03" E | Feb-1999 |
| Güzelyayla | 2065 | Snow-met | 40° 12' 01" N 41° 28' 22" E | Oct-2001 |
| Hacımahmut | 1965 | Snow-met | 39° 48' 21" N 40° 43' 45" E | Feb-1999 |
| DSI 21-01 Kırkgöze | 1830 | SGS | 40° 05' 51" N 41° 22' 59" E | Oct-2003 |
| EIE 2154 A. Kağdariç | 1675 | SGS | 39° 56' 20" N 40° 45' 35" E | Oct-2004 |
| EIE 2119 Kemah | 1123 | SGS | 39° 39' 01" N 39° 21' 36" E | Oct-2004 |

Tables 4.5 through 4.7 show the instrumentation with respect to meteorological, radiation and snow sensors present in each station and Table 4.8 provides the means of data collection and transfer from different snow-met and stream gaging stations in and around Karasu basin.

In the following sections, the type of data collected within each station is discussed with further details including tables, photographs and charts to give an idea of the conditions at site.

Table 4.5 Meteorological instrumentation at the sites

| Station | Prec | Temp | Wind Speed | Wind Direction | Relative Humidity | Air Press |
|---------|------|------|------------|----------------|-------------------|-----------|
| Çat (2340 m) | | ✔ | ✔ | ✔ | ✔ | ✔ |
| Sakaltutan (2150 m) | | ✔ | | | | |
| Ovacık (2130 m) | ✔ | ✔ | ✔ | ✔ | ✔ | |
| Güzelyayla (2065 m) | ✔ | ✔ | ✔ | ✔ | ✔ | ✔ |
| Hacımahmut (1950 m) | | ✔ | ✔ | ✔ | ✔ | ✔ |

Table 4.6 Radiation instrumentation at the sites

| Station | Solar Radiation | Albedo | Net Longwave Radiation | Net Total Radiation |
|---------|-----------------|--------|------------------------|---------------------|
| Çat (2340 m) | ✔ | | | ✔ |
| Sakaltutan (2150 m) | | | | |
| Ovacık (2130 m) | ✔ | ✔ | ✔ | |
| Güzelyayla (2065 m) | ✔ | ✔ | | ✔ |
| Hacımahmut (1950 m) | ✔ | | | |

Table 4.7 Snow instrumentation at the sites

| Station | Snow Pillow | Snow Depth | Snow Lysimeter |
|---|---|---|---|
| Çat (2340 m) | Hypalon (6.5 m$^2$) | Ultrasonic Depth Sensor | --- |
| Sakaltutan (2150 m) | Steel (4.0 m$^2$) | Ultrasonic Depth Sensor | --- |
| Ovacık (2130 m) | Hypalon (6.5 m$^2$) | Ultrasonic Depth Sensor | Yes (1.60 m$^2$) |
| Güzelyayla (2065 m) | Hypalon (6.5 m$^2$) | Ultrasonic Depth Sensor | Yes (1.53 m$^2$) |
| Hacımahmut (1950 m) | Steel (4.0 m$^2$) | Ultrasonic Depth Sensor | --- |

Table 4.8 Data collection and transfer system

| Station | Data Collection | Data Transfer |
|---|---|---|
| Çat (2340 m) | 2-hour and daily | Inmarsat Mini-M |
| Sakaltutan (2150 m) | Daily | Inmarsat Mini-M |
| Ovacık (2130 m) | 2-hour and daily | Telephone Modem |
| Güzelyayla (2065 m) | 2-hour and daily | Telephone Modem |
| Hacımahmut (1950 m) | Daily | GSM |
| DSI 21-01 Kırkgöze (1830 m) | 15-minute | GSM |
| EIE 2154 A. Kağdariç (1675 m) | 15-minute | GSM |
| EIE 2119 Kemah (1125 m) | 15-minute | GSM |

## 4.3.1 Snow Data

The collection of snow data in conventional manner by snow poles and tubes in the region stared in mid 1960 s by the governmental organizations. During a snow season, usually monthly or bimonthly snow course measurements are conducted. These measurements indicate the high snow potential of the region but are far from providing sufficient information for snow modeling.

In order to automatically collect continuous snow data in the study area, snow pillows connected to a pressure transducer and ultrasonic depth sensors are installed to each of the snow-met stations. With this, snow pillows would measure the weight of the snow on top of them and at the same time depth sensors would measure the snow depth over the pillow, hence, snow water equivalent over the snow pillows can be calculated. At first, the snow pillows were made of steel sheets buried under the soil. At each station, four of these pillows were placed together (2 m by 2 m) and connected with pipes. These pillows were not very sensitive to the shallow snow depth above them producing spurious values. Therefore, they were replaced by rubber made hypalon pillows which covered a larger area (approx. 6.5 m$^2$) than the metal pillows and more sensitive to weight changes because of its material. The hypalon pillows were placed on a uniform soil insulated by rubber lining and covered by a wire mesh to protect them from rats. They are filled with water, antifreeze and alcohol in order to prevent the fluid from freezing as well as keeping the density close to 1000 kg/m$^3$. All the air inside the pillow should be evacuated so that snow load is transferred directly by the mixed fluid to the pressure transducer whereby measured and logged to the data logger. Figure 4.5 shows the installation of a snow pillow in Çat station.

October 2003

Figure 4.5 Snow pillow installation in Çat station

The snow depth and snow water equivalent at a station is monitored continuously being measured every 30 seconds and averaged over a 2-hour period. Also daily minimum and maximum values along with the time of occurrences of these events are summarized at the end of each day in the loggers. As these valuable data are measured and recorded by the station equipment, snow measurements are also conducted manually from time to time by snow sampling tubes around or close to each station in order to compare the readings. Figure 4.6 and Figure 4.7 show such a comparison of snow depth and snow water equivalent respectively from Güzelyayla station during 2004 water year. As seen from the figures, snow depths show a better match than the SWE values. This may be considered as an expected result because the accuracy of measuring the snow depth is much more than the SWE. Small discrepancies can be attributed to the errors in the manual snow tube weighing as well as load decrease over the snow pillow due to ice bridging. Even if these errors are small, the snow sampling points are in any case different than the area over the snow pillow and this might be another reason for the mismatch of the values which may be explained by wind drift and forming of the ice lenses or frozen layers in the snow.
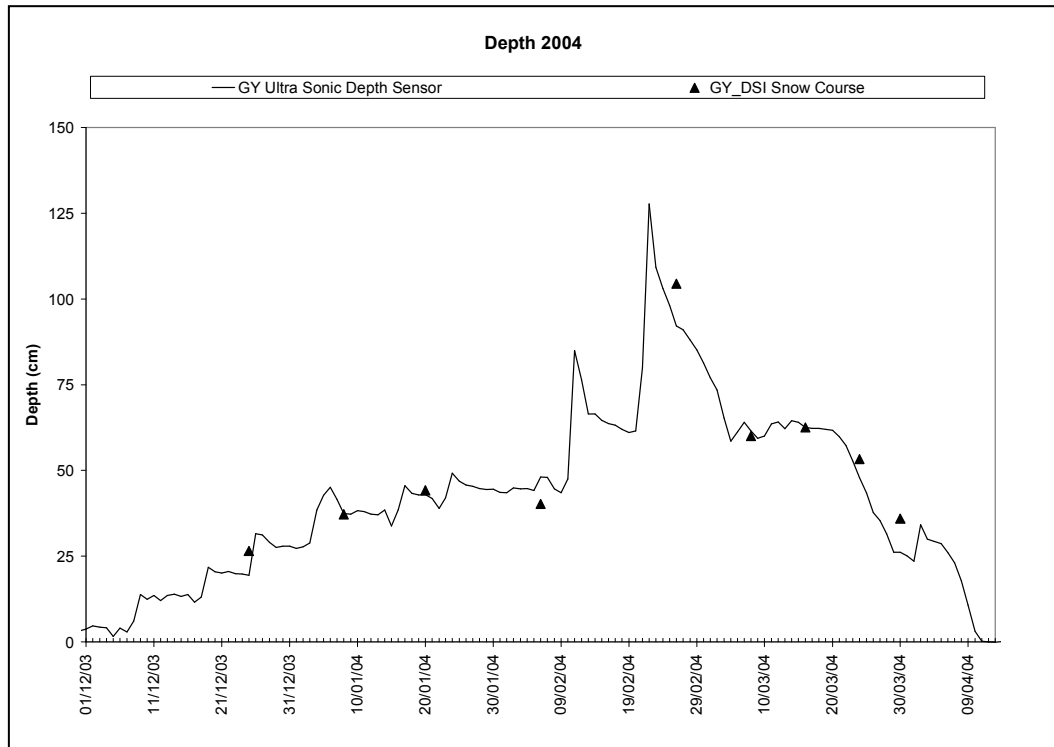
Figure 4.6 Manual and automatic snow depth measurements (cm), Güzelyayla station, 2004 water year
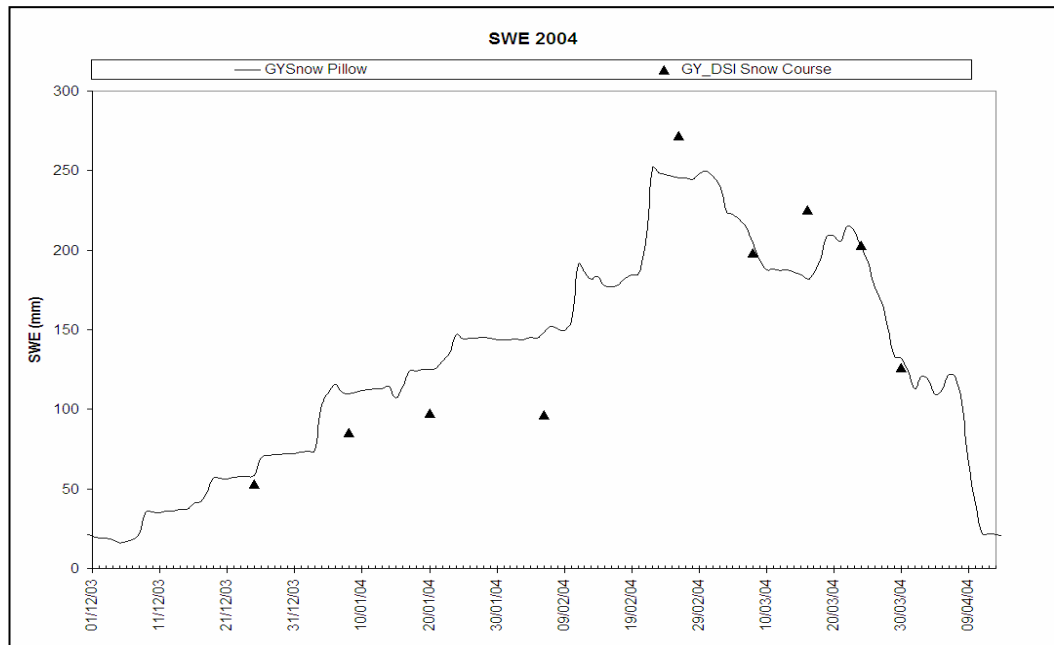


Figure 4.7 Manual and automatic snow water equivalent measurements (mm), Güzelyayla station, 2004 water year

72

As seen from Table 4.5, currently, Çat (replaced in 2003), Ovacık (replaced in 2002) and Güzelyayla (installed in 2001) stations have hypalon snow pillows where as Sakaltutan and Hacımahmut sites continue to work with steel snow pillows. But all the snow-met stations have ultrasonic depth sensors over the pillows.

Long term manual snow course measurements for snow water equivalent between 1976-2003 around Güzelyayla, Ovacık, Çat and Sakaltutan sites is depicted in Figure 4.8. This analysis is done to show the general pattern of SWE distribution at different locations and altitudes in the basin during a snow season. Snow water equivalent values are grouped into ten day composites since the observation dates are unevenly distributed within a month. Unfortunately, snow course data are generally carried out during accumulation periods hence missing out snow melt. But in any case, these long term SWE data may give an indication on the average conditions to determine dry and wet snow seasons.
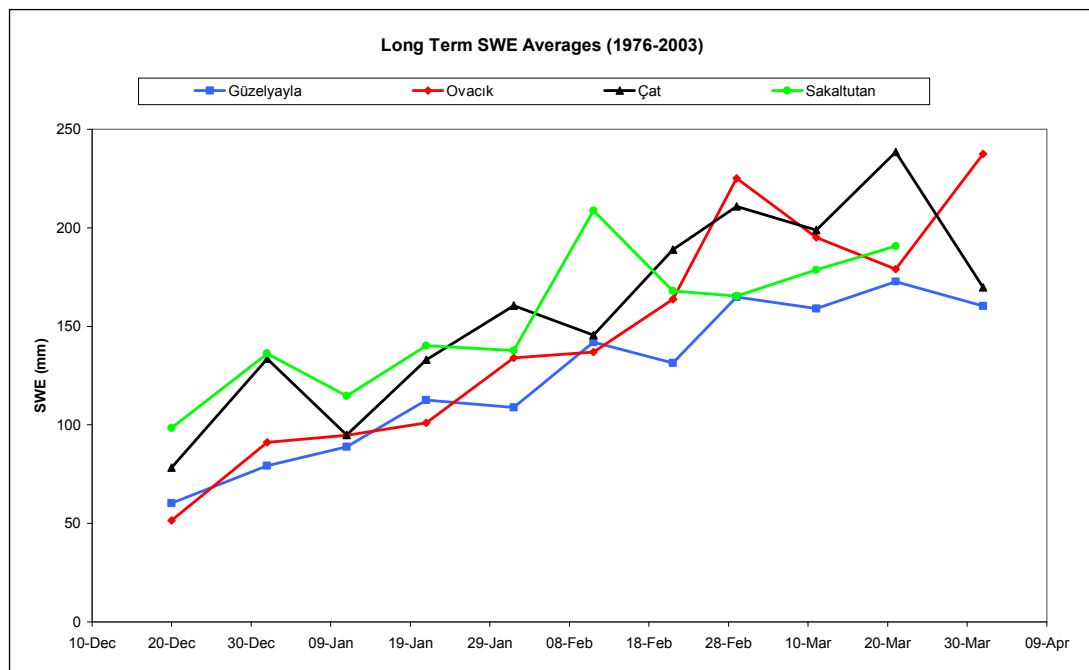


Figure 4.8 Long term average manual snow water equivalent values (1976-2003)

## 4.3.2 Meteorological Data

## 4.3.2.1 Radiation

Radiation is the only form of energy transfer that can be measured directly in the natural environment. Greatest use of radiometers in hydrology is in the studies related with evaporation and snowmelt. For most studies of evaporation, incident all wave radiation data are adequate, since the reflectivity of water is nearly constant. The reflectivity of snow, however, is highly dependent upon wavelength and albedo, which may range from 30 to 90 percent. Hence, both incident shortwave and longwave radiation data are required.

Also under clear sky conditions the distribution of incident radiation can be modeled over complex terrain for both solar (shortwave) (Dozier, 1980) and thermal (longwave) (Marks and Dozier, 1979) wavelength ranges, but under cloudy conditions, measurements are necessary because the separate contributions of direct and diffuse solar and emitted thermal radiation from the atmosphere and clouds are not easily predicted or modeled. Since Eastern Anatolia has a rough topography, clouds are mainly present during winter and spring seasons. Therefore, rather than modeling solar and thermal radiations in the region, incident radiation is reliably and accurately measured in broad wavelength band widths using well established instrumentation.

Incident radiation is monitored with a combination of sensors in Çat, Ovacık, Güzelyayla and Hacımahmut stations. Net radiometers in the spectral range of 0.3-100 $\mu$m are used in Çat and Güzelyayla stations. Pyronometers are used to measure solar radiation in the spectral range of 0.305-2.8 $\mu$m at Çat, Ovacık, Güzelyayla and Hacımahmut stations. Net pyrgeometers are placed at Ovacık station to measure both the incoming and outgoing longwave radiation within the spectral range of 5-25 $\mu$m. Measurements of albedo is accomplished through the use of two pyronometers possessing hemispherical fields of view. One pyronometer measures the incident and the other the reflected flux and albedo is

calculated by ratioing these fluxes. Albedo measurements are conducted in Ovacık and Güzelyayla stations. Forms of net solar and net total radiation are measured at Çat and Güzelyayla stations whereas, net solar and net thermal radiation is measured at Ovacık station to derive net total radiation. Therefore, a combination of different radiation forms are being measured and derived in the stations providing a kind of verification with each other. Table 4.6 summarizes the radiation instrumentation in the study area. Figure 4.9 illustrates the combination of pyronometers and pyrgeometers at Ovacık station.
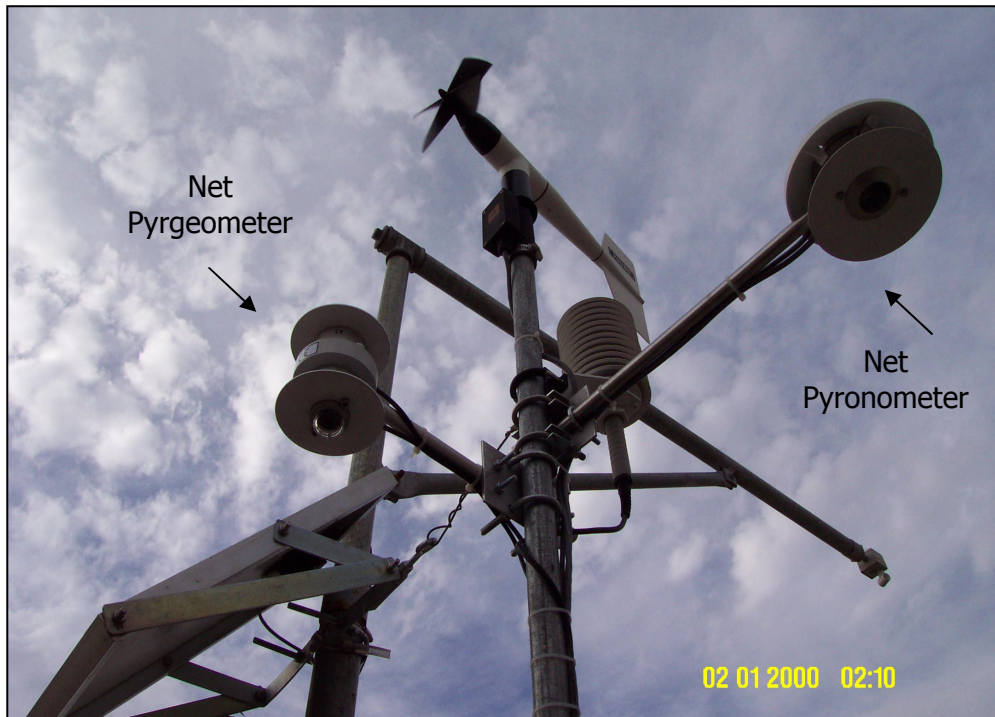


Figure 4.9 Net pyronometer and net pyrgeometer at Ovacık station

Figure 4.10 depicts 2-hourly average solar radiation (W/m$^2$) for a diurnal cycle at Güzelyayla station over a 15-day period in mid-January and mid-June of the 2003 water year. As seen from the figure, in June, the sun rises about 2 hours earlier and sets about 2 hours later and the radiation difference is nearly 3-fold than in January. Figure 4.11 shows 2-hourly average net radiation (W/m$^2$) again at Güzelyayla station for the same diurnal periods in January and June of the 2003 water year. The significant difference in net radiation magnitude and sunlit period can easily be seen between the two periods.
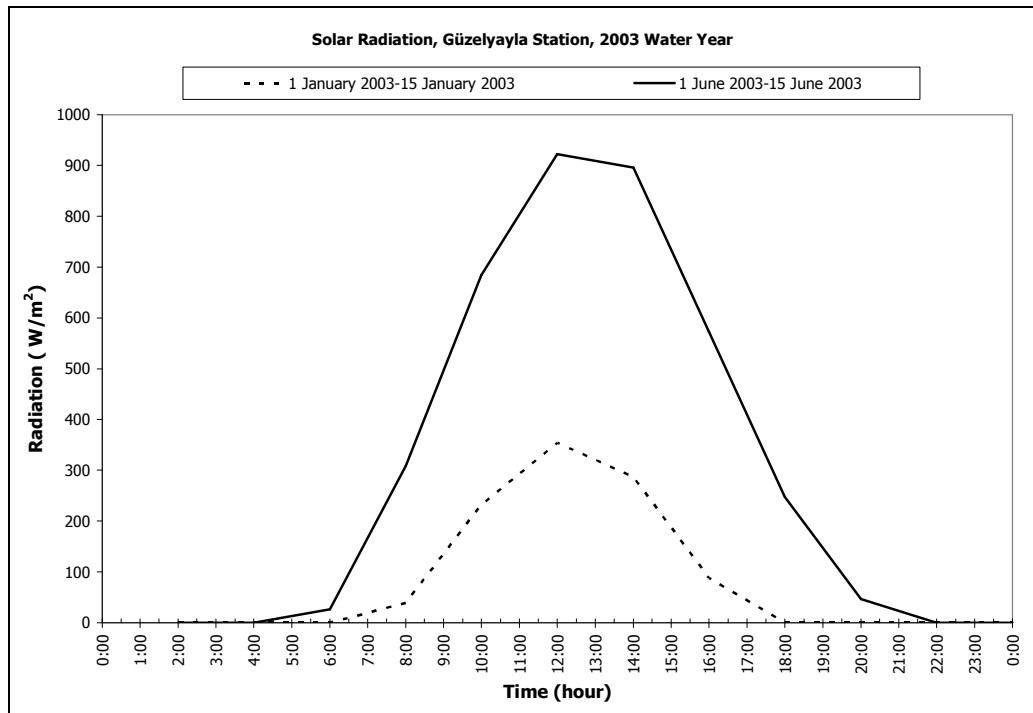
Figure 4.10 Winter and summer diurnal average solar radiation (W/m$^2$), Güzelyayla station, 2003 water year
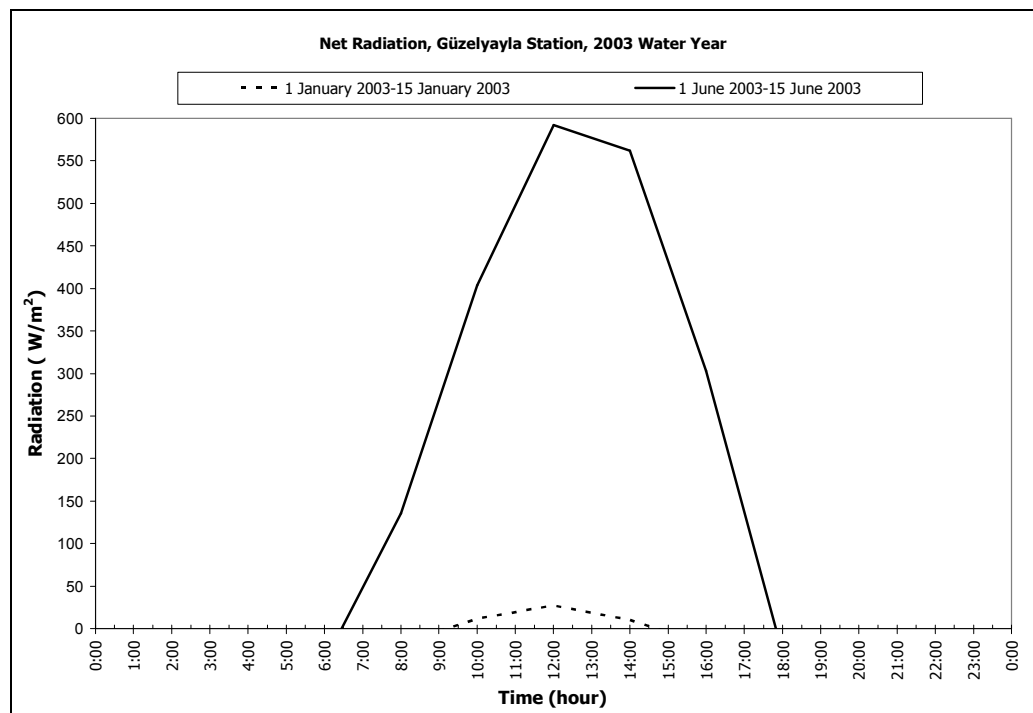


Figure 4.11 Winter and summer diurnal average net radiation (W/m$^2$), Güzelyayla station, 2003 water year

Topographic differences in elevation, shading and exposure between the measurement stations may cause distinct differences in measured solar radiation (Marks et al., 1992). The contribution of solar and thermal radiation to the energy balance of snow cover during 2002, 2003 and 2004 water years are discussed in detail in Şensoy (2005).

## 4.3.2.2 Air Temperature

The most common meteorological data collected anywhere are of air temperature. Ideally, these measurements should be made at a specified height above the snow surface, shielded from the effects of radiation or conduction from sources other than the atmosphere. In practice, this is seldom the case. Some radiant heating or cooling of the instrument shelter is inevitable, but in most locations this produces only a minor affect (Marks et al., 1992).

Air temperature measurements are present in all five snow-met stations in the study area as indicated in Table 4.7. Daily minimum, average and maximum air temperatures are presented in Figure 4.12 and monthly minimum, average and maximum air temperatures are tabulated in Table 4.9 for the 2003 water year at Güzelyayla station to give a better insight about the region. These values point out that even at an elevation of 2065 m above sea level (a.s.l.) (Güzelyayla station), air temperatures may range from -30 °C to +30 °C showing how extremely this parameter may vary during a year's cycle.
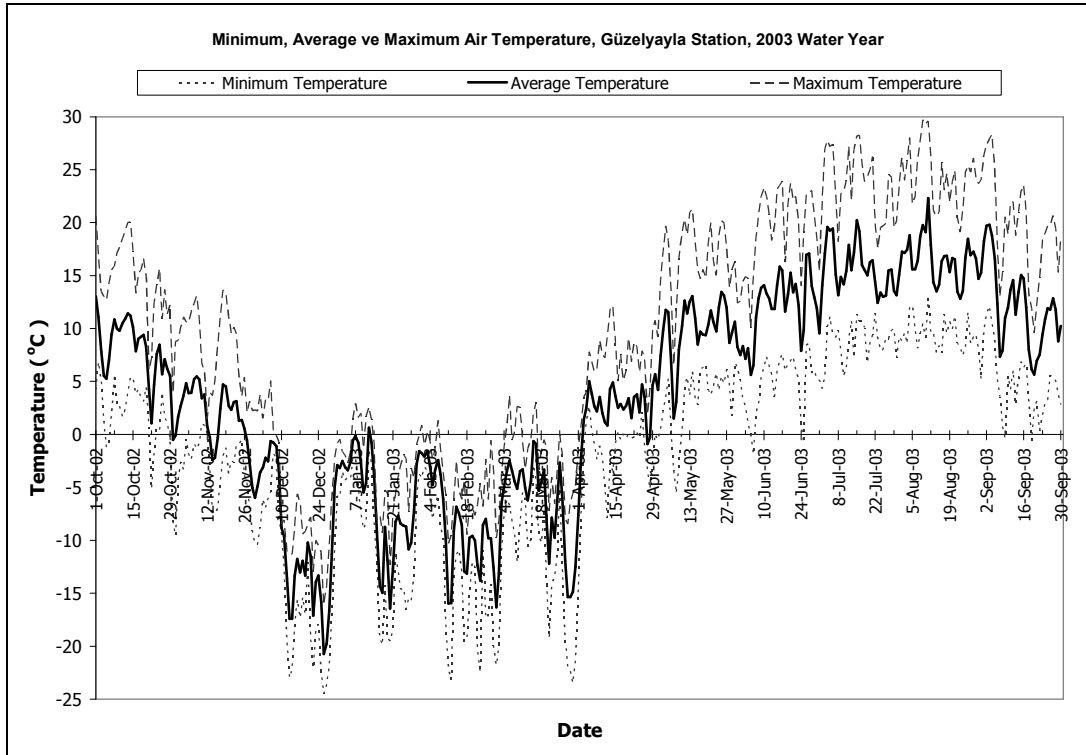
Figure 4.12 Daily air temperatures ($^{o}$C), Güzelyayla station, 2003 water year

Table 4.9 Monthly air temperatures ($^{o}$C), Güzelyayla station, 2003 water year

| Month | Minimum | Average | Maximum |
|-----------|---------|---------|---------|
| October | -9.57 | 7.67 | 20.63 |
| November | -10.38 | 1.71 | 13.65 |
| December | -24.52 | -10.03 | 5.08 |
| January | -19.89 | -6.31 | 2.89 |
| February | -23.20 | -8.32 | 1.32 |
| March | -23.47 | -7.10 | 3.71 |
| April | -14.43 | 2.35 | 12.17 |
| May | -5.54 | 9.75 | 21.28 |
| June | -1.85 | 12.03 | 23.90 |
| July | 4.32 | 15.49 | 28.26 |
| August | 5.23 | 16.53 | 29.73 |
| September | -0.57 | 12.02 | 28.32 |

## 4.3.2.3 Snow Surface Temperature

Snow surface temperature is difficult to measure by physical thermometry. Davis et al. (1984) showed that the near snow surface temperature tends to follow the air temperature as long as the air temperature is less than $0^{\circ}C$. This occurs because the insulating characteristics of the snow cover allow the surface layer to come into temperature equilibrium with the atmosphere even though this may create large temperature differences between the surface and lower layers. However, once the air temperature is above $0^{\circ}C$, the snow surface is constrained ($\leq 0^{\circ}C$) and the temperature difference can increase in magnitude.

Manual spot measurements of snow surface temperature using a radiant thermometer were taken at Güzelyayla and Ovacık stations during 2003 water year. A linear relationship is found between air temperature and snow surface temperature. These estimates of snow surface temperature should be reasonable for the top few centimeters of the snow cover during windy or daylight conditions. However, they may substantially differ especially under calm conditions at night due to radiative cooling.

## 4.3.2.4 Soil Temperature

Even though ground heat flux in the energy balance calculations is not a dominant factor, it is measured only in Güzelyayla station during 2003 water year. A thermistor probe was buried in soil to a depth of 15-20 cm for it to represent the upper soil layer. The recorded results from 2003 water year were not satisfactory because the upper soil temperature was always above $0^{\circ}C$ during the winter season. Even when the air and snow surface temperatures are well below the freezing point, a positive ground temperature would mean a very high ground heat flux in the energy balance calculations and a continuous melting from the snow-ground interface which is not believed to be the case. Therefore, the thermistor probe is replaced by a better thermocouple probe in Güzelyayla station in the

beginning of 2004 water year in the hope to measure more realistic upper soil layer temperatures.

## 4.3.2.5 Wind Speed and Direction

The movement of air is an important part of weather process; wind exerts considerable influence in evaporation and snowmelt processes. Wind speed is measured by anemometers and wind direction by vanes of which there are several types. Wind is highly variable in both time and space and is difficult to characterize by sampling in either of these dimensions. It is generally deemed site-specific. Wind direction is greatly influenced by orientation of orographic barriers. With a weak pressure system, diurnal variation of wind direction may occur in mountainous regions, the winds blowing upslope in the daytime and downslope at night.

Wind speed and direction are measured in all the snow-met stations except Sakaltutan. Wind speeds are more pronounced in Çat and Güzelyayla stations especially during snow accumulation period with an average around 3 - 4 m/s and a prevailing wind direction of north-east south-west. Wind speeds are rather low at Ovacık station with an average of 1.5 m/s. Daily mean wind speed and wind direction are shown in Figure 4.13 and Figure 4.14 respectively at Güzelyayla snow-met station during 2003 water year.
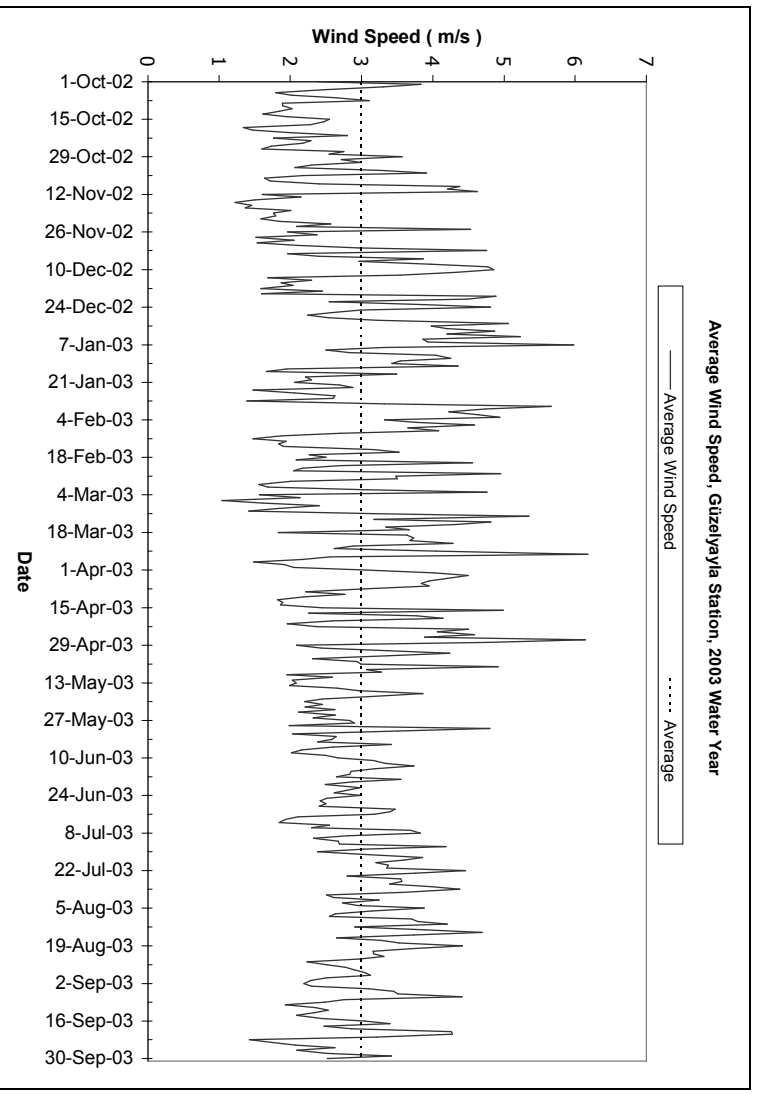
Figure 4.13 Daily mean wind speed (m/s), Güzelyayla station, 2003 water year
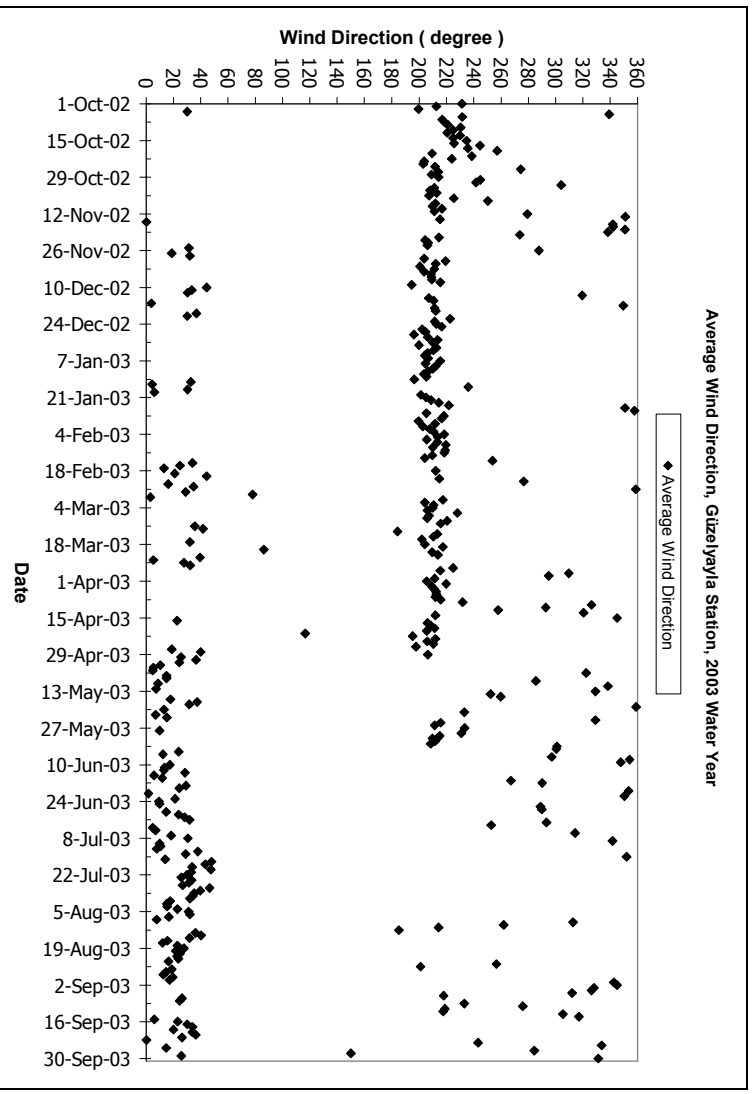


Figure 4.14 Daily mean wind direction (degree),Güzelyayla station,2003 water year

81

## 4.3.2.6 Relative Humidity and Air Pressure

Relative humidity or the water vapor content of the air is monitored in all the snow-met stations except Sakaltutan. Capacitance-type humidity instruments are installed at the stations as these are preferred to be used at remote alpine sites. These sensors are also affected by radiant heating and cooling, though to a lesser degree than are air temperature sensors.

Air pressure is monitored in Çat, Güzelyayla and Hacımahmut snow-met stations. A barometer with a silicon capacitive sensor is used to measure barometric pressure on a 600 to 1060 mb range.

## 4.3.2.7 Precipitation

Precipitation in Karasu Basin falls mainly as snow during November through March and rain at other times. But sleet (mixed rain and snow) is also quite frequent in the transition periods between rain and snow depending on air temperature.

There are precipitation gages located at Ovacık and Güzelyayla stations. These gages are equipped with an electrical heater, but due to lack of power supply at a remote location, the heater could not be operated. Since snow accumulation may present gaging problem due to gage freezing, capping of gage by snow and high winds, precipitation gages are generally used to measure rainfall amounts and snowfall data are computed according to snow pillow and depth sensor variations. During 2003 water year, 612 mm of precipitation is measured in Güzelyayla snow-met station as shown in Figure 4.15.
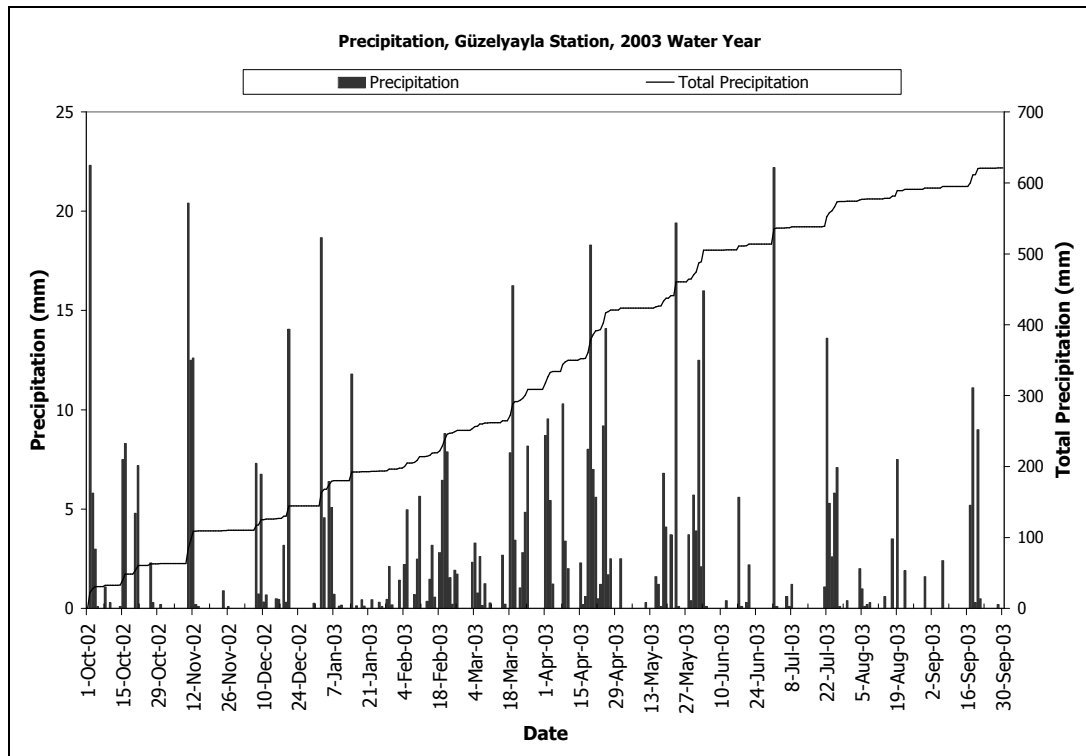
Figure 4.15 Daily and yearly cumulative precipitation (mm), Güzelyayla station, 2003 water year

## 4.3.3 Hydrological Data

### 4.3.3.1 Snowmelt Lysimeter

Snowmelt runoff models are mainly evaluated based on the reproducing capability of an observed hydrograph that are not direct measurements of snow melt. Improvements in these model components would lead to a stronger physical basis and for this reason, water released from the base of the snow pack is an ideal variable because it serves as the output of the snowmelt routine and the input to the runoff production routine. Hence, snowmelt lysimeters are designed to collect and measure the melt water released from the snow pack, thus they are excellent tools for quantifying the snowmelt timing and volume requirements of snowmelt studies, such as water-supply forecasting and hydrologic model-improvement studies (Kattelmann, 2000). In the snow free season, snowmelt lysimeter can be

83

used as an efficient precipitation gage since it is less affected by wind due to its large area (Killingtveit and Saelthun, 1995).

In this sense, unenclosed snowmelt lysimeters are constructed and installed at Güzelyayla (2002) and Ovacık (2003) snow-met stations. Tekeli et al. (2005b) discusses the types, construction and installation of the two snowmelt lysimeters in detail. Both of the snowmelt lysimeters are placed at a higher elevation than ground level to minimize lateral flows in the snow pack but the wind drift effect could not be diminished. The outflow from the snowmelt lysimeters are measured with a tipping bucket rain gauge placed at the bottom of the lysimeter outlet with a screen to eliminate any debris entering into the rain gage. The installed snowmelt lysimeter at Güzelyayla snow-met station is seen in Figure 4.16. The snowmelt lysimeter at Güzelyayla station worked quite well for the two water years (2003 and 2004) but problems hindered the operation in Ovacık snow-met station. Freezing of outlet flow and debris blockage were the main problems faced in Ovacık station.

The results of the snowmelt lysimeter outflow timing are quite comparable with snow melt and rainfall values especially in Güzelyayla station. Lysimeter data and basin outlet runoff in micro (Kırkgöze Basin, 242 km$^2$) and macro (Keban Basin, 67,500 km$^2$) catchment scales also show an interesting match for the 2003 water year as seen in Figure 4.17. For more results of the snowmelt lysimeter operation Tekeli et al. (2005b) may be referred.

Figure 4.16 Snowmelt lysimeter at Güzelyayla station
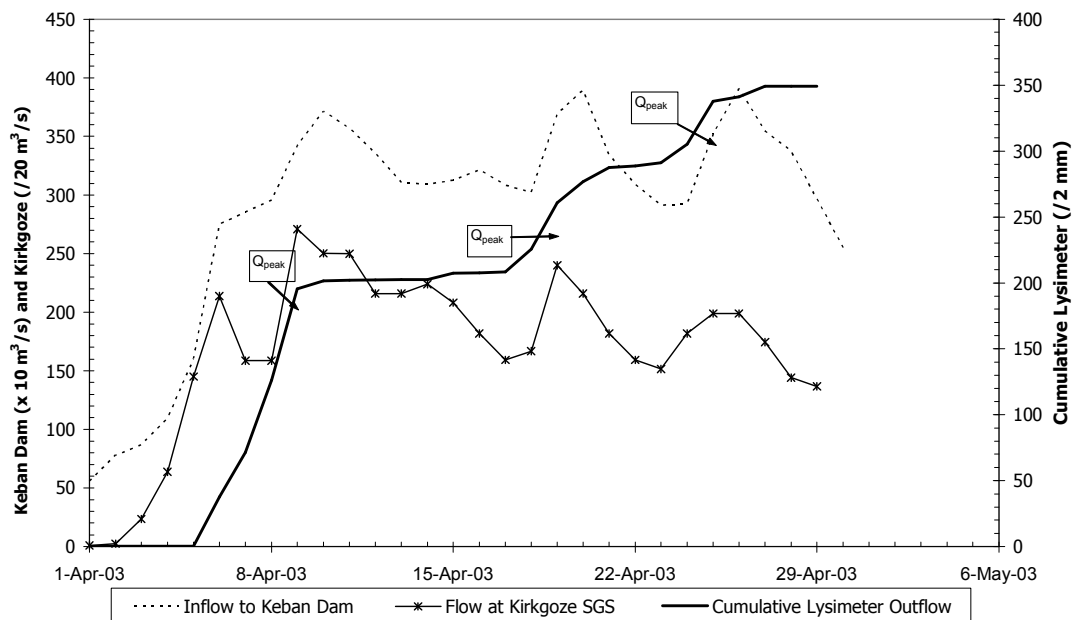


Figure 4.17 Güzelyayla snowmelt lysimeter outflow comparison with different basin
scale discharges

### 4.3.3.2 Streamflow

Measurement of stage and discharge is a very central part of operational hydrology and hence, most data available for model calibration and verification are runoff data. Having a long runoff series for a basin enables the researchers to understand the behavior of the catchment better under different conditions. Although long runoff records are important, nowadays, monitoring real time runoff data is as crucial for real time operations and forecasting.

Based on this idea, besides monitoring five snow-met stations, three main stream gaging stations are selected in Karasu Basin where real time runoff data are also observed. These stream gaging stations are EIE 2119, EIE 2154 and DSI 21-01 from downstream to upstream. Table 4.4 and Table 4.8 present more information on the stream gauging stations. DSI 21-01 station is equipped with real time shaft encoder system in the beginning of 2004 water year, but replaced by a pressure transducer system instead in the beginning of 2005 water year. The other two stream gaging stations are established with real time instrumentation in the beginning of 2005 water year both using a shaft encoder system. The real time communication with all three stream gaging stations is managed using a GSM system which is probably the most efficient and reliable way of communication in Turkey at the moment. By chance, the early unexpected flooding in Turkey which occurred during 29 February - 9 March 2004 has shown the vital importance of accessing real time runoff data especially on Euphrates River where large dams are located (Şorman et al., 2004).

# CHAPTER 5

# REMOTE SENSING IN SNOW HYDROLOGY

## 5.1 Introduction

In the hydrological field, modeling needs spatial data from the consideration of the area being studied. In the past, hydrologists relied mostly on conventional data network systems based on manual ground measurements. As the technological progress brought new impulses, automatic meteorological stations furnished data from remote mountain areas which was particularly important for snow hydrology.

Remote sensing is one of the new techniques being applied in hydrology and in particular in snow hydrology. Characterized by insufficient spatial and temporal coverage of the Earth's surface, the conventional networks are being supplemented by remotely sensed data network systems because of several unique aspects. First, remote sensing techniques have the ability to measure spatial information as opposed to point data. Second, remote sensing techniques have the ability to measure the state of the Earth's surface over large and especially remote areas. Finally, they have the ability to assemble long term data for multi purposes especially those which utilize satellite sensors (Engman and Gurney, 1991).

## 5.2 History of Remote Sensing of Snow

Earth Observation (EO) data have been successfully applied in snowmelt hydrology only in the past few decades. Some of the first attempts were conducted by Rango et al. (1977) showing the effective application of EO data to predict snowmelt runoff and Rott (1978) demonstrating the application of frequent snow cover mapping in the Alps using different sensors. Early attempts at snow mapping using EO data are summarized in Hall and Martinec (1985). An illustration of the usefulness of satellite derived snow cover data for hydrological modeling was given by Martinec and Rango (1987). Wiesnet et al. (1987) outlined the importance of remote sensing methods for snow cover mapping in general.

Haefner (1980 cited in Rott, 2000) stated that within Europe at the time snow cover monitoring from satellite was not yet undertaken on a routine basis whereas several such activities were being conducted in North America during the 1980's resulting in applications still operational today (Carroll, 1990). An online example is available at the National Operational Hydrologic Remote Sensing Center (NOHRSC, URL-2).

Individual snow cover monitoring activities have frequently been reported, Frank et al. (1988), Harrison and Lucas (1989), Hu et al. (1993), Seidel et al. (1994), Baumgartner and Rango (1995), Rango (1996), Nagler and Rott (1997), but joint approaches resulting in methods and applications shared with a large community of users, especially in Europe, have begun recently with the HydAlp (Rott et al., 2000) and SnowTools (Guneriussen et al., 2000) projects. Following the achievements in these projects, other joint works have been undertaken such as EnviSnow (URL-3) and SnowMan (URL-4) projects which are still being continued.

## 5.3 Spectral Characteristics of Snow

Every object emits radiation in all wavelengths in the electromagnetic spectrum, Figure 5.1. Therefore, sensors that operate from gamma ray wavelengths to the very high frequency of microwave portions have been employed for remote sensing of snow and ice. However, it may be more advantageous to use discrete portions of the spectrum for specific task at hand, since there may be distinguishing key wavelength portions enabling easy detection of the object under search.
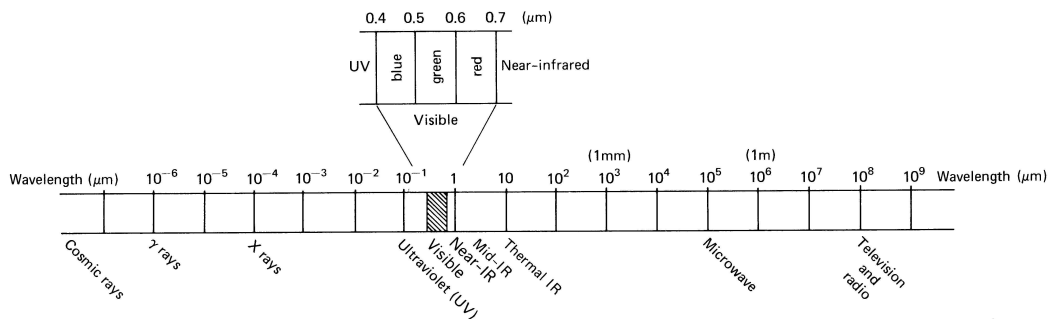


Figure 5.1 Electromagnetic Spectrum

Snow has a unique reflectance behavior; illuminated by the sun; snow is one of the brightest objects in nature in the optical and near infrared range (~0.410 µm), but is rather dark in the medium infrared (~1.5-2.5 µm) (Seidel and Martinec, 2004). Freshly fallen snow has a very high reflectance in the visible wavelengths as seen in Figure 5.2, but as it ages the reflectivity decreases in the visible and especially in the longer near infrared region. The aging is characterized by melting and refreezing cycles leading to a gain in crystal grain size as well as contamination with impurities. An advantage of using visible and near infrared data is the easy interpretation of the image as well as its spatial resolution, but on the other hand clouds may degrade the use of such wavelengths.
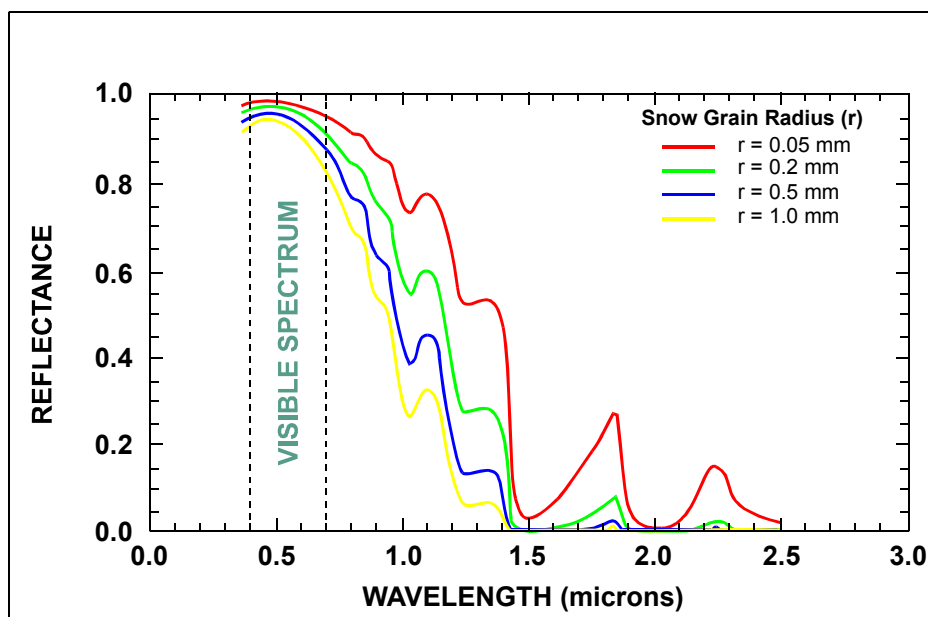
Figure 5.2 Reflective properties of snow

Thermal infrared part of the spectrum measure the radiation emitted by the Earth's surface which is dependent on surface temperature. Therefore these channels are mostly used to measure snow surface temperature. If the snow surface temperature stays at 0°C in a diurnal cycle, then it is highly likely that the snow pack has reached an isothermal stage indicating the process of snowmelt. Clouds may again limit the usability of thermal infrared images because cloud top temperatures would be measured instead of surface temperatures.

Microwave radiation measured at different wavelengths and at different polarizations enables the extraction of information related to the physical characteristics of the snow pack. Depth, water equivalent, liquid water capacity, grain size and shape, temperature, stratification are some of the properties that can be detected on microwave region. Since the response of snow varies with its state, regular monitoring may allow the detection on the onset of melt. Superiority of microwave with respect to the visible imagery is the independency of measurements from weather conditions and illumination. Thus cloud covered or night time data can also be used. However, their low spatial resolutions prevent their usability in mountainous basins (Rango, 1996).

Table 5.1 shows the relation between some of the snow properties and spectral bands and Table 5.2 gives the snow properties that affect its reflectance values (Engman and Gurney, 1991).

Table 5.1 Relation between snow properties and spectral bands (Engman and Gurney, 1991).

| Property | Visible/Near Infrared | Thermal | Microwave |
|---|---|---|---|
| Snow cover area | Yes | Yes | Yes |
| Depth | If very shallow | Weak | Moderate |
| Snow water equivalent | If very shallow | Weak | Strong |
| Stratigraphy | No | Weak | Strong |
| Albedo | Strong | No | No |
| Liquid water content | Weak | Weak | Strong |
| Temperature | No | Strong | Weak |
| All weather capability | No | No | Yes |
| Current best resolution | A few meters | Hundreds of meters | Tens of meters |

Table 5.2 Snow properties affecting its reflectance (Engman and Gurney, 1991).

| Property | Visible Reflectance | Near Infrared Reflectance | Thermal Infrared Emissivity | Microwave Emissivity |
|---|---|---|---|---|
| Grain size | * | Yes | No | Yes |
| Zenith Angle | No | Yes | Yes | Yes |
| Depth | Yes | No | No | Yes |
| Contaminants | Yes | No | No | |
| Liquid water content | No | * | No | Yes |
| Temperature | No | No | No | Yes |
| Density | No | No | No | Yes |

## 5.4 Satellite Remote Sensing of Snow

Snow cover mapping in mountainous areas is demanding due to the interfering topography and the heterogeneous ground properties. According to Rango (1994), the only efficient way to monitor the dynamically changing seasonal snow cover on a sufficiently large scale is by satellite remote sensing. But, one must judiciously select the proper sensor to use for a particular analysis taking into consideration factors such as wavelengths, resolution or frequency and timing of ground coverage (Hall and Martinec, 1985).

A high temporal resolution is important; particularly for monitoring changes in snow extent due to melt or accumulation. Although snow cover can be detected and monitored with a variety of remote sensing devices, the greatest application has been found in the visible (VIS) and the near infrared (NIR) region of the electromagnetic spectrum (Hall et al., 2002). For operational snow cover monitoring, satellites with moderate spatial resolution but with high repetition rate are important for the advantage of obtaining a cloud free image. Although cloud problem is removed with the use of microwave data (either passive or active), interpretation of the images are much more difficult with respect to optical satellites because they are highly affected from surface and subsurface properties.

Sensor systems presently in orbit are listed in Table 5.3. The multi-spectral sensors differ in terms of spatial and time resolution. The acquainted spectral information ranges in bands (or channels) from the visible, near-infrared (NIR) and up to the thermal-infrared (TIR) wavelengths. Operational snow cover monitoring requires as many sensors in orbit as possible with repetition rates as high as possible in order to take advantage of some cloud free or partially cloud covered scenes. A comprehensive survey of missions and sensors both from the past and the present in orbit has been compiled by Kramer (2002).

Table 5.3 Characteristics of satellites for snow cover mapping (Status: June 2003) (adapted from Seidel and Martinec, 2004)

| Satellite | Sensors | Spectral bands | Spatial Resolution | Repetition rate | Launched by |
|---|---|---|---|---|---|
| Meteosat-7 | VIS/IR | 3 | 2.5 km × 2.5 km | 0.5 hours | EUMETSAT (1997) |
| Meteosat-8 | VIS/IR | 12 | 1 km × 1 km | 0.25 hours | EUMETSAT (2002) |
| NOAA-14, -16 | AVHRR | 5 | 1 km × 1 km | 12-24 hours | USA (2000) |
| TERRA, AQUA | MODIS-XS | 36 | 250 m, 500 m, 1000 m | 1-2 days | USA (1999, 2002) |
| ENVISAT | MERIS | 15 | 300 m × 300 m | 3 days | ESA (2002) |
| Landsat-4, -5 | MSS | 4 | 59 m × 79 m | 16 days | USA (1972, 1984) |
| | TM | 7 | 30 m × 30 m | | |
| Landsat-7 | ETM+ | 7 | 30 m × 30 m | 16 days | USA (1999) |
| | PAN | 1 | 15 m × 15 m | | |
| SPOT-2, -3, -4 | XS | 3 | 20 m × 20 m | 26 days | France (1990, 1993, 1998) |
| | PAN | 1 | 10 m × 10 m | | |
| SPOT-5 | XS | 3 | 10 m × 10 m | 26 days | France (2002) |
| | | | 5 m × 5 m | | |
| IRS-1C | PAN | 1 | 5.8 m × 5.8 m | 5 days | India (1995) |
| | LISS-3 | 4 | 23 m × 23 m | | |
| IRS-P3 | WIFS | 3 | 188 m × 188 m | 24 days | India (1996) |
| IKONOS | XS | 4 | 4 m × 4 m | 3 days | USA (1999) |
| | PAN | 1 | 1 m × 1 m | | |
| QUICKBIRD-2 | XS | 4 | 2.44 m × 2.88 m | 3 days | USA (2001) |
| | PAN | 1 | 0.61 m × 0.72 m | | |

The satellites tabulated in Table 5.3 can further be classified into High and Medium Resolution Optical Imagers (HROI and MROI), optical in this sense does include the infrared part of the electromagnetic spectrum. The most obvious advantage of MROI sensors is their high repetition rate and the possibility of near real time access to data. Hence, in terms of logistics, this makes MROI data highly suitable for regular and efficient SCA mapping. Although spatial resolution of MROI sensors limit the application to large basins, snow cover mapping at regional or larger scales can again be benefited from wide area coverage and low data cost.

Studies performed in literature indicate the effective use of medium optical imagery satellites. Among the available MROI sensors, AVHRR has been utilized for the longest time and in the largest number of studies dealing with SCA mapping. Snow cover maps of the Northern Hemisphere have been available since 1966 from the National Oceanic and Atmospheric Administration (NOAA, URL-1). Snow cover maps derived from NOAA-AVHRR are commonly used from small scale area analysis. More detailed maps for larger scale studies are deduced from the high resolution multi-spectral sensors such as on board of Landsat or SPOT satellites. The recently launched Moderate Resolution Imaging Spectroradiometer (MODIS) by NASA as part of the first Earth Observing System (EOS) platform is of special interest for snow hydrology with respect to global and continental surveys. This sensor is discussed in more detail in the following section.

## 5.5 Moderate Resolution Imaging Spectroradiometer (MODIS)

Earth Observation System (EOS) launched the Moderate Resolution Imaging Spectroradiometer (MODIS) instruments, on the Terra platform in 18 December 1999 and on the Aqua platform in 4 May 2002. MODIS provides imagery of the Earth's surface and clouds in 36 discrete, narrow spectral bands from approximately 0.4 to 14 μm in wavelengths with a temporal resolution of near to one day and spatial resolution of 250 m (bands 1-2), 500 m (bands 3-7) and 1000 m (bands 8-36). Table 5.4 shows the 36 discrete MODIS bands and their corresponding Landsat TM and NOAA-AVHRR bands. The EOS project is designed to observe and monitor the surface of the Earth for 15 years in order to differentiate short-term and long-term trends, as well as, regional and global phenomena.

MODIS has a very comprehensive workforce behind it consisting of several universities and organizations around the world under the directives of NASA. MODIS Science Team is divided into four discipline groups: Atmosphere, Calibration, Land and Ocean under which 44 standard MODIS data products are generated. A MODIS data product summary chart is shown in Table 5.5. Among the many MODIS products, MODIS snow and ice products are distributed through the National Snow and Ice Data center (URL-5) Distributed Active Archive Center (DAAC) at the University of Colorado in Boulder, Colorado since September 2000.

With the increased spectral band number and daily global 500 m spatial resolution offered by MODIS, MODIS snow cover products are prone to improve and/or enhance the currently available operational products (Hall et al., 2002) such as NOAA-AVHRR. Also, daily as well as 8-day composite snow cover maps are produced. Main distinguishing characteristics of MODIS snow data is the fact that the processing chain is automated thus reducing or eliminating biases due to human subjectivity. This enables the production of a consistent data set required for long-term climate studies. Moreover, the quality assurance (QA) information embedded within the data set is very informative about the snow extent.

Table 5.4 MODIS band centers and corresponding Landsat TM and NOAA-AVHRR bands. (Hall et al., 1998)

| MODIS band | Center Wavelength (μm) | Spatial Res.(m) | TM band | AVHRR band |
|---|---|---|---|---|
| 1 | 0.645 | 250 | | 1 |
| 2 | 0.858 | 250 | 4 | 2 |
| 3 | 0.469 | 500 | 1 | |
| 4 | 0.555 | 500 | 2 | |
| 5 | 1.240 | 500 | | |
| 6 | 1.640 | 500 | 5 | |
| 7 | 2.130 | 500 | 7 | |
| 8 | 0.412 | 1000 | | |
| 9 | 0.443 | 1000 | | |
| 10 | 0.488 | 1000 | | |
| 11 | 0.531 | 1000 | | |
| 12 | 0.551 | 1000 | | |
| 13 | 0.667 | 1000 | 3 | 1 |
| 14 | 0.678 | 1000 | 3 | 1 |
| 15 | 0.748 | 1000 | | 2 |
| 16 | 0.869 | 1000 | 4 | 2 |
| 17 | 0.905 | 1000 | | 2 |
| 18 | 0.936 | 1000 | | 2 |
| 19 | 0.940 | 1000 | | 2 |
| 20 | 3.750 | 1000 | | 3 |
| 21 | 3.959 | 1000 | | 3 |
| 22 | 3.959 | 1000 | | |
| 23 | 4.050 | 1000 | | |
| 24 | 4.465 | 1000 | | |
| 25 | 4.515 | 1000 | | |
| 26 | 1.375 | 1000 | | |
| 27 | 6.715 | 1000 | | |
| 28 | 7.325 | 1000 | | |
| 29 | 8.550 | 1000 | | |
| 30 | 9.730 | 1000 | | |
| 31 | 11.030 | 1000 | 6 | 4/5 |
| 32 | 12.020 | 1000 | | 5 |
| 33 | 13.335 | 1000 | | |
| 34 | 13.635 | 1000 | | |
| 35 | 13.935 | 1000 | | |
| 36 | 14.235 | 1000 | | |

## 5.5.1 MODIS File Format

Hierarchical Data Format – Earth Observation System (HDF-EOS) is the standard format for EOS-Data Information System (EOSDIS) products. The snow product files contain two layers, which are namely, the meta data including the attributes and the Scientific Data Sets (SDS) including the data arrays.

Table 5.5 MODIS data product summary chart

**Calibration**
MOD 01 - Level-1A Radiance Counts
MOD 02 - Level-1B Calibrated Geolocated Radiances
MOD 03 - Geolocation Data Set

**Atmosphere**
MOD 04 - Aerosol Product
MOD 05 - Total Precipitable Water (Water Vapor)
MOD 06 - Cloud Product
MOD 07 - Atmospheric Profiles
MOD 08 - Gridded Atmospheric Product
MOD 35 - Cloud Mask

**Land**
MOD 09 - Surface Reflectance
MOD 10 - Snow Cover
MOD 11 - Land Surface Temperature & Emissivity
MOD 12 - Land Cover/Land Cover Change
MOD 13 - Gridded Vegetation Indices (Max NDVI & Integrated MVI)
MOD 14 - Thermail Anomalies, Fires & Biomass Burning
MOD 15 - Leaf Area Index & FPAR
MOD 16 - Evapotranspiration
MOD 17 - Net Photosynthesis and Primary Productivity
MOD 29 - Sea Ice Cover
MOD 43 - Surface Reflectance BRDF/Albedo Parameter
MOD 44 - Vegetation Cover Conversion

**Ocean**
MOD 18 - Normalized Water-leaving Radiance
MOD 19 - Pigment Concentration
MOD 20 - Chlorophyll Fluorescence
MOD 21 - Chlorophyll_a Pigment Concentration
MOD 22 - Photosynthetically Available Radiation (PAR)
MOD 23 - Suspended-Solids Concentration
MOD 24 - Organic Matter Concentration
MOD 25 - Coccolith Concentration
MOD 26 - Ocean Water Attenuation Coefficient
MOD 27 - Ocean Primary Productivity
MOD 28 - Sea Surface Temperature
MOD 31 - Phycoerythrin Concentration
MOD 36 - Total Absorption Coefficient
MOD 37 - Ocean Aerosol Properties
MOD 39 - Clear Water Epsilon

## 5.5.2 MODIS Snow Products

MODIS snow products are provided as a sequence of products beginning with a swath (scene) and progressing through spatial and temporal transformations to an 8-day gridded product (Riggs et al., 2003). A summary of the six different MODIS snow data products are shown in Table 5.6.

Table 5.6 Summary of the MODIS snow data products

| Earth Science Data Type (ESDT)* | Product Level | Nominal Data Array Dimensions | Spatial Resolution | Temporal Resolution | Map Projection |
|---|---|---|---|---|---|
| MOD10_L2 | L2 | 1354 km by 2000 km | 500 m | swath(scene) | None |
| MOD10L2G | L2G | 1200 km by 1200 km | 500 m | $n^{th}$ day | Sinusoidal |
| MOD10A1 | L3 | 1200 km by 1200 km | 500 m | day | Sinusoidal |
| MOD10A2 | L3 | 1200 km by 1200 km | 500 m | 8-day | Sinusoidal |
| MOD10C1 | L3 | $360^{o}$ by $180^{o}$ (global) | $0.05^{o}$ | day | Geographic |
| MOD10C2 | L3 | $360^{o}$ by $180^{o}$ (global) | $0.05^{o}$ | 8-day | Geographic |

ESDT*: short name used for identifying snow data product

The MODIS snow maps will augment the valuable record of Northern Hemisphere snow cover that was started in 1966 by NOAA which provided weekly maps (Matson et al., 1986) and continues today with the daily snow products from the Interactive Snow and Ice Mapping System (IMS) (Ramsay, 1998).

## 5.5.3 MODIS Snow Detection Algorithm

The MODIS snow mapping (Snowmap) and ice mapping (Icemap) algorithms identify snow, lake ice and sea ice by their reflectance and emittance properties and generate global daily and 8-day composited snow/ice cover products. The basic techniques used in these algorithms are threshold-based criteria tests, the normalized difference between bands and decision rules. MODIS bands 1, 2, 4, 6, 31 and 32 are the main inputs to the snow cover algorithm.

The MODIS snow mapping is a fully automated algorithm that is based on Normalized Difference Snow Index (NDSI) and a set of thresholds. The NDSI is useful for the identification of snow and ice for separating snow/ice and most cumulus clouds. The NDSI is a measure of the relative magnitude of the characteristic reflectance difference between the visible and short infrared reflectance of snow as shown in Equation 5.1.

$$NDSI = \frac{(MODIS)\,Band\,4 - (MODIS)\,Band\,6}{(MODIS)\,Band\,4 + (MODIS)\,Band\,6} \qquad \text{Equation 5.1}$$

The NDSI is insensitive to a wide range of illumination conditions, is partially normalized for atmospheric effects and does not depend on the reflectance in a single band (Hall et al., 2001).

The high reflectance of snow in the visible compared to mid-infrared portion of the spectrum yields high NDSI values for snow compared to other surface materials. After numerous comparison tests with Landsat-TM scenes, the NDSI threshold is set to be greater than 0.4 for snow. Since water may also have an NDSI $\geq$ 0.4, an additional test is necessary to separate water from snow. Snow and water may be discriminated by MODIS Band 2 (0.841-0.876 $\mu$m) test. If MODIS Band 2 reflectance is $\geq$ 11% and NDSI $\geq$ 0.4 then the pixel is initially mapped as snow.

Forests are among the dark objects that cause a classification problem in NDSI because many snow covered pixels in forested areas have an NDSI lower than 0.4. To eliminate this confusion Normalized Difference Vegetation Index (NDVI) (Tucker, 1979; Tucker, 1986 and Townshend and Tucker, 1984), which has been proven to be an effective method for monitoring global vegetation conditions throughout a year, is utilized. The NDVI for MODIS is calculated using Band 1 and Band 2 as shown in Equation 5.2.

$$NDVI = \frac{(MODIS)\,Band\,2 - (MODIS)\,Band\,1}{(MODIS)\,Band\,2 + (MODIS)\,Band\,1} \qquad \text{Equation 5.2}$$

High values of NDVI indicate healthy and denser vegetation. Thus by using the NDVI and NDSI in combination, it is possible to lower the NDSI threshold in forested areas without compromising the algorithm performance in other land covers (Hall et al., 2001). If a pixel has NDSI and NDVI values within an irregular polygon as determined from canopy-reflectance modeling as discussed in Klein et al. (1998), it is mapped as snow.

To improve the snow mapping accuracy and eliminating the spurious snow, especially from cloud intrusion, aerosol effects, snow/sand confusion on coastlines, a thermal mask was implemented in fall of 2001. A split window technique using MODIS Band 31 (10.78-11.28 $\mu$m) and Band 32 (11.77-12.27 $\mu$m) is performed to estimate surface temperature values. A pixel is not mapped as snow if the estimated surface temperature is greater than 277°K. It is reported that this technique has improved the snow covered area especially in warm tropical regions (Hall et al., 2001).

MODIS snow algorithm is executed on land and inland lake pixels. In this content, oceans are skipped using the land/water mask in MODIS geolocation product MOD03. Also Snowmap is applied to pixels that have a clear view of the surface. Clouds are masked using MODIS cloud mask data product MOD35 (Riggs et al., 2003).

For further details on MODIS technical specifications, data products, algorithms and ordering, one may refer to Hall et al. (2001), Hall et al. (2002), Riggs et al. (2003) and MODIS internet web page (MODIS, URL-6).

## 5.6 Geographic Information Systems in Remote Sensing

In order for the application of remote sensing to be successful, key ancillary support systems must be available. Beyond the initial computer data processing of the digital remote sensing imagery, Geographic Information Systems (GIS) are used to supply all other important spatial, temporal and statistical information at low cost to further integrate and analyze the remote sensing data with relative ease (WMO, 1999a).

A GIS is an organized collection of computer hardware, software and geographic data designed to efficiently capture, store, update, manipulate, analyze and display all forms of geographically referenced information (Johnson et al., 1992). The information pertaining to various spatial or temporal features are stored typically as attributes in tabular files linked to the feature, often in special database management systems (DBMS).

GIS is extensively used to delinate drainage systems either from a DEM (Digital Elevation Model) or TIN (Triangulated Irregular Network) for any location and then quantify the characteristics of that system. Watersheds, stream networks, slope, aspect and many other topographic characteristics can be generated to assist in the analysis of remotely sensed images. For example, when a basin is only partially obscured by cloud, it is possible to extrapolate snow cover information from cloud-free areas to cloud covered areas by equating areas of similar elevation, aspect and slope (Rango, 1996).

RS and GIS are both tools for managing spatially distributed information in large quantities and at a variety of scales. Both increase the capabilities of human decision maker and planners to grasp relationships at larger scales and in more complex settings than has been possible before.

Processing of remote sensing data is getting less expensive since technical tools for multi-spectral image analysis and management of results using Geographic Information Systems are commonly available. In addition, the availability of Earth Observation data on a global scale with reasonable time and ground resolutions is steadily increasing.

GIS coupled with remote sensing is a well-established tool and routinely used in applied hydrology today. Results of the analysis give a digital representation of the temporal and spatial variations of selected variables (e.g. snow cover, vegetation) and can serve as input into hydrological models.

# CHAPTER 6

# HBV MODEL APPLICATION

## 6.1 Introduction

The expanding use and increased complexity of hydrological runoff models has given rise to a concern about overparameterization and risks for compensating errors. In this sense, an accurate simulation of runoff is no guarantee for correctly estimated internal variables of a conceptual model. An error in the description of one process may be compensated by an error in another part of the model. One proposed way out is the calibration and validation against additional observations, such as snow, soil moisture, groundwater or water quality.

The HBV model was initially intended for runoff simulation and hydrological forecasting, but as the scope of applications grew rapidly, the physical credibility of the model became critical. Some of these applications were focused on site-specific details in the water balance, which opened opportunities for internal validation of the model (Bergström et al., 2002). It became important to make sure that the model was not 'right for the wrong reason' (Klemes, 1986).

The Nordic HBV model (Saelthun, 1996) used in this study is a modified version of the HBV model (Bergström, 1992) developed for the Nordic project "Climate Change and Energy Production" as a synthesis of several versions used in different Nordic countries. The model structure is a sequence of three submodels for snow, soil and response with a usual daily time step as described in Chapter 3. The model is divided into ten elevation intervals and the observed model inputs are precipitation, temperature and potential evapotranspiration. The main output from

the simulations is runoff, but snow pack and snow covered area for each elevation interval can also be simulated. The HBV model is applied to Kırkgöze Basin in Upper Euphrates River, where details are provided in the following section, as a pioneer application of the model in Turkey.

Since HBV model is a semi-distributed conceptual hydrologic model with several parameters, it needs calibration. In this section of the thesis, determination of the confined model parameters as well as calibration of the specified free parameters in the model is undertaken. A multi-variable calibration procedure, using optical satellite derived snow covered area data as well as runoff, in the HBV model application is tested to assess if internal simulations of the model could be improved without deteriorating the runoff results. In this sense, Earth Observation data can play a valuable role to increase the confidence in the model performance.

## 6.2 Basin Description

Kırkgöze basin, located at the headwaters of Karasu basin as shown in Figure 6.1 with the outlet DSI 21-01 under the supervision of General Directorate of State Hydraulic Works, is selected as the test area in this study. Kırkgöze basin has an area of 242.42 km$^2$ and an elevation range from 1830 m to 3140 m as shown on a Digital Elevation Model (DEM), Figure 6.1, derived from 1:25,000 scaled contour maps using GIS spatial analysis. The median elevation in the basin is calculated around 2342 m. Figure 6.2 depicts the slope map of the basin which has a mean total slope of 24.6%. In terms of aspect, 20.8% is facing north, 22.1% is facing east, 23.4% is facing south, 30.7% is facing west and 3.0% is on a flat surface in Kırkgöze basin as presented in Figure 6.3. For a better visual understanding of the site, a 3-dimensional view of the basin is shown in Figure 6.4. A land use map of the area is generated by performing a hierarchical classification technique on a Landsat TM June 2000 satellite image (Akyürek and Şorman, 2002) as shown in Figure 6.5. Most of the area is pasture (86%) along with bare land and forest contributing 7% and 4% respectively to the basin. The general climatologic

conditions indicate a cold, dry and windy area which can also be observed by the figures given in Chapter 4.

The main reasons for concentrating on this certain basin rather than the whole Karasu basin is that there is no significant human interaction to the catchment either from urbanization or reservoir regulation. Although the basin can be considered as small in terms of scale, it has a large elevation difference that makes it possible to conduct a snow study. Finally, Kırkgöze basin is located close to the city of Erzurum and therefore the region is accessible to reach at regular intervals.
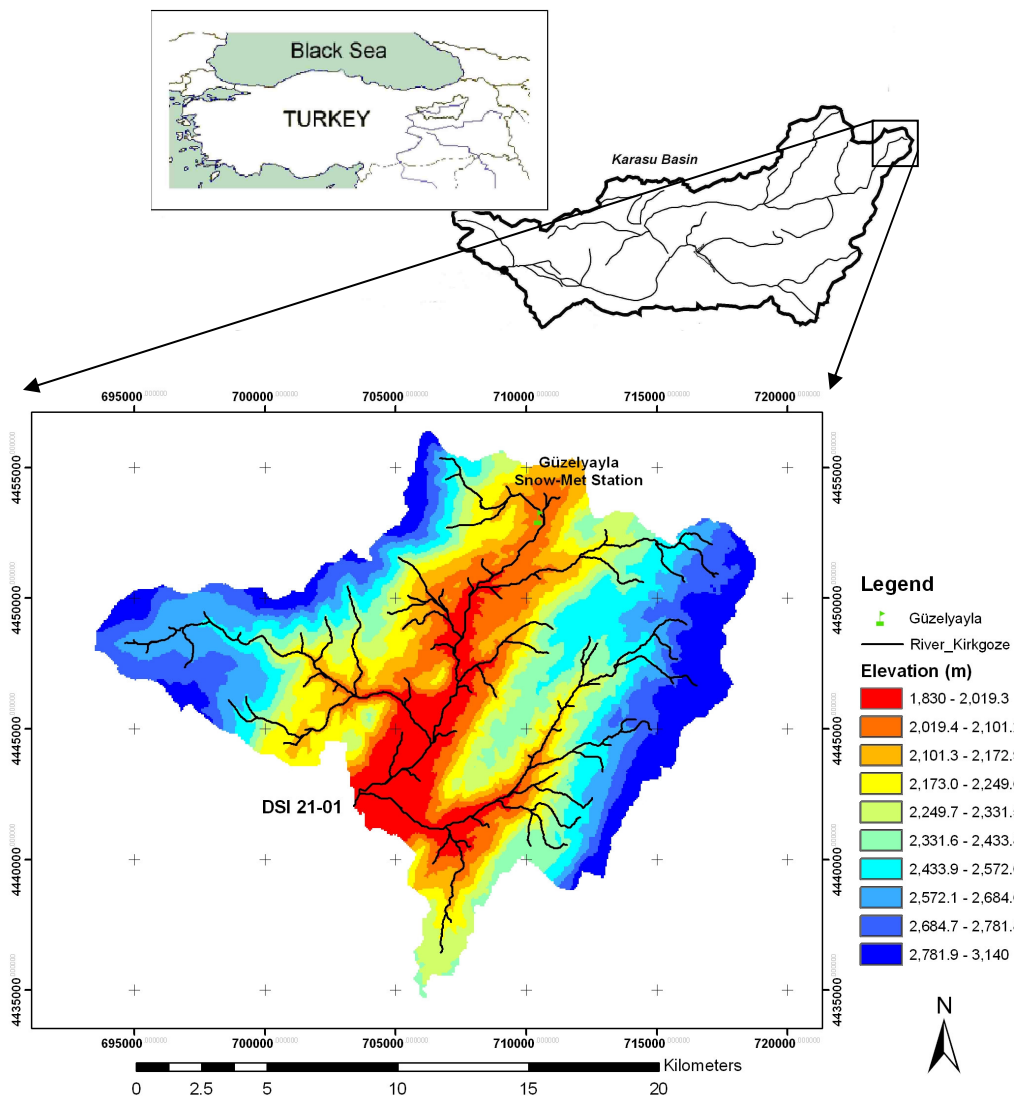


Figure 6.1 Location and Digital Elevation Model of Kırkgöze Basin
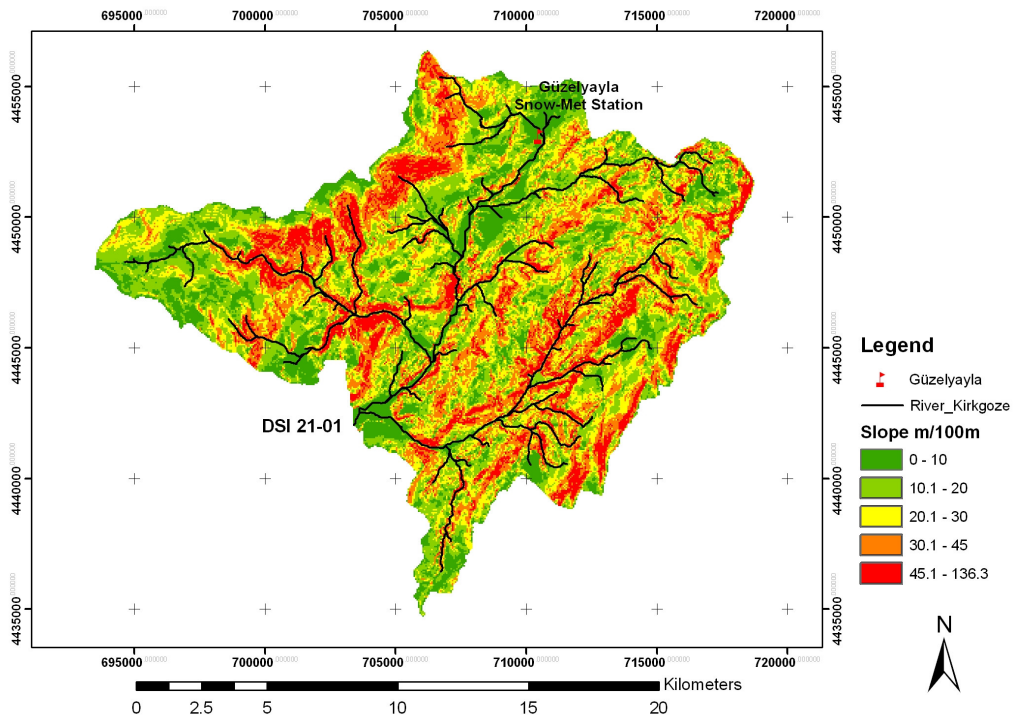
Figure 6.2 Slope map of Kırkgöze Basin
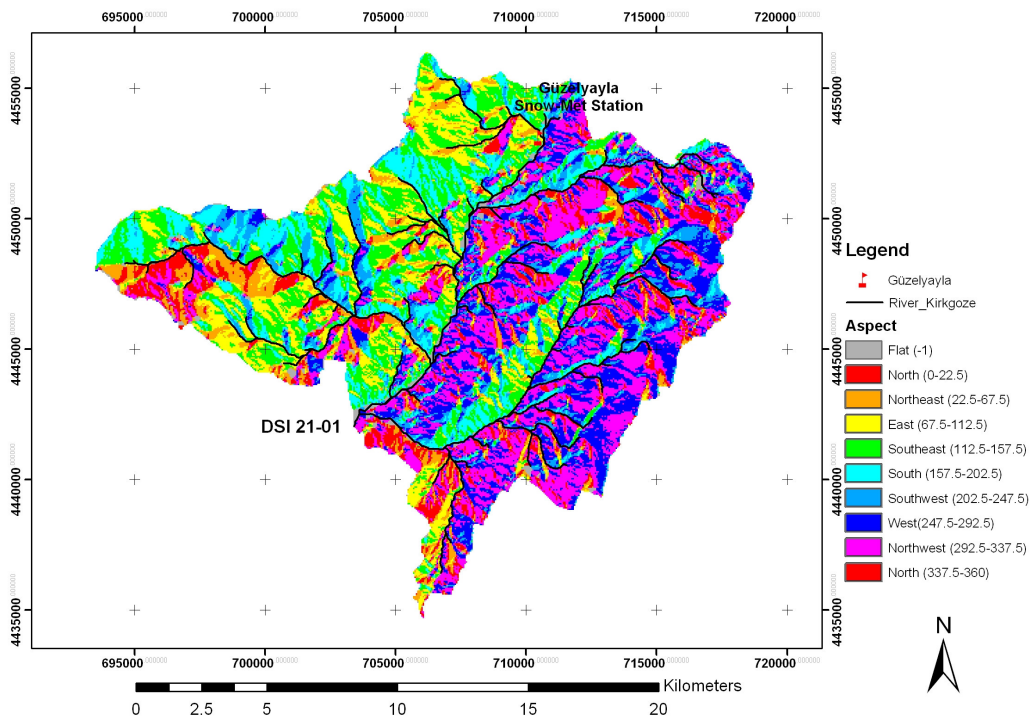


Figure 6.3 Aspect map of Kırkgöze Basin
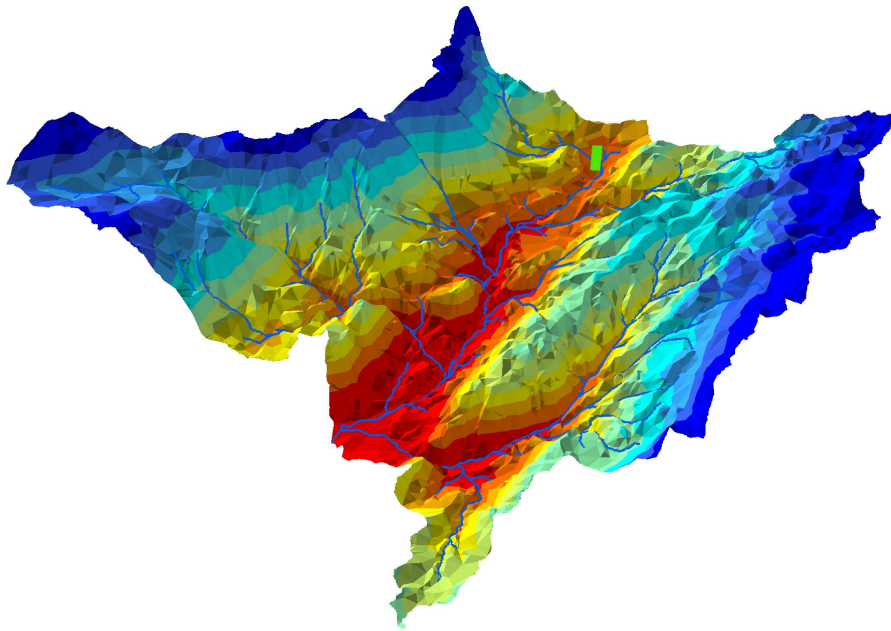
Figure 6.4 3-dimensional view of Kırkgöze Basin



Legend

Wkirkgoze_basin

**Class_Names**

- bare land
- buit-up area
- fallow
- forest
- grass-high GWT
- irrigated
- pasture
- poor pasture
- road
- unclassified
- water
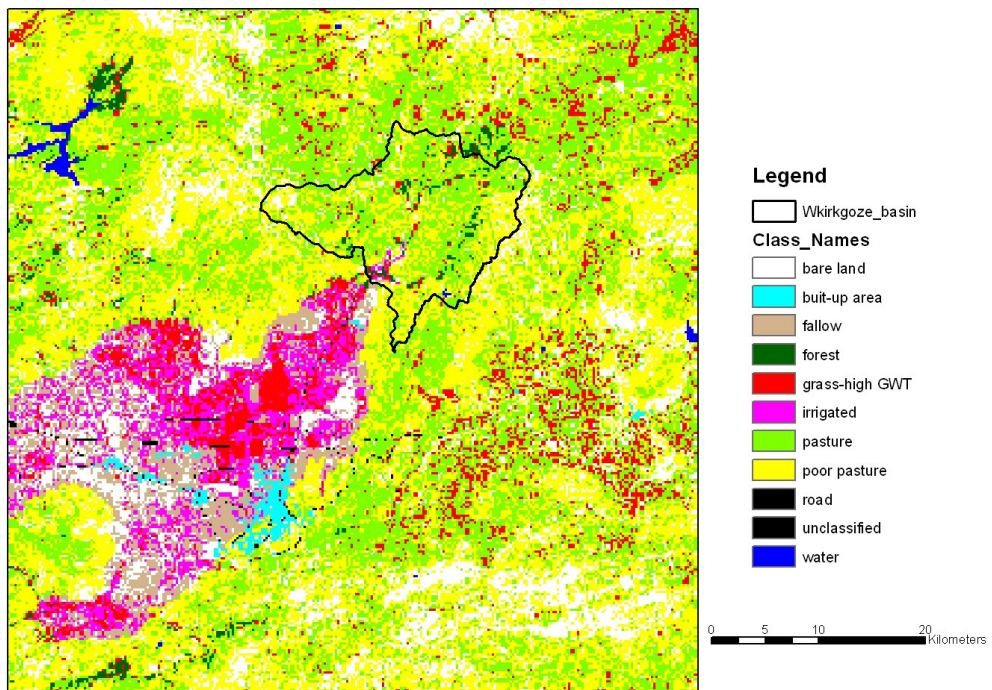
Figure 6.5 Land cover classes for Kırkgöze Basin derived from Landsat TM image, June 2000

## 6.3 Hydro-meteorological Data

Güzelyayla snow and meteorological station is located within Kırkgöze basin as seen in Figure 6.1. This automatic station measures several snow and meteorological variables every 30 seconds and records the averages of these measurements every 2 and 24 hours. Since there are no synoptic or climate stations in the catchment operated by the governmental organizations, mean daily temperature and total precipitation data for the HBV model is used only from Güzelyayla station.

Discharge data for Kırkgöze basin is supplied from DSI 21-01 stream gaging station which is positioned at the outlet of the basin. Both a shaft encoder and pressure transducer equipment measure the stages at the outlet which are converted into discharge values using rating curves updated frequently.

Table 6.1 summarizes the hydrometeorological data (precipitation, temperature and discharge) used for modeling in Kırkgöze basin.

Table 6.1 Hydro-meteorological data used for modeling in Kırkgöze basin
(P: Precipitation, T: Temperature, Q: Discharge)

| Station Name | Type | Parameters | Start Year | Latitude Longitude | Elevation (m) |
|---|---|---|---|---|---|
| Güzelyayla | Snow and Meteorological | P, T | 2001 | 40° 12′ 01″ N 41° 28′ 22″ E | 2065 |
| Kırkgöze | Stream Gaging | Q | 1963 | 40° 05′ 51″ N 41° 22′ 59″ E | 1830 |

## 6.4 Snow Cover Data

The Earth Observation data used in the study are daily MODIS snow products MOD10A1, details given in Chapter 5, downloaded from National Snow and Ice Data Center (NSIDC, URL-5), Boulder, Colorado, USA, through file transfer protocol (ftp). MODIS images are stored in tiles as shown in Figure 6.6 and the study area corresponds to a single tile namely, h21v04. Downloaded images are then processed using MODIS Reprojections Tools (MRT, URL-7) software to define the projection, cell size and if needed to mosaic several other tiles. Using MRT software, MODIS MOD10A1 products are reprojected into World Geodetic System 1984 (WGS84) Universal Transverse Mercator (UTM) Zone 37 projection system which is originally Sinusoidal. The spatial resolution of the product is kept as 500 m as default and since there is only one MODIS tile used, no mosaicking is performed.
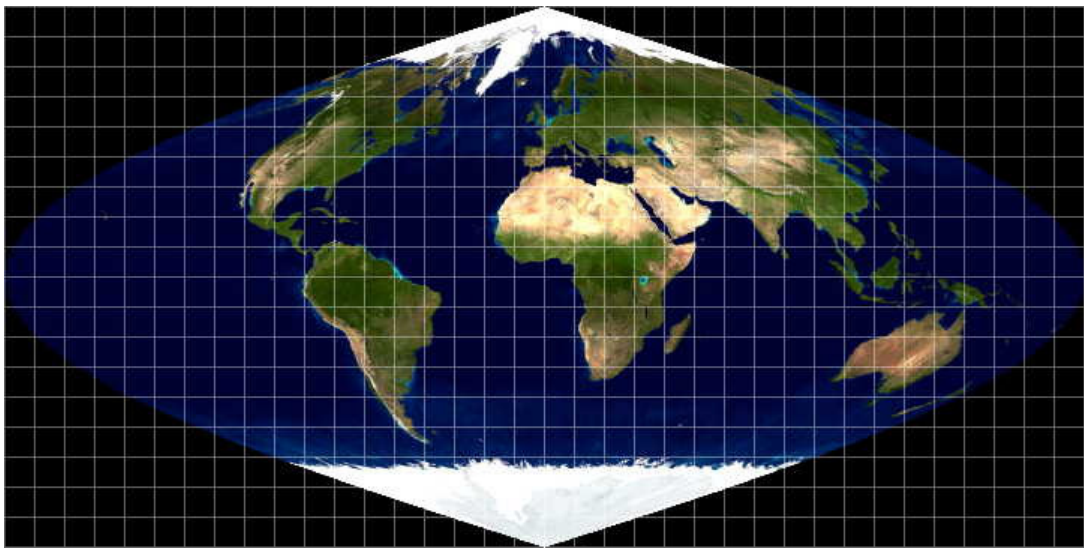


Figure 6.6 View of MODIS tiles

Three melt seasons, 2002, 2003 and 2004 are chosen for comparison of HBV snowpack predictions with snow cover maps derived from MODIS satellite. This is mainly because there are no reliable temperature and precipitation data within the region before this time since Güzelyayla station was installed in late 2001. Also, even there were meteorological data for the area of study, MODIS satellite images are only present from September 2000 since MODIS is one of the recent satellites in space. Before this time, if snow covered area is the point of interest, other Medium Range Optical Instrumentation (MROI) satellites need to be used, one such example would be NOAA-AVHRR which is not as superior as MODIS in terms of spatial and spectral resolution.

Daily images from the three melt periods, 2002, 2003 and 2004 are processed using MRT software which are later imported into ERDAS Imagine software. With a module written in Spatial Modeler of ERDAS Imagine software, the 8-bit continuous MODIS image is converted into a thematic snow cover product with names and color attributes. The thematic snow cover product of the whole MODIS tile is cut for the area of interest which is Kırkgöze basin for an overlay analysis of snow, cloud and land cover percentages in the region for each daily image. Clear images from cloud coverage are preferred to be used in modeling, hence images that have cloud cover less than 25% are processed as a first step that correspond to a period just before, during and just after all the snow has melted. A total of 28 images in 2002, 20 images in 2003 and 27 images in 2004 are classified with the above given criteria. Afterwards, these images are further decreased in number because of a stricter criterion in which images that fall into only the main mid-melting period, excluding beginning and ending snowmelt periods, as well as a cloud cover percentage of less than around 10-15% is preferred. The reasons for the second criteria are that a model can easily simulate the beginning and ending of the melt periods but may have problems within this portion and also a further clear image from clouds is more reliable. Hence in the end, 6 images in 2002, 6 images in 2003 and 7 images in 2004 are selected to be used for snow covered area determination in Kırkgöze basin. Finalized image dates with snow and cloud cover percentages are tabulated in Table 6.2 and are depicted in Figure 6.7.

Table 6.2 Dates with cloud and snow coverage for the available classified MODIS images in Kırgöze basin.

| 2002 (6 images) | | | 2003 (6 images) | | | 2004 (7 images) | | |
|---|---|---|---|---|---|---|---|---|
| Date | Cloud % | Snow % | Date | Cloud % | Snow % | Date | Cloud % | Snow % |
| 13-Apr-02 | 7.7 | 88.0 | 11-Apr-03 | 9.2 | 75.7 | 25-Mar-04 | 6.6 | 89.0 |
| 29-Apr-02 | 1.9 | 47.6 | 13-Apr-03 | 3.4 | 55.5 | 8-Apr-04 | 11.7 | 77.4 |
| 7-May-02 | 1.1 | 36.8 | 2-May-03 | 6.7 | 34.7 | 9-Apr-04 | 7.3 | 65.8 |
| 20-May-02 | 0.0 | 24.9 | 3-May-03 | 0.1 | 28.8 | 18-Apr-04 | 16.6 | 70.2 |
| 27-May-02 | 0.0 | 11.8 | 9-May-03 | 2.3 | 20.6 | 26-Apr-04 | 6.7 | 42.7 |
| 7-Jun-02 | 2.2 | 4.6 | 13-May-03 | 3.5 | 9.2 | 22-May-04 | 11.2 | 18.7 |
| | | | | | | 1-Jun-04 | 11.6 | 7.6 |

As mentioned by Klein et al. (1998), Metsamaki et al. (2002) and Vikhamar and Solberg (2003), remote sensing of the snow pack works best for open areas. Since the basin under study does not contain a dense vegetation land cover, there is no need to mask out an area where remote sensing images can give erroneous results.
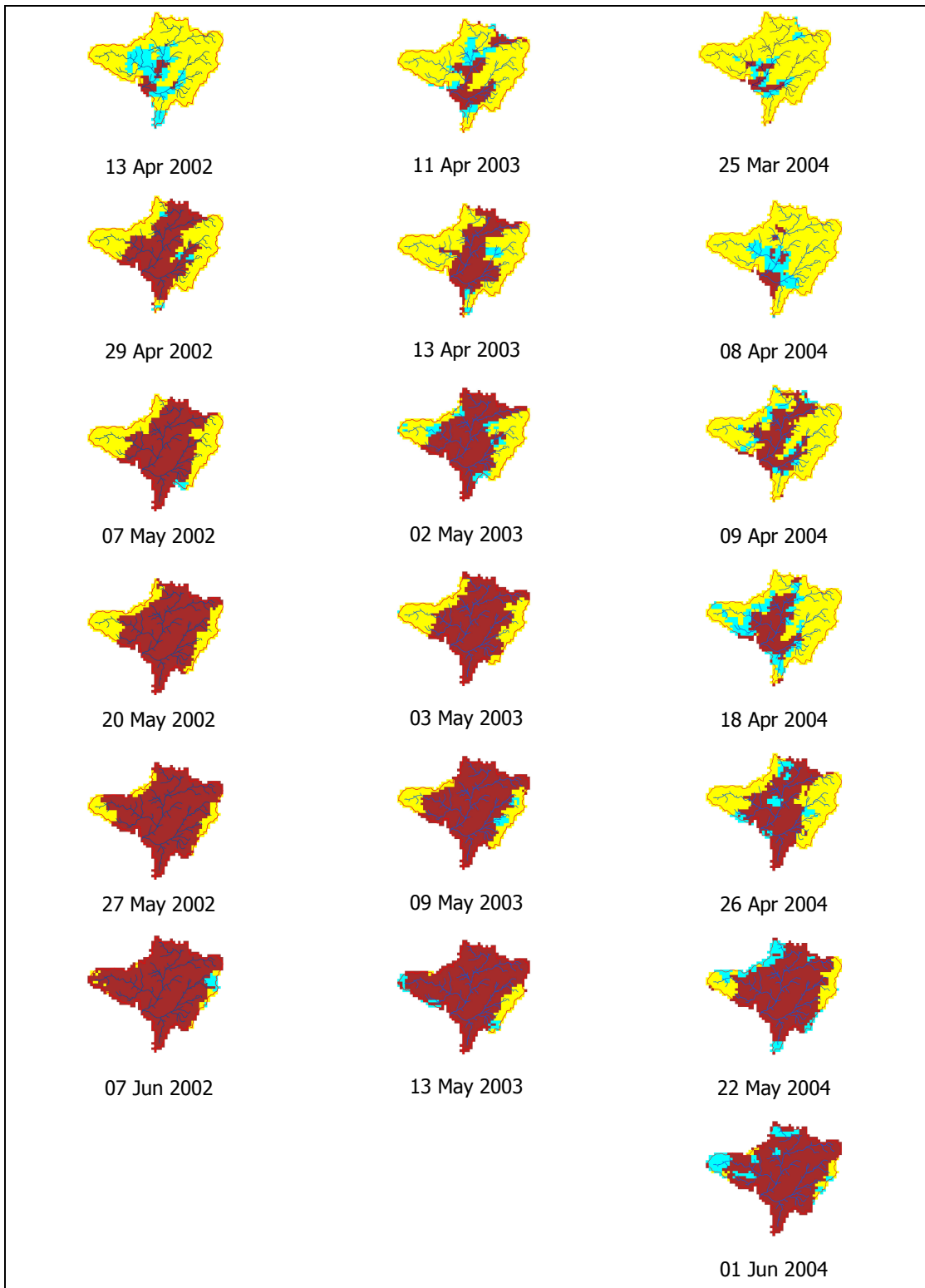
Figure 6.7 Classified MODIS images from the study period (yellow=snow, brown=land, blue=cloud or unclassified).

## 6.5 Model Parameters

As described in Chapter 3, HBV model parameters consist of two categories named as confined and free parameters. Confined parameters are values that are provided to the model once and never changed whereas free parameters must be determined by a process of calibration.

## 6.5.1  Confined Model Parameters

The confined parameters of HBV model are listed and further discussed below:

❋  Area and area-elevation curve
❋  Potential monthly evapotranspiration
❋  Land use and vegetation (land cover)
❋  Initial conditions

<u>Area and Area-Elevation Curve</u>

Through the use of GIS analysis, several basin characteristics are determined as shown in Figure 6.1 through Figure 6.4. In this sense, the area of the basin is calculated as 242.42 km$^2$ and the area-elevation (hypsometric) curve is computed using the Digital Elevation Model (DEM) of Kırkgöze basin given in Figure 6.8. Since HBV model requires the basin to be described in ten equal percentage elevation intervals, this process is done using a GIS query and tabulated in Table 6.3 along with their slope values in percentage.
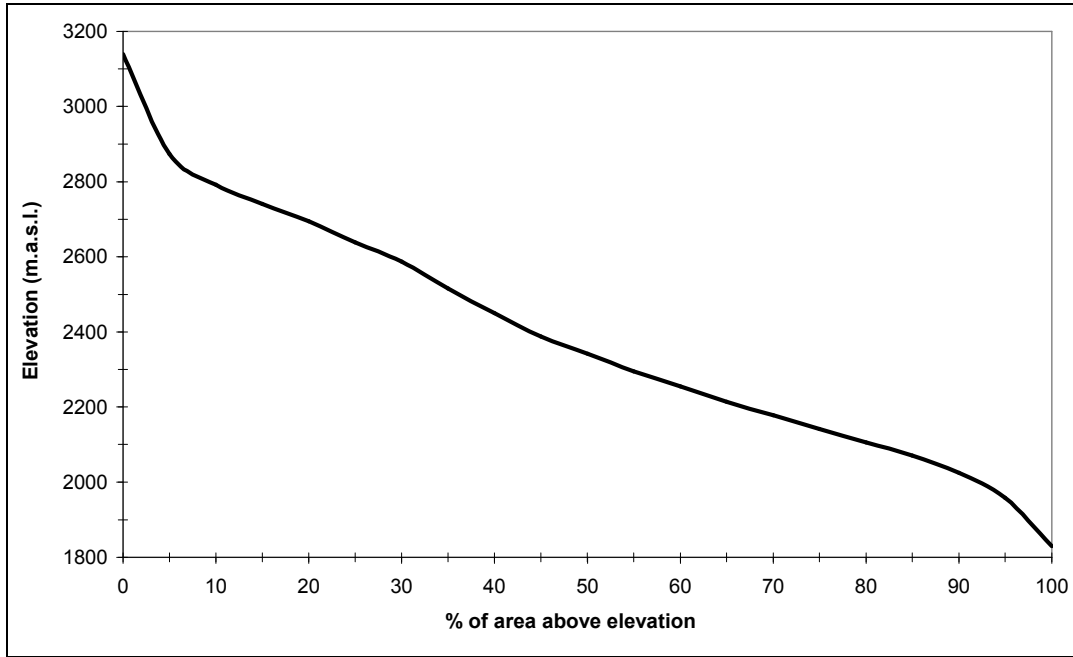
Figure 6.8 Hypsometric curve of Kırkgöze Basin

Table 6.3 Ten equal elevation intervals of Kırkgöze basin and their corresponding slope values

| Basin Area (%) | Elevation Range (m) | Slope (%) |
|---|---|---|
| 0 - 10 | 1830 - 2026 | 19.66 |
| 10 - 20 | 2026 - 2107 | 21.32 |
| 20 - 30 | 2107 - 2178 | 23.78 |
| 30 - 40 | 2178 - 2254 | 24.91 |
| 40 - 50 | 2254 - 2342 | 26.41 |
| 50 - 60 | 2342 - 2440 | 27.90 |
| 60 - 70 | 2440 - 2589 | 30.32 |
| 70 - 80 | 2589 -2692 | 25.12 |
| 80 - 90 | 2692 -2791 | 20.94 |
| 90 - 100 | 2791 - 3140 | 25.41 |
| **0 - 100** | **1830 - 3140** | **24.62** |

Potential Monthly Evapotranspiration

Evapotranspiration is the term used to describe the two almost inseparable processes of evaporation (physical process of the conversion of liquid water to water in a vapour form) and transpiration (loss of water by plants). The maximum and actual rates of evapotranspiration are called potential and actual evapotranspiration respectively. In the determination of potential evaporation, Thornthwaite (1948), Blaney-Criddle (1950) and Penman (1956) as cited in Usul (2001) are some of the most well known methods.

The potential evapotranspiration for the HBV model is calculated in monthly terms using Thornthwaite and Blaney-Criddle formulae because of the simple and reliable applicability of the two methods. The results of the two approaches were quite similar for each month hence an average is calculated and given in Table 6.4.

Table 6.4 Monthly potential evapotranspiration (PET) used in the HBV model

| Month | Oct | Nov | Dec | Jan | Feb | Mar | Apr | May | Jun | Jul | Aug | Sep |
|---|---|---|---|---|---|---|---|---|---|---|---|---|
| PET (mm/month) | 35 | 9 | 2.5 | 2.5 | 2.5 | 9 | 30 | 65 | 85 | 95 | 95 | 70 |

Land Cover

The land cover classes are determined by performing a hierarchical classification technique on a Landsat TM June 2000 satellite image (Akyürek and Şorman, 2002) as shown in Figure 6.5. There are more land cover classes in this classification than HBV model can recognize, therefore, they are joined into four classes which are field, forest, lake and glacier to be used as input into the HBV model. With this grouping, there are no lake or glacier components whereas 96% of the area is considered as field and the rest 4% is taken as forest in the model.

Table 6.5 Study catchment characteristics

| Catchment | River | Area (km²) | Elevation (m a.s.l) | | | Field (%) | Forest (%) | Lake (%) | Glacier (%) |
|---|---|---|---|---|---|---|---|---|---|
| | | | Median | Max | Min | | | | |
| DSI 21-01 Kırkgöze | Karasu | 242.42 | 2342 | 3140 | 1830 | 96 | 4 | 0 | 0 |

<u>Initial Conditions</u>

Contents of the HBV model storages (upper and lower) at the beginning of simulation periods are important but generally unknown values. In literature, generally two methods are used to prevent problems linked to inappropriate initial conditions so as not to jeopardize the simulations. First, the initial levels in model storages are set to average seasonal values for the corresponding time of the year. Second, a warm-up period, a few months to a year are common values, is inserted at the beginning of each simulation period to attenuate the effect of the storage initialization (Seibert, 1997; Uhlenbrook, 1999; Perrin, 2001). Model results for the warm-up period are ignored in the computation of goodness-of-fit criteria.

In this study, both methods are tried to be applied. Firstly, several runs are performed to determine the seasonal average conditions in the basin and then each simulation period is also given a warm-up period of nearly half a month. A longer warm-up period would not be practical to use in this case because already not a long simulation period is present for model calibration (3 years of data).

## 6.5.2  Free Model Parameters

Being a general hydrological model that can simulate both rainfall and snowfall, HBV model has quite a number of free parameters to adjust for calibration. These parameters are listed in Table 3.1. Although HBV is a conceptual model, most of its parameters do have a physical meaning. Therefore, in order to calibrate the free parameters of the model if there are measurements related to the model

parameters, these parameters are rather taken as fixed values to decrease the number of calibrable parameters in the model and hence the uncertainty.

As the HBV model is highly-overparameterized, standard values are assigned to some of the calibration parameters in this study. Internal model parameters, like maximum content of liquid water (LV) and the refreezing coefficient (CFR), are not calibrated and literature based values are used since they are not very sensitive free parameters. The number of model parameters to be calibrated with their default values and feasible parameter space are given in Table 6.6.

## 6.6 Automatic Calibration Routine coupled with HBV Model

Once all the confined parameters are calculated and those less sensitive free parameters are decided upon, the rest of the free parameters need to be calibrated. As discussed in Chapter 3, this procedure can either be done manually or in an automatic manner. In this study, an automatic calibration technique is utilized to determine the selected 16 free parameters in HBV model. The automatic calibration is carried out by an independent computer package outside the HBV model using two different search methods namely GML (Gauss-Marquardt-Levenberg) and SCE_UA (Shuffled Complex Evolution, University of Arizona) which are discussed in the following sections.

Table 6.6 HBV model free parameters with their upper and lower ranges and assigned default values for calibration

| Name | Meaning | Default value | Value range Min | Max | Units |
|------|---------|---------------|-----|-----|-------|
| Snow routine | | | | | |
| Tx | Threshold temperature for rain/snow | 0.0 | -2.5 | 2.5 | °C |
| Ts | Threshold temperature for snowmelt | 0.0 | -2.5 | 2.5 | °C |
| Cx | Degree-day factor | 3.5 | 1 | 7 | mm/°C/day |
| PKOR | Precipitation correction rainfall | 1.0 | 0.5 | 1.7 | --- |
| SKOR | Precipitation correction snowfall | 1.0 | 0.5 | 1.7 | --- |
| TTGD | Temperature lapse rate for clear days | - 0.6 | -1.1 | -0.3 | °C/100 m |
| TVGD | Temperature lapse rate during precipitation | - 0.4 | -0.8 | -0.2 | °C/100 m |
| PGRD | Precipitation lapse rate | 0.01 | 0.0 | 0.1 | --- |
| Soil routine | | | | | |
| FC | Field capacity in soil moisture zone | 250 | 50 | 450 | mm |
| LP | Threshold value for PET in soil moisture | 0.9 | 0.6 | 1.0 | frac. of FC |
| β | Parameter in soil moisture routine | 1.0 | 1.0 | 4.0 | --- |
| Response routine | | | | | |
| KUZ2 | Fast recession constant in Upper zone | 0.2 | 0.1 | 0.6 | 1/day |
| UZ | Threshold level for quick runoff in Upper zone | 20 | 5 | 65 | mm |
| KUZ1 | Slow recession constant in Upper zone | 0.1 | 0.01 | 0.3 | 1/day |
| PERC | Percolation from Upper to Lower zone | 0.9 | 0.5 | 2.0 | mm/day |
| KLZ | Recession constant in Lower zone | 0.001 | 0.0005 | 0.01 | 1/day |

## 6.6.1 Model-independent Parameter ESTimation (PEST)

PEST (an acronym for Parameter ESTimation) is a powerful nonlinear parameter estimation computer package, developed by Doherty et al. (1994) and later updated Doherty (2003, 2004) and, that exists independently of any particular model, yet can be applied to a wide range of model types.

The purpose of PEST is to assist in data interpretation, model calibration and predictive analysis. If there are field or laboratory measurements corresponding to model-generated numbers, PEST can adjust model parameter and/or excitation data until model-generated numbers fit a set of observations as closely as possible, provided certain continuity conditions are met. It will decrease the discrepancies between modeled and observed values to a minimum in the weighted least squares sense. It does this by taking control of the model and running it as many times as is necessary in order to determine this optimal set of parameters and/or excitations. The universal applicability of PEST lies in its ability to perform these tasks for any model that reads its input data from one or a number of ASCII (i.e. text) input files and writes the outcomes of its calculations to one or more ASCII output files. Thus a model does not have to be recast as a subroutine and recompiled before it can be used within a parameter estimation process. PEST adapts to the model, the model does not need to adapt to PEST.

## 6.6.1.1 An Overview of PEST

PEST is subdivided into three functionally separate components which are:
- parameter and/or excitation definition and recognition,
- observation definition and recognition,
- the nonlinear estimation and predictive analysis algorithm.

## Parameter definition and recognition

Of the masses of data of all types that may reside on a model's input files, those numbers must be identified which PEST is free to alter and optimize. Fortunately, this is a simple process which can be carried out using input file "templates". To construct a template file, each space occupied by a parameter is replaced by a set of characters that both identify the parameter and define its width on the input file. Then whenever PEST runs the model it copies the template to the model input file, replacing each parameter space with a parameter value as it does so.

PEST requires that upper and lower bounds be supplied for adjustable parameters; this information is vital to PEST, for it informs PEST of the range of permissible values that a parameter can take. Many models produce nonsensical results, or may incur a run-time error, if certain inputs transgress permissible domains.

PEST allows logarithmic transformation of selected parameters to hasten the rate of convergence to optimal parameter values. PEST also allows to incorporate a prior information into the estimation process to increase the value of the objective function (i.e. the sum of squared deviations between model and observations).

## Observation definition and recognition

PEST requires that for each model output file which must be opened and perused for observation values, an instruction file be provided detailing how to find those observations. This instruction file can be prepared using any text editor.

Once interfaced with a model, PEST's role is to minimize the weighted sum of squared differences between model-generated observation values and those actually measured in the laboratory or field; this sum of weighted, squared, model-to-measurement discrepancies is referred to as the "objective function". The fact that these discrepancies can be weighted makes some observations more

important than others in determining the optimization outcome. Weights should be inversely proportional to the standard deviations of observations, "trustworthy" observations having a greater weight than those which cannot be trusted as much. Also, if observations are of different types (for example solute concentration and solvent flow rates in a chemical process model) they can be grouped by the user so that the weights assigned to each group can reflect the relative magnitudes of the numbers used to express different quantities; in this way the set of larger numbers will not dominate the parameter estimation process just because the numbers are large. A particular observation can be provided with a weight of zero if the user does not wish it to affect the optimization process at all.

Parameter estimation algorithm

PEST uses a nonlinear estimation technique known as the Gauss-Marquardt-Levenberg (GML) algorithm. For linear models (ie. models for which observations are calculated from parameters through a matrix equation with constant parameter coefficients), optimization can be achieved in one step. However for nonlinear problems (most models fall into this category), parameter estimation is an iterative process. At the beginning of each iteration, the relationship between model parameters and model-generated observations is linearized by formulating it as a Taylor series expansion about the currently best parameter set; hence the derivatives of all observations with respect to all parameters must be calculated. This linearized problem is then solved for a better parameter set and the new parameters tested by running the model again. By comparing parameter changes and objective function improvement achieved through the current iteration with those achieved in previous iterations, PEST can tell whether it is worth undertaking another optimization iteration; if so the whole process is repeated.

The strength of this method lies in the fact that it can generally estimate parameters using fewer model runs than any other estimation method, a definite bonus for large models whose run times may be considerable. However the

method requires that the dependence of model-generated observation counterparts on adjustable parameters and/or excitations be continuously differentiable.

As it calculates derivatives, PEST records the sensitivity of each parameter with respect to the observation dataset to a file which is continuously available for inspection. If it is judged that PEST's performance is being inhibited by the behaviour of certain parameters (normally the most insensitive ones) during the optimization process, these parameters can be temporarily held at their current values while PEST calculates a suitable upgrade for the rest of the parameters. This whole process can be automated using PEST's "automatic user intervention" functionality.

PEST uses a number of different criteria to determine when to halt its iterative process. Note that only one of them (zero-valued objective function) is a guarantee that the objective function minimum has been obtained. In difficult circumstances, any of the other termination criteria could be satisfied when the objective function is well above its minimum and parameters are far from optimal. If these criteria are properly set through user provided PEST input variables, the user can be reasonably assured that when PEST terminates the parameter estimation process, either the optimal parameter set has been found or further PEST execution will not find it.

At the end of the parameter estimation process (the end being determined either by PEST or by user) PEST writes a large amount of useful data to its run record file. PEST records the optimized value of each adjustable parameter together with that parameter's 95% confidence interval. It tabulates the set of field measurements, their optimized model-calculated counterparts, the difference between each pair, and certain functions of these differences. (These are also recorded on a special file ready for immediate importation into a spreadsheet for further processing.)

As a summary, PEST requires three types of input files which are:

- template files, one for each model input file which PEST must write prior to a model run,
- instruction files, one for each model output file which PEST must read after a model run, and
- a PEST control file which "brings it all together", supplying PEST with the names of all template and instruction files together with the model input/output files to which they pertain. It also provides PEST with the model name, parameter initial estimates, field or laboratory measurements to which model outcomes must be matched, prior parameter information, and a number of PEST variables which control the implementation of the Gauss-Marquardt-Levenberg method.

For a more detailed explanation of the PEST package, one can refer to Doherty (2003, 2004).

## 6.6.2 Shuffled Complex Evolution (SCE-UA)

The SCE-UA method, developed at the University of Arizona, is a global search optimization method designed to handle difficult, nonlinear response surfaces encountered in the calibration of conceptual watershed models. SCE-UA method is not problem specific and can be used for a broad class of problems effectively as well. SCE-UA method is capable of handling high parameter dimensionality and it does not rely on derivatives. The method is based on the notion of sharing information and on concepts drawn from principles of natural biological evolution.

A number of studies have been conducted that compare SCE-UA with other existing global and local optimization methods, including the Adaptive Random Search (ARS) method, Multi Start Simplex (MSX) method and Genetic Algorithm (GA) for calibrating conceptual rainfall–runoff models (e.g. Duan et al., 1992; Duan et al., 1994; Gan and Biftu, 1996; Cooper et al., 1997; Kuczera, 1997; Franchini et

al., 1998; Freedman et al., 1998; Thyer et al., 1999). These studies demonstrate that the SCE-UA method is an effective and efficient search algorithm in finding the global optimum. The SCE-UA method has been widely applied for calibration of various conceptual rainfall–runoff models, including the Sacramento model (Sorooshian et al., 1993; Duan et al., 1994; Gan and Biftu, 1996; Yapo et al., 1996; Gan et al., 1997), the Tank model (Tanakamaru and Burges, 1996; Cooper et al., 1997), the Xinanjiang model (Gan and Biftu, 1996; Gan et al., 1997) and for the first time with HBV model in this study.

The SCE-UA method is based on a synthesis of the best features from several existing search strategies, including the simplex procedure (Nelder and Mead, 1965), competitive evolution (Holland, 1975), controlled random search (Price, 1987) and introduces the new concept of complex shuffling.

The SCE-UA method begins by dividing the sample of all possible parameter values into a number of complexes (ngs), each containing a specified number of points (npg). Each complex is allowed to perform a modified simplex process. After a specified number of steps (nspl), the points within the complexes are shuffled to form a new set of sub-complexes each containing a number of points (nps) from the previous generation of complexes. The shuffling process reduces the risk of optimizing to a local minimum. As the search progresses, the entire population tends to converge towards the neighborhood of the global optimum, provided the initial population size is sufficiently large.

The SCE method includes various algorithmic parameters. The most important parameter is the number of complexes (ngs). Sensitivity tests show that the dimensionality of the calibration problem (number of calibration parameters) is the primary factor determining the proper choice of (ngs) (Duan et al., 1994). In general, the larger the value of (ngs) chosen the higher the probability of converging into the global optimum but at the expense of a larger number of model simulations (the number of model simulations is virtually proportional to ngs) and vice versa.

For a more detailed structure of the SCE-UA algorithm, one can refer to Duan et al. (1992, 1993, 1994) and Singh (1995).

## 6.6.3 A Comparison of PEST and SCE_UA Search Methods

Although two different search methods for model calibration process are described in the preceding sections, both can be run on the same platform. SCE_UA algorithm is linked to the PEST package (Doherty, 2003) which allows the use of already prepared input files (template, instruction and control files) under PEST platform. This saves time and effort to the user in the data preparation stage by which the input files are created and checked once and can be used for both of the search methods afterwards.

The strength of global optimization methods such as, SCE-UA and other such methods, is their ability to incorporate a certain degree of randomness into the search for the minimum of the objective function. There are costs and benefits associated with this strategy. The computational cost of adding such randomness to the selection of trial parameter values lies in the fact that many such values must often be selected for these methods to work properly; the selection of every such parameter set requires that a model run be undertaken in order to evaluate the objective function associated with that set. However the benefit of this strategy lies in the fact that it is only through the inclusion of such randomness in the global search strategy that it can be guaranteed that all "regions of attraction" within parameter space are "felt" at various stages of the optimization process; the global objective function minimum lies at the base of one of these regions of attraction. The efficiency with which different global optimization methods can locate this global minimum depends in part on the extent to which they can "learn from experience" in pursuing parameter trajectories which lead towards local, rather than global, objective function minima.

The Gauss-Marquardt-Levenberg (GML) method employed by PEST is stated not to be a global optimization method (Doherty, 2004). Where there is only one minimum of the objective function, the GML method is normally the fastest way to find it, involving far fewer model runs than any other method. However if parameter starting values are located in the catchment area of a local minimum, rather than the global minimum, then the GML method will very efficiently find its way to the local minimum.

## 6.7 Model Calibrations

In this study, the HBV model is automatically calibrated using GML and SCE_UA search algorithms for Kırkgöze basin. Data from the three-year period, 1 October 2001 to 30 September 2004, are used in the calibration process both in individual water year terms and in a combined form. The calibration process is carried out in two modes: 1) against runoff only as traditionally done (Q-model) 2) against runoff and snow covered area (SCA) using Earth Observation data (QS-model).

Such work was firstly initiated within the SnowTools (Guneriussen et al., 2000) and HydAlp (Rott et al., 2000) projects. The evaluations carried out in these projects showed that updating of the HBV model with remotely sensed SCA data tended to reduce the model performance. But Engeset et al. (2003) and later Alfnes et al. (2004, 2005) stated that the main reason for this could be the SCA data which was not used in the model calibrations. Using SCA in the calibration process, Engeset et al. (2003) and Alfnes et al. (2004, 2005) found that calibrating against both SCA and runoff together resulted in models that simulated SCA better than models calibrated against runoff alone. The improved SCA simulations did not seem to reduce the precision in the runoff simulations. Similar studies to evaluate the use of Earth Observation data on snow in the HBV model are conducted by Metsämäki et al. (2003) and Johansson et al. (2003).

The difference of this study from the above mentioned literature is that SCE_UA global optimization search method is applied for the first time with the HBV model along with the additional snow covered area data from MODIS satellite for a multi-variable calibration. Above all, this is the first application of the HBV model in Turkey. The objective of the study is to investigate if using SCA data from MODIS satellite in the HBV model calibrations would improve the final model performance that does not depend on runoff only.

The HBV model input and necessary calibration files are prepared in PEST platform so that both GML and SCE_UA search methods could be automatically applied for the calibration process. An example of the template, instruction and control files are presented in Appendix A.

As mentioned earlier, PEST platform uses the sum of weighted squared residuals ($\Phi$) as the objective function, Equation 6.1. The best parameter set for a single-variable calibration is decided upon the lowest objective function under the given weight conditions for each observation.

$$\Phi = \sum_{i=1}^{m \text{ or } n} \left( w_i \, r_i \right)^2 \qquad \text{Equation 6.1}$$

where:   $r_i$   = residual (difference between the observed and simulated value
            for a variable)

   $w_i$   = weight of each observation

   m or n = number of observations depending of the criterion variable

The weighting factor of the observations is of great importance in the automatic calibration process. For a multi-variable calibration case where different observation types are used (runoff in $m^3/s$ and snow covered area in %), weight of each observation is adjusted such that different objective functions ($\Phi_1$ for runoff and $\Phi_2$ for snow covered area) are of about the same magnitude, Equation 6.2. The reason for this adjustment is that no one of the variable groups should

127

dominate during the calibration process even when their number of observations are different.

$$\Phi = \Phi_1 + \Phi_2 = \sum_{i=1}^{n} \left( w_i \, r(Q)_i \right)^2 + \sum_{j=1}^{m} \left( w_j \, r(SCA)_j \right)^2 \qquad \text{Equation 6.2}$$

Several simulation trails are undertaken using both GML and SCE_UA automatic calibration procedures. The original method of PEST package, which is the GML algorithm, converges to a result far before SCE_UA does. On a PC with Pentium IV processor and 512 MB RAM, a GML run for a combined three-year simulation takes around 3-5 minutes whereas, for a SCE_UA simulation at least 120 minutes are approximately needed for the completion of a run. In this sense, GML method is more advantageous. However, during the GML and SCE_UA simulation trials, both methods generally give different results when minimizing the objective function. By large, SCE_UA provides lower objective function values as compared to GML algorithm. The only explanation of this result can be mentioned as, although GML search method converges faster to minimize the objective function, it seems to reach a local minimum most of the time. Hence it can be concluded that GML is very dependent on the starting parameter values as have been mentioned by some other authors as well (Alfnes et al., 2005; Doherty, 2004; Engeset et al., 2003). When the final parameter estimation values determined by SCE_UA method are fed back into GML algorithm, the GML method does not improve on the objective function. As a result it can be deduced that although taking longer to complete the shuffling process, SCE_UA search method is a more powerful method than the GML algorithm in nonlinear parameter estimation when applied to hydrologic modeling to find the global optimum.

During the multi-variable calibration procedure, the SCE_UA method used in the study provides only the total minimum objective function ($\Phi$) from both variables at the end of a simulation. Hence the weight of each variable ($\Phi_1$ and $\Phi_2$) can not be observed. To examine and make sure that one variable group does not

dominate over the other, GML method is run with the SCE_UA output results once again to see the effect of each variable group on the objective function separately.

As a means to judge the performance of the calibration, two widely used goodness-of-fit criterion are applied. The first one is the Root Mean Square Error (RMSE), Equation 6.3, that has the units of the evaluated variable. The lower the RMSE means the better the calibration process has been undertaken.

$$RMSE = \sqrt{\frac{\sum_{i=1}^{n} \left(x_{obs,i} - x_{sim,i}\right)^2}{n}} \qquad \qquad \text{Equation 6.3}$$

where:      $x_{obs}$   = observed value

$x_{sim}$   = simulated value

n      = number of observations

The second goodness-of-fit criterion is the well-known Nash and Sutcliffe (1970) $R^2$ criterion, Equation 6.4, mainly applied in rainfall-runoff modeling. It is dimensionless and may obtain a value ranging from $-\infty$ to 1. A value greater than zero means that the simulated model gives a better estimate than a long-term mean of the observations. Also termed as the model efficiency, this equation actually shows the percentage of explained variance over the total variance (or in other words one minus the unexplained variance) between the observed and simulated values. Being dimensionless, it has an advantage over RMSE in the sense that different variables may be comparable. But it does depend on a meaningful average value.

$$R^2 = 1 - \frac{\sum_{i=1}^{n}\left(x_{obs,i} - x_{sim,i}\right)^2}{\sum_{i=1}^{n}\left(x_{obs,i} - \overline{x}_{obs}\right)^2} \qquad \text{Equation 6.4}$$

where:    $x_{obs}$    = observed value

$x_{sim}$    = simulated value

$\overline{x}_{obs}$    = average value during the observation period

n        = number of observations

The above-mentioned criterion are transformed to the equations given in Table 6.7 to judge the performance of the calibration simulations for single-variable and multi-variable cases with runoff and snow covered area as the variables. Usually in literature RMSE and $R^2$ criterion are applied to runoff which is probably the easiest but at the same time the most important measured field variable. But for the multi-variable calibration procedure, these criterion are applied to snow covered area as well that describe the accuracy of the temporal variation of SCA. For SCA variable, unlike runoff, all of the daily values during a snowmelt season are not present mostly due to the cloud problem of the optical satellite used. Therefore, the number of observations for runoff and SCA are different. One additional criterion with respect to runoff is added to the goodness-of-fit table which is the accumulated relative volume error ($V_E$) during the modeled period. This criterion is general and used both in the single and multi-variable calibration simulations. Although, daily volume differences can be noticeable, during the overall model calibration period, results may practically yield no volume error. But this criterion is still important for the verification and forecasting periods.

Table 6.7 Goodness-of-fit criterion used in the calibration process

| Objective Functions | Equation | Value for 'perfect' fit |
|---|---|---|
| $RMSE_Q$ | $\sqrt{\dfrac{\sum\limits_{i=1}^{n}\left(Q_{obs,i}-Q_{sim,i}\right)^2}{n}}$ | 0 |
| $RMSE_{SCA}$ | $\sqrt{\dfrac{\sum\limits_{i=1}^{m}\left(SCA_{obs,i}-SCA_{sim,i}\right)^2}{m}}$ | 0 |
| $R_Q^2$ | $1-\dfrac{\sum\limits_{i=1}^{n}\left(Q_{obs,i}-Q_{sim,i}\right)^2}{\sum\limits_{i=1}^{n}\left(Q_{obs,i}-\overline{Q}_{obs}\right)^2}$ | 1 |
| $R_{SCA}^2$ | $1-\dfrac{\sum\limits_{i=1}^{m}\left(SCA_{obs,i}-SCA_{sim,i}\right)^2}{\sum\limits_{i=1}^{m}\left(SCA_{obs,i}-\overline{SCA}_{obs}\right)^2}$ | 1 |
| $V_E$ | $\dfrac{\sum\limits_{i=1}^{n}\left(Q_{obs,i}-Q_{sim,i}\right)}{\sum\limits_{i=1}^{n}Q_{obs,i}}$ | 0 |

where Q represents discharge in m$^3$/s and SCA is snow covered area in %. n and m values are the number of discharge and snow covered area observations respectively. $V_E$ is the accumulated relative volume error.

During the calibration of the HBV model, each of the above mentioned goodness-of–fit criterion are calculated for the calibration period and will be presented in the subsequent sections. The RMSE terms for each variable have their own units of measurement so as to give an idea of the error. On the other hand, $R^2$ terms are dimensionless. Due to this advantage, a weighted combination of the dimensionless criterion can be used to yield an optimal goodness-of-fit as shown in Equation 6.5. $R_{TOT}^2$ criterion combines the criterion for snow covered area as well as runoff with a penalty for any volume error. This combined multi-variable

technique can be used to take into account all the variables subject to calibration or validation. An advantage of the proposed formulation is that all variables are given about the same weight owing to the dimensionless nature of the $R^2$ criterion. No re-scaling of the different criteria due to differences in magnitude or variance is needed.

$$R_{TOT}^2 = w_1 R_Q^2 + w_2 R_{SCA}^2 - w_3 |V_E| \qquad \text{Equation 6.5}$$

The choice of weights $w_i$ introduces some subjectivity into the automatic process. The default choice should be to set all weights equal however, different weights could be chosen, taking into account for example the reliability and sampling frequency of the different variables. Although runoff may be the most important end product of a hydrological model especially during a flood season, in this study, the internal variable of SCA in the HBV model is as worthy to be correctly simulated. Therefore, equal weights are given to both runoff and snow covered area criterion because it is thought that one should not dominate over the other if their effect is to be tested. In this sense, $w_1$ and $w_2$ are both given a weight of 0.5 and $w_3$ is specified as 0.1 as proposed by Lindström et al. (1997) and Bergström et al. (2002) to be a decent penalty for any volume error occurring.

## 6.7.1 Simulations without EO data (single-variable)

The first of the calibration modes is the traditional single-variable runoff simulations (Q-model) without the use of Earth Observation data. 16 HBV model free parameters are automatically calibrated using SCE_UA method firstly taking each year individually and then in a combined form. By this way it will be possible to see how the model tries to replicate the observed values for certain years and as a whole. The goodness-of-fit criterion is calculated for runoff and SCA separately along with the volume penalty and the total model efficiency is determined by assigning certain weights to these criterion. Figure 6.9 shows the model simulation runs for discharge and snow covered area using the single criterion as runoff for individual years and Figure 6.10 plots the model simulation runs for combined years. Table 6.8 and Table 6.9 tabulate the results.

It looks like the individual year 2003 is simulated the best out of the three by considering each of the goodness-of-fit criterion. The simulated hydrograph fits well with the observed values and the snow covered area depletion shows a smooth decline over the melt period except once in late April 2003.

For individual years of 2002 and 2004, time-wise the start of the melt season is simulated correctly, but the observed peak discharge values in the hydrograph are not met. This mismatch is compensated later in the season which also includes the rainfall-runoff process even after snowmelt has ceased. During 2002, there are two times when SCA has increased (snowfall occurrence) in the melt period whereas, the same process has occurred several times in the 2004 season showing a more fluctuating snow cover over the basin.

As of the combined calibration runs, 2003-2004 combination has the best discharge efficiency, but SCA is represented best within the 2002-2003 water years. This is probably because 2004 discharge values are better modeled as compared to 2002 simulations but at the same time since 2004 SCA depletion has

a more complicated decreasing trend, this is why SCA goodness-of-fit values decrease when 2004 is taken into consideration.

Also as expected, as more data are made available for calibration, both discharge and snow covered area efficiencies decline which can be seen from 2002-2004 three year combination results. Although this is the case, the lowering of the efficiencies also correspond to a more sound model parameter calibration values. On the overall, model efficiency values above 80% are categorized as good results in hydrological terms.

Table 6.8 Calibration results of Q-models for individual years

| Water Year | 2002 | 2003 | 2004 |
|---|---|---|---|
| Simulation Period | 1/10/2001 - 30/9/2002 | 1/10/2002 - 30/9/2003 | 1/10/2003 - 30/9/2004 |
| $RMSE_Q$ | 0.435 | 0.168 | 0.363 |
| $RMSE_{SCA}$ | 8.758 | 5.476 | 12.956 |
| $R^2_Q$ | 0.880 | 0.980 | 0.920 |
| $R^2_{SCA}$ | 0.898 | 0.939 | 0.794 |
| $V_E$ | 0.002 | 0.000 | 0.001 |
| $R^2_{TOT}$ | 0.889 | 0.960 | 0.857 |
| Figure 6.9 | a.1 + b.1 | a.2 + b.2 | a.3 + b.3 |

Table 6.9 Calibration results of Q-models for combined years

| Water Year | 2002-2003 | 2003-2004 | 2002-2004 |
|---|---|---|---|
| Simulation Period | 1/10/2001 - 30/9/2003 | 1/10/2002 - 30/9/2004 | 1/10/2001 - 30/9/2004 |
| $RMSE_Q$ | 0.427 | 0.414 | 0.455 |
| $RMSE_{SCA}$ | 5.040 | 10.537 | 10.065 |
| $R^2_Q$ | 0.880 | 0.900 | 0.870 |
| $R^2_{SCA}$ | 0.958 | 0.847 | 0.863 |
| $V_E$ | 0.000 | 0.002 | 0.000 |
| $R^2_{TOT}$ | 0.919 | 0.874 | 0.867 |
| Figure 6.10 | a.1 + b.1 | a.2 + b.2 | a.3 + b.3 |
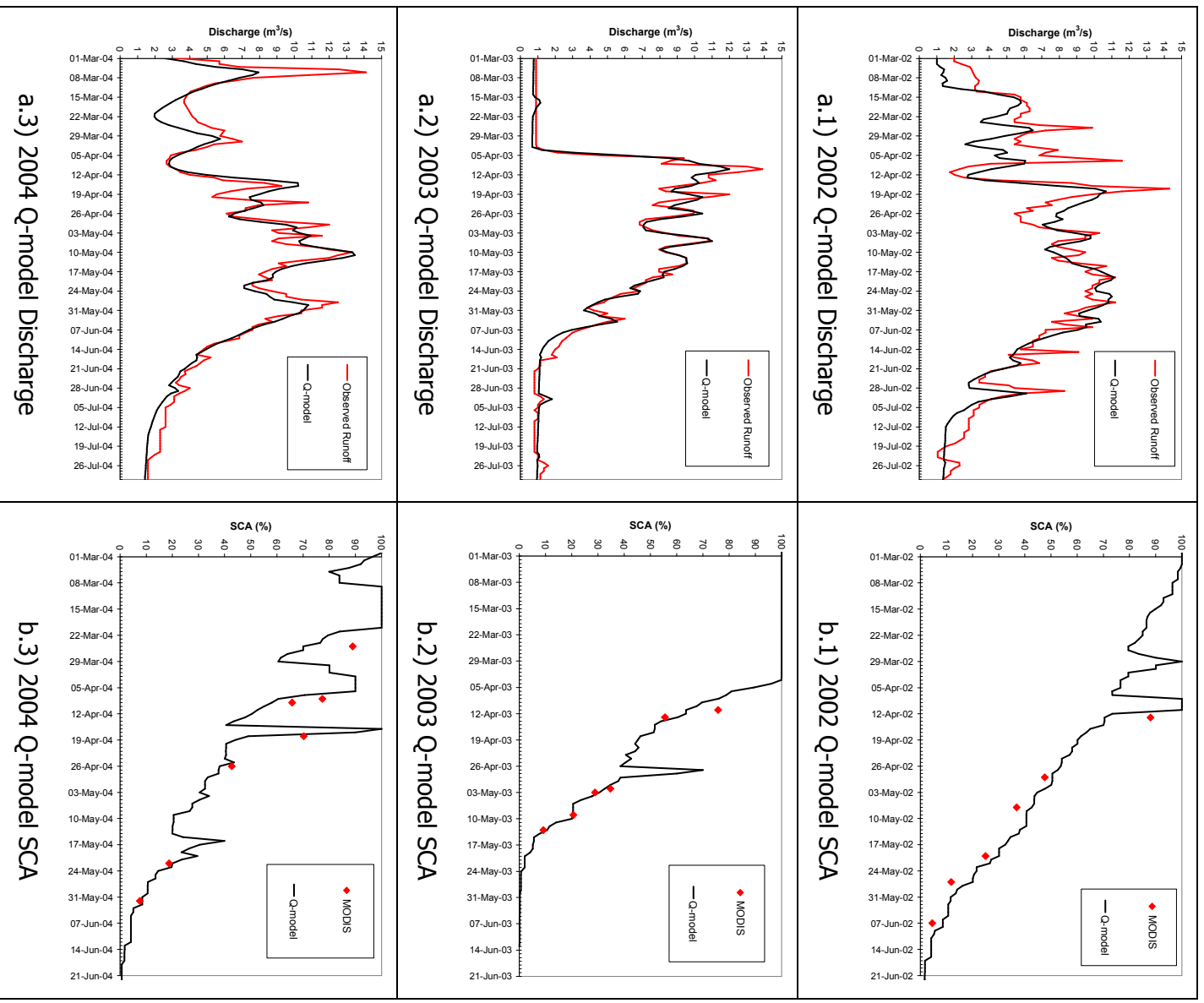
Figure 6.9 Single-variable model simulations (Q-model) for individual years using a) discharge (m³/s) and b) snow covered area (%)

135
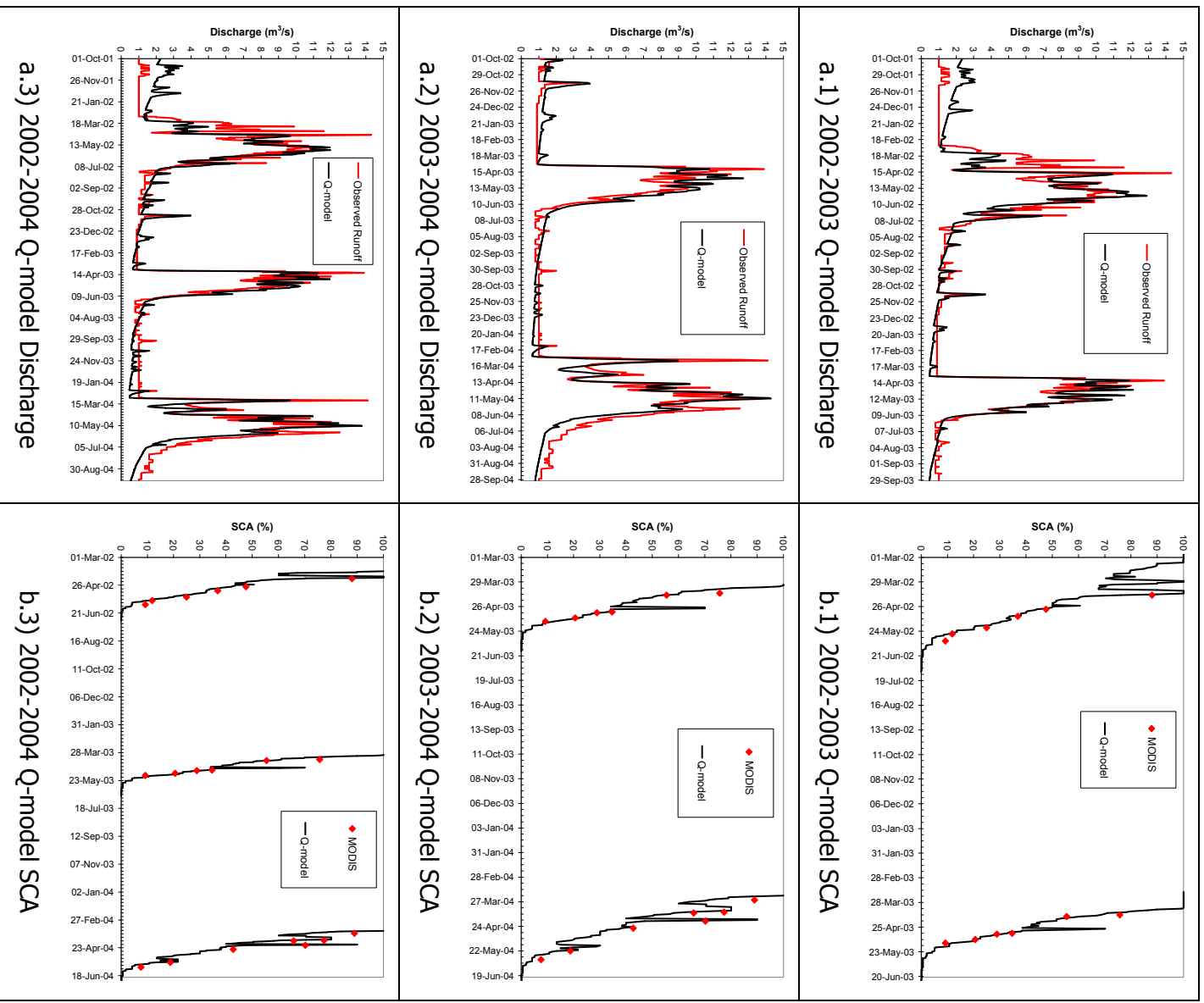
Figure 6.10 Single-variable model simulations (Q-model) for combined years using
a) discharge (m³/s) and b) snow covered area (%)

136

## 6.7.2 Simulations with EO data (multi-variable)

The second calibration mode is the multi-variable runoff and snow covered area simulations (QS-models). Again SCE_UA method is utilized to automatically calibrate the selected 16 free parameters individually and in a combined form for the three respective years 2002, 2003 and 2004. Figure 6.11 and Figure 6.12 depict the model simulation runs for individual years and in a combined form respectively. The goodness-of-fit criterion is calculated for each variable and given in Table 6.10 and Table 6.11 for the two different combinations.

The best representation of the simulated hydrographs among individual years is again 2003, while 2002 and 2004 year early snowmelt runoff peaks can still not be matched. In terms of SCA, 2002 shows a better agreement with the MODIS images. On the overall for the individual years, 2003 is far better than the rest.

For the combined years, the two-year combined calibrations give similar results for discharge and a small decrease of 0.01 in the three-year combined. The best SCA values are achieved in 2003-2004 combination and interestingly 2002-2004 SCA is the next best. On the overall, the total model efficiencies for the combined years are very close to each other.
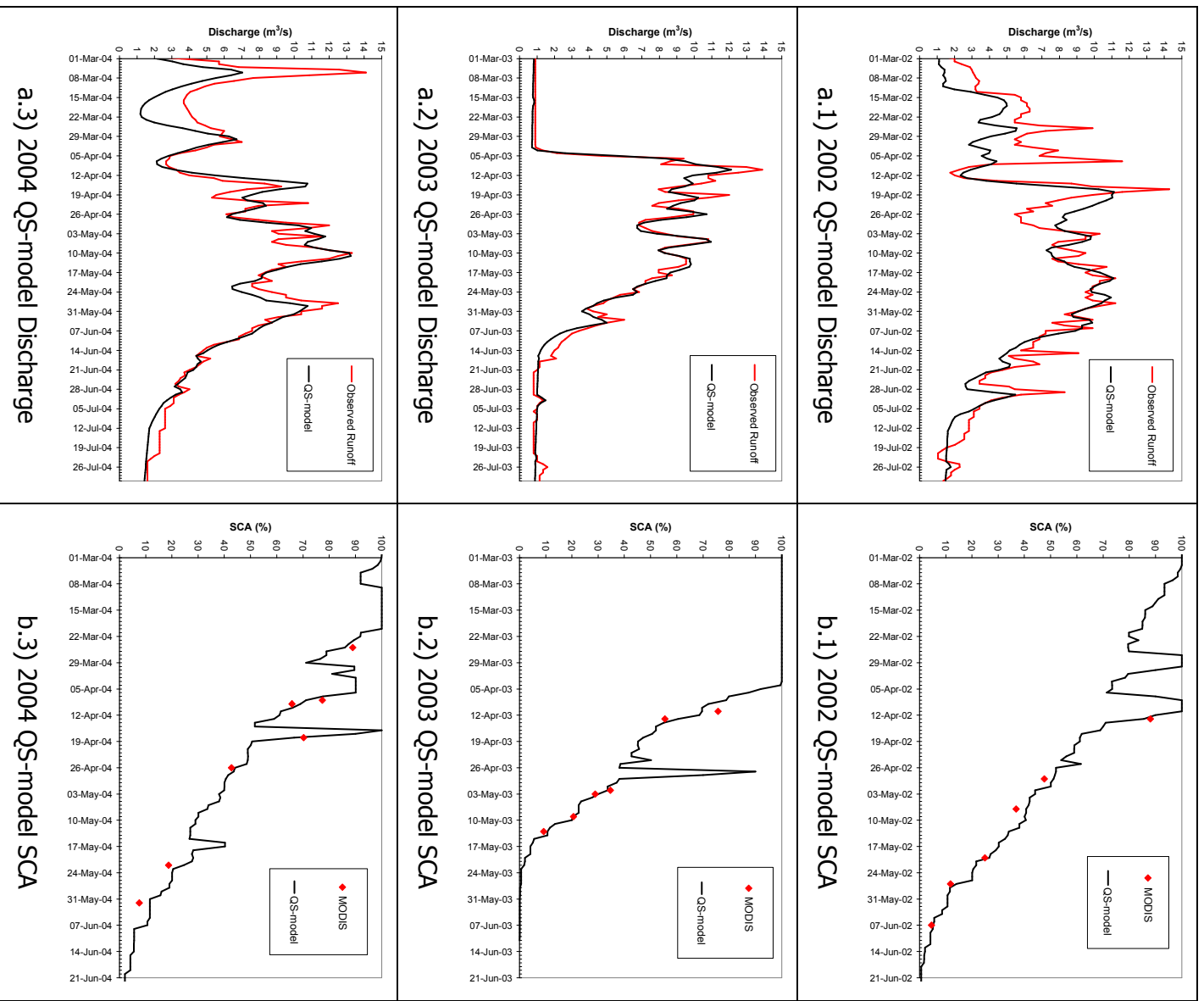
Figure 6.11 Multi-variable model simulations (QS-model) for individual years using
a) discharge (m³/s) and b) snow covered area (%)
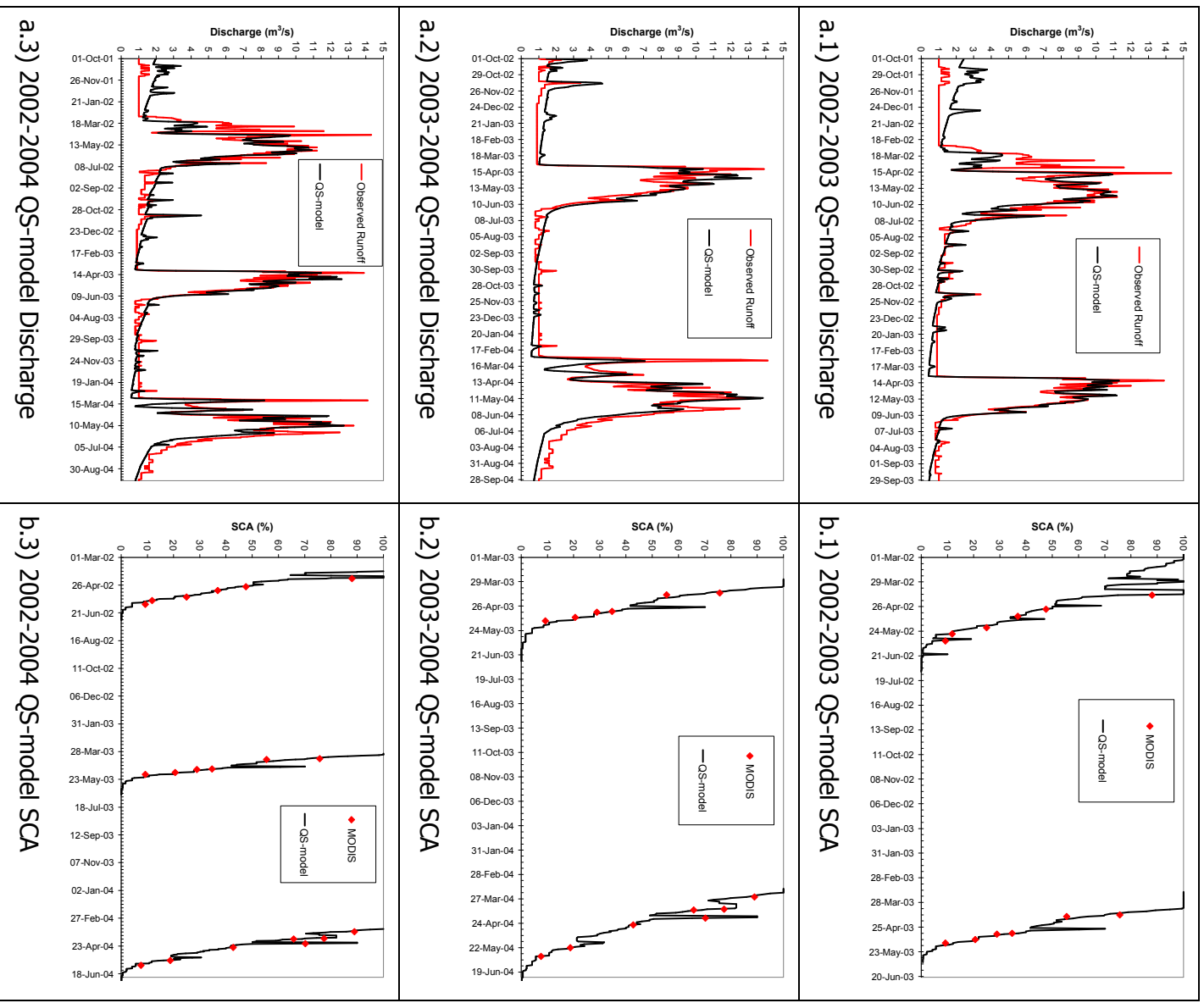
Figure 6.12 Multi-variable model simulations (QS-model) for combined years using
a) discharge (m³/s) and b) snow covered area (%)

139

Table 6.10 Calibration results of QS-models for individual years

| Water Year | 2002 | 2003 | 2004 |
|---|---|---|---|
| Simulation Period | 1/10/2001 - 30/9/2002 | 1/10/2002 - 30/9/2003 | 1/10/2003 - 30/9/2004 |
| $RMSE_Q$ | 0.507 | 0.244 | 0.510 |
| $RMSE_{SCA}$ | 2.629 | 3.338 | 4.196 |
| $R^2_Q$ | 0.840 | 0.980 | 0.880 |
| $R^2_{SCA}$ | 0.991 | 0.977 | 0.978 |
| $V_E$ | 0.000 | 0.001 | 0.001 |
| $R^2_{TOT}$ | 0.916 | 0.979 | 0.929 |
| Figure 6.11 | a.1 + b.1 | a.2 + b.2 | a.3 + b.3 |


Table 6.11 Calibration results of QS-models for combined years

| Water Year | 2002-2003 | 2003-2004 | 2002-2004 |
|---|---|---|---|
| Simulation Period | 1/10/2001 - 30/9/2003 | 1/10/2002 - 30/9/2004 | 1/10/2001 - 30/9/2004 |
| $RMSE_Q$ | 0.484 | 0.531 | 0.562 |
| $RMSE_{SCA}$ | 5.236 | 4.078 | 4.914 |
| $R^2_Q$ | 0.880 | 0.880 | 0.870 |
| $R^2_{SCA}$ | 0.954 | 0.977 | 0.967 |
| $V_E$ | 0.000 | 0.001 | 0.000 |
| $R^2_{TOT}$ | 0.917 | 0.929 | 0.919 |
| Figure 6.12 | a.1 + b.1 | a.2 + b.2 | a.3 + b.3 |

### 6.7.3 Comparison of Model Calibrations

The HBV model calibration is carried out for the three water years, 2002, 2003 and 2004 in several different yearly combinations to see the change in model response both in terms of runoff and snow covered area variables. The goodness-of-fit criterion values on these two variables are computed individually and in a combined weighted manner. Model parameter uncertainty is tested to see the difference between single-variable and multi-variable model calibration.

When the calibration results are compared using Q-model and QS-model for the individual years, it can be concluded that at a small expense of discharge efficiency, SCA measures increase. Individual year 2003 has been affected the least in these two calibration modes, where the discharge efficiency stayed the same while SCA efficiency increased giving a total increase on the overall as can be seen in Table 6.12. Individual years 2002 and 2004 both show a 0.04 decrease for discharge measure but a 0.093 to 0.184 increase for SCA $R^2$ terms. As a total, 0.019 to 0.072 increase in the individual year calibration is observed when weights are distributed equally to discharge and snow covered area.

In the comparison for the combined years, Table 6.13, a decrease of 0.02 in discharge efficiency is observed for the 2003-2004 combination whereas no change is detected for the 2002-2003 and 2002-2004 simulations. In terms of SCA, an interesting small decrease is calculated for the 2002-2003 combination as compared to a significant increase for the 2003-2004 and 2002-2004 calibration combinations.

As an overall result on the calibration process it can be concluded that, both individual and combined year QS-model simulations show a considerable increase in the total model efficiency including runoff, snow covered area and accumulated volume terms as compared to the Q-model runs. A small trade-off in discharge efficiency is compensated by a larger increase in the SCA measure giving an overall increase for the model goodness-of-fit terms. In all the calibration simulations, the

relative accumulated volume error is very small which does not affect the total model efficiency results.

Table 6.12 Calibration result comparison for individual years

| Water Year | 2002 | 2003 | 2004 |
|---|---|---|---|
| Simulation Period | 1/10/2001 - 30/9/2002 | 1/10/2002 - 30/9/2003 | 1/10/2003 - 30/9/2004 |
| $RMSE_Q$ | -0.072 | -0.076 | -0.147 |
| $RMSE_{SCA}$ | +6.129 | +2.138 | +8.760 |
| $R^2_Q$ | -0.040 | 0.000 | -0.040 |
| $R^2_{SCA}$ | +0.093 | +0.038 | +0.184 |
| $V_E$ | +0.002 | -0.001 | 0.000 |
| $R^2_{TOT}$ | +0.027 | +0.019 | +0.072 |

Table 6.13 Calibration result comparison for combined years

| Water Year | 2002-2003 | 2003-2004 | 2002-2004 |
|---|---|---|---|
| Simulation Period | 1/10/2001 - 30/9/2003 | 1/10/2002 - 30/9/2004 | 1/10/2001 - 30/9/2004 |
| $RMSE_Q$ | -0.057 | -0.117 | -0.107 |
| $RMSE_{SCA}$ | -0.196 | +6.459 | +5.151 |
| $R^2_Q$ | 0.000 | -0.020 | 0.000 |
| $R^2_{SCA}$ | -0.004 | +0.130 | +0.104 |
| $V_E$ | 0.000 | +0.001 | 0.000 |
| $R^2_{TOT}$ | -0.002 | +0.055 | +0.052 |

The best parameter sets for individual and combined year calibration cases with Q-model and QS-model are tabulated in Table 6.14 and Table 6.15 respectively. In order to better visualize the changes in parameter values between individual and combined years, the parameter values are normalized along the feasible parameter space, given in Table 6.6, using Equation 6.6 to obtain a value in the range of zero and one.

$$\text{Normalized Value} = \frac{(x - x_{min})}{(x_{max} - x_{min})}$$
Equation 6.6

where:  x  = optimum parameter value for each model variable

     $x_{min}$ = lowest value in the feasible parameter space

     $x_{max}$ = highest value in the feasible parameter space

Figure 6.13 through Figure 6.16 depict the normalized ranges of the 16 HBV model parameters with individual and combined Q-model and QS-model simulations. Simulation results indicate that only few of the model parameters are found to be well-defined, while for the others, good fits are obtained over broad ranges.

For the Q-model runs parameters tx, ts, skor, tvgd, uz1 and perc show a narrow range distribution (< 0.2) while lp and β are the parameters which have the largest range. The rest are scattered in between 0.2 and 0.4 values. For the QS-model simulations, parameters in the narrow range are ts, cx, tvgd, prgd, fc, kuz2. Parameters tx, lp, uz1, perc and β show the largest change within the parameter set. Interestingly, narrow ranged parameters in Q-model runs are not seen in the QS-model simulations. ts and tvgd are the only two parameters to be well-defined in both model calibration results. For an easier comparison among all the model parameters between single and multi-variable calibrations for combined years, the ratios are computed by dividing QS-model ranges for each parameter with the Q-model ranges where the results are plotted in Figure 6.17. It can be seen that some of the model parameters are well over and some under the equilibrium line (line passing from QS/Q Range=1). Parameter uncertainty, i.e. the problem to find one unique set of parameters, increases with the number of model parameters and

decreases with increasing information about the system. Hence in the calibration of the HBV model, it was hoped that the use of additional data, snow covered area in this case, would help to constrain the ranges of parameter values. It is not very clear to say that parameter uncertainty has been decreased in this study as expected. There could be several reasons to this. Firstly, calibration data of three years may not be enough to give such a judgement as well as including the quality of this data. Another reason could be the overparameterization of the model to obtain only one optimal parameter set. There could be several different parameter sets spread throughout the parameter space that can provide almost equally good fits. And finally, other objective functions beside the sum of squared differences as used in this study, could be utilized to make more use of the data in hand. Although parameter uncertainty may be a significant source of the combined modeling uncertainty, other sources such as natural randomness, data errors and the model structure itself may pose uncertainty on their own.

One thing that needs to be stressed on besides parameter uncertainty is that it is important to distinguish between an insensitive and an uncertain parameter. As stated by Seibert (1997) that if good simulations of the measured runoff could be obtained with different values for one parameter, this does not necessarily mean that the simulations are  insensitive to changes in this parameter, but that changes are compensated for by the other parameters. Hence in order to decrease overparameterization of the model, parameter sensitivity analysis may be employed to decrease the number of calibrable model parameters and set constant values to the insensitive model parameters at a small expense of model efficiency. By this way, better calibration and validation processes can be applied for a basin hence resulting in a more reliable hydrological modeling.

Table 6.14 Model parameter values for individual years

| Parameter | Units | 2002 Q-model | 2002 QS-model | 2003 Q-model | 2003 QS-model | 2004 Q-model | 2004 QS-model |
|---|---|---|---|---|---|---|---|
| Ts | °C | -2.4612 | -0.9911 | -0.0811 | 0.2397 | -1.0725 | -0.4407 |
| Tx | °C | -2.4863 | -2.4950 | -2.3191 | -1.2820 | -2.4676 | -2.4835 |
| Cx | mm/°C/day | 2.5340 | 2.8554 | 4.0697 | 4.3252 | 4.3712 | 2.4529 |
| PKORR | --- | 0.6798 | 0.7244 | 0.7509 | 0.6516 | 0.8969 | 0.7811 |
| SKORR | --- | 1.3849 | 1.1665 | 0.9681 | 0.8669 | 0.6206 | 0.6802 |
| TTGRAD | °C/100 m | -1.0796 | -1.0785 | -0.8086 | -0.7997 | -1.0986 | -0.9738 |
| TVGRAD | °C/100 m | -0.7490 | -0.7520 | -0.7902 | -0.5934 | -0.9079 | -0.7950 |
| PGRAD | --- | 0.0312 | 0.0107 | 0.0243 | 0.0500 | 0.0513 | 0.0696 |
| FC | mm | 188.0497 | 148.1461 | 385.2775 | 291.1822 | 205.5851 | 192.6434 |
| LP | frac. of FC | 0.9771 | 0.8786 | 0.8981 | 0.7971 | 0.7331 | 0.8109 |
| β | --- | 3.2396 | 1.9494 | 2.1591 | 1.9270 | 2.6919 | 3.1854 |
| KUZ2 | mm | 0.1009 | 0.1001 | 0.1024 | 0.1000 | 0.1009 | 0.1041 |
| UZ | 1/day | 12.0458 | 24.1698 | 49.5994 | 46.0404 | 64.9398 | 56.9710 |
| KUZ1 | 1/day | 0.2344 | 0.1284 | 0.1311 | 0.1334 | 0.0764 | 0.1098 |
| PERC | mm/day | 1.3253 | 1.2942 | 1.3227 | 1.2030 | 1.4944 | 1.7162 |
| KLZ | 1/day | 0.0051 | 0.0045 | 0.0037 | 0.0037 | 0.0042 | 0.0056 |

Table 6.15 Model parameter values for combined years

| Parameter | Units | 2002-2003 Q-model | 2002-2003 QS-model | 2003-2004 Q-model | 2003-2004 QS-model | 2002-2004 Q-model | 2002-2004 QS-model |
|---|---|---|---|---|---|---|---|
| Ts | °C | -1.1466 | 0.8477 | -2.0272 | -1.9815 | -2.0348 | -1.7032 |
| Tx | °C | -2.4383 | -2.4984 | -2.3007 | -2.3814 | -2.4436 | -2.4362 |
| Cx | mm/°C/day | 2.6201 | 2.7956 | 4.7678 | 2.7195 | 4.6102 | 3.1742 |
| PKORR | --- | 0.7760 | 0.6866 | 0.9921 | 0.9153 | 0.7664 | 0.7462 |
| SKORR | --- | 0.7344 | 0.9151 | 0.6614 | 0.6667 | 0.8849 | 0.9790 |
| TTGRAD | °C/100 m | -0.7559 | -0.6937 | -1.0978 | -0.8229 | -1.0960 | -0.9512 |
| TVGRAD | °C/100 m | -0.7438 | -0.7039 | -0.7998 | -0.7990 | -0.7955 | -0.7499 |
| PGRAD | --- | 0.0436 | 0.0487 | 0.0186 | 0.0320 | 0.0419 | 0.0315 |
| FC | mm | 176.0250 | 167.1741 | 259.1700 | 207.3383 | 154.0874 | 134.4047 |
| LP | frac. of FC | 0.8671 | 0.6321 | 0.7654 | 0.8549 | 0.6848 | 0.6951 |
| β | --- | 2.2465 | 1.4090 | 3.1350 | 3.2392 | 1.3522 | 1.1233 |
| KUZ2 | mm | 0.5175 | 0.1008 | 0.1004 | 0.1009 | 0.1007 | 0.1014 |
| UZ | 1/day | 68.7396 | 28.4374 | 58.2409 | 41.0517 | 64.5592 | 18.1054 |
| KUZ1 | 1/day | 0.1423 | 0.1420 | 0.0644 | 0.0748 | 0.0842 | 0.1128 |
| PERC | mm/day | 1.4391 | 1.3139 | 1.4988 | 1.4994 | 1.4914 | 1.9748 |
| KLZ | 1/day | 0.0061 | 0.0063 | 0.0037 | 0.0037 | 0.0053 | 0.0053 |
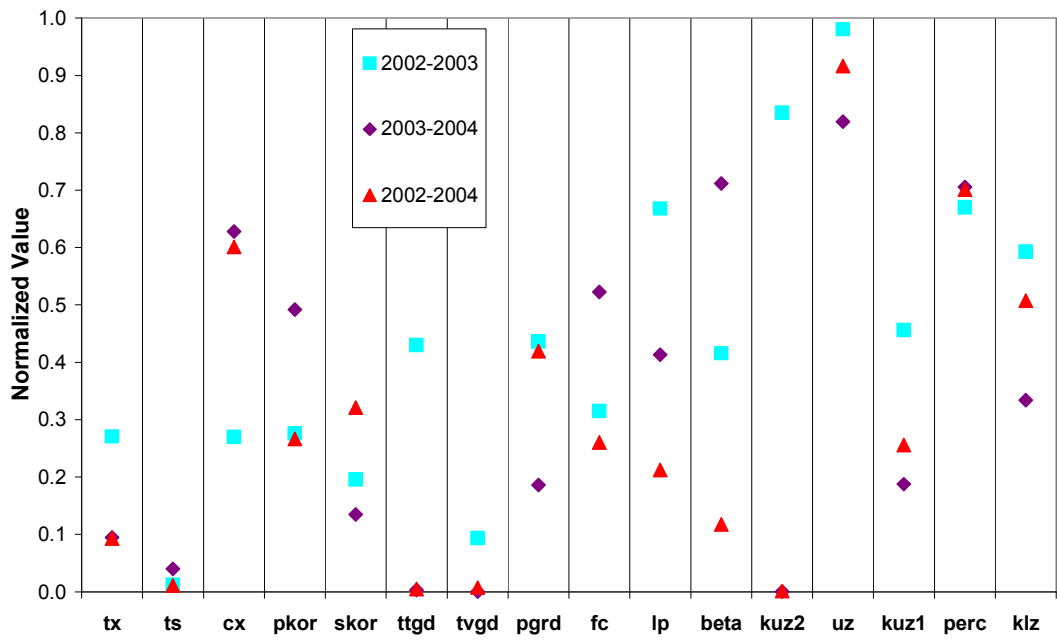
Figure 6.13 Q-model normalized values for combined years
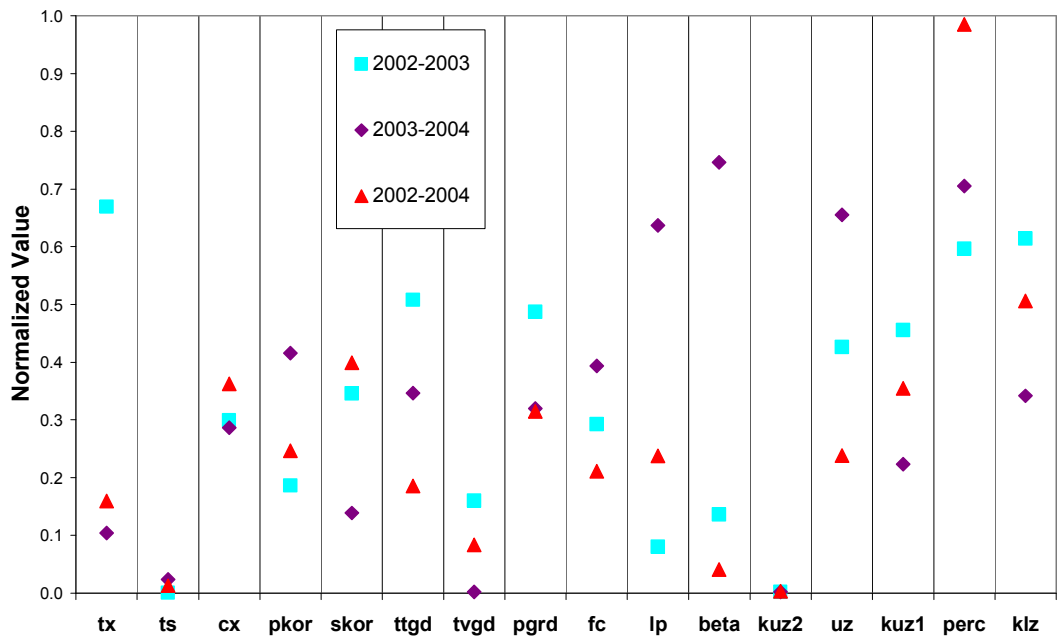


Figure 6.14 QS-model normalized values for combined years

146
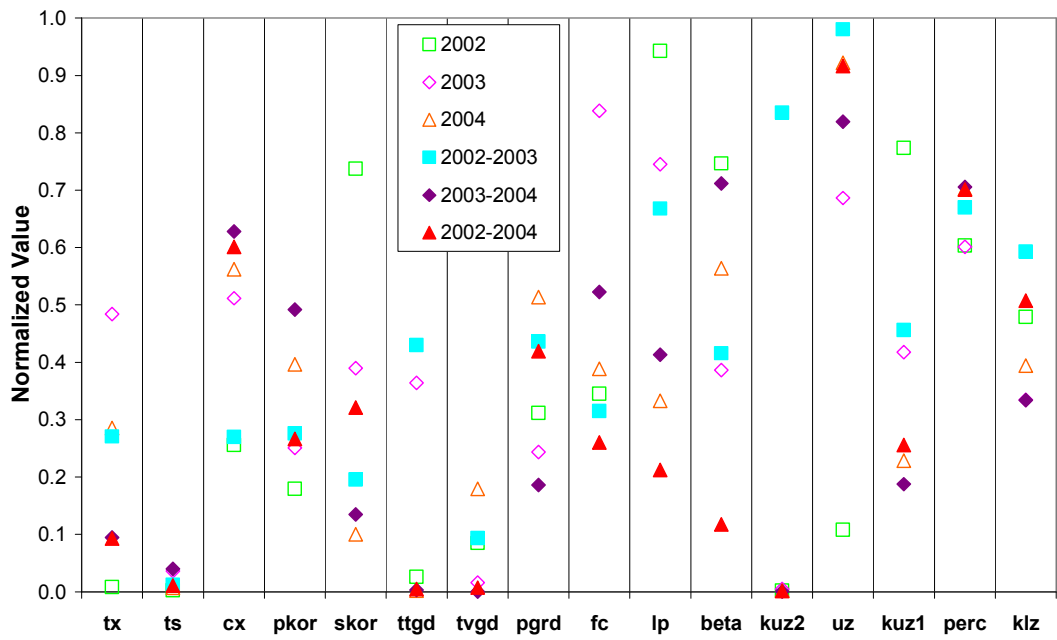
Figure 6.15 Q-model normalized values for individual and combined years
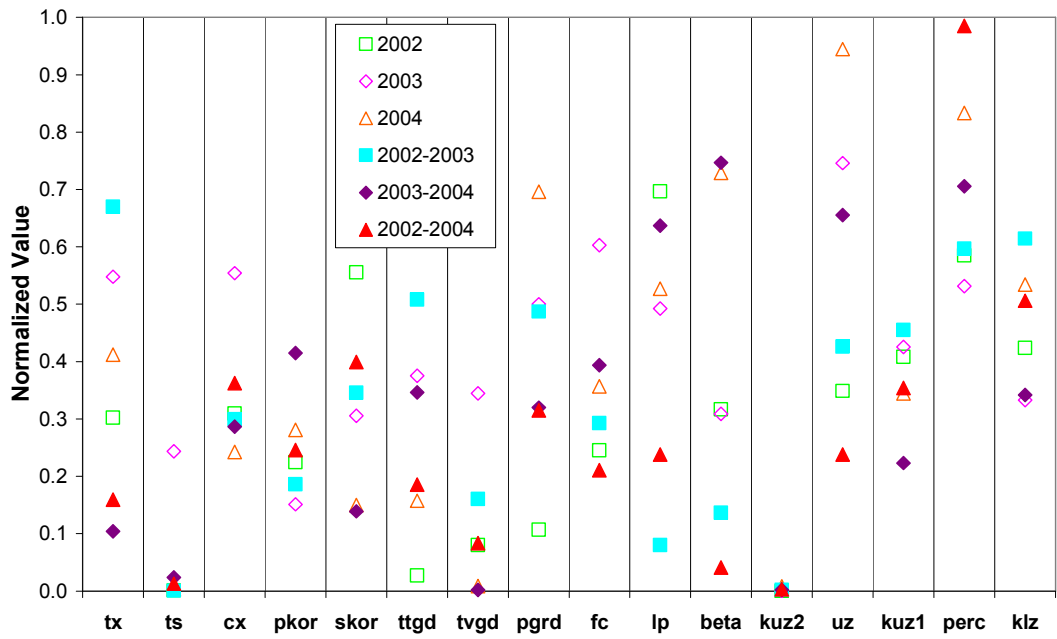


Figure 6.16 QS-model normalized values for individual and combined years
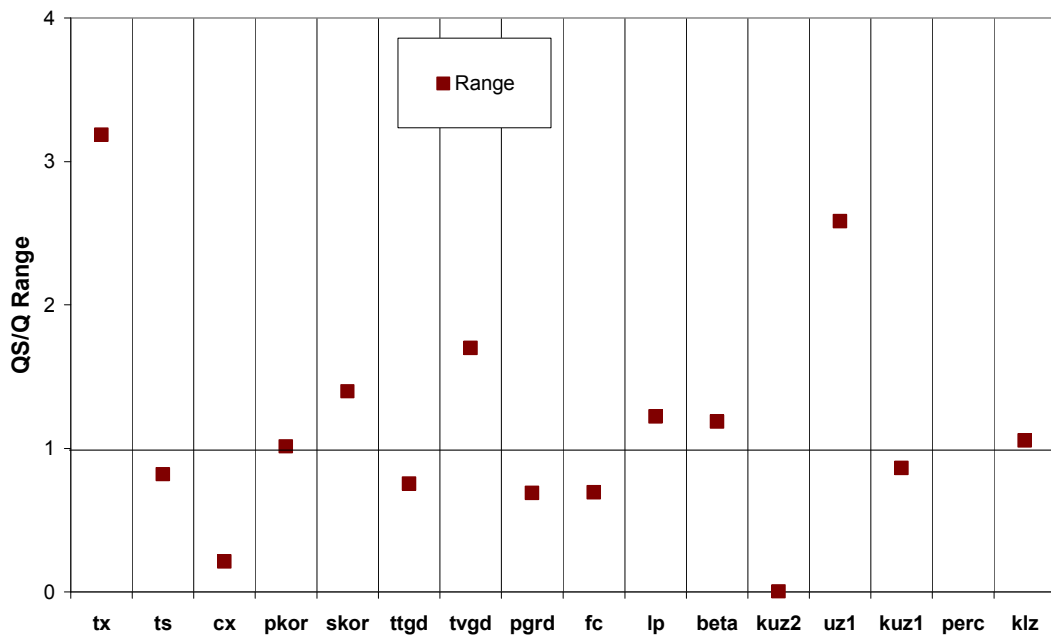
Figure 6.17 Calibrated parameter variations between Q-model and QS-model for combined years

Unfortunately, model calibration does not guarantee reliability of model predictions. The parameter values obtained during calibration and the subsequent predictions made using the calibrated model are only as realistic as the validity of the model assumptions for the study watershed and the quality and quantity of actual watershed data used for calibration and simulation. Therefore, even after calibration, there is potentially a great deal of uncertainty in results that arises simply because it is too unlikely to find error-free observational data (e.g. precipitation, streamflow, topography) and because no simulation model is an entirely true reflection of the physical process being modeled.

## 6.8 Model Validation

Once the HBV model parameters have been optimally fitted to the observed data by automatic calibration using single and multi-variable cases, the goodness-of-fit should be tested (validated) on an independent set of data. This is often referred to as a split sample test. Since not a very long input data set is in hand considering only three water years, 2002, 2003 and 2004, again a combination of these years are used to validate the model. This is done in two cases; 1) the model parameters found by calibrating 2002-2003 years are used to validate the water year 2004 and 2) 2003-2004 parameters are used to validate the water year 2002.

As the first case, 2004 water year is validated both in terms of runoff and snow covered area using Q-model and QS-model parameters. The results are plotted in Figure 6.18 and tabulated in Table 6.16. For the second case, 2002 water year is validated using runoff and snow covered area with Q-model and QS-model parameters respectively. These results are shown in Figure 6.19 and tabulated in Table 6.17.

Commenting on the results, goodness-of-fit criterion values for the validation of 2004 year are all lower than the calibration period of 2002-2003 water years both in terms of Q-model and QS-model results. This is an expected finding in general, but as the calibration period increases the difference between the calibration and validation results are expected to decrease.

For the 2002 validation case using 2003-2004 water years, the values are a little different than the 2004 validation. Interestingly, the SCA measures seem to give better results during the validation stage only for the Q-model parameters, whereas, QS-model parameters for SCA show a decreasing trend as expected. On the overall, the calibration results are still higher. 2002 validation measures show a better fit as compared to the 2004 validation results by 3-4%, but there is no clear indication to conclude that QS-model parameters perform better than Q-model parameters for this period of study.

a.1) 2004 Q-model Discharge

b.1) 2004 Q-model SCA

a.2) 2004 QS-model Discharge

b.2) 2004 QS-model SCA
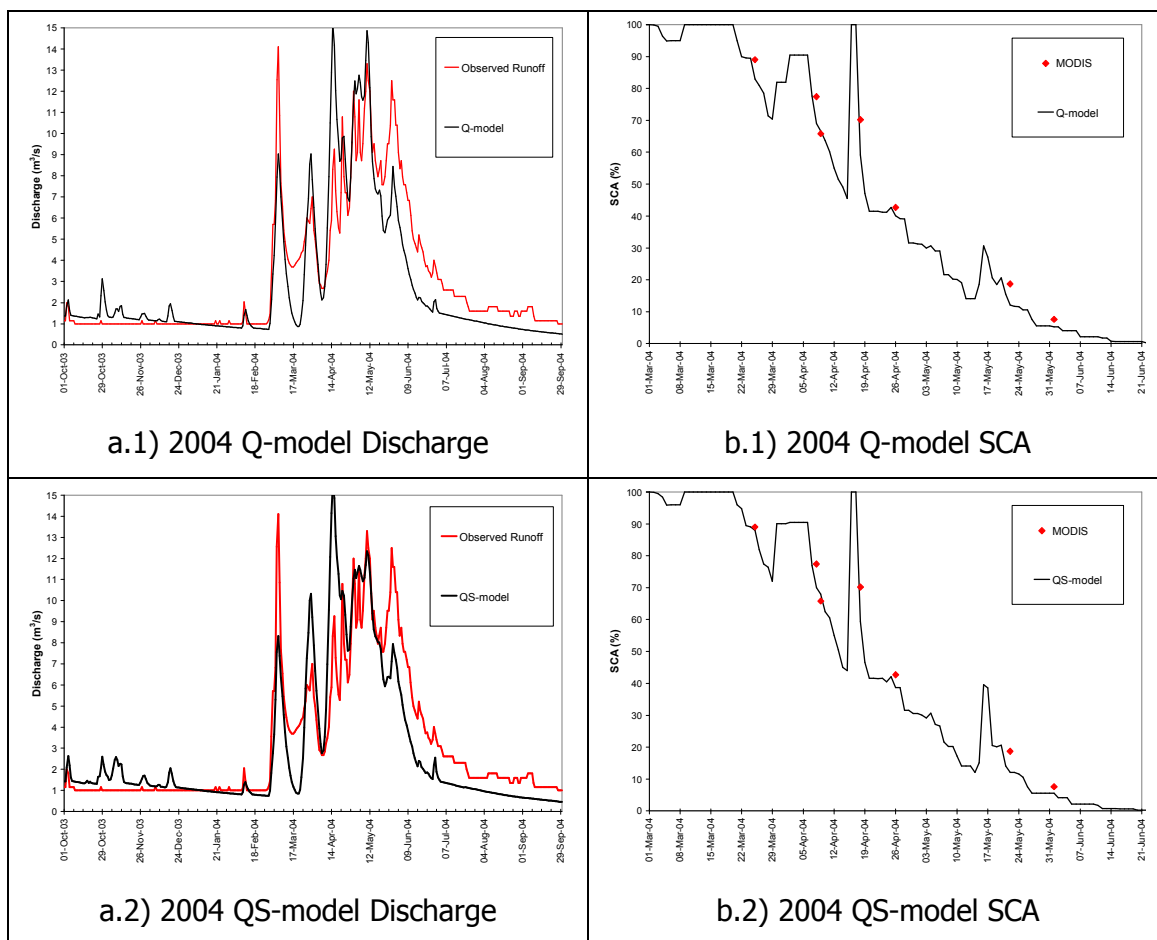
Figure 6.18 Model validation results for 2004 water year using a) discharge ($m^3$/s) and b) snow covered area (%)

Table 6.16 Validation of 2004 using 2002-2003 calibration results

| Criterion | Q-model | | QS-model | |
|---|---|---|---|---|
| | Calibration | Validation | Calibration | Validation |
| $RMSE_Q$ | 0.427 | 0.562 | 0.484 | 0.609 |
| $RMSE_{SCA}$ | 5.040 | 6.411 | 5.236 | 5.841 |
| $R^2_Q$ | 0.880 | 0.740 | 0.880 | 0.700 |
| $R^2_{SCA}$ | 0.958 | 0.949 | 0.954 | 0.958 |
| $V_E$ | 0.000 | 0.123 | 0.000 | 0.093 |
| $R_{Tot}$ | 0.919 | 0.832 | 0.917 | 0.820 |
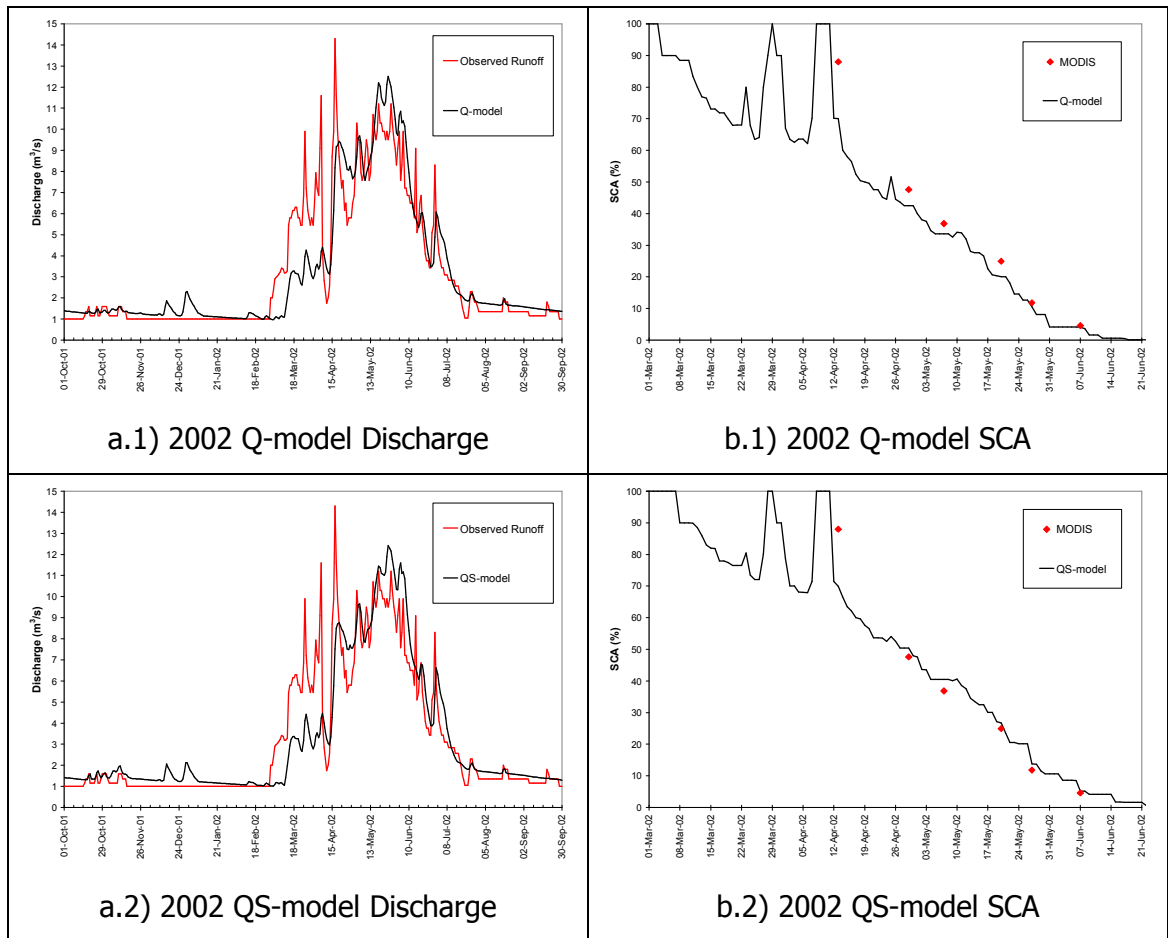
Figure 6.19 Model validation results for 2002 water year using a) discharge ($m^3/s$) and b) snow covered area (%)

Table 6.17 Validation of 2002 using 2003-2004 calibration results

| Criterion | Q-model | | QS-model | |
|---|---|---|---|---|
| | Calibration | Validation | Calibration | Validation |
| $RMSE_Q$ | 0.414 | 0.478 | 0.531 | 0.484 |
| $RMSE_{SCA}$ | 10.537 | 8.024 | 4.078 | 7.705 |
| $R^2_Q$ | 0.900 | 0.810 | 0.880 | 0.800 |
| $R^2_{SCA}$ | 0.847 | 0.915 | 0.977 | 0.921 |
| $V_E$ | 0.002 | 0.002 | 0.001 | 0.010 |
| $R^2_{Tot}$ | 0.874 | 0.862 | 0.929 | 0.860 |

## 6.9 Investigation of Pareto Front

As described in Chapter 3, the solution of Equation 3.3 will not, in general, be a single unique set of parameters but will consist of the so called Pareto set of solutions (non-dominant solutions), according to various trade-offs between different objectives. Thus, a number of tests are carried out in order to estimate the Pareto front and analyze the trade-offs between runoff and snow covered area variables for the combined three consecutive water years (2002 - 2004) only. For this study, Equation 6.2 (weighted sum of squared differences) is utilized for the two variables of runoff and snow covered area. To explore the Pareto front, ten different calibration runs are conducted with different weightings on the objective functions runoff ($\Phi_1$) and snow covered area ($\Phi_2$); two calibration runs using only one of the variables for estimation of the tails of the front and eight runs to estimate the intermediate part. The root mean square error (RMSE), Equation 6.3, is determined from the objective function of weighted sum of squared differences corresponding to the estimated Pareto front and plotted in Figure 6.20. From a multi-objective point of view, these ten parameter sets are equally good but obviously for practical applications some points are more relevant than others.
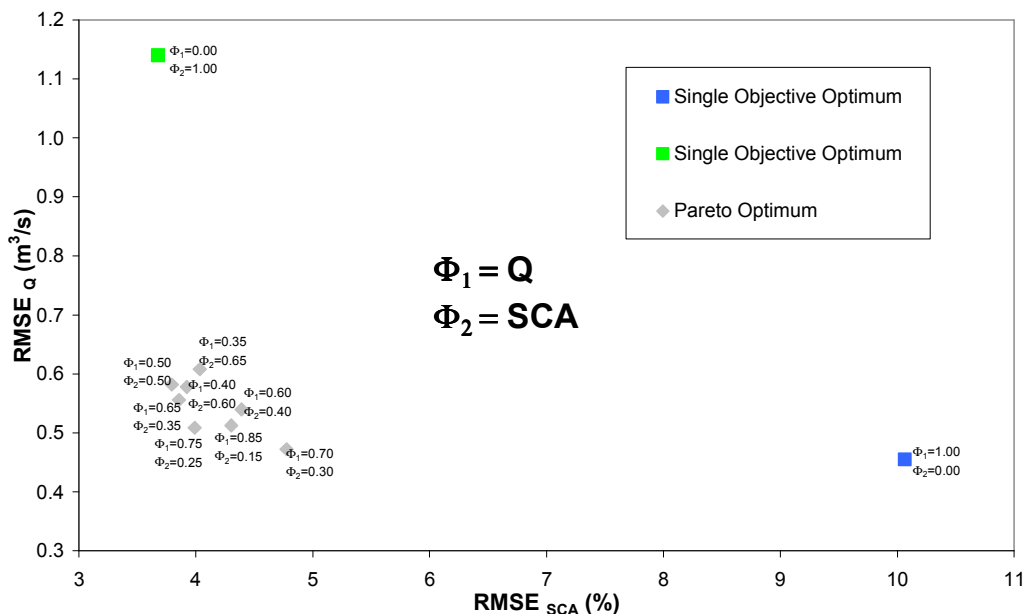


Figure 6.20 Estimated Pareto front without transformation constants

When solving the multi-objective calibration problem, the problem is usually transformed into a single-objective optimization problem by defining a scalar that aggregates the various objective functions. One such aggregate measure is the Euclidean distance as given in Equation 6.7 and used by Madsen (2000a).

$$F(\theta)_{agg} = \sqrt{\left( \left( F(\theta)_1 + A_1 \right)^2 + \left( F(\theta)_2 + A_2 \right)^2 + .... + \left( F(\theta)_p + A_p \right)^2 \right)} \quad \text{Equation 6.7}$$

where $A_i$ are transformation constants assigned to the different objectives, which allows to select relative priorities to certain objectives. The two objectives in this case are RMSE of runoff ($RMSE_Q$) and snow covered area ($RMSE_{SCA}$). Hence Equation 6.7 can be rewritten to reflect the variables of the study as Equation 6.8.

$$RMSE_{agg} = \sqrt{\left( \left( RMSE_Q + A_1 \right)^2 + \left( RMSE_{SCA} + A_2 \right)^2 \right)} \quad \text{Equation 6.8}$$

The selection of the transformation constants, however, is not straight forward, since the priority also depends on the value of the objective function. For instance, if all $A_i$ are set to zero, implicitly larger weights are given to objectives with larger RMSE values. For investigating the entire Pareto front, the aggregated distance measure can be adopted by performing several optimization runs using different values of $A_i$. This in practical applications may be too tedious to calculate where one is only interested in part of the Pareto optimal solutions. In this case, it is proposed to use an aggregated objective function that puts equal weights on the different objectives. A balanced measure can be defined by assigning transformation constants in Equation 6.8 such that all ($RMSE_x + A_i$) have about the same distance to the origin. When using a population-based optimization algorithm, SCE_UA as considered here, an initial population within the feasible region is evaluated. The minimum values of $F_i$ ($F_{i,min}$) are estimated from this initial population and each of the objective functions is transformed to having the same distance to the origin as the objective function with the largest minimum value of $F_i$ as given in the equation below;

$$A_i = \text{Max}\left(F_{j,min}, j = 1,2,...,p\right) - F_{i,min} \qquad \text{when } i = 1,2,...,p \qquad \text{Equation 6.9}$$

The distances to the origin of all the plotted simulation points in Figure 6.20 are calculated with the abovementioned Euclidean distances procedure and a balanced optimum is determined along the intermediate part of the Pareto front as indicated in Figure 6.21. The compromise solution corresponds to a break point on the Pareto front; that is, moving along the front in either direction implies only a small decrease of one of the objective functions at the expense of a pronounced increase of the other objective function defining a Pareto front with a very sharp structure.
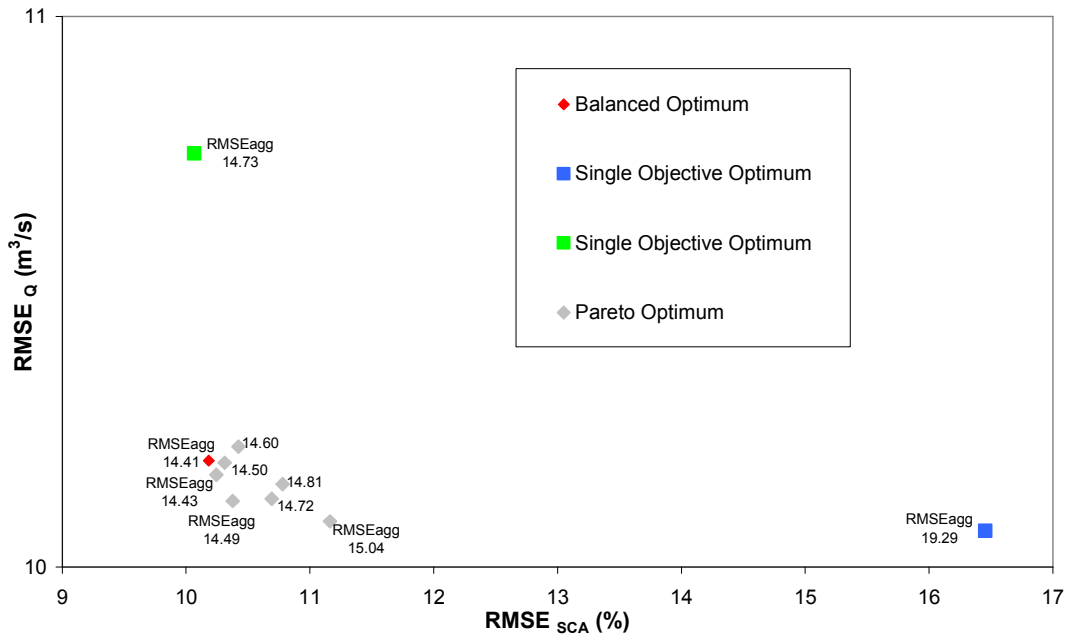


Figure 6.21 Balanced Pareto front with transformation constants

The variation of the optimum model parameter sets along the Pareto front is given in Figure 6.22. The parameter values are normalized with respect to the upper and lower limits of the hypercube search space shown in Table 6.6 so that the feasible range of all parameters is between 0 and 1. A remarkably large variability is observed in the parameter values when moving along the Pareto front. The range is larger than 50% of the feasible range for some of the parameters, ttgd, pgrd, fc, beta, kuz2 and uz. For the others, a trend is apparent when moving along the

Pareto front. For instance, tx, ts, ttgd, kuz1 and klz increase with respect to increasing weight on snow covered area objective. Focusing on either of the two objectives result in distinctly different parameter combinations. The variation of parameter combinations along the Pareto front also implies a large variability on the simulated hydrograph as shown in Figure 6.23.

As a conclusion, although the traditional concept of model calibration is built on the hypothesis that a unique optimum set of parameter values exist, it is clear from the above analysis that such unique global solution does not exist. In a multi-objective context, there is a multitude of parameter combinations that are "equally good". Depending on the priority of the objectives one may shift either way on the Pareto front although a balanced optimum is preferred most of the time for a hydrologically sound application. Table 6.18 show the calibrated HBV model parameter values for the balanced optimum point on the Pareto front.
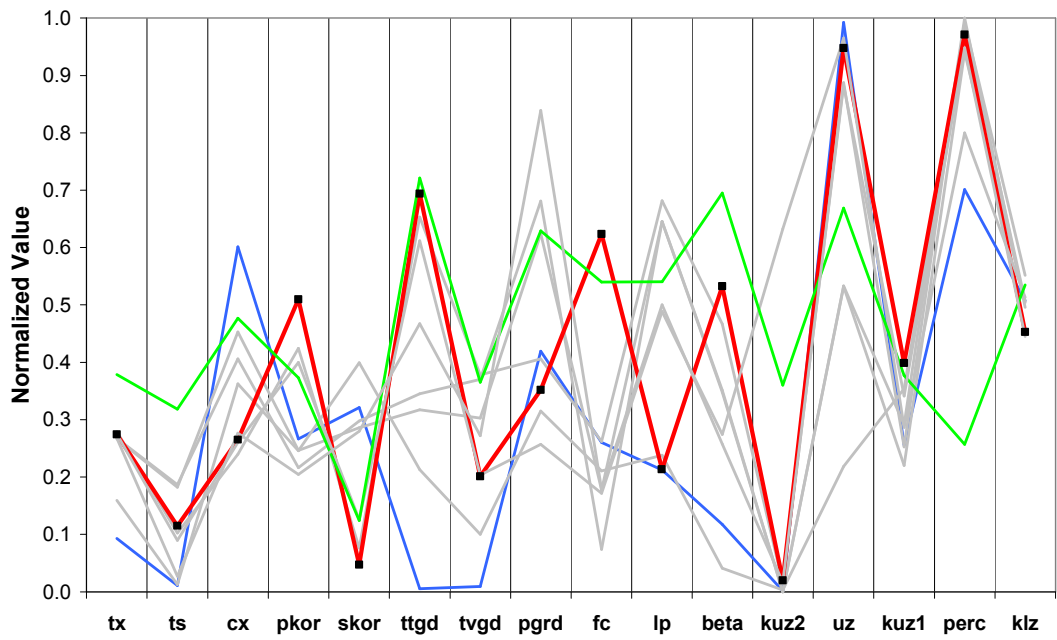
Figure 6.22 Normalized range of parameter values along the Pareto front (coloring correspond to parameter sets in Figure 6.21)
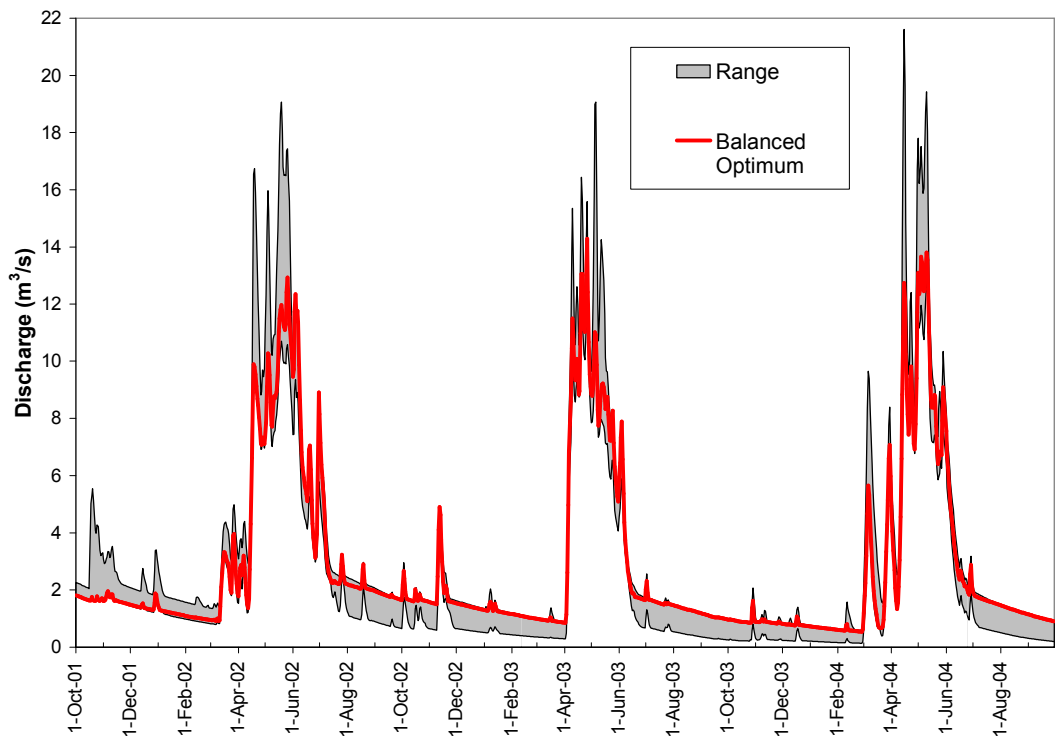


Figure 6.23 Range of simulated hydrographs corresponding to parameter sets along the Pareto front

Table 6.18 Calibrated balanced optimum HBV model parameters values on the Pareto front

| Name | Meaning | Units | Default value | Value range Min | Max | Calibrated Parameter Value |
|------|---------|-------|---------------|-----------------|-----|----------------------------|
| | Snow routine | | | | | |
| Tx | Threshold temperature for rain/snow | °C | 0.0 | -2.5 | 2.5 | -1.1629 |
| Ts | Threshold temperature for snowmelt | °C | 0.0 | -2.5 | 2.5 | -2.3632 |
| Cx | Degree-day factor | mm/°C/day | 3.5 | 1 | 7 | 2.6604 |
| PKOR | Precipitation correction rainfall | --- | 1.0 | 0.5 | 1.7 | 0.7049 |
| SKOR | Precipitation correction snowfall | --- | 1.0 | 0.5 | 1.7 | 0.8361 |
| TTGD | Temperature lapse rate for clear days | °C/100 m | - 0.6 | -1.1 | -0.3 | -0.7729 |
| TVGD | Temperature lapse rate during precipitation | °C/100 m | - 0.4 | -0.8 | -0.2 | -0.6642 |
| PGRD | Precipitation lapse rate | --- | 0.01 | 0.0 | 0.1 | 0.0839 |
| Soil routine | | | | | | |
| FC | Field capacity in soil moisture zone | mm | 250 | 50 | 450 | 121.3990 |
| LP | Threshold value for PET in soil moisture | frac. of FC | 0.9 | 0.6 | 1.0 | 0.8001 |
| β | Parameter in soil moisture routine | --- | 1.0 | 1.0 | 4.0 | 1.7734 |
| Response routine | | | | | | |
| KUZ2 | Fast recession constant in Upper zone | 1/day | 0.2 | 0.1 | 0.6 | 0.1084 |
| UZ | Threshold level for quick runoff in Upper zone | mm | 20 | 5 | 65 | 58.0023 |
| KUZ1 | Slow recession constant in Upper zone | 1/day | 0.1 | 0.01 | 0.3 | 0.1089 |
| PERC | Percolation from Upper to Lower zone | mm/day | 0.9 | 0.5 | 2.0 | 1.9118 |
| KLZ | Recession constant in Lower zone | 1/day | 0.001 | 0.0005 | 0.01 | 0.0047 |

# CHAPTER 7

# HBV MODEL FORECASTS USING NUMERICAL WEATHER PREDICTION MODELS

## 7.1 Introduction

Hydrological models require meteorological input data for computation of watershed runoff values. These required meteorological values show variation both in time and space. A common source of spatially and temporarily varying meteorological data are the outputs of numerical weather prediction models.

Numerical weather prediction (NWP) is the name given to the technique used to forecast the weather by computer from its present, measured state up to several days ahead (URL-8). Hydrological forecast analyses are highly dependent on the forecasted meteorological data. As the accuracy of the meteorological forecast data increase, better results of the hydrological analysis can be derived. Such accurate hydrological analyses enable better hydropower production, optimization of water supply and flood control. Thus, future weather situations are the key interest of hydrological and meteorological model forecasts.

Operational runoff forecasts are being carried out in many countries of the world since decades using hydrological models of various complexity. In critical situations, the forecasts are required for flood warning purposes, otherwise they are used for planning of hydropower production and reservoir operation. Mainly in the eastern part of Turkey, snowmelt plays an important role in the formation of runoff where the highest peaks as well as the highest runoff volumes normally

occur during the melt season. Besides the work done by Şorman et al. (2004) and Tekeli (2005) so far, no real-time hydrological forecasting has been conducted according to author's knowledge by coupling atmospheric and hydrological models in the region.

This chapter will give a brief description about each of the numerical weather prediction models used in the study and the procedures followed in coupling the necessary atmospheric model outputs into the HBV model for runoff forecasting.

## 7.2 Numerical Weather Predictions (NWP) Models

### 7.2.1 European Center for Medium-Range Weather Forecasts (ECMWF)

Recognizing the economic and social benefits to be derived from more accurate medium-range forecasts, the European States agreed to combine their scientific and technical resources in this aspect of weather forecasting and decided to establish the European Centre for Medium-Range Weather Forecasts (ECMWF). The European Centre for Medium-Range Weather Forecasts (ECMWF, the Centre) is an international organization supported by 25 European States. Currently, its member states are Belgium, Denmark, Germany, Spain, France, Greece, Ireland, Italy, Luxembourg, the Netherlands, Norway, Austria, Portugal, Switzerland, Finland, Sweden, Turkey and United Kingdom. The states that have concluded co-operation with ECMWF are Croatia, Czech Republic, Iceland, Hungary, Romania, Slovenia and Serbia and Montenegro.

Originally a COST (European Cooperation in Science and Technology) project, the Centre was established in 1973 by a convention. The first real-time medium-range forecasts were made in June 1979 and the Centre has been producing operational medium-range weather forecasts since 1 August 1979.

ECMWF is a consequence of hundred year's development in dynamic and synoptic meteorology, fifty years of which are related with the development of the numerical weather prediction (NWP) methods. The principle objectives of ECMWF can be summarized as:

❉ the development of numerical methods for medium-range weather forecasting;
❉ the preparation, on a regular basis, of medium-range weather forecasts for distribution to the meteorological services of the Member States;
❉ scientific and technical research directed to the improvement of these forecasts;
❉ collection and storage of appropriate meteorological data.

Every day, ECMWF prepares 10-day weather forecasts and shares the numerical products with the meteorological offices of the member states by a dedicated telecommunications network. Turkey, being one of the member states since November 1975, uses these products to prepare medium-range forecasts for the end users.

## 7.2.1.1 Medium-Range Forecasts

ECMWF predicts the behavior of the atmosphere in the medium-range up to ten days ahead. In this time, the future state of the atmosphere at any point can be influenced by phenomena at very distant geographical locations. Thus, many applications of medium-range forecasting, for example ship routing or pollution dispersion, are not confined to limited areas of the globe. Therefore, the whole atmosphere is included in the model from the earth's surface to a height of 65 km. The discretization that can be afforded at the moment depends on the computer power available and how efficiently it is used.

The horizontal resolution of the discretization of the Centre's current model is equivalent to having 40 km evenly spaced grid points geographically around the globe. This network of points is then repeated at 60 levels in the vertical. The model forecasts wind, temperature and humidity at 20,911,680 points throughout the atmosphere. Even though very small scale effects, such as, heating of the soil by the sun, turbulence of the air near the ground and at high levels in the atmosphere and cumulus cloud systems, can not be represented properly with the most powerful computers available today, much effort is placed to take into account their influence on the behavior of the parameters of the large scales. Even so, with today's resolution it is possible, for example, to distinguish clearly the French Massif Central from the Alps and the Po valley in northern Italy. Hence it can be said that with this detail the Centre's model can produce a realistic forecast of the near surface weather parameters, such as local winds and temperature at the level of the measurement stations.

## 7.2.1.2 Making the Forecast and Products

In order to start the computer model, initial or starting conditions are required. Observations are used to calculate the weather (wind etc.) at each point throughout the model atmosphere. The forecast is made in short steps, of about 15 minutes ahead, with each forecast providing initial conditions for the next forecast step.

The preparation of initial conditions is both a delicate and demanding task which in the ECMWF forecasting system requires almost as much computer resources as a ten day forecast.

Initial conditions for the ECMWF global model are prepared by making an appropriate synthesis of observed values of atmospheric fields taken over a 24 hour period and short-range forecasts provided by the global model itself. This synthesis is a process of assimilating observed values into a model. The use of

both observations and model forecasts in the construction of initial values is required. High quality data are sparsely and irregularly distributed over the globe. Short-range model forecasts carry forward in time knowledge of earlier observations and also provide a crucial background for extracting useful information from expensive satellite observations.

The model variables for the computation of the forecasts are temperature, wind and specific humidity. These primary parameters are converted into other atmospheric parameters. A subset of parameters is available to ECMWF Member States through the operational dissemination system as shown in Table 7.1, where all parameters are available in lat-long grid form. These products are computed at 3 hourly intervals from 3 to 72 hours and at 6 hourly intervals from 72 to 240 hours.

## 7.2.1.3 Data Archives

Weather forecasting makes use and generates very large volumes of data that need to be stored for long periods including observations, analysis, forecast and also research experiments. These data represent a valuable asset, providing a detailed record of worldwide weather and weather forecasts over the past 25 years. To accommodate these data, ECMWF has a dedicated Data Handling System. In order to manage and access this large archive, ECMWF has developed a dedicated software: the Meteorological Archive and Retrieval System (MARS). Data is stored in standard formats agreed with the World Meteorological Organization, namely GRIB (GRIdded Binary) format for meteorological fields and BUFR (Binary Universal Form of Representation of meteorological data) format for meteorological observations.

Table 7.1 ECMWF dissemination products

| Operational products | Additional experimental products |
|---|---|
| Upper air parameters (on pressure levels and model levels<br><br>Mean sea level pressure<br><br>to day 7 | Upper air parameters (on pressure levels and model levels<br><br>Mean sea level pressure<br><br>from day 7 ½ to day 10 |
| 2 meter temperature<br>2 meter dew point<br>10 meter wind<br>10 meter wind gust<br>total precipitation<br>total cloud cover<br>to day 7 (every 3 h up to day 3, every 6 h beyond) | 2 meter temperature<br>2 meter dew point<br>10 meter wind<br>10 meter wind gust<br>total precipitation<br>total cloud cover<br>to day 7 (every 3 h up to day 3, every 6 h beyond)<br>Additional weather parameters:<br>large scale precipitation<br>convective precipitation<br>low cloud cover<br>medium cloud cover<br>high cloud cover<br>snowfall<br>snowdepth<br>throughout the forecast range |

## 7.2.2 Mesoscale Model (MM5)

The PSU/NCAR mesoscale model is a limited-area, nonhydrostatic or hydrostatic, terrain-following sigma-coordinate model designed to simulate or predict mesoscale and regional-scale atmospheric circulation. It has been developed at the Pennsylvania State University (PSU) and National Center for Atmospheric Research (NCAR) as a community mesoscale model and is continuously being improved by contributions from users at several universities and government laboratories (URL-9).

The Fifth-Generation NCAR / Penn State Mesoscale Model (MM5) is the latest in a series that developed from a mesoscale model used by Anthes at Penn State in the early 70's that was later documented by Anthes and Warner (1978 cited in URL-9). Since that time, it has undergone many changes designed to broaden its usage. These include (i) a multiple-nest capability, (ii) nonhydrostatic dynamics, which allows the model to be used at a few-kilometer scale, (iii) multitasking capability on shared- and distributed-memory machines, (iv) a four-dimensional data-assimilation capability, and (v) more physics options.

## 7.2.2.1 Components of MM5

The model (known as MM5) is supported by several auxiliary programs, which are referred to collectively as the MM5 modeling system.

A schematic diagram is provided to facilitate discussion of the complete modeling system in Figure 7.1. It is intended to show the order of the programs and the flow of the data and to briefly describe their primary functions. Documentation for various programs in the modeling system is available online (URL-10).
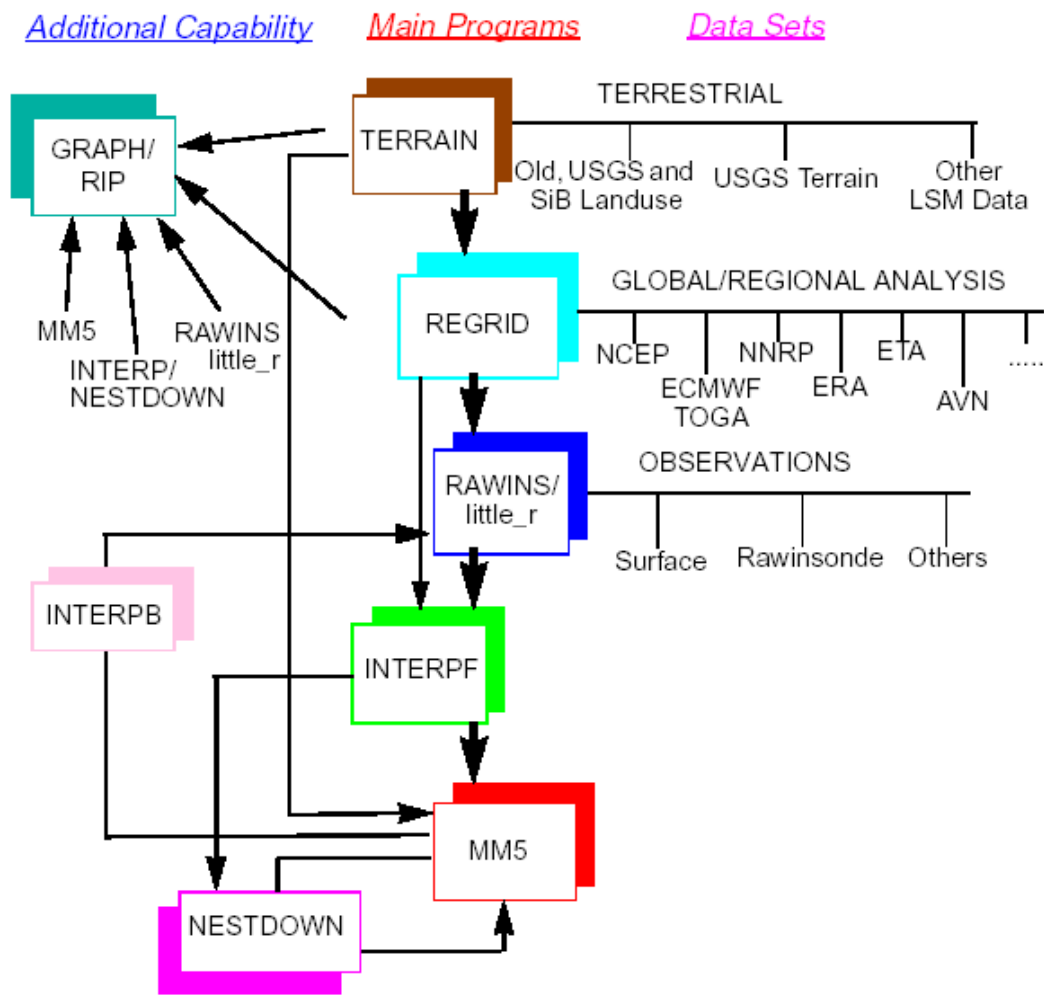
Figure 7.1 MM5 modeling system data flowchart (URL-10)

Terrestrial and isobaric meteorological data are horizontally interpolated (programs
TERRAIN and REGRID) from a latitude-longitude mesh to a variable high-resolution
domain on either a Mercator (low latitudes), Lambert Conformal (mid latitudes), or
Polar Stereographic (high latitudes) projection system. Since the interpolation does
not provide mesoscale detail, the interpolated data may be enhanced (program
RAWINS or little_r) with observations from the standard network of surface and
rawinsonde stations using either a successive-scan Cressman technique or
multiquadric scheme. Program INTERPF performs the vertical interpolation from

165

pressure levels to the sigma coordinate system of MM5. Sigma surfaces near the ground closely follow the terrain and the higher-level sigma surfaces tend to approximate isobaric surfaces. Since the vertical and horizontal resolution and domain size are variable, the modeling package programs employ parameterized dimensions requiring a variable amount of core memory. Some peripheral storage devices are also used. After the MM5 run, the data from sigma coordinate levels are interpolated back to the pressure levels by INTERPB. On the other hand, NESTDOWN can be used to interpolate model level data to a finer grid for preparation of a new model integration. Model outputs both on pressure and sigma surface levels can be viewed by graphic programs RIP or GRAPH.

## **Program Functions**

❉ TERRAIN

- Define model domain and map projection
- Generate terrain, and landuse catagory data on model grids
- Generate vegetation/soil catagory data for MM5 model's land-surface model option (V3 only)
- Calculate map-scale factors and Coriolis parameter for the model (V3 only)

❉ REGRID / (DATAGRID V2 only)

- Generate first-guess pressure-level fields on model grids from another model dataset
- Calculate map-scale factors and Coriolis parameter for the model (V2 only)

❉ RAWINS / LITTLE_R

- Perform objective analysis: blend first-guess fields with radiosonde and surface observations

❉ INTERPF / (INTERP V2 only)

- Interpolate pressure-level data from either RAWINS/LITTLE_R or REGRID/ (DATAGRID V2) to model's sigma coordinate

❉ MM5

- Perform time integration

❈ NESTDOWN
  • Generate fine mesh model input from coarse mesh model output   (1-way option). Capability of changing vertical sigma levels.
  • Generate fine mesh model input from coarse mesh model input
❈ INTERPB
  • Interpolate model sigma-level data to pressure levels
  • Generate first guess for RAWINS/LITTLE_R
  • Generate intermediate files for REGRID/regridder
❈ GRAPH/RIP
  • Generate plots from the output of modeling system programs (based on NCAR Graphics)

## 7.2.2.2 Data Required to Run MM5 Modeling System

For a successful MM5 run, the following data sets are required:
❈ Topography data
❈ Land use data
❈ Gridded atmospheric data having at least: sea level pressure, wind, temperature, relative humidity and geopotential height at the following pressure levels, surface, 1000, 850m 700m 500, 400, 300, 250, 200, 150, 100 mb
❈ Soundings and surface observations data

Topography, land use, vegetation and soil data with global coverage in varying resolutions are available from NCAR website (URL-11). The modeling system is able to run on various computer platforms such as Cray, SGI, IBM, Alpha, Sun, HP, and PCs running Linux.

### 7.2.2.3 Lateral Boundary Conditions

Since MM5 is a regional model, it requires an initial condition as well as lateral boundary condition to run. To produce lateral boundary condition for a model run, one needs gridded data to cover the entire time period that the model is integrated. In MM5, all four boundaries have specified horizontal winds, temperature, pressure and moisture fields and can have specified microphysical fields (such as cloud) if these are available. Thus, before any model run, boundary values have to be set in addition to the initial values.

The boundary values can come from any of the following three places:

❈ Analyses at the future times

❈ Previous coarser mesh simulation

❈ Another model's forecast

### 7.2.3 Use of Numerical Weather Prediction Models in Turkey

Turkish State Meteorological Organization (DMI) is the responsible government organization for providing weather forecasts both in quantitative and qualitative form to other organizations and the public. Since Turkey is one of the member states of the ECMWF, Turkish State Meteorological Organization receives forecast products to prepare medium-range forecasts. By using ECMWF data as boundary conditions to MM5 modeling system, DMI also generates MM5 products to provide forecast data to the end users.

With a protocol signed between State Meteorological Organization (DMI) and Middle East Technical University (METU), Water Resources Laboratory (WRL), some of the ECMWF and MM5 products (temperature and precipitation data) are transferred from DMI to METU-WRL through file transfer protocol (ftp) to be used in snowmelt runoff forecasting in the Eastern Anatolian region of Turkey.

The advantage of MM5 over ECMWF is the temporal and spatial resolution improvements. As described earlier, ECMWF model forecasts are produced every 3 to 6 hours with 0.5° grid resolution whereas MM5 products are produced every 1 hour with 0.1° grid resolution. It is difficult to display the temporal resolution but spatial resolution difference between the two NWP models can be seen in Figure 7.2 which presents the air temperature grid forecasts.

a)



b)
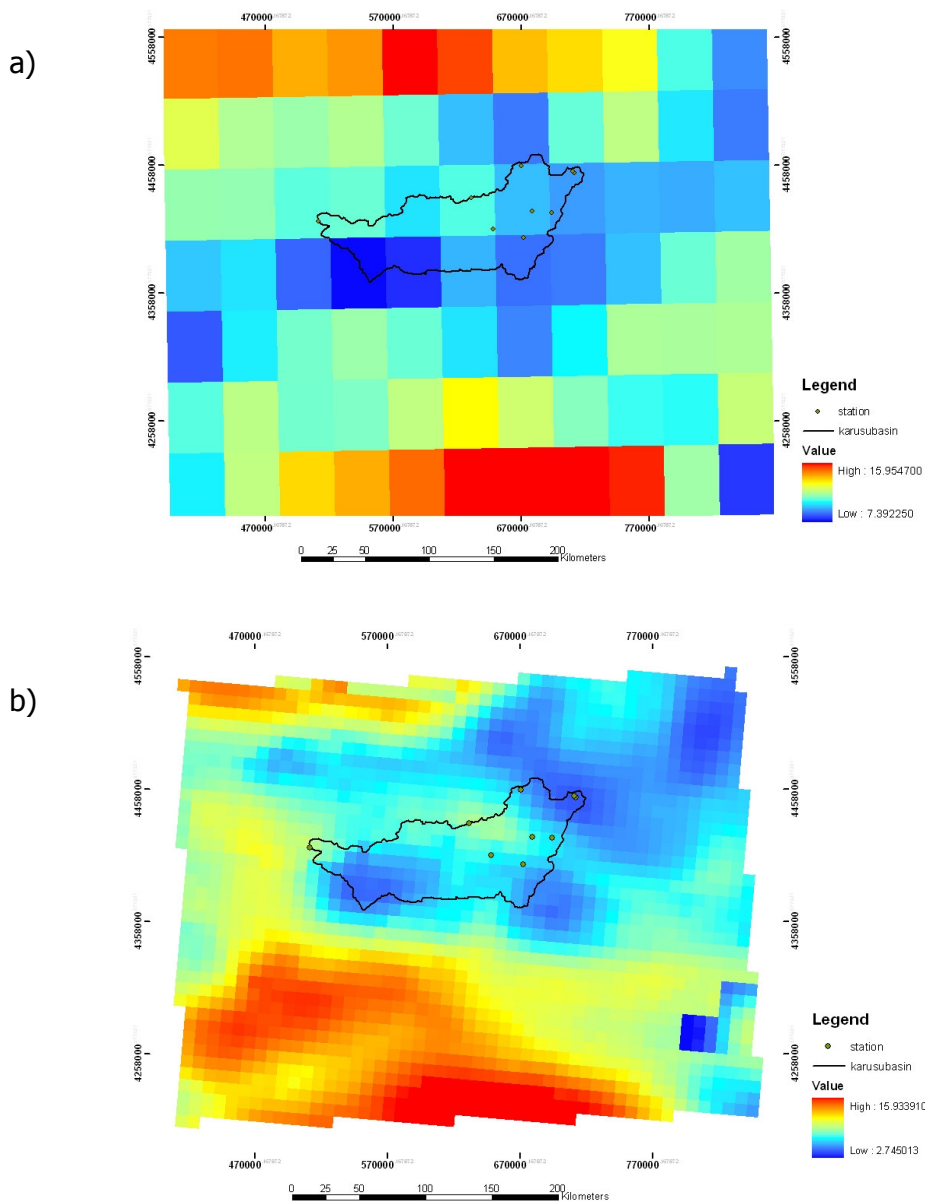


Figure 7.2 Forecast of air temperature (°C) in and around Karasu basin by

a) ECMWF    b) MM5

Another major difference between ECMWF and MM5 models is the topographic data layer used to predict and distribute the atmospheric conditions as depicted by Figure 7.3. It can be seen that MM5 layer has a finer elevation resolution than ECMWF data.

a)



b)
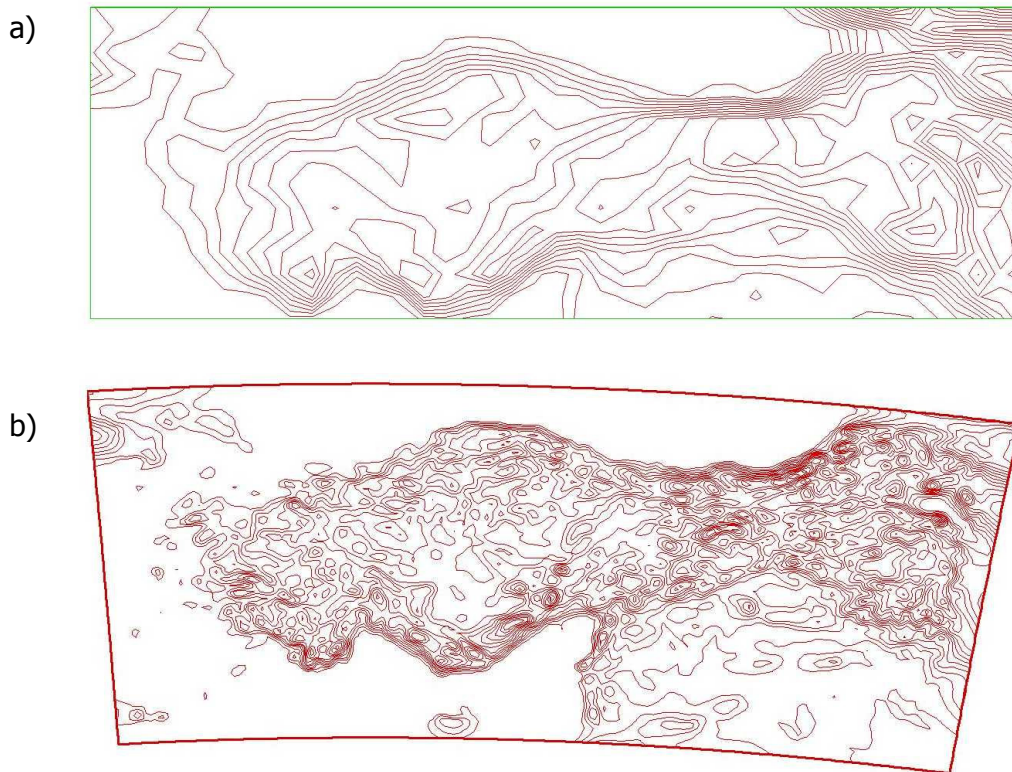


Figure 7.3 Elevation contours over Turkey by   a) ECMWF   b) MM5

Finally, MM5 modeling system also utilizes a land use layer during the generation of the forecasts whereas ECMWF does not make use of such a layer. This land use layer for the area of Karasu basin is shown in Figure 7.4. The higher elevated parts of the basin are classified mainly as crop/wood mosaic while the lower parts are composed of grassland, pasture and savanna formation. Although there are several different land use groups in and around the basin, it may still seem to be a very broad classification as compared to the land use groups determined by Landsat TM satellite images shown in Figure 6.5.
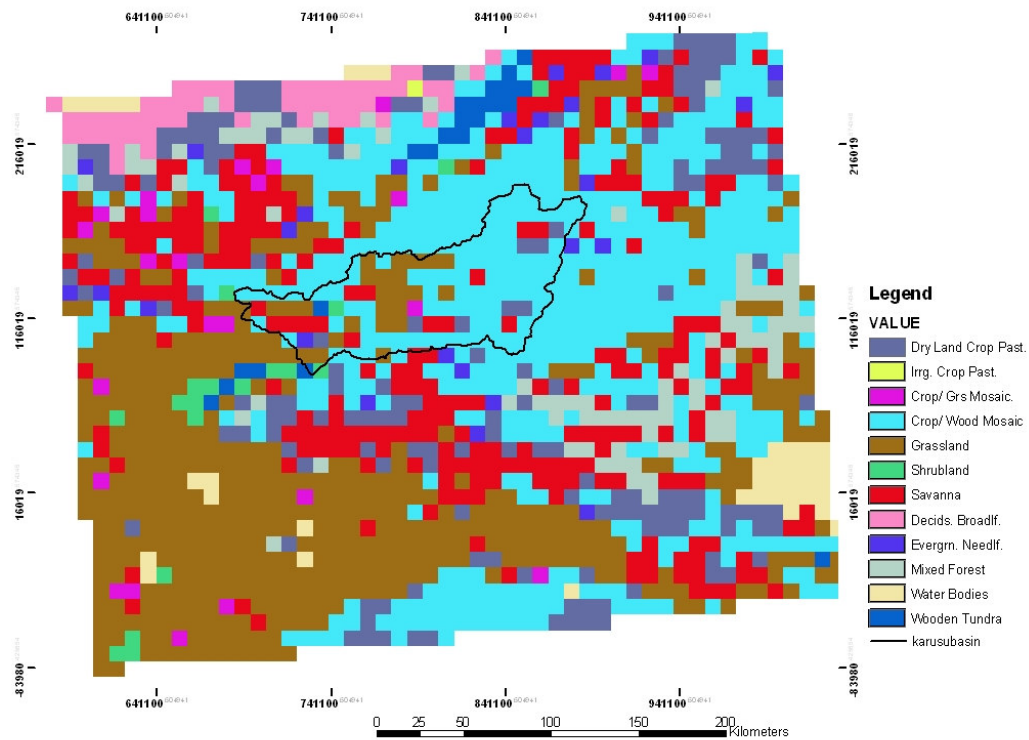
Figure 7.4 Land use layer utilized in MM5 forecasts

## 7.3 Snowmelt Runoff Forecasting in the Upper Euphrates Basin

Snow in the Eastern Anatolia starts to accumulate in late autumn and may stay on ground until early summer depending on the elevation. Since 60-70% of the total volume comes during the snowmelt season, early forecasting of the snowmelt runoff would enable optimum reservoir regulation which is very important as there are several large dams located in series on the Euphrates River.

In this respect, snowmelt runoff forecasting is conducted in the Upper Euphrates basin during the 2004 snowmelt season for the first time using numerical weather forecast models. Daily average temperature and total precipitation products of ECMWF and MM5 data are used as input data for the calibrated HBV model in the representative study area of Kırkgöze basin. As being a pioneer study in the region, this work could not be conducted in a real time form during its first

171

application due to several reasons stated below:

�test time limitations due to manual processing of the forecast data

✳ malfunction of the stream gaging station DSI 21-01 (outlet of Kırkgöze basin)

✳ missing forecast data at times

An interesting coincidence is that 2004 water year has evolved an untimely snowmelt event that occurred during late February and early March right after a significant snowfall in the eastern and southern parts of Turkey. This situation has resulted in the loss of human lives due to flooding and avalanches as well as in the inundation of many areas causing considerable damage to houses and farmlands. This situation has been reported by several national and international organizations and media at the time (URL-12; URL-13; URL-14; URL-15). Therefore, it was an important opportunity to evaluate how good the flooding situation could be predicted if the short term forecast products of numerical weather prediction models had been used in advance.

## 7.3.1 Forecast Processing Chain

There are basically four different data sets used in the forecasting process where the main steps of the processing chain are outlined in Figure 7.5. The processing chain is composed of a series of programs written for Unix and Windows environments. Fortran and Perl codes are mainly used under Unix environment whereas, custom-made Visual Basic scripts are complied in Windows media. Data sets are received from various platforms and are passed through different processes which are explained in more detail in the following sections. In the end, all the data are compiled to prepare the model input for runoff forecasts. Since different data are received and processed in different platforms, a fully automatic forecast processing chain could not be performed during the study although, such automation is necessary and should be considered as a future progress.
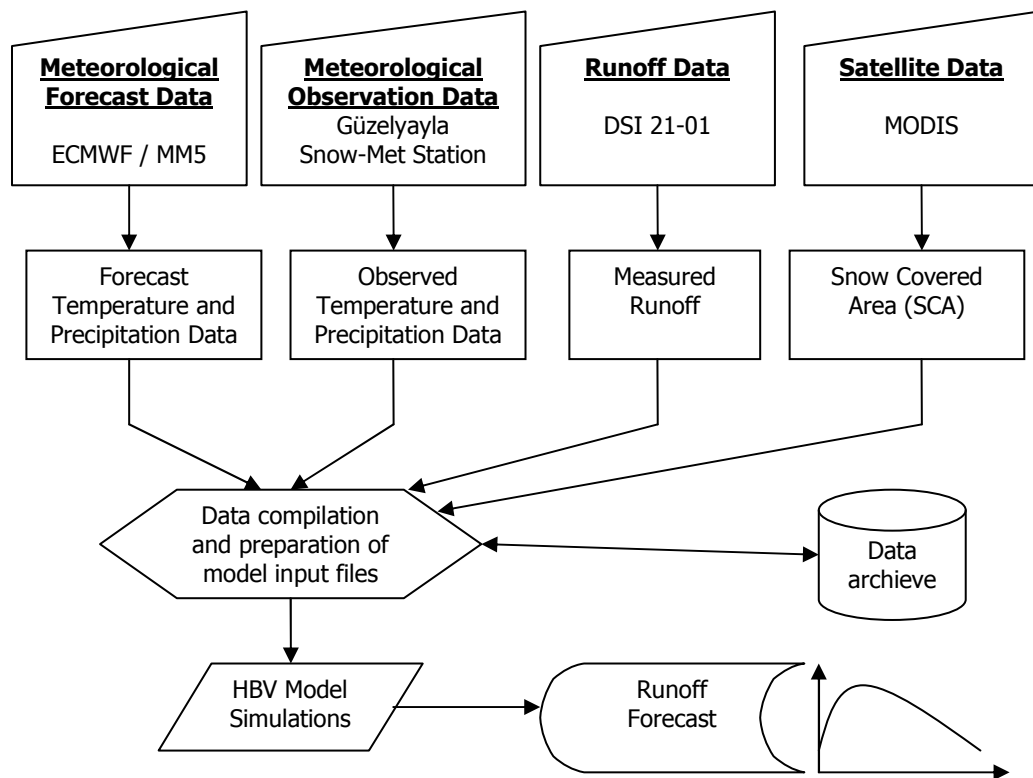
Figure 7.5 Data processing chain for runoff forecasts

Meteorological Forecast Data

ECMWF forecasts are transferred to Turkish State Meteorological Organization (DMI) via file transfer protocol. Using these ECMWF data as boundary conditions for Turkey, a nested MM5 forecast is determined at a finer resolution. Both of the NWP model outputs are then uploaded to METU server from DMI via shell scripts at the beginning of each day (around 4:00 am).

The two NWP model data come in different formats. ECMWF data are available in GRIB (GRIdded Binary) format, whereas, MM5 data are in RIP (Read-Interpolate-Plot) format. Since each output format is unique, different strategies are developed to decode the data sets. The flowchart for the processing chains of ECMWF and MM5 output are given in Figure 7.6. Following the decoding process, both data sets are imported into a GIS environment where necessary projection information are firstly added in order to perform several GIS spatial analysis.

**a)**

```
┌─────────────────────────────┐
│    ECMWF Headquarters       │
│   (execution of model runs) │
└─────────────────────────────┘
              │
              ▼
┌─────────────────────────────┐
│    Data transfer to DMI     │
│        (via FTP)            │
└─────────────────────────────┘
              │
              ▼
┌─────────────────────────────┐
│    Data transfer to METU    │
│        (via FTP)            │
└─────────────────────────────┘
              │
              ▼
┌─────────────────────────────┐
│   Data download to WRL      │
│ (from Unix to PC environment)│
└─────────────────────────────┘
              │
              ▼
┌─────────────────────────────┐
│    Decode of GRIB data      │
│   (custom-made BAT code)    │
└─────────────────────────────┘
              │
              ▼
┌─────────────────────────────┐
│   Subset Area of Interest   │
│    (custom-made VB code)    │
└─────────────────────────────┘
              │
              ▼
┌─────────────────────────────┐
│      Import to ArcGIS       │
│    (GIS spatial analysis)   │
└─────────────────────────────┘
              │
              ▼
┌─────────────────────────────┐
│ Preparation of Model Input Files│
│    (table, graph, report)   │
└─────────────────────────────┘
```

**b)**

```
┌─────────────────────────────┐
│            MM5              │
│ (execution of model runs using│
│  ECMWF as boundary conditions)│
└─────────────────────────────┘
              │
              ▼
┌─────────────────────────────┐
│    Data transfer to METU    │
│        (via FTP)            │
└─────────────────────────────┘
              │
              ▼
┌─────────────────────────────┐
│     Decode of RIP data      │
│ (custom made FORTRAN code - │
│           UNIX)             │
└─────────────────────────────┘
              │
              ▼
┌─────────────────────────────┐
│   Subset Area of Interest   │
│  (custom-made FORTRAN code -│
│           UNIX)             │
└─────────────────────────────┘
              │
              ▼
┌─────────────────────────────┐
│  Determination of daily ave.│
│ temp and total prec. (custom-│
│    made PERL code - UNIX)   │
└─────────────────────────────┘
              │
              ▼
┌─────────────────────────────┐
│   Data download to WRL      │
│ (from Unix to PC environment)│
└─────────────────────────────┘
              │
              ▼
┌─────────────────────────────┐
│      Import to ArcGIS       │
│    (GIS spatial analysis)   │
└─────────────────────────────┘
              │
              ▼
┌─────────────────────────────┐
│ Preparation of Model Input Files│
│    (table, graph, report)   │
└─────────────────────────────┘
```

Figure 7.6 NWP model data processing chains

a) ECMWF GRIB data          b) MM5 RIP data

174

Meteorological Observation Data

Ground based meteorological data are provided from the five automatic snow-met stations set up in and around Karasu basin where details are given in Chapter 4. For this study on the Kırkgöze basin, only Güzelyayla snow-met station is used as the representative in situ station for validation purposes of the forecast data since it is located within the basin boundary. Although data from other stations may also be used to compare in case of a break-down or malfunction of any instrumentation at Güzelyayla snow-met station. The flowchart of this process is given in Figure 7.7.
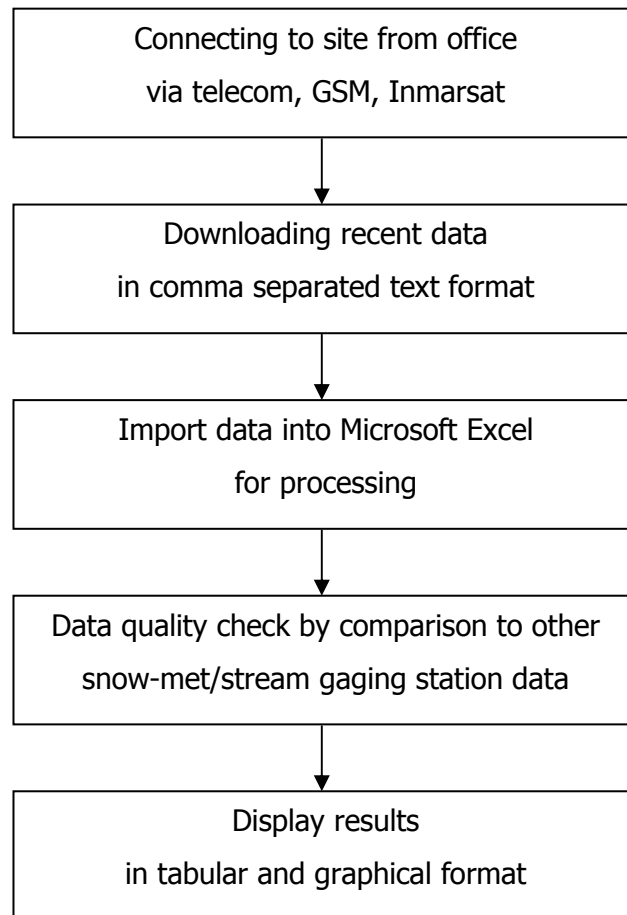


Figure 7.7 Hydro-meteorological data processing chain

<u>Runoff Data</u>

As given in Chapter 4, there are three automatic stream gaging stations located in Karasu basin. But for this study, runoff from only DSI 21-01 station is taken into account that drains Kırkgöze basin although measurements from the other stations are also monitored for data comparison purposes and to be used in case of instrumentation malfunction. The flowchart of this process is identical to meteorological observation data hence can be related to Figure 7.7.

<u>Satellite Data</u>

MODIS satellite images are used in this study to determine snow covered area depletion in Kırkgöze basin especially during the 2004 snowmelt period. Daily MODIS images of snow cover (MOD10A1), where the algorithm is explained in Chapter 5, are downloaded from NSIDC by FTP. These images are later processed in the order as shown by Figure 7.8 to be used in the snow covered area comparison derived from the HBV model simulations.

## 7.3.2 Model Input Data

Since data arrive from several different sources in various formats, the preparation of input files into the HBV model are performed manually. Two parameter sets on the Pareto front determined in Chapter 6 are utilized to predict snowmelt runoff at the outlet of Kırkgöze basin (DSI 21-01) for the 2004 snowmelt season. One set is the Pareto tail point that minimizes the discharge error (Q-model) and the second set is the balanced optimum point (QS-model). The model input data are composed of four main data sets as described in the forecast process chain. In this section, the necessary model input data and their timing are described for a real-time runoff forecasting process.

```
┌─────────────────────────────────────┐
│     Ordering MODIS daily snow cover  │
│     images from NSIDC                │
└─────────────────────────────────────┘
                  │
                  ▼
┌─────────────────────────────────────┐
│     Downloading the ordered MODIS    │
│     images from NSIDC by FTP         │
└─────────────────────────────────────┘
                  │
                  ▼
┌─────────────────────────────────────┐
│   Mosaicking MODIS images if         │
│   necessary and reprojecting to      │
│   UTM coordinate system              │
└─────────────────────────────────────┘
                  │
                  ▼
┌─────────────────────────────────────┐
│     Importing into a RS/GIS software │
│     to add color and name attributes │
└─────────────────────────────────────┘
                  │
                  ▼
┌─────────────────────────────────────┐
│     Overlay analysis to determine    │
│     snow covered area percentages    │
└─────────────────────────────────────┘
                  │
                  ▼
┌─────────────────────────────────────┐
│     Display results                  │
│     in tabular and graphical format  │
└─────────────────────────────────────┘
```
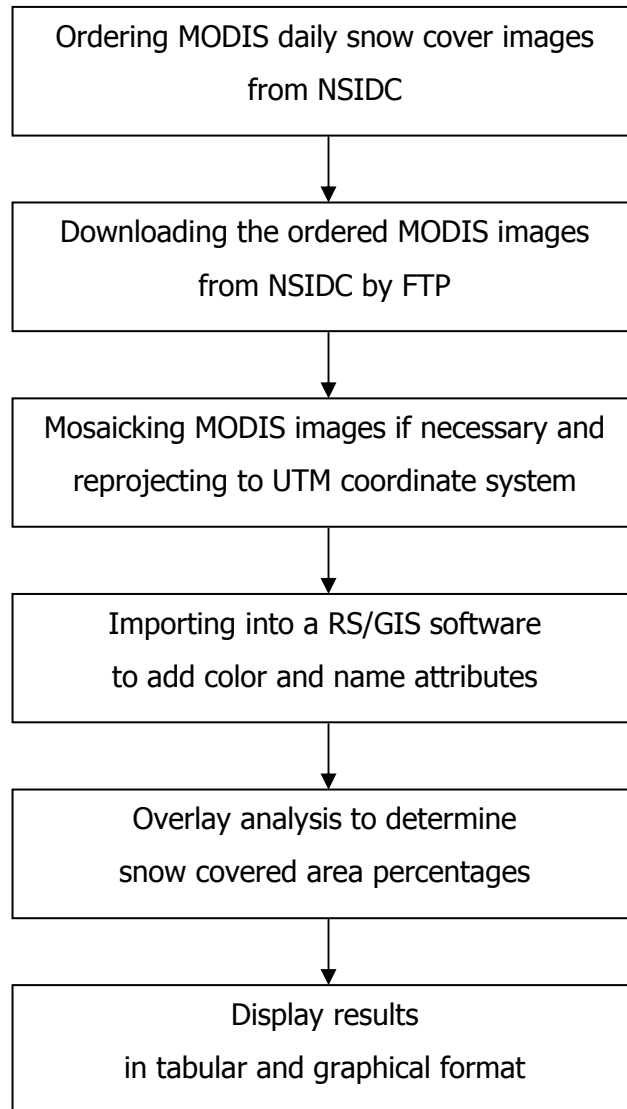
Figure 7.8 Flowchart of MODIS snow covered area determination

Meteorological Forecast Data

The meteorological forecasts are composed of temperature and precipitation data in a daily format as used by the HBV model from numerical weather predictions models of ECMWF and MM5. The basin under study is represented by 1 grid of ECMWF or 9 grids of MM5 data, as can be seen in Figure 7.9 showing two forecast day examples. The ECMWF forecasts consist of a 1-day ahead (t+24 hour) daily average temperature and daily total precipitation data. The MM5 forecast data

ECMWF Temperature (°C) 6 Mar 2004

ECMWF Precipitation (mm) 6 Mar 2004

MM5 Temperature (°C) 6 Mar 2004

MM5 Precipitation (mm) 6 Mar 2004

ECMWF Temperature (°C) 28 May 2004

ECMWF Precipitation (mm) 28 May 2004

MM5 Temperature (°C) 28 May 2004

MM5 Precipitation (mm) 28 May 2004
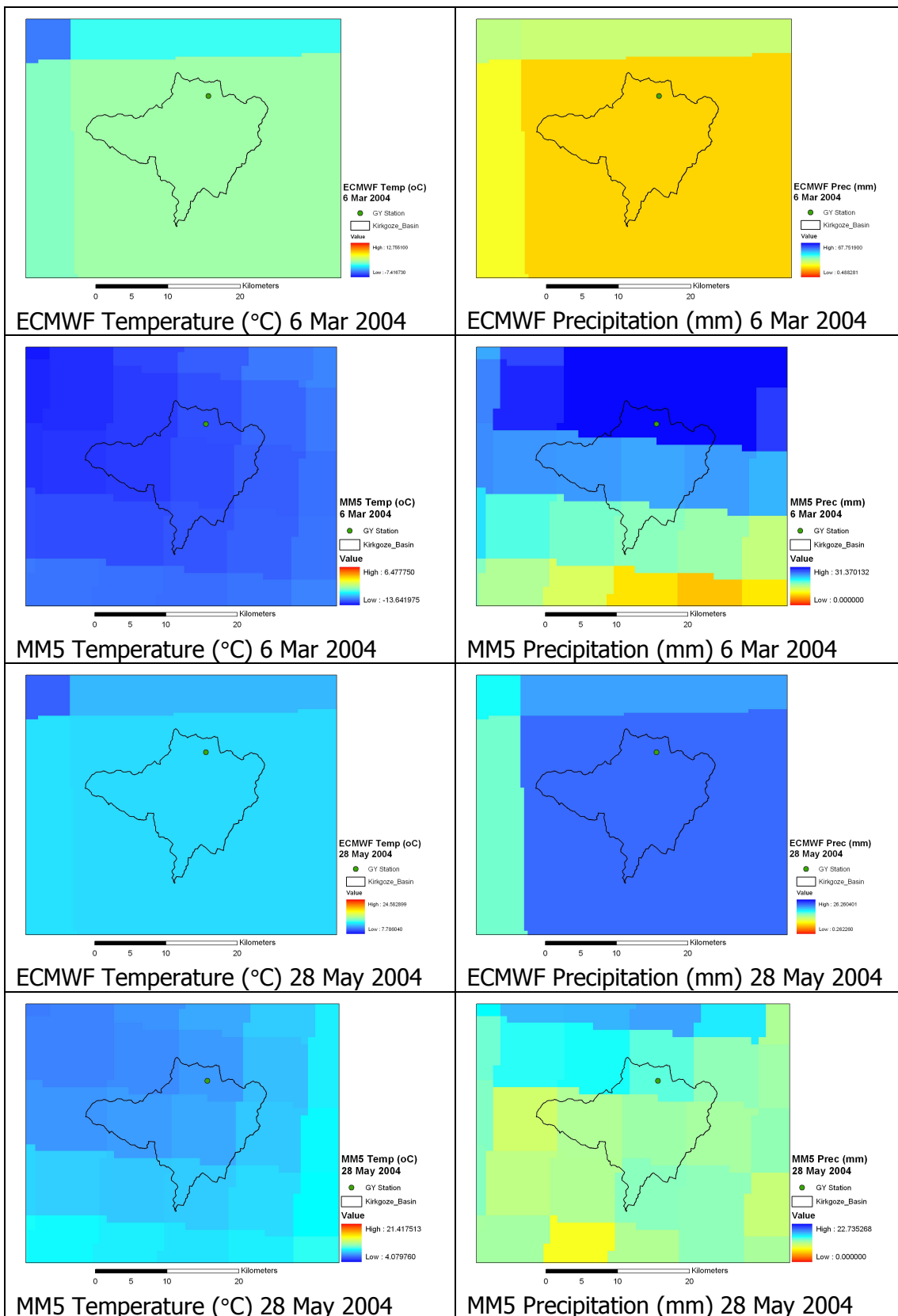
Figure 7.9 Daily forecasts of ECMWF and MM5 data

include again 1-day ahead (t+24 hour) temperature values for 07:00, 14:00 and 21:00 local times. Although hourly MM5 forecast data are available in DMI, the use of such data would have considerably increased the memory size as well as the processing time needed to conduct this study. Hence daily average temperature is calculated from the given three values as would generally be done on a ground climate station. The daily total precipitation from MM5 data are determined by the addition of convective and non-convective precipitation values for the related day.

The meteorological forecast data are available from the beginning of the snowmelt season which is marked by 29 February 2004 until 30 June 2004. MM5 forecasts are preferred to be used when available because of its finer spatial resolution, but at times when they were missing generally due to a problem in the FTP uploading from DMI, ECMWF data back up the missing days for model input. The acquisition timing and method of meteorological forecast data availability are presented in Table 7.2.

Meteorological Observed Data

Daily forecast temperature and precipitation data are validated with ground station measurements from Güzelyayla (GY) automatic snow-met station inside the Kırkgöze basin each day. The differences between the observed and forecast values for both temperature and precipitation data are compared and plotted in Figure 7.10 and 7.11 respectively. Daily forecast results for each day are replaced with the observed values for the next day's model simulation throughout the forecast period. The collected 2-hourly and daily observed data can be reached online 24-hours a day using telephone modem as summarized in Table 7.2.
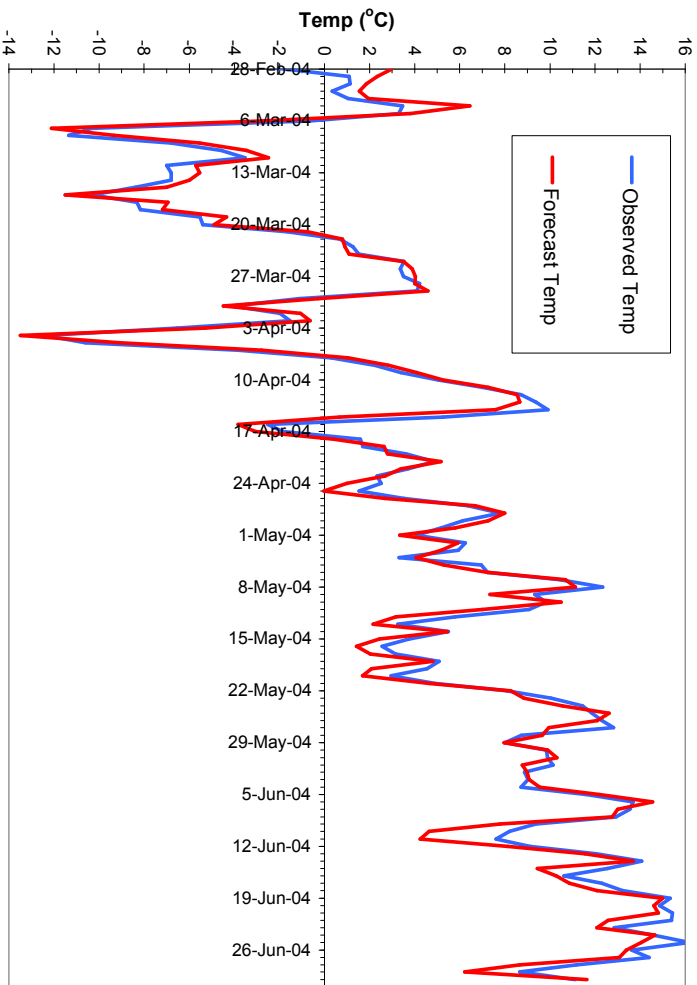
Figure 7.10 Observed and forecast temperature comparison
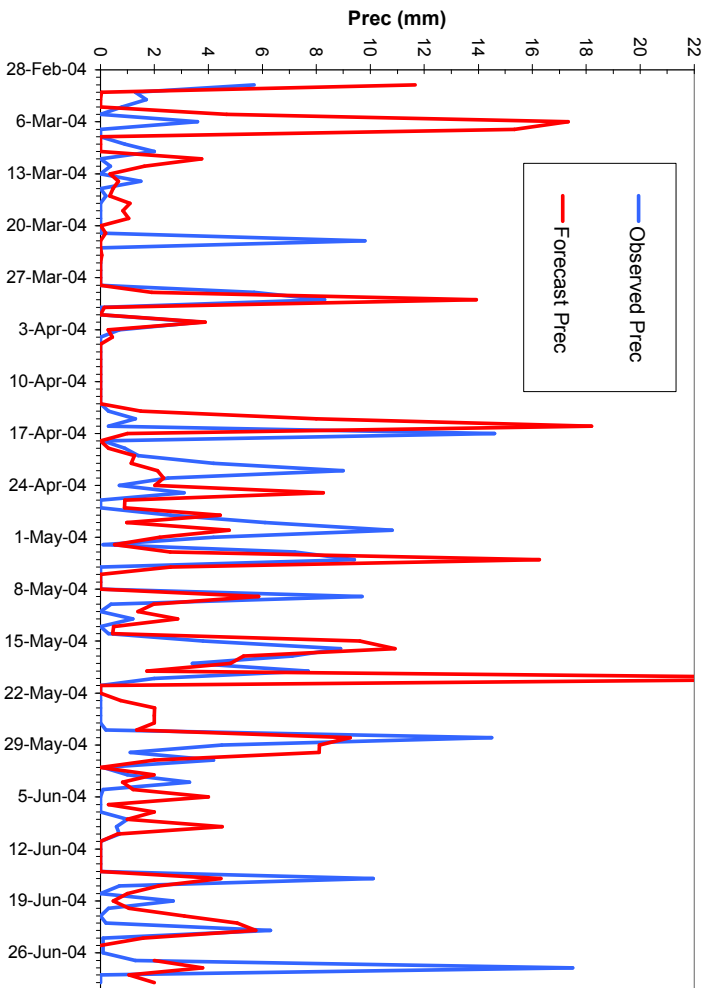


Figure 7.11 Observed and forecast precipitation comparison

180

Runoff Data

For a real-time runoff study, the model discharge simulations computed with the 1-day lead time forecast data need to be validated and updated continuously. Therefore, stream gaging station DSI 21-01 at the Kırkgöze basin outlet was automated for the 2004 water year to collect discharge data every 15 minutes and transmit this data when connected via GSM. But the instrumentation failed to work properly during the melt season. As a result, discharge data could not be collected in a real-time form and was instead obtained manually from time to time when the data logger was downloaded from in situ. Because of this inconvenience, for the 2005 water year, the shaft encoder instrumentation measuring water level at the stream gaging station is replaced by a pressure sensor. This equipment is working without a problem for the continuing 2005 water year transmitting the collected data by GSM when needed. For runoff forecast validation, the availability and timing of the measured runoff data are given in Table 7.2.

Snow Cover Data

Although discharge can be regarded as the most important output for any hydrological model, the internal model variables should also be physically consistent. Otherwise the model would be working right for the wrong reason. Hence, snow cover in the melt season is tracked by MODIS satellite images in order to compare with the model simulation results. Daily MODIS snow cover data (MOD10A1 for Terra platform and MYD10A1 for Aqua platform) are downloaded from NSIDC for the 2004 melt season. Each snow cover image is processed as described earlier in the chapter and those least affected by cloud obstruction are selected. Each MODIS image is ordered from NSIDC by a delay of 3-4 days and has to be downloaded by ftp. The availability and timing of MODIS SCA images are presented in Table 7.2.

Table 7.2 Availability of input data

| Forecast meteorological data | | | |
|---|---|---|---|
| **Data Type** | **Availability** | **Via** | **Arrival Time** |
| MM5 | Daily | FTP from DMI | ~ 4:00 am each day |
| ECMWF | Daily | FTP from DMI | ~ 4:00 am each day |
| Observed meteorological data | | | |
| **Station Name** | **Availability** | **Via** | **Arrival Time** |
| Güzelyayla (GY) | 2-hour and daily | Telephone modem | Online 24 hours |
| Runoff data | | | |
| **Station Name** | **Availability** | **Via** | **Arrival Time** |
| Kırkgöze DSI 21-01 | 15-min and daily | GSM | Online 24 hours |
| Snow cover data | | | |
| **Satellite Name** | **Availability** | **Via** | **Arrival Time** |
| MODIS (Terra/Aqua) | Daily (3-4 days delay) | FTP from NSIDC | ~ ½ day after ordering |

## 7.3.3 Forecast Simulations

The above mentioned four data sets are utilized to forecast daily runoff and snow covered area using the HBV model and compare the results with the observed values for the snowmelt period starting from 29 February and continuing until 30 June during the 2004 water year. The results of the Q-model parameter set for runoff and snow covered area are plotted in Figure 7.12 and Figure 7.13 respectively. Figure 7.14 and Figure 7.15 show the same results for the QS-model parameter set. Apart from the visual comparison, Table 7.3 is prepared to evaluate the differences between the two model runs for the forecast period using various goodness-of-fit criteria described earlier in Chapter 6.
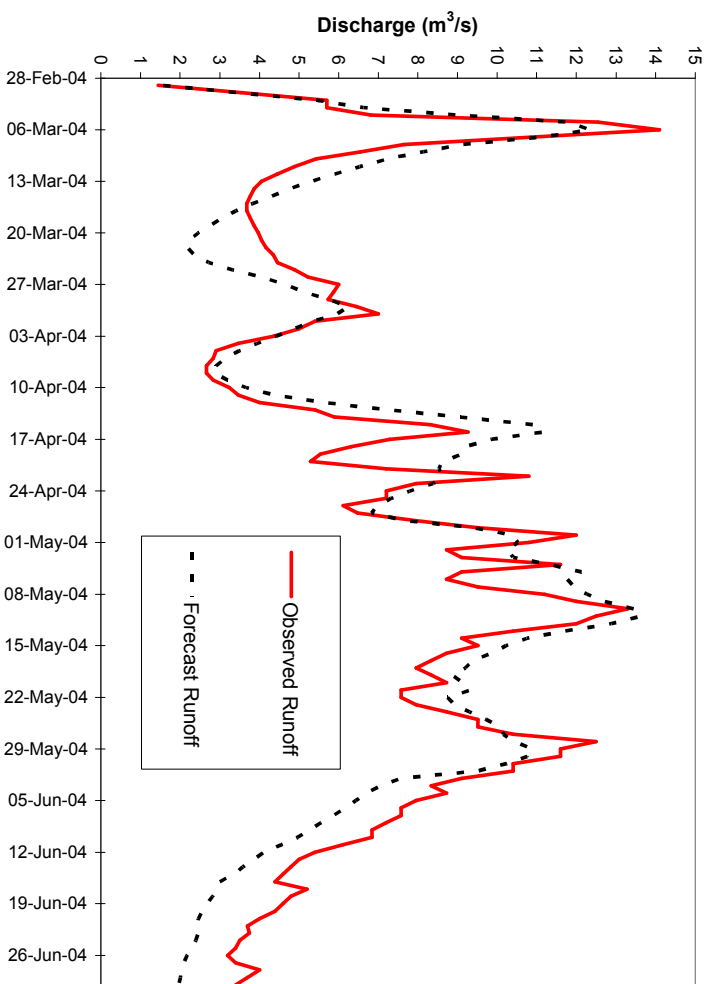
Figure 7.12 Forecast runoff for 2004 with Q-model parameters
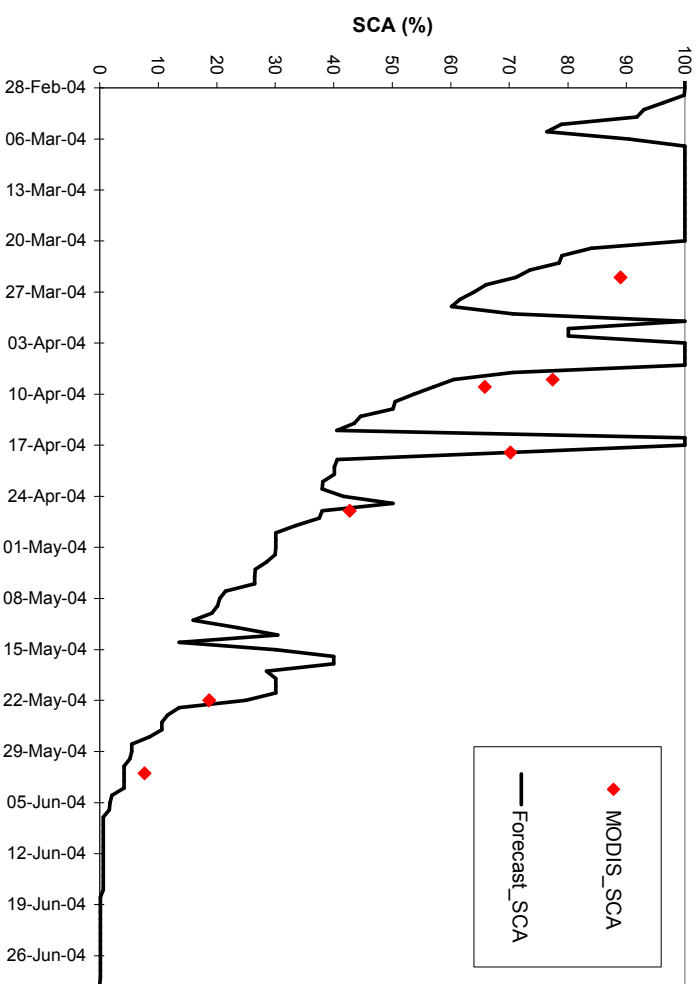


Figure 7.13 Forecast SCA for 2004 with Q-model parameters

183
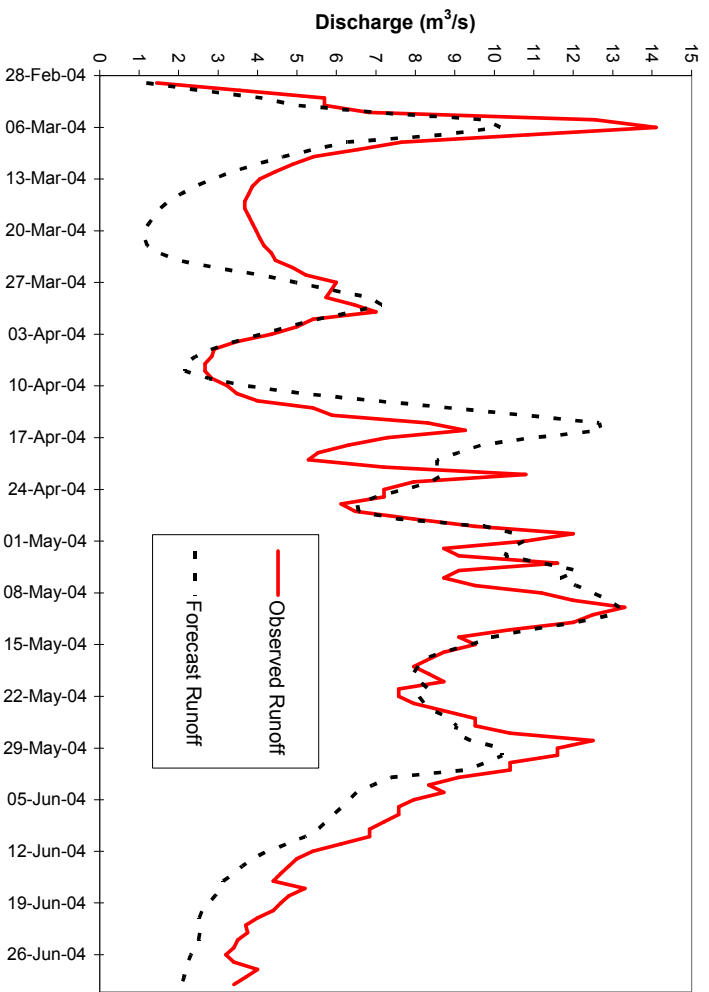
Figure 7.14 Forecast runoff for 2004 with QS-model parameters
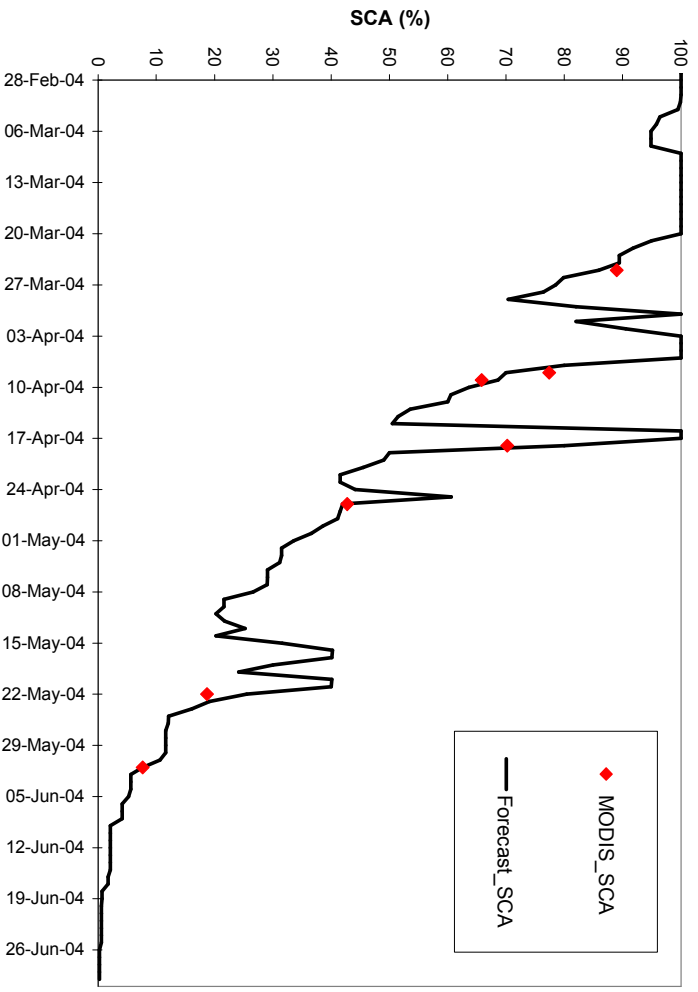


Figure 7.15 Forecast SCA for 2004 with QS-model parameters

184

Table 7.3 Forecast simulation results of the two models

| Model | Q-model | QS-model | Difference |
|---|---|---|---|
| Water Year | 2004 | 2004 | 2004 |
| Simulation Period | 29/2/2004 - 30/6/2004 | 29/2/2004 - 30/6/2004 | 29/2/2004 - 30/6/2004 |
| $RMSE_Q$ | 1.432 | 1.727 | -0.295 |
| $RMSE_{SCA}$ | 10.391 | 5.542 | +4.849 |
| $R^2_Q$ | 0.750 | 0.637 | -0.113 |
| $R^2_{SCA}$ | 0.867 | 0.962 | +0.095 |
| $V_E$ | 0.0014 | 0.0648 | -0.0634 |
| $R^2_{TOT}$ | 0.808 | 0.794 | -0.014 |

On the overall, the two models both simulated runoff and snow covered area quite well even when using 1-day lead time numerical weather prediction data for the HBV input parameters. Runoff in the Q-model is predicted better than the QS-model but on the contrary snow covered area is better estimated using the QS-model parameters compared to the Q-model. The volume error, which is used as a penalty on the total, increases with the QS-model parameters. Hence on the overall goodness-of-fit giving equal weight to runoff and snow covered area with a minor penalty for volume error, Q-model gives a slightly better fit than the QS-model.

Generally in the region, the initial increase on runoff usually occurs when the ripe snowpack first starts to melt during mid-march. But the timing of the first peak in the 2004 snowmelt season occurred earlier than expected with a high magnitude, beginning on 29 February 2004, which was the main reason for the flooding in the region. Comparing the hydrographs, Q-model simulates this high initial peak better than the QS-model, most probably because of the higher degree-day factor parameter. In relation to the same time period, the SCA depletion is greater for the Q-model as expected since more snow is allowed to melt. Having the lower initial peak for the QS-model hydrograph, the following two runoff peaks are higher than

the Q-model. Since the SCA line approximately indicates 40% at the beginning of May in both models, this shows that nearly equal amount of snow has melted until the beginning of May in which the Q-model melts the pack more in the earlier part of the season whereas QS-model has a slower start for the beginning but with an increasing reaction. Both models show a similar reaction during the mid melt period simulating the timing and peaks quite well. In the same manner, both of the model hydrographs do not give a good fit for the final part of the melt season always indicating an underestimation. This could be related to an incorrect precipitation correction in the model parameters (pkor), a missed precipitation representation for the model input from NWP models or with a small probability an incorrect computation of the observed hydrograph itself from the varying rating curve due to sedimentation.

The study shows that meteorological output from numerical weather prediction models (MM5 and ECMWF) give valuable information on the early prediction of runoff. Although only 1-day lead time is presented in this work, further increase on the lead time (from a couple of days to a week) can be evaluated but with an increasing uncertainty (Johansson et al., 2001). This uncertainty is especially higher for the precipitation values which are difficult to forecast accurately for periods longer than 1-2 days in advance (Vehvilainen and Huttunen, 2001).

Even though quite satisfying results have been achieved in coupling atmospheric and hydrologic models for runoff forecasting, there are a couple of points that may need to be addressed for a more representative watershed modeling. Firstly, not all the information supplied by the NWP models are utilized in the HBV model. Meteorological variables other than temperature and precipitation, such as radiation and wind, are known to affect snow melt and evaporation significantly. Also, the distribution of meteorological variables within the watershed and through time is simplified in the HBV model. Instead of using gridded data, HBV can only represent subbasins and zone levels.

Keeping these points in mind, improvements both on atmospheric and hydrologic modeling continuously follow one another with the rapidly growing collaboration of hydrologists and atmospheric scientists. Through these developments, hopefully in the very near future, coupling of atmospheric and hydrologic modeling especially for runoff forecasting will become a standard tool for better planning of hydropower production, reservoir operation and especially for flood warning purposes.

# CHAPTER 8

# CONCLUSIONS AND RECOMMENDATIONS

## 8.1 Introduction

This chapter summarizes the main results of the preceding chapters and addresses the question on how successfully the aims have been achieved. The important limitations faced during the study are outlined and suggestions on to how they might be improved and additional recommendations for future work are put forward.

The two major aims initially stated at the beginning of the study were:

i) To apply one of the well-known conceptual hydrological models in a basin in Turkey for the first time not in a traditional manner using only runoff but also including satellite snow covered area as an additional variable. This would enable the generation of Pareto front (non-dominant solutions) between runoff and snow covered area to determine the balanced optimum parameter sets.

ii) To use numerical weather predictions model output as input into the calibrated hydrological model and perform operational runoff forecasts with a 1-day lead time for part of the 2004 water year when snowmelt is dominant.

These aims were accomplished through a combined monitoring and modeling approach within the general framework of numerical model application in hydrology. The extent to which these objectives have been achieved and the main results arising from the work presented are discussed below.

## 8.2 Conclusions

In the first part of the thesis, the automatic calibration of the HBV model is carried out in Kırkgöze basin using two different procedures. The first one against runoff data alone (Q-model) and the other is using both runoff and snow covered area (SCA) together (QS-model). The results prove that the HBV model can be calibrated against SCA in addition to runoff with only a small reduction in the model performance. The improved performance in SCA was considerably higher than the loss of performance in runoff. Consequently, on the overall, the total model performance increases around 3.7% for the QS-model including both runoff and SCA as compared to Q-models simulations.

Inspecting the variation for the normalized ranges of the calibrated HBV model parameters, only a few of the model parameters are found to be well-defined while for the others, good fits are obtained over broad ranges. Although it was expected that the use of additional data would help to decrease the model parameter uncertainty by constraining the ranges of parameter values, it was not so clear to state it in this study. The study did, however, rely upon a relatively short duration of recorded data for the watershed under consideration. The capability of the automatic calibration algorithm and the uncertainty analysis methodology, as well as the behavior of the simulation model could be more effectively tested if the calibration, verification, and uncertainty analysis efforts could be applied to a 'data rich' watershed.

In the last part of the calibration process, the Pareto front is investigated for the non-dominant set of solutions using runoff at one axis and snow covered area on the other. A number of tests have been carried out to determine the tails of the front as well as the balanced optimum values located at the intermediate part of the front closer to the origin. From a multi-objective point of view all the points lying on the Pareto front are equally as good, but obviously for practical applications some points are more relevant than others. For example, the tail point that minimizes SCA is not a very realistic approach in modeling, as runoff is

189

probably the most important output in any hydrological model. But in the same sense, considering runoff as the only relevant model result could approach to a reasoning where a model may predict runoff correctly regardless of the internal parameters. Hence, depending on the priority of the objectives, one may shift either way in the Pareto front although a balanced optimum is preferred most of the time, as done in this case, for a hydrologically sound application.

The result of the first part of study indicates that integration of satellite observed SCA in hydrological modeling requires persistence. Therefore, the benefit from the Earth Observation data may not be obvious for years when the snowpack is well simulated by the model, although showing a confirmation of the model estimate. But during unusual snow distribution conditions where large deviations are present as in the distributed case of Şensoy (2005), snow covered images may be of valuable help allowing an updating of the model to represent the actual conditions in the area of concern (Engeset et al, 2003; Alfnes et al., 2005).

The techniques for model calibration may need to be further developed which requires substantial amount of reliable data for evaluation. In this lies an obvious obstacle. Without reliable data, there will be no model development. Without an active end user, remote sensing experts may not give their best efforts to produce high quality data (Johansson et al., 2003).

As a remark, one should also bring attention to the obvious shortcomings of the hydrological model (HBV) itself. It is unsatisfactory that the performance in predicting runoff deteriorates when additional information like that of SCA is included. This is a commonly known feature of the HBV model and the same behaviour is observed when including other observations of, say, groundwater, extension of saturated areas, or environmental tracers (Bergstrom et al., 2002). This brings attention to the problem of overparameterization in the HBV model that is quite effective in disguising flawed process descriptions. This study has obtained positive results when including SCA data, but part of the problem of not obtaining

even better results are not entirely related to imperfect SCA observations but also on inadequate description of the hydrological processes in the HBV model.

For the second part of the thesis, the calibrated HBV model using both Q-model and QS-model parameters are applied to forecast runoff with a 1-day lead time in the study area, although longer lead times are possible to use with increasing uncertainty. During the forecasts, the two models had the better of one another in different aspects, Q-model having a better runoff model performance whereas QS-model predicting SCA with a better fit. On the overall, the total model performances were quite similar with Q-model (0.808) having a small edge over the QS-model (0.794). Accordingly it can be concluded that, in its first attempt for the Upper Euphrates basin, the concept of hydrologic forecasting using numerical weather prediction model data gave promising results especially in the timing of the high runoff events. Consequently, it is shown that the possibility of operational runoff forecasting in the Eastern part of Turkey could be made applicable if such studies are put into operational use.

During the forecast simulations, the uncertainty of the predicted input data should not be underestimated. The reason is that a grid data ($0.1°$ spatial resolution corresponding to approximately 9 km) represents a point on the ground. Hence to improve the NWP output, especially for a rugged mountainous terrain, several ground stations at different locations and altitudes should be compared with the NWP data either using a downscaling or upscaling procedure.

Also to mention that especially during the period when rapid melting of snowpack starts at low and medium altitudes at which high deviation of SCA are expected to occur between simulated models runs and observed satellite products, rather than the number of satellite images in larger quantity, the quality (being free of clouds) as well as the timing of the images are more important (Tekeli et al., 2005a).

The present evaluation of the HBV model confirms that any major breakthroughs may not be expected in hydrological modeling as long as we limit ourselves to standard input data and judge the models by analysis of river runoff only. But by using additional data and improved calibration strategies, small improvements could be made possible to increase the confidence in the model and to take a step closer to physical reality.

As a final conclusion, it can be inferred with great confidence that real-time or at least near-real time monitoring of snow and hydro-meteorological data is a necessity for operational hydrologic modeling which can be utilized for the better management of water resources.

## 8.3 Recommendations

- Instrumentation malfunction occurred several times during the study period. Better sheltering and maintenance to some of the equipment is necessary. For example, the snow pillow pressure has to be adjusted before snow accumulation so that correct measuring of the weight above the pillow can be conducted. Also, special care must be taken for the snow lysimeter because the main operational function of this equipment is to show when ripe snow starts to generate flow. If any blockage in the equipment takes place due to icing or debris, the main snowmelt period could be missed.

- Some of the instrumentation in the current snow-met stations need updating. Since temperature is one of the easier meteorological variables to measure, precipitation should be measured more accurately especially as being one of the HBV model input. To measure precipitation both in the liquid and solid form somehow snow has to be melted to convert into water equivalent. This can be done either by heating the equipment or by using an antifreeze solution. The disadvantage of the first method is that it may increase the sublimation process whereas in the latter method, a lag time may occur before snow melts in the antifreeze liquid to be measured. But in

any case either of the methods would be very efficient to decrease the uncertainty for the "skor" model parameter.

- Further reliable data should be collected for a couple of more years in order to understand the basin response in different situations such as, quick melt on temperature increase only, rain-on-snow events, different snow depletion patterns and the range of runoff values during different snowmelt periods. This would also be useful enabling longer warm-up periods to determine the initial state of the model which has a significant effect on model results.

- Additional snow and meteorological stations need to be installed in Euphrates basin especially to represent Murat catchment where more of the snowmelt runoff is contributed compared to Karasu basin. For the selection of the new sites, different locations, elevation, slope, aspect and accessibility to the point should be taken into account.

- Additional snow and meteorological station data should be used considering a larger basin as the study area to see the response of scale factor on the calibration and forecast results.

- In order to test the overparameterization in the HBV model, a parameter identification procedure could be applied as in the case of Muleta (2005). Firstly, screening those parameters that could be reasonably estimated based on field data. Then a parameterization technique for transferring model parameters of a given spatial unit to other spatial units in the watershed using a selected representative subbasin. Finally, applying a parameter sensitivity analysis particularly for watersheds that lack long years of recorded data to reduce the number of calibrable parameters.

- As well as reducing the number of parameters for model calibration, adjusting the parameter range also needs careful attention. Although several limits can be found in literature, appropriate values should be tested that do not affect the model efficiency significantly.

- Besides determining the sensitive model parameters, uncertainty analysis should also be performed because uncertainty in models and data leads to uncertainty in model parameters and model predictions. Bevin and Binley

(1992) proposed a method called generalized likelihood uncertainty estimation (GLUE) that uses prior distributions of parameter sets and a method for updating these distributions, as new calibration data become available, to make probabilistic estimates of model outputs. In order to determine uncertainty GLUE method could be applied to the data set in hand.

- The simplified HBV model structure could be improved by additional input variables such as radiation (as one of the dominant energy fluxes for snowmelt), wind, humidity, cloud cover etc. and at the same time the daily time step for model simulations could be lowered. With these improvements a simple conceptual model can be turned into a more physically based model but for such changes to take place, a long test period with sufficient amount of reliable data at various geographical locations need to be conducted to make sure that the additional variables are beneficial for the operational use of the model.

- A log normal snow distribution is used in the HBV model applied in this study. According to Alfnes et al. (2005) a dynamic snow distribution using gamma sums is applied to represent the snow reservoir more correctly. Hence using new distribution functions could improve the model results especially on snow water equivalent and snow cover.

- Present version of the HBV model divides the basin into subbasins and further into elevation zones. Although the results achieved so far in literature are satisfactory, to improve on the current situation by better representing the physical conditions, delineation of subbasins into hydrologic response units (HRUs) based on physical characteristics of the watershed (i.e. elevation, slope, aspect, soil, land use) could be beneficial (Nagler, 2005).

- Besides the use of optical satellites to determine snow covered area, microwave remote sensing could be utilized to reflect other properties of snow such as snow water equivalent that could be verified by the ground snow-met stations and made use of as an additional variable in hydrologic modeling.

- Satellites providing snow covered area, such as NOAA and MODIS, represent a pixel in binary terms as either snow or no snow. But it is known that as the snowmelt season progresses patchy areas of snow appear. Such areas are generally depicted as snow covered because of the brighter snow reflectance. To represent such conditions, subpixel snow classification concept is being applied where a percentage of snow cover is expressed for each pixel of the image (Appel and Salomonson, 2005; Painter et al., 2005).

- MM5 forecast data may be improved by using a finer topographic layer from a Digital Elevation Model and a better land use layer obtained from satellite remote sensing such as MODIS or Landsat. Also inclusion of data assimilation would enable more accurate forecasts.

- A step ahead of the forecasting process is "nowcasting" where radar images can be utilized for runoff prediction. Such measurements may not give a lengthy time in advance but on the other hand could be much more accurate than an event which has not yet taken place.

- For the selection of model parameters, effects of weather phenomena, El Nino and La Nina, can be investigated.

- The current snow-met stations are set up by Middle East Technical University (METU) and State Hydraulic Works (DSI) personnel financed by State Planning Organization (DPT) projects conducted in METU. So far the operation and maintenance of this equipment are largely undertaken by the METU personnel but both the equipment and knowledge of use of the collected data has to be transferred to the government organizations and used operationally in the most appropriate manner possible besides continuing research studies in the universities.

# REFERENCES

Akyürek, Z. and Şorman, A.Ü. (2002), Accuracy Assessment of a Landsat Assisted Land-cover Mapping Case Study: City of Erzurum and its Vicinity-Turkey, *3rd International Remote Sensing Symposium of Urban Areas*, Istanbul, Turkey, 11-13 June 2002, Vol. 2, pp. 529-536.

Alfnes, E., Langsholt, E., Skaugen, T. and Udnaes H-C, (2005) *Updating snow reservoir in hydrological models from satellite observed snow covered areas*, Report No.4-2005, Norwegian Water Resources and Energy Directorate (NVE), Oslo, Norway.

Alfnes, E., Udneas, H.C. and Andreassen, L. (2004) Satellite-observed snow covered area and spring flood prediction in the HBV model, *The XXIII. Nordic Hydrological Conference*, Fresh Water Resources Management, Estonia.

Altınbilek, D. (2004) Development and Management of Euphrates-Tigris Basin, *Water Resources Development*, Vol. 20, No. 1, pp. 15-33.

Ambroise, B., Perrin, J.L. and Reutenauer, D. (1995) Multicriterion validation of semidistributed conceptual model of the water cycle in the Fecht Catchment, *Water Resources Research*, 31 (6), 1467-1481.

Appel I. and Salomonsaon V.V. (2005) Global Estimate of Fractional Snow Cover from MODIS, *4th EARSeL Workshop: Remote Sensing of Snow and Glaciers-Important Water Resources of the Future*, 21-23 February 2005, University of Berne, Switzerland.

Bathurst, J.C., Wicks, J.M., O'Connell, P.E. (1995) The SHE/SHESED basin scale water flow and sediment transport modeling system, in *Computer models of watershed hydrology*, ed V.P. Singh, Water Resources Pub., pp165-214.

Baumgartner, M.F. and Rango, A. (1995) A microcomputer based alpine snowcover analysis system (ASCAS), *Photogrammetric Engineering and Remote Sensing*, 61 (12), 1475-1486.

Bergström, S., Lindström, G. and Pettersson, A. (2002) Multi-variable parameter estimation to increase confidence in hydrological modeling, *Hydrological Processes*, 16, 413-421.

Bergström, S. (1995) The HBV model, in *Computer models of watershed hydrology*, ed. V.P. Singh, Water Resources Pub., p165-214.

Bergström, S. (1992) The HBV Model-Its Structure and Applications, *SMHI Hydrology*, RH No.4, Norrköping, 35 pp.

Beven, K.J. (2001) *Rainfall-runoff modeling*, Wiley, 360pp.

Beven, K.J. (1993) Prophecy, reality and uncertainty in distributed hydrological modeling, *Advances in Water Resources*, 16, 41-51.

Beven, K.J. and Binley, A.M. (1992) The future of distributed models: model calibration and uncertainty prediction, *Hydrological Processes*, 6, 279-298.

Burnash, R.J.C. (1995) The NWS river forecast system-catchment modeling, in *Computer models of watershed hydrology*, ed. V.P. Singh, Water Resources Pub., p165-214.

Carroll, T. R. (1990) Operational Airborne and Satellite snow cover products of the National Hydrologic Remote Sensing Center, *Proceedings of the 47th Annual Eastern Snow Conference*, 87-98.

Cazorzi, F., and Fontana, G.D. (1996) Snowmelt modeling by combining air temperature and a distributed radiation index, *Journal of Hydrology*, 181 (1-4), 169-187.

Cooper, V.A., Nguyen, V.T.V. and Nicell, J.A. (1997) Evaluation of global optimization methods for conceptual rainfall-runoff model calibration, *Wat. Sci. Tech.*, 36 (5), 53-60.

Davis, R.E., Dozier, J. and Marks, D. (1984) Micrometeorological measurements and instrumentation in support of remote sensing observations of an alpine snow cover, *Proceedings of the Western Snow Conference*, 52, 161-164.

Doherty, J. (2004) *PEST - Model Independent Parameter Estimation*, User Manual: Fifth Edition, Watermark Computing, Australia.

Doherty, J. (2003) *PEST – Surface Water Utilities*, Watermark Numerical Computing and University of Idaho.

Doherty, J., L. Brebber, and P. Whyte (1994) *PEST - Model Independent Parameter Estimation*, Watermark Computing, Corinda, Australia.

Dozier, J. (1980) A clear sky spectral radiation model for snow-covered mountainous terrain, *Water Resources Research,* 16**,** 709-718.

Duan, Q., Gupta, V., Sorooshian, S. and Rousseau, A., Turcotte, R. (2003) *Calibration of Watershed Models*, ed. Duan Q. et al., Water Science and Application 6, American Geophysical Union, Washington DC.

Duan, Q., Sorooshian, S. and Gupta, V. (1994) Optimal use of the SCE-UA global optimization method for calibrating watershed models, *Journal of Hydrology*, No. 158, 265-284.

Duan, Q., Sorooshian, S. and Gupta, V. (1993) A Shuffled Complex Evolution Approach for Effective and Efficient Optimization, *Journal of Optimization Theory Application*, Vol.76, No.3, 501-521.

Duan, Q., Sorooshian, S. and Gupta, V. (1992) Effective and efficient global optimization for conceptual rainfall-runoff models, *Water Resources Research*, 28 (4), 1015-1031.

Engeset, R.V., Udnaes, H.C., Guneriussen, T., Koren, H., Malnes, E., Solberg, R. and Alfnes, E. (2003) Improving Runoff Simulations Using Satellite-Observed and Time-Series of Snow Covered Area, *Nordic Hydrology,* 34 (4), 281-294.

Engman, E.T. and Gurney, R.J. (1991) *Remote Sensing in Hydrology,* Chapman and Hall, 225 pp

Franchini, M., Galeati, G. and Berra, S. (1998) Global optimization techniques for the calibration of conceptual rainfall-runoff models, *Hydrological Sciences Journal*, 43 (3), 443-458.

Frank C., Itten I. K., Staez K. (1988) Improvement in NOAA-AVHRR snow cover determination for runoff prediction, *IEEE IGARSS*, pp.433-435.

Freedman V.L., Lopez V.L., Hernandez M. (1998) Parameter identifiably for catchment-scale erosion modeling: A comparison of optimization algorithms, *Journal of Hydrology*, 207 (1-2), 83-97

Gan, T.Y., Dlamini, E.M. and Biftu, G.F. (1997) Effects of model complexity and structure, data quality and objective functions on hydrological modeling, *Journal of Hydrology*, 192, 81-103.

Gan, T.Y. and Biftu, G.F. (1996) Automatic calibration of conceptual rainfall-runoff models, optimization algorithms, catchment conditions and model structure, Water Resources Research, 32 (12), 3513-3524.

Gray, D.M. and Prowse, T.D. (1992) Snow and floating ice, *Handbook of Hydrology*, D.R. Maidment ed., McGraw-Hill, Inc., New York: 7.1-7.58.

Grosbois, D.E., Hooper, R.P. and Christopherson, N. (1988) A multisignal automatic calibration methodology for hydrochemical models-A case study of the Birkenes model, *Water Resources Research*, 24 (8), 1299-1307.

Guneriussen, T., Bjerke, P.L., Hallikainen, M., Hiltbrunner, D., Johnsen, H., Jaaskelainen, V., Kolberg, S.A., Koskinen, J., Maltzer, C., Pullianen, J., Sand, K., Solberg, R. Standley, A. and Wiesmann, A. (2000) *Research and Development of Earth Observation Methods for Snow Hydrology*, *SnowTools Final Report*, NORUT Report, 431/47-00.

Gupta, H.B., Sorooshian, S. and Yapo, P.O. (1998) Toward improved calibration of hydrological models: Multiple and noncommensurable measures of information, *Water Resources Research*, 34 (4), 751-763.

Hall, D.K., Riggs, G.A., Salomonson, V.V., DiGirolamo, N.E., Bayr, K.J. (2002) MODIS snow cover products, *Remote Sensing of Environment*, 83, pp. 181-194.

Hall, D.K., Riggs, G.A., Salomonson, V.V., Barton, J.S., Casey, K., Chien, J.Y.L., DiGirolamo, N.E., Klein, A.G., Powell, H.W., Tait, B.A. (2001) *Algorithm Theoretical Basis Document (ATBD) for MODIS snow and sea-ice mapping algorithms*.

Hall, D.K., Foster J.L., Verbyla D.L., Klein A.G. and Benson C.S. (1998) Assessment of snow-cover mapping accuracy in a variety of vegetation-cover densities in central Alaska, *Remote Sensing of Environment*, 66:129-137.

Hall, D.K. and Martinec, J. (1985) *Remote sensing of ice and snow,* Chapmen and Hall, London, pp189.

Harrison, A.R. and Lucas, R. M. (1989) Multi-spectral classification using NOAA/AVHRR imagery, *International Journal of Remote Sensing*, Vol. 10, 907-916.

Hendersen-Sellers, A., Yang, Z.L., Dickinson, R.E., (1993) The project for intercomparison of land-surface parameterization schemes, *Bull. Amer. Meteor. Soc.*, 74(7), 1335-1349.

Hill, M.C. (1998) Methods and guidelines for effective model calibration, U.S. Geological Survey, *Water Resources Investigations Report* 98-4005.

Hock, R. (1999) A distributed temperature index ice and snowmelt model including potential direct solar radiation, *Journal of Glaciology*, 45 (149), 101-111.

Holland, J. (1975) *Adaptation in natural and artificial systems*, Ann Arbor, University of Michigan Press, 211 pp.

Hooper, R.P., Stone, A., Christopherson, N., Grosbois, E.D. and Seip, H.M. (1988) Assessing the Birkenes model of stream acidification using a multisignal calibration methodology, *Water Resources Research*, 24 (8), 1308-1316.

Hu, X., Bailey, J.O., Barret, E.C. and Kelly, E.J. (1993) Monitoring snow area and depth with integration of remote sensing and GIS*, International Journal of Remote Sensing*, Vol. 14, No. 17, 3529-3268.

Johansson, B., Andreasson, J. and Jansson, J. (2003) Satellite data on snow cover in the HBV model. Method development and evaluation. *SMHI Hydrology*, RH No.90, Norrköping.

Johansson, B., Caves, R., Ferguson, R. and Turpin, O. (2001) Using remote sensing data to update the simulated snow pack of the HBV runoff model. In: *Remote Sensing and Hydrology*, IAHS publ., No. 267, 595-597.

Johnson, A.I., Petterson, C.B. and Fulton, J.L. (1992) *Geographic Information Systems (GIS) and mapping – Practices and standards*, ASTM Publication STP 1126, 346 pp.

Kattelmann, R. (2000) Snowmelt lysimeters in the evaluation of snowmelt models, *Annals of Glaciology*, 31, 406-410.

Kaya, H.I. (1999), *Application of Snowmelt Runoff Model using remote sensing and geographic information systems*, M.Sc. Dissertation, Dept. of Civil Engineering, Middle East Technical University, Ankara, Turkey.

Killingtveit, A. and Saelthun, N.R. (1995) *Hydrology, Hydropower Development Volume No. 7*, Norwegian Institute of Technology, Division of Hydraulic Engineering, Trondheim, Norway.

Killingtveit, A. and Sand, K. (1991) Areal Distribution of snow cover in mountainous areas, *Northern Research Basin 1990*, National Hydrology Research Institute, Saskatoon.

Killingtveit A. (1976) *En studie av vannbalansen i Sagelva hydrologiske forskningsfelt*, Instittutt for vassbygging, NTH, Trondheim, Norway.

Klein, A.G., Hall, D.K. and Riggs, G.A. (1998) Improving snow cover mapping in forests through use of a canopy reflectance model, *Hydrological Processes*, 12, 1723-1744.

Klemes, V. (1986) Operational testing of hydrological simulation models, *Hydrological Sciences Journal*, 31 (1), 13-24.

Kramer, H.J. (2002) Earth Observation History, Observation of the Earth and its Environment – Survey of Missions and Sensors, Springer.

Kuczera, G. and Mroczkowski, M. (1998) Assessment of hydrologic parameter uncertainty and the worth of multi-response data, *Water Resources Research*, 34, 1481-1489.

Kuczera, G. (1997) Efficient subspace probabilistic parameter optimization for catchment models, *Water Resources Research*, 33 (1), 177-185.

Kuczera, G. (1983) Improved parameter inference in catchment models, 2. Combining different kinds of hydrological data and testing their compatibility, *Water Resources Research*, 19, 1163-1172.

Kustas, W.P. and Rango, A. (1994) A simple energy budget algorithm for the snowmelt runoff model, *Water Resources Research*, Vol. 30, No. 5, pp. 1515-1527.

Kuusisto, E. (1980) On the values and variability of degree-day melting factor in Finland, *Nordic Hydrology*, 11, pp. 235-242.

Larson, L.W. and Peck E.W. (1974) Accuracy of precipitation measurements for hydrologic modeling, *Water Resources Research*, Vol. 10, 857-863.

Leavesley, G.H. and Stannard, L.G. (1995) The precipitation-runoff modeling system, in *Computer models of watershed hydrology*, ed. V.P. Singh, Water Resources Pub., p165-214.

Lindström G., Johansson B., Persson M., Gardelin M., Bergström S. (1997) Development and test of the distributed HBV-96 model, *Journal of Hydrology*, 201, pp 272-288.

Madsen, H. and Jacobsen, T. (2001) Automatic calibration of the MIKE SHE integrated hydrological modeling system, *4$^{th}$ DHI Software Conference*, 6-8 June 2001, Scanticon Conference Center, Helsingør, Denmark.

Madsen, H. (2000a) Automatic calibration of a conceptual rainfall-runoff model using multiple objectives, *Journal of Hydrology*, 235, 276-288.

Madsen, H. (2000b) Automatic calibration and uncertainty assessment in rainfall-runoff modeling, *2000 Joint Conference on Water Resources Engineering and Water Resources Planning and Management*, Hyatt Regency Minneapolis, USA, July 30 -August 2, 2000.

Male, D.H. and Gray, D.M. (1981) *Snow cover ablation and runoff*, D.H. Male and D.M. Gray ed. Toronto, Ontario, Pergamon Press**:** 360-436

Marks, D., Dozier, J. and Davis, R. (1992) Climate and energy exchange at the snow surface in the alpine region of the Sierra Nevada 1. Meteorological measurements and monitoring, *Water Resources Research*, Vol.28, No. 11: 3029-3042.

Marks, D., McGurk, B., Berg, N. and Dawson, D. (1988) Snow volume comparisons for atmospheric deposition monitoring, *Proc. West. Snow Conf.*, 56, 124-136.

Marks, D. and Dozier, J. (1979) A clear sky longwave radiation model for remote alphine areas, *Arch. Meteorol., Geophys. Bioclimatol. Ser*. B. 27, 159-187.

Marsh, P. and Woo, M. K. (1984) Wetting front advance and freezing of meltwater within a snow cover 2: A Simulation Model, *Water Resources Research*, Vol. 20, No. 12: 1865-1874.

Martinec, J. and Rango, A. (1987) Interpretation and utilization of areal snow cover data from satellites, *Annals of Glaciology*, Vol. 19, pp. 166-169.

Matson, M., Ropelewski C.F. and Varnadore M.S. (1986) *An atlas of satellite derived northern hemisphere snow cover frequency*, National Weather Service, Washington, D.C., 75 pp.

McLaughlin, D. and Townley, L.R. (1996) A reassessment of the groundwater inverse problem, *Water Resources Research*, 32 (5), 1131-1161.

Metsamaki, S., Huttunen, M., Anttila, S. (2003) The operative remote sensing of snow covered area in a service of hydrological modeling in Finland, Proceedings of the 23rd EARSeL Symposium and Workshops, Gent, Belgium, 2-7 June 2003.

Metsamaki, S., Vepsalainen, J., Pulliainen, J. and Suckdorff, Y. (2002) Improved linear interpolation method for the estimation of snow covered area from optical data, *Remote Sensing of Environment*, 82, 64-78.

Muleta, M. and Nicklow, J. (2005) Sensitivity and uncertainty analysis coupled with automatic calibration for a distributed watershed model, *Journal of Hydrology*, 306, 127-145.

Nagler T. (2005) Personal contact.

Nagler, T. and Rott H. (1997) The application of ERS-1 SAR for snowmelt runoff modeling. In: M.F. Baumgartnet, G.A. Schultz, and A.I. Johnson (eds), *5th Scientific Assembly of the International Association of Hydrological Sciences*, Rabat, Morocco, 28-30 April, 1997 (IAHS Publication No.242, pp. 119-126)

Nash, J.E. and Sutcliffe, J.V. (1970) River flow forecasting through conceptual models. Part I: A discussion of principles, *Journal of Hydrology*, Vol. 10, 282-290.

Nelder, J.A. and Mead, R. (1965) A simplex method for function minimization, *Comput. J.*, 7 (4), 308-313.

Ohmura, A. (2001) Physical basis for the temperature based melt index method, *J. Applied Meteorology*, 40 (4), 753-761.

Painter T.H., Bales R., Dozier J. (2005) Enhanced subpixel snow cover products from MODIS in snowmelt hydrological applications, *4th EARSeL Workshop: Remote Sensing of Snow and Glaciers-Important Water Resources of the Future*, 21-23 February 2005, University of Berne, Switzerland.

Pellicciotti, F., Strasser, U., Brock, B., Burlando, P., Funk, M. and Corrippio, J., (2002), An enhanced albedo accounting degree-day melt model for distributed application, *American Geophysical Union (AGU) Fall Meeting*, San Francisco.

Perrin, C., Michel C., Andreassian, V. (2001) Does a large number of parameters enhance model performance? Comparative assessment of common catchment model structures on 429 catchments, *Journal of Hydrology*, 242, pp 275-301.

Price, W.L. (1987) Global optimization algorithms for a CAD workstation, *Journal of Optimization Theory and Applications*, 55 (1), 133-146.

Ramsay, B. (1998) The interactive multisensor snow and ice mapping system, *Hydrological Processes*, 12, pp.1537-1546.

Rango, A. (1996) Spaceborne remote sensing for snow hydrology applications, *Hydrological Sciences Journal*, Vol. 41, 477-494.

Rango, A. (1994) Application of remote sensing methods to hydrology and water resources, *Hydrological Sciences Journal*, 34 (4), 309-320.

Rango, A., Salomonson, V.V., and Foster, J.L. (1977) Seasonal streamflow estimation in the Himalayan region employing meteorological snowcover observations, *Water Resources Research*, Vol. 13 (1), 109-112.

Refsgaard, J.C. (1997) Parameterization, calibration and validation of distributed hydrological models, *Journal of Hydrology*, 198, 69-97.

Riggs, G.A., Barton, J.S., Casey K., Hall, D.K., Salomonson, V.V. (2003) *MODIS snow products user guide for collection 4 data products*.

Rott, H., Nagler, T., Glendinning, G., Wright, G., Miller, D., Gauld, J., Caves, R., Ferguson, R., Quegan, S., Turpin, O., Clark, C., Johansson, B., Gyllander, A., Baumgartner, M., Kleindienst, H., Voigt, S. and Pirker, O. (2000) HYDALP. *Hydrology of Alpine and High Latitude Basins. Final Report*. Institut für Meteorologie and Geophysik, Universitat Innsbruch, Mitteilungen, 4.

Rott, H. (1978) *Zur* Schneekartierung in alpinen Einzugsbebieten aus Satellitenbildern, *Zeitschrift fur Gletscherkunde und Glaziologie*, Vol 14(1), 81-93.

Saelthun, N.R. (1996) The 'Nordic' HBV Model. Description and documentation of the model version developed for the project climate change and energy production, Norges Vassdrags-og Energiverk Report No.7.

Seibert, J (2003) The quest for an improved dialogue between modeler and experimentalist, *Calibration of Watershed Models*, ed. Duan Q. et al., Water Science and Application 6, American Geophysical Union, Washington DC.

Seibert, J. (2000) Multi-criteria calibration of a conceptual runoff model using a genetic algorithm, *Hydrology and Earth System Science*, 4 (2), 215-224.

Seibert, J. (1997) Estimation of parameter uncertainty in the HBV model, *Nordic Hydrology*, 28(4/5), 247-262.

Seidel, K. and J. Martinec (2004). Remote Sensing in Snow Hydrology; Runoff Modeling, Effect of Climate Change, Springer, 150pp.

Seidel, K., Brüsh, W. and Steinmeier, C. (1994) Experiences from real time runoff forecasts by snow cover remote sensing, *IEEE IGARSS*.

Singh, V.P. and Frevert, D.K. (2000a) *Mathematical models of large watershed hydrology*, Water Resources Pub., 891pp.

Singh, V.P. and Frevert, D.K. (2000b) *Mathematical models of small watershed hydrology and applications*, Water Resources Pub., 950pp.

Singh, V.P. (1995) *Computer models of watershed hydrology*, Water Resources Pub., 1130pp.

Sorooshian, S. and Gupta, V.K. (1995) Model calibration, in *Computer models of watershed hydrology* , V.P. Singh (ed.), Water Resources Pub., Littleton, Colorado, 23-68.

Sorooshian, S., Duan, Q. and Gupta, V.K. (1993) Calibration of rainfall-runoff models: application of global optimization to the Sacramento soil moisture accounting model, *Water Resources Research*, 29 (4), 1185-1194.

Sorooshian, S. and Dracup, J.A. (1980) Stochastic parameter estimation of hydrologic rainfall-runoff models, Correlated and heteoroscedastic error cases, *Water Resources Research*, 16 (2), 430-442.

Spear, R.C. and Hornberger, G.M. (1980) Eutrophication in peel inlet. II: Identification of critical uncertainities via generalized sensitivity analysis, *Water Res.*, 14, 43-49.

Sugawa, M. (1995) Tank model, in *Computer models of watershed hydrology*, ed. V.P. Singh, Water Resources Pub., p165-214.

Şensoy, A. (2005), *Physically based point snowmelt modeling and its distribution in Upper Euprates Basin*, Ph.D. Dissertation, Dept. of Civil Engineering, Middle East Technical University, Ankara, Turkey.

Şensoy, A. (2000), *Spatially distributed hydrologic modeling approach using geographic information systems*, M.Sc. Dissertation, Dept. of Civil Engineering, Middle East Technical University, Ankara, Turkey.

Şorman, A.A., Tekeli A.E., Şensoy A., Şorman A.Ü. (2004) Forecasting the Early Snowmelt Flood of 2004 – A Case Study from Upper Euphrates Basin, *6th International Congress on Advances in Civil Engineering*, 6-8 October 2004, Boğaziçi University, Istanbul, Turkey.

Tanakamuru, H. and Burges, S.J. (1996) Application of global optimization to parameter estimation of the Tank Model. In Proceedings of the *International Conference on Water Resources and Environmental Research*, 29-31 October, Kyoto, Japan, Vol.2, 39-46.

Tekeli, A.E. (2005), *Operational hydrological forecasting of snowmelt runoff model by RS-GIS Integration*, Ph.D. Dissertation, Dept. of Civil Engineering, Middle East Technical University, Ankara, Turkey.

Tekeli A.E., Akyürek Z., Şorman A.A., Şensoy A., Şorman A.Ü. (2005a) Using MODIS snow cover maps in modeling snowmelt runoff process in the Eastern part of Turkey, *Remote Sensing of Environment* (accepted for publication).

Tekeli A.E., Şorman A.A., Şensoy A., Şorman A.Ü., Bonta J., Schaefer G. (2005b), Snowmelt lysimeters for real time snowmelt studies in Turkey, *Turkish Journal of Engineering and Environmental Sciences*, Vol.29, No.1, pp 29-40.

Tekeli, A.E. (2000), *Integration of remote sensing and geographic information systems on snow hydrology modeling*, M.Sc. Dissertation, Dept. of Civil Engineering, Middle East Technical University, Ankara, Turkey.

Thyer, M., Kuczera, G. and Bates, B.C. (1999) Probabilistic optimization for conceptual rainfall-runoff models: A comparison of the shuffled complex evolution and simulated annealing algorithms, *Water Resources Research*, 35 (3), 767-773.

Townshend, J.R.G. and Tucker, C.J. (1984) Objective assessment of Advanced Very High Resolution Radiometer data for land cover mapping, *International Journal of Remote Sensing*, 5, 497-504.

Troutman, B.M. (1985) Errors and parameter estimation in precipitation-runoff modeling 1. Theory, *Water Resources Research*, Vol. 21(8), pp 1195-1213.

Tucker, C.J. (1986) Maximum normalized difference vegetation index images for sub-Saharan Africa for 1983-1985, *International Journal of Remote Sensing*, 7, 1383-1394.

Tucker, C.J., (1979) Red and photographic infrared linear combinations for monitoring vegetation, *Remote Sensing of Environment*, 8, pp 127-150.

Uhlenbrook, S., Seibert, J., Leibundgut, C., Rodhe, A. (1999) Prediction uncertainty of conceptual rainfall-runoff models caused by problems in identifying model parameters and structure, *Hydrological Sciences Journal*, 44(5), 779-797.

UNEP (2001) The Mesopotamian Marshlands: Demise of an Ecosystem, *Early Warning and Assessment Technical Report No.3*, UNEP/DEWA/TR.0103, Geneva.

USACE (1998) *Engineering and Design: Runoff from Snowmelt*, U.S. Army Corps of Engineers, Washington DC.

USACE (1956) *Snow Hydrology: Summary report of the snow investigations*, U.S. Army Corps of Engineers, North Pacific Division, Portland, Oregon.

Usul, N. (2001) *Engineering Hydrology*, METU Press Publishing Company.

Uzunoğlu, E. (1999), *Application of the SLURP model using remote sensing and geographic information systems*, M.Sc. Dissertation, Dept. of Civil Engineering, Middle East Technical University, Ankara, Turkey.

Van Griensven, A. and Bauwens, W. (2001) Multi-objective calibration in integrated river basin modeling, *Geophysical Research Abstracts*, Vol.3, European Geophysical Society, 26th General Assembly.

Vehvilainen, B. and Huttunen, M. (2001) Hydrological forecasting and real time monitoring in Finland: The watershed simulation and forecasting system (WSFS), Finnish Environment Institute.

Vikhamer, D. and Solberg, R. (2003) Subpixel mapping of snow cover in forests by optical remote sensing, *Remote Sensing of Environment*, 84, 69-82.

Wang, Q.J. (1991) The genetic algorithm and its application to calibrating conceptual rainfall-runoff models, *Water Resources Research*, 27 (9), 2467-2471.

Wiesnet, D.R., Ropelevski, C.F., Kukla, G.J. and Robinson, D.A. (1987) A discussion of the accuracy of NOAA satellite derived global seasonal snow cover measurements, *IAHS publications,* Vol. 166, 291-304.

Winther, J-G. (1993) *Snow and Glacier Ice Characteristics measured using Landsat TM Data*, Norwegian Institute of Technology, Dept. of Hydraulic and Environmental Engineering, IVB Report B-2-1993-5, Trondheim, Norway.

WMO (1999a) *Current operational applications of remote sensing in hydrology*, Publication No. 884, Operational Hydrology Report No. 43, World Meteorological Organization, Geneva, Switzerland.

WMO (1999b) *Areal modeling in hydrology using remote sensing data and geographical information system*, Publication No. 885, Operational Hydrology Report No. 44, World Meteorological Organization, Geneva, Switzerland.

WMO (1992) *Simulated real-time intercomparison of hydrological models*, Publication No. 779, Operational Hydrology Report No. 38, World Meteorological Organization, Geneva, Switzerland.

WMO (1986) *Intercomparison of models of snowmelt runoff*, Publication No. 646, Operational Hydrology Report No. 23, World Meteorological Organization, Geneva, Switzerland.

WMO (1975) *Intercomparison of conceptual models used in hydrological forecasting*, Operational Hydrology Technical Report No: 7, WMO, Geneva.

Yapo, P.O. (1996) *A multi-objective global optimization algorithm with application to calibration of hydrological models*, PhD. Thesis, Department of Hydrology and Water Resources, University of Arizona, Tucson, Az.

Yapo, P.O., Gupta, V., Sorooshian, S. (1996) Calibration of Conceptual Rainfall-Runoff Models: Sensitivity to Calibration Data, *Journal of Hydrology*, 181, 23-48.

## **Web References**

URL-1, NOAA, National Oceanic and Atmospheric Administration
http://www.ssd.noaa.gov/PS/SNOW
(Last accessed 20/03/2005)

URL-2, NOHRSC, National Operational Hydrologic Remote Sensing Center
http://www.nohrsc.nws.gov
(Last accessed 20/10/2004)

URL-3, EnviSnow, Development of Generic Earth Observation Based Snow Parameter Retrieval Algorithms
http://projects.itek.norut.no/EnviSnow
(Last accessed 20/06/2005)

URL-4, SnowMan, Snow Parameter Retrieval from Remote Sensing data for Improved Monitoring and Management of Water Resources
http://projects.itek.norut.no/snowman
(Last accessed 20/06/2005)

URL-5, NSIDC, National Snow and Ice Data Center
http://www.nsidc.org
(Last accessed 14/03/2005)

URL-6, MODIS, Moderate Resolution Imaging Spectroradiometer
http://modis.gsfc.nasa.gov
(Last accessed 20/03/2005)

URL-7, MRT, MODIS Reprojection Tools
http:// lpdaac.usgs,gov/landdaac/tools/modis/index.html
(Last accessed 25/10/2004)

URL-8, ECMWF, European Center for Medium-Range Weather Forecasts
http://www.ecmwf.int
Last accessed 20/03/2005)

URL-9, MM5, Mesoscale Model 5
http://www.mmm.ucar.edu/mm5/overview.html
(Last accessed 20/06/2005)

URL-10, MM5, Mesoscale Model 5
http://www.mmm.ucar.edu/mm5/mm5v3/v3model.html
(Last accessed 20/06/2005)

URL-11, MM5, Mesoscale Model 5
ftp://ftp.ucar.edu/mesouser/MM5V3/TERRAIN_DATA
(Last accessed 20/06/2005)

URL-12, Anadoluajansı
http://www.hri.org/news/turkey/anadolu/2004/04-03-06.anadolu.html
(Last accessed 20/10/2004)

URL-13, Dartmouth Flood Observatory
http://www.dartmouth.edu/%7Efloods/Archives/2004global.jpg
(Last accessed 20/10/2004)

URL-14, Poleshiftprepare
http://www.poleshiftprepare.com/earth_changesJanMar2004.htm
(Last accessed 20/10/2004)

URL-15, Turkishpress
http://www.turkishpress.com/turkishpress/news.asp?ID=18205
(Last accessed 20/10/2004)

# APPENDIX A

# Parameter ESTimation (PEST) Input Files

```
ptf #
START  2KIRK
  2     0              1    PNO       Number of precipitation stations
  2     0  GY_P             PID1      Identification for precip station 1
  2     0         2065.     PHOH1     Altitude precip station 1
  2     0          1.0      PWGT1     Weight precipitation station 1
  2     0              1    TNO       Number of temperature stations
  2     0  GY_T             TID1      Identification for temp station 1
  2     0         2065.     THOH1     Altitude temp station 1
  2     0          1.0      TWGT1     Weight temp station 1
  2     0              1    QNO       Number of discharge stations
  2     0  Kirkgoze         QID       Identification for discharge station
  2     0          1.       QWGT      Scaling factor for discharge
  2     0       242.42      AREAL     Catchment area                   [km2]
  2     4        0.000      MAGDEL    Regulation reservoirs            [1]
  2     5     1890.000      HYPSO ( 1,1), low point            [m]
  2     6     2026.000      HYPSO ( 2,1)
  2     7     2107.000      HYPSO ( 3,1)
  2     8     2178.000      HYPSO ( 4,1)
  2     9     2254.000      HYPSO ( 5,1)
  2    10     2341.000      HYPSO ( 6,1)
  2    11     2440.000      HYPSO ( 7,1)
  2    12     2589.000      HYPSO ( 8,1)
  2    13     2692.000      HYPSO ( 9,1)
  2    14     2791.000      HYPSO (10,1)
  2    15     2957.000      HYPSO (11,1), high point
  2    16        0.000      HYPSO ( 1,2), Part of total area below HYPSO (1,1) = 0
  2    17        0.100      HYPSO ( 2,2)
  2    18        0.200      HYPSO ( 3,2)
  2    19        0.300      HYPSO ( 4,2)
  2    20        0.400      HYPSO ( 5,2)
  2    21        0.500      HYPSO ( 6,2)
  2    22        0.600      HYPSO ( 7,2)
  2    23        0.700      HYPSO ( 8,2)
  2    24        0.800      HYPSO ( 9,2)
  2    25        0.900      HYPSO (10,2)
  2    26        1.000      HYPSO (11,2), Part of total area below HYPSO (11,1) = 1
  2    27        0.000      BREPRO( 1), Glacier area, part of total area, below HYPSO( 1,1) (=0.0)
  2    28        0.000
  2    29        0.000
  2    30        0.000
  2    31        0.000
  2    32        0.000

  2    33        0.000
  2    34        0.000
  2    35        0.000
  2    36        0.000
  2    37        0.000      BREPRO(11), Glacier area, part of total area, below HYPSO(11,1)
  2    38
  2    39      270.000      NDAG      Day no for conversion of glacier snow to ice
  2    40 #     tx   #      TX        Threshold temperature for snow/ice          [C]
  2    41 #     ts   #      TS        Threshold temperature fo no melt            [C]
  2    42 #     cx   #      CX        Melt index                         [mm/deg/day]
  2    43        0.050      CFR       Refreeze efficiency                         [1]
  2    44        0.080      LV        Max rel. water content in snow              [1]
  2    45 #    pkor  #      PKORR     Precipitaion correction for rain            [1]
  2    46 #    skor  #      SKORR     Additional precipitation corection for snow at gauge [1]
```

Figure A.1 PEST template file example for HBV model

```
2   47                    GRADALT   Altitude for change in prec. grad.        [m]
2   48                    PGRAD1    Precipitation gradient above GRADALT       [1]
2   49        0.020       CALB      Ageing factor for albedo              [1/day]
2   50        0.330       CRAD      Radiation melt component                  [1]
2   51        0.340       CONV      Convection melt component                 [1]
2   52        0.330       COND      Condensation melt component               [1]
2   60        1.1         CEVPL     lake evapotranspiration adjustment fact   [1]
2   61        0.5         ERED      evapotranspiration red. during interception [1]
2   62        30.0        ICEDAY    Lake temperature time constant            [d]
2   63 #  ttgd    #       TTGRAD    Temperature gradient for days without precip [deg/100 m]
2   64 #  tvgd    #       TVGRAD    Temperature gradient for days with precip [deg/100 m]
2   65 #  pgrd    #       PGRAD     Precipitation altitude gradient        [1/100 m]
2   66        1.500       CBRE      Melt increase on glacier ice              [1]
2   67        0.008       EP        EP( 1), Pot evapotranspiration, Jan   [mm/day] or [1]
2   68        0.008       EP        EP( 2), Pot evapotranspiration, Feb   [mm/day] or [1]
2   69        0.300       EP        EP( 3)
2   70        1.000       EP        EP( 4)
2   71        2.000       EP        EP( 5)
2   72        2.800       EP        EP( 6)
2   73        3.000       EP        EP( 7)
2   74        3.000       EP        EP( 8)
2   75        2.300       EP        EP( 9)
2   76        1.100       EP        EP(10)
2   77        0.300       EP        EP(11)
2   78        0.008       EP        EP(12)), Pot evapotranspiration, Dec   [mm/day] or [1]
2   79 #  fc      #       FC        Maximum soil water content            [mm]
2   80 #  lp      #       FCDEL     Pot.evapotr when content = FC*FCDEL    [1]
2   81 #  beta    #       BETA      Non-linearity in soil water zone      [1]
2   82        50.00       INFMAX    maximum infiltration capacity         [mm/day]
2   83
2   84
2   85 #  kuz2    #       KUZ2      Quick time constant upper zone        [1/day]
2   86 #   uz1    #       UZ1       Threshold quick runoff                [mm]
2   87 #  kuz1    #       KUZ1      Slow time constant upper zone         [1/day]
2   88 #  perc    #       PERC      Percolation to lower zone             [mm/day]
2   89 #   klz    #       KLZ       Time constant lower zone              [1/day]
2   90        0.00        ROUT      (1), Routing constant (lake area, km2)
2   91        0.00        ROUT      (2), Routing constant (rating curve const)
2   92        0.00        ROUT      (3), Routing constant (rating curve zero)
2   93        0.00        ROUT      (4), Routing constant (rating curve exp)
2   94        0.00        ROUT      (5), Routing constant (drained area ratio)
2   95        0.00        DECAY     (1), Feedback constant
2   96        0.00        DECAY     (2), Feedback constant
2   97        0.00        DECAY     (3), Feedback constant
2   98        0.17        CE        Evapotranspiration constant           [mm/deg/day]
2   99        1.0         DRAW      "draw up" constant                    [mm/day]
2  100        40.0        LAT       Latitude                              [deg]
2  101        -0.6        TGRAD(1)  Temperature gradient Jan              [deg/100m]
2  102        -0.6        TGRAD(2)  Temperature gradient Feb              [deg/100m]
2  103        -0.6        TGRAD(3)  Temperature gradient Mar              [deg/100m]
2  104        -0.6        TGRAD(4)  Temperature gradient Apr              [deg/100m]
2  105        -0.6        TGRAD(5)  Temperature gradient May              [deg/100m]
2  106        -0.6        TGRAD(6)  Temperature gradient Jun              [deg/100m]
2  107        -0.6        TGRAD(7)  Temperature gradient Jul              [deg/100m]
2  108        -0.6        TGRAD(8)  Temperature gradient Aug              [deg/100m]
2  109        -0.6        TGRAD(9)  Temperature gradient Sep              [deg/100m]
2  110        -0.6        TGRAD(10) Temperature gradient Oct              [deg/100m]
2  111        -0.6        TGRAD(11) Temperature gradient Nov              [deg/100m]
2  112        -0.6        TGRAD(12) Temperature gradient Dec              [deg/100m]
2  113        20.0        SPDIST    Uniformly distributed snow acc        [mm]
2  114        80.0        SMINI     Inital soil moisture content          [mm]
2  115        0.0         UZINI     Initial upper zone content            [mm]
2  116        135.0       LZINI     Initial lower zone content            [mm]
2  121           1        VEGT(1,1) Vegetation type 1, zone 1
2  122           0        VEGT(2,1) Vegetation type 2, zone 1
2  123        0.0         VEGA(1)   Vegetation 2 area, zone 1             [1]
2  124        0.0         LAKE(1)   Lake area,      zone 1                [1]
2  125           1        VEGT(1,2) Vegetation type 1, zone 2
2  126           0        VEGT(2,2) Vegetation type 2, zone 2
2  127        0.0         VEGA(2)   Vegetation 2 area, zone 2             [1]
2  128        0.0         LAKE(2)   Lake area,      zone 2                [1]
2  129           1        VEGT(1,3) Vegetation type 1, zone 3
2  130           0        VEGT(2,3) Vegetation type 2, zone 3
2  131        0.0         VEGA(3)   Vegetation 2 area, zone 3             [1]
2  132        0.0         LAKE(3)   Lake area,      zone 3                [1]
2  133           1        VEGT(1,4) Vegetation type 1, zone 4
```

Figure A.1 (cont'd) PEST template file example for HBV model

```
 2  134          0      VEGT(2,4) Vegetation type 2, zone 4
 2  135          0.0    VEGA(4)   Vegetation 2 area,  zone 4          [1]
 2  136          0.0    LAKE(4)   Lake area,          zone 4          [1]
 2  137          1      VEGT(1,5) Vegetation type 1, zone 5
 2  138          0      VEGT(2,5) Vegetation type 2, zone 5
 2  139          0.0    VEGA(5)   Vegetation 2 area,  zone 5          [1]
 2  140          0.0    LAKE(5)   Lake area,          zone 5          [1]
 2  141          1      VEGT(1,6) Vegetation type 1, zone 6
 2  142          0      VEGT(2,6) Vegetation type 2, zone 6
 2  143          0.0    VEGA(6)   Vegetation 2 area,  zone 6          [1]
 2  144          0.0    LAKE(6)   Lake area,          zone 6          [1]
 2  145          1      VEGT(1,7) Vegetation type 1, zone 7
 2  146          0      VEGT(2,7) Vegetation type 2, zone 7
 2  147          0.0    VEGA(7)   Vegetation 2 area,  zone 7          [1]
 2  148          0.0    LAKE(7)   Lake area,          zone 7          [1]
 2  149          1      VEGT(1,8) Vegetation type 1, zone 8
 2  150          0      VEGT(2,8) Vegetation type 2, zone 8
 2  151          0.0    VEGA(8)   Vegetation 2 area,  zone 8          [1]
 2  152          0.0    LAKE(8)   Lake area,          zone 8          [1]
 2  153          1      VEGT(1,9) Vegetation type 1, zone 9
 2  154          0      VEGT(2,9) Vegetation type 2, zone 9
 2  155          0.0    VEGA(9)   Vegetation 2 area,  zone 9          [1]
 2  156          0.0    LAKE(9)   Lake area,          zone 9          [1]
 2  157          1      VEGT(1,10) Vegetation type 1, zone 10
 2  158          0      VEGT(2,10) Vegetation type 2, zone 10
 2  159          0.0    VEGA(10)   Vegetation 2 area, zone 10         [1]
 2  160          0.0    LAKE(10)   Lake area,         zone 10         [1]
FINIS
```

Figure A.1 (cont'd) PEST template file example for HBV model

```
pif *
l200  [sc01]66:73
l16   [sc02]66:73
l8    [sc03]66:73
l13   [sc04]66:73
l7    [sc05]66:73
l11   [sc06]66:73
l308  [sc07]66:73
l2    [sc08]66:73
l19   [sc09]66:73
l1    [sc10]66:73
l6    [sc11]66:73
l4    [sc12]66:73
l317  [sc13]66:73
l14   [sc14]66:73
l1    [sc15]66:73
l9    [sc16]66:73
l8    [sc17]66:73
l26   [sc18]66:73
l10   [sc19]66:73
```

Figure A.2 PEST instruction file example

```
pcf
* control data
restart estimation
16 20 14 0 2
1 2 single point 1 0 0
5.0 2.0 0.3 0.03 10
3.0 3.0 0.001
0.1 aui
30 0.01 3 3 0.01 3
1 1 1
* automatic user intervention
8 1 0.9 0
10 0 3
0.8 0.95 3
* parameter groups
tcrt relative  0.03    0.01  always_2  2 parabolic
tres relative  0.03    0.01  always_2  2 parabolic
cx   relative  0.0125  0.05  always_2  2 parabolic
kor  relative  0.025   0.025 always_2  2 parabolic
tgrd relative  0.02    0.001 always_2  2 parabolic
pgrd relative  0.02    0.001 always_2  2 parabolic
fc   relative  0.025   1.0   always_2  2 parabolic
lp   relative  0.02    0.001 always_2  2 parabolic
beta relative  0.02    0.05  always_2  2 parabolic
kuz2 relative  0.03    0.01  always_2  2 parabolic
uz1  relative  0.025   1.0   always_2  2 parabolic
kuz1 relative  0.05    0.005 always_2  2 parabolic
perc relative  0.05    0.005 always_2  2 parabolic
klz  relative  0.02    0.001 always_2  2 parabolic
* parameter data
tx   none  relative   0.000   −2.0     2.5    tcrt  1.0   0.0 1
ts   none  relative   0.000   −2.0     2.5    tres  1.0   0.0 1
cx    log  factor     3.500    1.0     7.0    cx    1.0   0.0 1
pkor  log  factor     1.000    0.5     1.5    kor   1.0   0.0 1
skor  log  factor     1.000    0.5     1.7    kor   1.0   0.0 1
ttgd none  factor    −0.600   −1.1    −0.4    tgrd  1.0   0.0 1
tvgd none  factor    −0.400   −0.7    −0.3    tgrd  1.0   0.0 1
pgrd none  relative   0.010    0.0     0.1    pgrd  1.0   0.0 1
fc    log  factor   250.000   50.0   450.0    fc    1.0   0.0 1
lp   none  relative   0.900    0.6     1.0    lp    1.0   0.0 1
beta none  relative   1.000    1.0     4.0    beta  1.0   0.0 1
kuz2 none  factor     0.200    0.1     0.5    kuz2  1.0   0.0 1
uz1   log  factor    20.00     5.0    65.0    uz1   1.0   0.0 1
kuz1 none  factor     0.100    0.01    0.3    kuz1  1.0   0.0 1
perc none  factor     0.600    0.30    2.0    perc  1.0   0.0 1
klz  none  factor     0.001    0.0005  0.01   klz   1.0   0.0 1
* observation groups
diff
sca
* observation data
accd  0.0   1.0   diff
sc01   88.0 1.0    sca
sc02   47.6 1.0    sca
sc03   36.8 1.0    sca
sc04   24.9 1.0    sca
sc05   11.8 1.0    sca
sc06    4.6 1.0    sca
sc07   75.7 1.0    sca
sc08   55.5 1.0    sca
sc09   34.7 1.0    sca
sc10   28.8 1.0    sca
sc11   20.6 1.0    sca
sc12    9.2 1.0    sca
sc13   89.0 1.0    sca
sc14   77.4 1.0    sca
sc15   65.8 1.0    sca
sc16   70.2 1.0    sca
sc17   42.7 1.0    sca
sc18   18.7 1.0    sca
sc19    7.6 1.0    sca
* model command line
hbv.exe < arda020304.txt
* model input/output
param.tpl param.dat
res_020304.ins PRTFIL.RES
snow_020304n.ins PRTFIL.RES
```

Figure A.3 PEST control file example

212

# CURRICULUM VITAE

## PERSONAL INFORMATION

Surname, Name: Şorman, Ali Arda
Nationality: Turkish (TC)
Date and Place of Birth: 30 January 1976, Ankara
Email: ardasor@metu.edu.tr
    asorman@anadolu.edu.tr

## EDUCATION

| Degree | Institution | Date of Graduation |
|--------|-------------|--------------------|
| Ph.D. | METU, Civil Engineering, Ankara, Turkey | June 2005 |
| M.Sc. | METU, Civil Engineering, Ankara, Turkey | December 1999 |
| B.Sc. | METU, Civil Engineering, Ankara, Turkey | July 1996 |
| High School | Continental School, Jeddah, Saudi Arabia | June 1992 |

## WORK EXPERIENCE

| Year | Place | Enrollment |
|------|-------|------------|
| Oct 2004 - Present | Anadolu University, Civil Engineering | Research Assistant |
| Jun 1997 - Sep 2004 | METU, Civil Engineering | Research Assistant |

## FOREIGN LANGUAGE

English (excellect)

## PUBLICATIONS

1. Tekeli A.E., Akyürek Z., Şorman A.A., Şensoy A., Şorman A.Ü. (2005) Using MODIS snow cover maps in modeling snowmelt runoff process in the Eastern part of Turkey, *Remote Sensing of Environment*, (accepted for publication).
2. Tekeli A.E., Akyürek Z., Şensoy A., Şorman A.A., Şorman A.Ü. (2005) Modeling the temporal variation in snow covered area derived from satellite images for simulating/forecasting of snowmelt runoff in Turkey, *Hydrological Sciences Journal*, (accepted for publication).
3. Tekeli, A.E., Şorman, A.A., Şensoy, A., Şorman, A.Ü., Bonta, J. and Schaefer, G. (2005) Snowmelt Lysimeters for Real-Time Snowmelt Studies in Turkey, *Turkish Journal of Engineering and Environmental Sciences*, 29 (1), 29-40.
4. Şensoy, A., Tekeli, A.E., Şorman, A.A. and Şorman, A.Ü. (2003) Simulation of event based snowmelt runoff hydrographs based on snow depletion curves and the degree-day method, *Canadian Journal of Remote Sensing*, 29 (6), 693-700.
5. Şorman, A.A. (1999) *A Hydrological Modeling Approach using Remote Sensing and Geographic Information Systems – A Case Study*, M.Sc. Thesis, Department of Civil Engineering, Middle East Technical University.